

# **Functionalization of Magnetic Nanoparticles and their Application as Recyclable Support for Scavengers and Catalysts**

**Dissertation**

**Zur Erlangung des Doktorgrades der Naturwissenschaften**

**Dr. rer. nat.**

**der Fakultät für Chemie und Pharmazie**

**der Universität Regensburg**



vorgelegt von

**Corina Monika Eichenseer**

aus Neumarkt i.d.OPf.

**im Jahr 2016**

Die Arbeit wurde angeleitet von: Prof. Dr. O. Reiser

Promotionsgesuch eingereicht am: 11. April 2016

Promotionskolloquium am: 19. Mai 2016

Prüfungsausschuss:                      Vorsitz: Prof. Dr. O. Tepner

1. Gutachter: Prof. Dr. O. Reiser

2. Gutachter: Prof. Dr. M. A. Pericàs

3. Gutachter: Prof. Dr. F.-M. Matysik

Der experimentelle Teil der vorliegenden Arbeit wurde in der Zeit von Oktober 2012 bis Januar 2016 unter der Gesamtleitung von Herrn Prof. Dr. O. Reiser am Lehrstuhl für Organische Chemie der Universität Regensburg angefertigt. Zusätzlicher Betreuer war von April 2014 bis Juni 2014 Prof. M. A. Pericàs am Institut Català d'Investigació Química (ICIQ), Tarragona (Spanien).

Besonders bedanken möchte ich mich bei Herrn Prof. Dr. O. Reiser für die Aufnahme in seinen Arbeitskreis, die Überlassung des äußerst interessanten und vielseitigen Themas, die anregenden Diskussionen und seine stete Unterstützung.





*Meiner Familie und Marco*

“Phantasie ist wichtiger als Wissen, denn Wissen ist begrenzt.” - Albert Einstein

# Table of contents

<b>A</b>	<b>Introduction</b>	<b>1</b>
1	Covalent functionalization	3
1.1	Uncoated Fe <sub>3</sub> O <sub>4</sub> nanoparticles	3
1.2	Silica-coated Fe <sub>3</sub> O <sub>4</sub> nanoparticles	4
1.3	Graphene-coated nanoparticles	5
2	Noncovalent functionalization	6
3	Conclusion and perspectives	9
4	References	10
<b>B</b>	<b>Main Part</b>	<b>12</b>
1	Reversible magnetic mercury extraction from water	12
1.1	Introduction	13
1.2	Results and discussion	14
1.3	Conclusion	29
1.4	Experimental section	30
1.5	References	46
2	Synthesis and application of magnetic Noyori-type ruthenium catalysts for asymmetric transfer hydrogenation reactions in water	48
2.1	Introduction	49
2.2	Results and discussion	50
2.3	Conclusion	62
2.4	Experimental section	64
2.5	References	107
3	Juliá-Colonna epoxidation catalyzed by poly( <i>L</i> -leucine) functionalized magnetic nanoparticles	110
3.1	Introduction	111
3.2	Results and discussion	112
3.3	Conclusion	124
3.4	Experimental section	125
3.5	References	144
<b>C</b>	<b>Summary</b>	<b>146</b>

<b>D</b>	<b>Zusammenfassung</b>	<b>149</b>
<b>E</b>	<b>List of abbreviations</b>	<b>152</b>
<b>F</b>	<b>Appendix</b>	<b>154</b>
<b>G</b>	<b>Acknowledgement – Danksagung</b>	<b>158</b>

# A Introduction<sup>i</sup>

By definition, a catalyst emerges from a reaction unchanged and can be reused, provided that a separation from the reaction solution is possible.<sup>[1]</sup> Both academic and industrial researchers have developed a number of efficient, homogenous catalysts for countless reactions, also including asymmetric transformations. However, only a few among those catalysts are applicable in industrial production as the separation from the reaction products is often complicated, expensive and laborious.

In the last decades, there has been a trend toward the development of heterogeneous catalysts to circumvent the isolation problem: thanks to the immobilization on a solid support, the catalyst is not soluble anymore in the reaction solution and can be readily separated. The many different types of solid supports can be divided into two major categories: on the one hand organic polymer resins and on the other hand inorganic materials like silica or titanium dioxide. In both cases, the separation from the reaction is performed by filtration or centrifugation, although the low mechanical stability, especially of polymer beads, is detrimental. The weak gel structure is likely to break if the resins are stirred or recycled repeatedly, which is limiting the lifetime of the solid support.

A remarkable alternative to traditional supports are magnetic nanoparticles (NPs). Their big advantage is the facile separation from the reaction mixture. An external magnet is collecting the nanoparticles to one side of the reaction vessel and the supernatant solution can be completely decanted in a fast and efficient way. Thus, a contamination of the product solution with the support is prevented and the immobilized catalyst can be retrieved quantitatively. As no filtration or extraction steps are required, the energy consumption as well as the volume of solvents used can be reduced. The immobilization of catalysts on spherical, magnetic nanoparticles combines the benefits of heterogeneous and homogeneous catalysis. Due to their small size the particles have a large surface area, and this is contributing favorably to the interaction of the anchored, catalytically active molecules with the reaction solution. The results thereof are high reaction rates similar to those of the homogenous counterparts. Hence, the immobilization of catalysts or reagents on such small supports is bridging the gap between homogeneous and heterogeneous catalysis, being called semi-heterogeneous catalysis.<sup>[2]</sup> Besides the facile separation, magnetic nanoparticles have further advantages. They are often more mechanically stable than the polymer resins, allowing for mechanical stirring and frequent recycling. Furthermore, magnetic nanoparticles can be moved in an external magnetic field

---

<sup>i</sup> Reprinted and adapted with permission of *Nachrichten aus der Chemie*: C. M. Eichenseer, O. Reiser, *Nachrichten aus der Chemie* **2015**, 63, 763–767. Copyright © 2015 Gesellschaft Deutscher Chemiker, Frankfurt am Main.

without actual physical contact. This makes them applicable in flow systems in which the nanocatalysts can be perfectly mixed with the reaction solution by external rotating magnetic fields.<sup>[3]</sup> Additionally to using magnetic nanoparticles as mere solid support, there are cooperative effects which can be utilized. To mention just one example, immobilized catalysts or reagents can be selectively heated in an external magnetic field by inductive heating.<sup>[4]</sup> However, the application of magnetic nanoparticles as support can also pose a problem. The metal from the core of the particles can leach into the reaction solution. This metal contamination is undesired and has to be prevented, for instance by the introduction of a protective layer around the core, making the particles more stable. All in all, the benefits gained from the application of magnetic nanoparticles outbalance the potential negative side effects which explains why the particles have already been applied as support in the field of catalysis for more than ten years.<sup>[5]</sup> Just recently, they attracted even broader interest, as proven by numerous review articles from the last two years.<sup>[6]</sup>

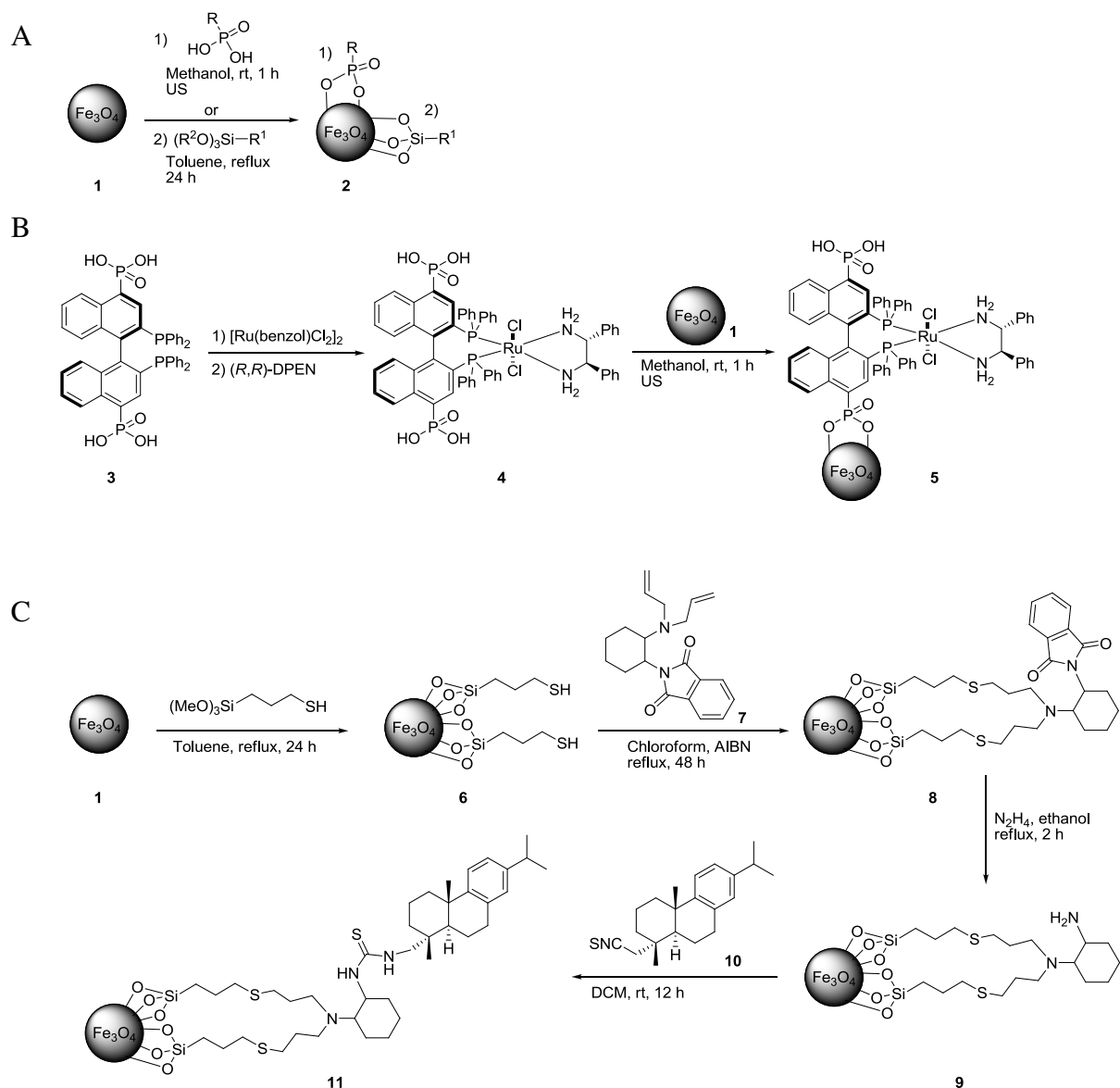
While there are many different types of magnetic nanoparticles they all have one thing in common: a magnetic core. This core can consist of metals like iron, cobalt or nickel, as well as of metal oxides such as iron oxide. Furthermore, alloys like FePt and CoPt or ferrites such as  $\text{CoFe}_2\text{O}_4$  are possible. Despite their beneficial high magnetization, pure metal nanoparticles suffer from oxidation when exposed to air. Therefore, the cores need to be coated by a protecting layer. However, also magnetic nanoparticles made of metal oxides, alloys or ferrites need a protective coating to ensure their stability under challenging reaction conditions. In addition to increasing the stability of the particles, this coating facilitates the surface functionalization. The established types of coatings are versatile and range from silica to graphene or polymers. There are two major strategies for the immobilization: the covalent and the noncovalent approach. The covalent immobilization of catalysts comprises again different possible routes depending on the functional groups on the surface of the magnetic nanoparticles. In summary, magnetic nanoparticles represent a customizable platform for the immobilization of different catalysts. In the following, functionalization strategies for uncoated as well as silica-coated iron oxide nanoparticles will be highlighted and the immobilization of catalysts on graphene-coated cobalt nanoparticles will be described. Various approaches for the noncovalent attachment of catalysts will be explored at last.

# 1 Covalent functionalization

## 1.1 Uncoated Fe<sub>3</sub>O<sub>4</sub> nanoparticles

Iron oxide nanoparticles have been widely used as data storage medium for a long time, for example in music tapes.<sup>[7]</sup> They are well known, readily available or can be prepared easily which explains their extensive application in chemistry, especially as support for catalysts.<sup>[8]</sup> When using iron oxide nanoparticles without an additional protective layer, two strategies for the functionalization are mostly applied. First of all, variable phosphonic acids can be anchored to the surface of Fe<sub>3</sub>O<sub>4</sub> nanoparticles **1** with the aid of ultrasound. The reaction takes place in methanol at room temperature and is complete within one hour (Scheme 1 A and B). Lin *et al.*<sup>[9]</sup> used this strategy for the synthesis of an immobilized chiral 4,4'-bisphosphonic acid-substituted 2,2'-bis(diphenylphosphino)-1,1'-binaphthyl-Ru-1,2-diphenyl-ethane-1,2-diamine (BINAP-Ru-DPEN) catalyst **5** (Scheme 1 B). Applied in the asymmetric transfer hydrogenation reactions, this catalyst showed both high activity (up to 50 TON h<sup>-1</sup>) and enantioselectivity (71–98% *ee*). Furthermore, its excellent recyclability was shown in 14 consecutive runs.

In another approach, Fe<sub>3</sub>O<sub>4</sub> nanoparticles can be functionalized via silanization of the surface. Substituted alkoxysilanes are hydrolyzed to highly reactive silanols which subsequently form stable Si-O-Si bonds *via* condensation with the free hydroxyl groups of the particle surface (Scheme 1 A and C).<sup>[10]</sup> Following this route, Li *et al.*<sup>[11]</sup> immobilized a rosin-derived tertiary amino thiourea catalyst on iron oxide nanoparticles (Scheme 1 C). The heterogeneous catalyst **11** was applied in asymmetric Mannich reactions, giving chiral β-amino acid precursors in good yields with excellent enantiomeric excess. Thanks to the magnetic properties of the support, the catalyst could be reisolated in a simple and efficient manner and could be reused in up to 15 runs without deactivation.

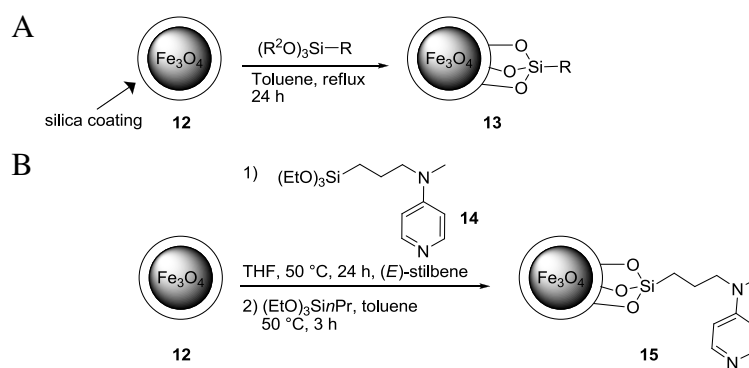


**Scheme 1.** (A) Strategies for the functionalization of uncoated  $\text{Fe}_3\text{O}_4$  NPs. (B) Immobilization of a BINAP-Ru-DPEN catalyst. (C) Attachment of an organocatalyst to iron oxide nanoparticles by silanization.

## 1.2 Silica-coated $\text{Fe}_3\text{O}_4$ nanoparticles

The coating of  $\text{Fe}_3\text{O}_4$  nanoparticles with an additional silica layer increases the stability of the particles, for example in aqueous medium, and enables its functionalization *via* silanization. The introduction of various functional groups is performed in just one reaction step (Scheme 2 A). According to this functionalization strategy, Gun'ko and Connon *et al.*<sup>[12]</sup> anchored a derivative of 4-(dimethylamino)-pyridine (DMAP) on silica-coated iron oxide NPs **12** (Scheme 2 B). The magnetic nanoparticle supported nucleophilic catalyst **15** showed high activity in acetylation reactions and could be easily recycled and reused in 30 runs without deactivation.



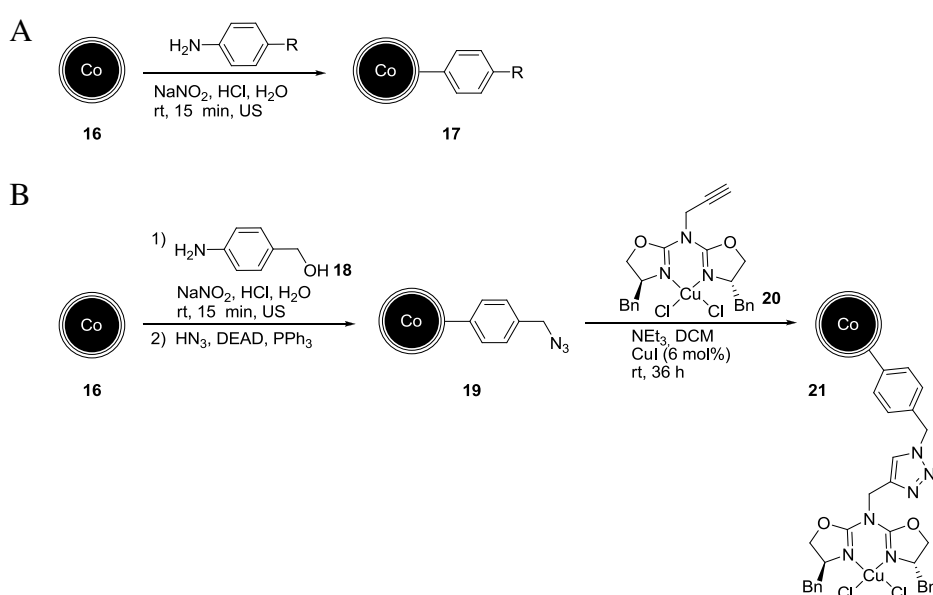


**Scheme 2.** (A) Strategy for the functionalization of silica-coated  $\text{Fe}_3\text{O}_4$  NPs. (B) Immobilization of an organocatalyst on silica-coated iron oxide NPs.

### 1.3 Graphene-coated nanoparticles

However, it needs to be stated that covalent bonds on silica as well as on metal oxides are labile under hydrolytic conditions, limiting the applicability of these materials. In contrast, carbon surfaces such as graphene can be chemically modified in a facile manner and at the same time the formed covalent bonds are more stable compared to those on silica or metal oxides. For the functionalization of graphene-coated nanoparticles, having, for example, a cobalt metal core, well-established diazonium chemistry is used.<sup>[13]</sup> The key step in this reaction is the electron transfer from the graphene shell to the corresponding diazonium salt, giving rise to a phenyl radical, which then reacts with the carbon surface to form a covalent bond.<sup>[14]</sup> This simple technique allows for the covalent attachment of a great number of functional groups to the graphene coating (Scheme 3 A).<sup>[15,16]</sup> Following this strategy, azide nanoparticles **19** could be synthesized, which turned out to be a versatile tool for further functionalization reactions and therefore, are also commercially available. These particles **19** could be easily functionalized by a copper(I)-catalyzed alkyne-azide cycloaddition (CuAAC) with various acetylene substituted compounds (Scheme 3 B).<sup>[15]</sup> Cu(II)-azabis(oxazoline) functionalized nanoparticles **21**, which were applied in the kinetic resolution of 1,2-diphenylethane-1,2-diol, represent one example for this strategy. The kinetic resolution with this heterogeneous catalyst was performed in batch, but also in a continuous-flow system. In the latter, external rotating magnetic fields were used to confine the immobilized catalyst locally while enabling effective mixing with the reaction solution. Excellent enantioselectivities could be obtained throughout several runs.<sup>[3]</sup>

However, all types of nanoparticles and coatings discussed above feature just a limited loading capacity. In order to increase the loading, polymers or dendrimers can be attached to the surface, which subsequently can be functionalized with catalysts.<sup>[17]</sup> Stark *et al.*<sup>[18]</sup> showed that a radical polymerization could be used to raise the typical loading of 0.1-0.2 mmol per gram nanoparticles to around 3 mmol per gram. Also a ring-opening metathesis polymerization (ROMP) could be applied to increase the catalyst loading on the magnetic nanoparticles significantly.<sup>[19]</sup> Furthermore, the degree of functionalization could be boosted by the attachment of radial dendrimers.<sup>[20]</sup>

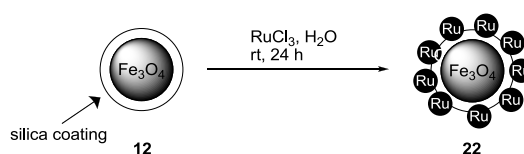


**Scheme 3.** (A) Strategy for the functionalization of graphene-coated cobalt nanoparticles. (B) Immobilization of a Cu(II)-azabis(oxazoline) complex *via* diazonium chemistry and CuAAC.

## 2 Noncovalent functionalization

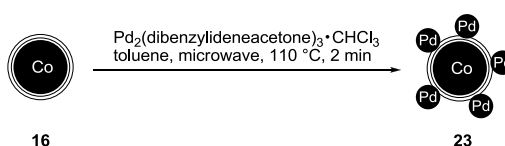
The noncovalent attachment of catalysts constitutes a completely different and alternative way of functionalization. It can be divided into two major subgroups: the immobilization of organic *vs.* inorganic catalysts. For the anchoring of inorganic catalysts different techniques are applicable. Metal salts can be reduced *in situ* and the so generated metal nanoparticles can be deposited on the surface of the magnetic nanoparticles. However, neither the size nor the morphology of the produced metal nanoparticles can be controlled using this method. Alternatively, the metal nanoparticles can be pre-synthesized. In this case, the properties of the metal nanoparticles can be controlled but the deposition on the magnetic nanoparticles might pose a problem. In 2013,

Varma *et al.*<sup>[21]</sup> published the synthesis of ruthenium nanoparticles on silica-coated  $\text{Fe}_3\text{O}_4$  nanoparticles (**22**) (Scheme 4). This catalyst was used in transfer hydrogenations of carbonyl compounds under microwave irradiation. The products could be isolated in very good yields and the magnetic catalyst could be recycled and reused in at least three runs without a loss of activity.



**Scheme 4.** Noncovalent attachment of ruthenium nanoparticles on silica-coated  $\text{Fe}_3\text{O}_4$  nanoparticles.

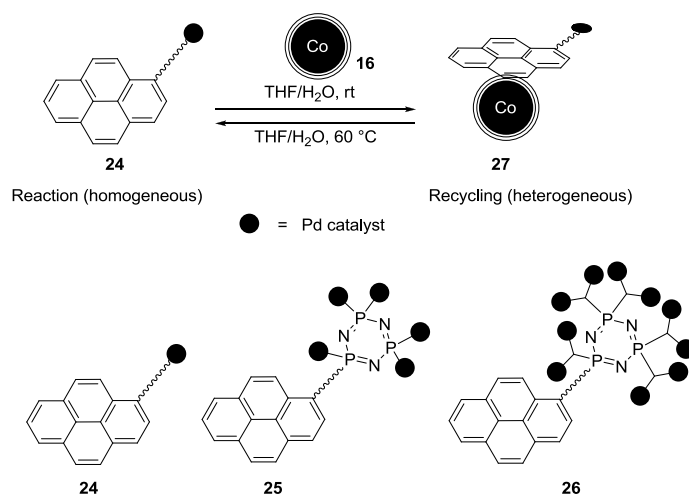
Another promising example for the noncovalent attachment of inorganic catalysts was the synthesis of a magnetic analog to palladium on charcoal. Starting from  $\text{Pd}_2(\text{dba})_3 \cdot \text{CHCl}_3$ , palladium nanoparticles could be deposited on graphene-coated cobalt nanoparticles within two minutes using microwave irradiation (Scheme 5).<sup>[22]</sup> Those nanocatalysts **23** were studied in hydrogenation reactions and showed a much higher catalytic activity compared to industrially applied palladium on charcoal. Furthermore, the catalyst could be easily recycled by magnetic decantation.



**Scheme 5.** Noncovalent attachment of palladium nanoparticles on graphene-coated cobalt nanoparticles.

For the noncovalent functionalization of magnetic nanoparticles with organic catalysts a different strategy has been developed. Reiser *et al.*<sup>[23]</sup> reported the reversible and noncovalent attachment of palladium catalysts on graphene-coated cobalt nanoparticles. The immobilization was accomplished via  $\pi$ - $\pi$  interaction between the pyrene-ligands and the graphene surface of the cobalt nanoparticles. The palladium complex desorbed by heating to  $100^\circ\text{C}$ , leading to a homogeneous catalyst which could be applied in hydroxycarbonylation reactions of aryl halides. Upon cooling to room temperature, the catalyst adsorbed again to the graphene surface of the magnetic nanoparticles, enabling a simple separation from the reaction solution by magnetic

decantation. Later on, Caminade, Majoral, Ouali *et al.*<sup>[24]</sup> combined this noncovalent functionalization strategy with a dendrimeric catalyst (Scheme 6). They developed a pyrene-tagged dendritic palladium phosphine catalyst which could be reversibly immobilized on graphene-coated cobalt nanoparticles by  $\pi$ - $\pi$  interactions (**24-26**). This strategy allowed for higher catalyst loadings thanks to the radial structure of the dendrimer as well as a fast and efficient recycling of the catalyst due to the magnetic properties of the support. The catalyst gave good to excellent yields in Suzuki coupling reaction and could be reused in four runs with no change in activity.



**Scheme 6.** Thermally-triggered, reversible noncovalent functionalization of graphene surface via  $\pi$ - $\pi$  interactions.

A more detailed overview on molecular catalysts immobilized on carbon surface will be given in a review article which is currently in preparation.<sup>[25]</sup>

### 3 Conclusion and perspectives

Catalysts immobilized on magnetic nanoparticles bridge the gap between homogeneous and heterogeneous catalysis. This technology has a great potential thanks to the variety of applicable nanoparticles and coatings, which can be chosen freely, depending on the demand. The majority of the magnetic supports is commercially available and the functionalization reactions are performed in a simple manner. A large number of functional groups can be introduced, giving access to various fields of application. One of the biggest advantages is the facile, fast and efficient separation of the immobilized catalysts from the reaction solution. Typical filtration and purification steps can be circumvented which saves energy as well as time. Altogether, magnetic nanoparticles as support for reagents or catalysts can be applied on lab scale but also in industry. Based on the simplicity and efficiency of this method, magnetic nanoparticles can have an even broader field of application in the future.

However, the implementation of this technique especially in industrial production requires further optimization work. To enable the application of magnetic nanoparticle supported reagents or catalysts in automated systems, the dispersibility in a large number of solvents needs to be established. In order to profit more from the magnetic properties of the support, the cooperative effects have to be explored further. Additionally, a commercial system for the agitation of the particles in rotating magnetic fields has to be developed. This would on the one hand guarantee an optimal mixing of the catalyst with the reaction solution and on the other hand redundantize conventional stirring which is especially important for miniaturized synthesis.

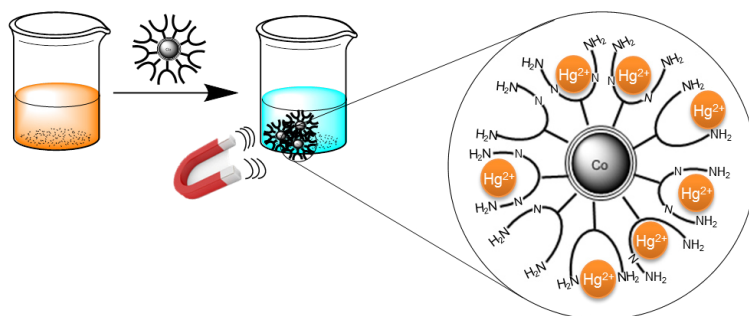
## 4 References

- [1] [http://www.oxforddictionaries.com/de/definition/englisch\\_usa/catalyst](http://www.oxforddictionaries.com/de/definition/englisch_usa/catalyst), **2016**.
- [2] a) S. Shylesh, V. Schünemann, W. R. Thiel, *Angew. Chem. Int. Ed.* **2010**, *49*, 3428–3459; b) V. Polshettiwar, R. S. Varma, *Green Chem.* **2010**, *12*, 743–754.
- [3] A. Schätz, R. N. Grass, Q. Kainz, W. J. Stark, O. Reiser, *Chem. Mater.* **2010**, *22*, 305–310.
- [4] S. Ceylan, C. Friese, C. Lammel, K. Mazac, A. Kirschning, *Angew. Chem. Int. Ed.* **2008**, *47*, 8950–8953.
- [5] a) M. Tamura, H. Fujihara, *J. Am. Chem. Soc.* **2003**, *125*, 15742–15743; b) S. Jansat, M. Gómez, K. Philippot, G. Muller, E. Guieu, C. Claver, S. Castellón, B. Chaudret, *J. Am. Chem. Soc.* **2004**, *126*, 1592–1593; c) A.-H. Lu, E. L. Salabas, F. Schüth, *Angew. Chem. Int. Ed.* **2007**, *46*, 1222–1244.
- [6] a) L. M. Rossi, Costa, Natalia J. S., F. P. Silva, R. Wojcieszak, *Green Chem.* **2014**, *16*, 2906–2933; b) J. Govan, Y. K. Gun'ko, *Nanomaterials* **2014**, *4*, 222–241; c) R. Dalpozzo, *Green Chem.* **2015**; d) R. B. Nasir Baig, M. N. Nadagouda, R. S. Varma, *Coord. Chem. Rev.* **2015**, *287*, 137–156; e) M. B. Gawande, S. N. Shelke, R. Zboril, R. S. Varma, *Acc. Chem. Res.* **2014**, *47*, 1338–1348; f) H. Duan, D. Wang, Y. Li, *Chem. Soc. Rev.* **2015**; g) H. Song, *Acc. Chem. Res.* **2015**, *48*, 491–499; h) D. Wang, D. Astruc, *Chem. Rev.* **2014**, *114*, 6949–6985.
- [7] a) A. S. Teja, P.-Y. Koh, *Prog. Cryst. Growth Charact. Mater.* **2009**, *55*, 22–45; b) S. F. Hasany, N. H. Abdurahman, A. R. Sunarti, R. Jose, *Current Nanoscience* **2013**, *9*, 561–575.
- [8] a) R. Abu-Reziq, H. Alper, D. Wang, M. L. Post, *J. Am. Chem. Soc.* **2006**, *128*, 5279–5282; b) A. J. Amali, R. K. Rana, *Green Chem.* **2009**, *11*, 1781–1786; c) S. Zhang, X. Zhao, H. Niu, Y. Shi, Y. Cai, G. Jiang, *J. Hazard. Mater.* **2009**, *167*, 560–566; d) S. Zhou, M. Johnson, J. G. C. Veinot, *Chem. Commun.* **2010**, *46*, 2411–2413; e) A. Hu, G. T. Yee, W. Lin, *J. Am. Chem. Soc.* **2005**, *127*, 12486–12487; f) P. D. Stevens, G. Li, J. Fan, M. Yen, Y. Gao, *Chem. Commun.* **2005**, 4435–4437; g) M. Ikenberry, L. Peña, D. Wei, H. Wang, S. H. Bossmann, T. Wilke, D. Wang, V. R. Komreddy, D. P. Rillema, K. L. Hohn, *Green Chem* **2014**, *16*, 836–843; h) P. D. Stevens, J. Fan, H. M. R. Gardimalla, M. Yen, Y. Gao, *Org. Lett.* **2005**, *7*, 2085–2088.
- [9] A. Hu, S. Liu, W. Lin, *RSC Adv.* **2012**, *2*, 2576–2580.
- [10] I. J. Bruce, T. Sen, *Langmuir* **2005**, *21*, 7029–7035.
- [11] H. Zhu, X. Jiang, X. Li, C. Hou, Y. Jiang, K. Hou, R. Wang, Y. Li, *ChemCatChem* **2013**, *5*, 2187–2190.
- [12] C. O Dálaigh, S. A. Corr, Y. Gun'ko, S. J. Connon, *Angew. Chem. Int. Ed.* **2007**, *46*, 4329–4332.
- [13] R. N. Grass, E. K. Athanassiou, W. J. Stark, *Angew. Chem. Int. Ed.* **2007**, *46*, 4909–4912.
- [14] F. M. Koehler, W. J. Stark, *Acc. Chem. Res.* **2013**, *46*, 2297–2306.
- [15] A. Schätz, R. N. Grass, W. J. Stark, O. Reiser, *Chem. Eur. J.* **2008**, *14*, 8262–8266.
- [16] a) A. Schaetz, M. Zeltner, T. D. Michl, M. Rossier, R. Fuhrer, W. J. Stark, *Chem. Eur. J.* **2011**, *17*, 10566–10573; b) Q. M. Kainz, S. Fernandes, C. M. Eichenseer, F. Besostri, H. Körner, R. Müller, O. Reiser, *Faraday Discuss.* **2014**, *175*, 27–40.
- [17] Q. M. Kainz, O. Reiser, *Acc. Chem. Res.* **2014**, *47*, 667–677.

- [18] A. Schätz, M. Zeltner, T. D. Michl, M. Rossier, R. Fuhrer, W. J. Stark, *Chem. Eur. J.* **2011**, *17*, 10566–10573.
- [19] a) A. Schätz, T. R. Long, R. N. Grass, W. J. Stark, P. R. Hanson, O. Reiser, *Adv. Funct. Mater.* **2010**, *20*, 4323–4328; b) C. M. Eichenseer, B. Kastl, M. A. Pericàs, P. R. Hanson, O. Reiser, *ACS Sustainable Chem. Eng.* **2016**, DOI 10.1021/acssuschemeng.6b00197.
- [20] A. Pourjavadi, S. H. Hosseini, S. T. Hosseini, S. A. Aghayeemeibody, *Catal. Commun.* **2012**, *28*, 86–89.
- [21] R. B. Nasir Baig, R. S. Varma, *ACS Sustainable Chem. Eng.* **2013**, *1*, 805–809.
- [22] Q. M. Kainz, R. Linhardt, R. N. Grass, G. Vilé, J. Pérez-Ramírez, W. J. Stark, O. Reiser, *Adv. Funct. Mater.* **2014**, *24*, 2020–2027.
- [23] S. Wittmann, A. Schätz, R. N. Grass, W. J. Stark, O. Reiser, *Angew. Chem. Int. Ed.* **2010**, *49*, 1867–1870.
- [24] M. Keller, V. Collière, O. Reiser, A.-M. Caminade, J.-P. Majoral, A. Ouali, *Angew. Chem. Int. Ed.* **2013**, *52*, 3626–3629.
- [25] S. Wittmann, R. Linhardt, C. M. Eichenseer, S. Fernandes, F. Besostri, O. Reiser, *ChemCatChem* Manuscript in preparation.

## B Main part

### 1 Reversible magnetic mercury extraction from water<sup>i</sup>



A facile and efficient way to decontaminate mercury(II) polluted water with the aid of highly stable and recyclable carbon-coated cobalt (Co/C) nanoparticles is reported. Comparing non-functionalized Co/C nanomagnets, which scavenge mercury by a redox mechanism, with particles that were functionalized with amino moieties, scavenging mercury by complexation, the latter one proved to be more effective with respect to extraction capacity and recyclability. A novel nanoparticle-poly(ethyleneimine) hybriide (Co/C-PEI), prepared by direct ring opening polymerization of aziridine initiated by an amino functionalized nanoparticle surface, led to a high capacity material (13 mmol amino groups/g nanomaterial) and thus proved to be the best material for scavenging toxic mercury at relevant concentrations (ppm/ppb) and scale for at least six consecutive cycles. On large-scale, 20 liters of water with an initial  $\text{Hg}^{2+}$  concentration of 30 ppb can be decontaminated to the level acceptable for drinking water ( $\leq 2$  ppb) with just 6 mg of Co/C-PEI particles.<sup>ii</sup>

<sup>i</sup> Reproduced with permission of The Royal Society of Chemistry: S. Fernandes,<sup>§</sup> C. M. Eichenseer,<sup>§</sup> P. Kreitmeier, J. Rewitzer, V. Zlateski, R. N. Grass, W. J. Stark, O. Reiser, *RSC Adv.* **2015**, 5, 46430-46436. Copyright © 2015 The Royal Society of Chemistry.

<sup>ii</sup> The manuscript was jointly written by C. M. Eichenseer and S. Fernandes. Synthesis of and extraction experiments with materials **30** and **33** were done by C. M. Eichenseer. S. Fernandes synthesized and evaluated Co/C-PAMAM **35** and Co/C-PS-PAMAM **37**. Synthesis of NovaPEG Amino Resin-PEI **42** was accomplished by C. M. Eichenseer. The large scale experiment was performed by S. Fernandes and V. Zlateski at the ETH Zürich. Magnetization measurements were done by H. Körner. TGA was measured by R. Müller. All other experiments were carried out by C. M. Eichenseer and S. Fernandes at the University of Regensburg.



## 1.1 Introduction

Removal of organic and inorganic waste from water has become an issue of major interest for the last few decades. In particular, the decontamination of heavy metals is still a matter of great concern, since these harmful substances can cause severe threats to human health. In this context, mercury is considered one of the most toxic pollutants to the environment and public health, being involved in several disasters of food poisoning in different countries around the world.<sup>[1,2]</sup> The cumulative character of this metal leads to an enrichment in the environment and the food chain,<sup>[3,4]</sup> which in turn may cause permanent adverse effects in the liver, lung, brain or kidney of living organisms, even at very low dose.<sup>[1,4]</sup> Furthermore, its solubility in water brings along additional problems concerning the toxicity, especially for the aquatic system.<sup>[5]</sup> Indeed, in its divalent form mercury is often found in fresh water, seawater, ground water and soil in considerable amounts.<sup>[1,4]</sup> Therefore, mercury and its derivatives are considered as priority hazardous substances (PHSs)<sup>[1,6]</sup> by several environmental associations that have started mercury monitoring programs worldwide.<sup>[1]</sup>

Facing the above-mentioned harms, different methodologies have been used for water treatment such as centrifugation, ultrafiltration, crystallization, sedimentation, solid-phase extraction and chemical precipitation.<sup>[1,2]</sup> Usually, the extraction of particular heavy metals is performed by using insoluble adsorbents.<sup>[7]</sup> However, this method requires further filtration which involves energy-intensive pumping and tedious recovery of the materials.<sup>[8]</sup>

In an attempt to develop more sensitive, simple and cost-effective materials, nanotechnology has attracted much attention in this field.<sup>[2,5]</sup> Magnetic nanoparticles in particular might contribute to such applications due to their distinct advantages like high surface area-to-volume ratio and therefore higher extraction capacity compared to micrometer-sized particles. The most important benefit is the facile and convenient separation of the nanoparticles by applying an external magnetic field, enabling an easy recovery and recycling of the scavenger,<sup>[1,4,6]</sup> potentially even in the open environment.

Additionally, materials that selectively bind  $\text{Hg}^{2+}$  in the presence of other metals are needed in order to prove feasibility in a real water decontamination situation. For instance, studies with 1-naphthylthiourea–methyl isobutyl ketone<sup>[9]</sup> or mesoporous crystalline material functionalized with mercaptopropyl<sup>[10]</sup> showed that these selectively extract  $\text{Hg(II)}$  from aqueous samples. Nevertheless, recovery and regeneration of the chelating agent proved to be impractical. Considering this, a selective magnetic mercury scavenger would make the entire process much easier and faster as well as enhance the reusability of the chelating agent.

Indeed, functionally modified magnetic nanobeads have already been used for the extraction of different metals from aqueous solution such as cadmium,<sup>[11,12]</sup> copper,<sup>[11,13]</sup> lead,<sup>[11,12]</sup> zinc,<sup>[13]</sup> mercury<sup>[12,14,15]</sup> cobalt<sup>[16,17]</sup> and nickel<sup>[16]</sup> under various conditions. However, concerning mercury, limitations related to selectivity in the presence of other metals and reusability of the scavengers are being encountered. Iron oxide nanoparticles were primarily considered as an attractive solution for magnetic separation. Recently, Pang *et al.*<sup>[15]</sup> reported the synthesis of functionalized iron oxide nanoparticles which efficiently remove mercury(II) from water samples (380 mg Hg<sup>2+</sup> extracted/ mol adsorbent) but selectivity in combination with other metals or recyclability of this scavenger material was not studied. Furthermore, Khani *et al.*<sup>[14]</sup> have developed magnetite nanoparticles functionalized with triazene groups showing selectivity towards mercury in binary systems, which could be used in two cycles with an extraction capacity of 10.26 mg Hg<sup>2+</sup> per gram nanomaterial. Mandel *et al.* have reported that thiol-modified magnetic microparticles are capable of extracting mercury preferentially over other metals. However, coadsorption of copper and cadmium was also observed in some cases. The release of adsorbed mercury (II) in order to recycle the scavenger was possible to an extent of about 30%, and the estimated extraction capacity was around 74 mg Hg<sup>2+</sup> per gram microparticles.<sup>[18]</sup> Magnetic Co/C nanoparticles, which exhibit excellent thermal and chemical stability as well as higher magnetization, recently appeared as a promising alternative for improving the extraction capacity and reusability of scavengers.<sup>[11,19]</sup> Such nanoparticles provide an additional carbon surface that stabilizes the metal core and allows for functionalization using established diazonium chemistry.<sup>[20,21]</sup>

Herein, the potential of Co/C nanomagnets to be used as magnetic scavengers for mercury extraction from water is reported. In addition, we studied the influence of amino functionalities on the nanoparticles to improve the extraction efficiency and selectivity, arriving at functional nanomagnets that show an extraction capacity for Hg<sup>2+</sup> of up to 550 mg/g nanoparticle.

## 1.2 Results and discussion

Carbon-coated nanobeads have proved their effectiveness in a variety of applications such as supports for scavengers, reagents or catalysts.<sup>[22,23–25]</sup> Relevant for this study, this type of nanoparticles was previously used for complexation/extraction of cadmium, copper, lead<sup>[11]</sup>, arsenic<sup>[26]</sup> as well as noble metals like gold<sup>[19,27]</sup> and platinum<sup>[27]</sup>. However, no studies for the removal of mercury(II) from contaminated water were reported.

In order to remove  $\text{Hg}^{2+}$  ions from contaminated water, pristine and commercially available Co/C NPs **16**<sup>[20]</sup> were initially investigated as possible scavengers. Two mercury solutions with different concentrations were prepared (15 and 30  $\text{mg}\cdot\text{L}^{-1}$ ) and the progress of extraction was monitored by ICP-OES during 10 minutes, aiming at practical decontamination times in real case scenarios, to study the adsorption kinetics and estimate the maximum extraction capacity of the nanobeads (Figure 1). From these results, using 5 mg of NPs to decontaminate 5 mL  $\text{HgCl}_2$  solution, it was concluded that approximately 13 mg  $\text{Hg}^{2+}$  can be scavenged using 1 g of nanoparticles within 10 minutes, even at low initial mercury concentrations of 15  $\text{mg}\cdot\text{L}^{-1}$ . However, also considerable leaching of  $\text{Co}^{2+}$  ions from the nanoparticle core was observed. The adsorption of  $\text{Hg}^{2+}$  onto the carbon layer of the nanoparticles was confirmed by x-ray photoelectron spectroscopy (XPS) analysis and is in agreement with the results obtained for multi-walled carbon nanotubes (MWCNTs).<sup>[28]</sup>

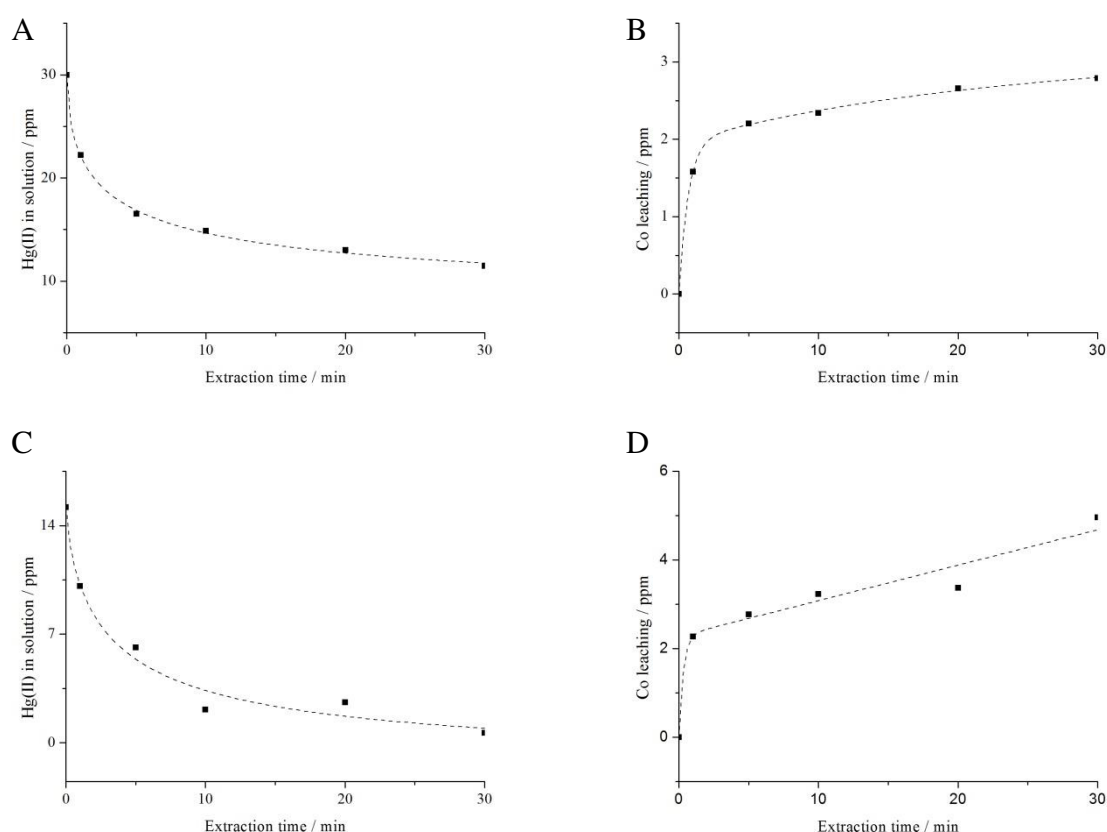
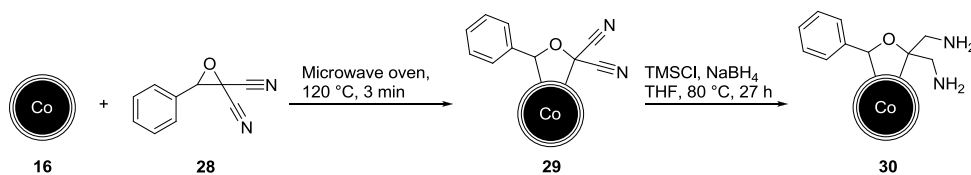


**Figure 1.** Mercury(II) extraction (A and C) and the corresponding cobalt leaching from the core of the magnetic Co/C nanoparticles (B and D). Conditions: 5 mg Co/C nanoparticles in 5 mL of an aqueous solution containing  $\text{HgCl}_2$  in an initial concentration of 30 ppm (A and B) and 15 ppm (C and D). Dashed curves for the extraction represent the logistic fit of the data set (logistic dose response in Chemistry). Dashed curves for the cobalt leaching represent the exponential decay fit of the data set.

Although the extraction of mercury using unmodified Co/C nanoparticles **16** proved to be efficient to some extent, there are three major limitations: (1) the occurring cobalt leaching leads to an undesired contamination that needs to be prevented. (2) The extraction capacity (13 mg  $\text{Hg}^{2+}$ / g NPs) is relatively low requiring a high amount of nanoparticles to remove  $\text{Hg}^{2+}$  on large scale. (3) An efficient release of mercury from the particles, thus allowing their recycling was not possible under various conditions tried (aqua regia; heating at 150 °C; aqua regia combined with high temperature).

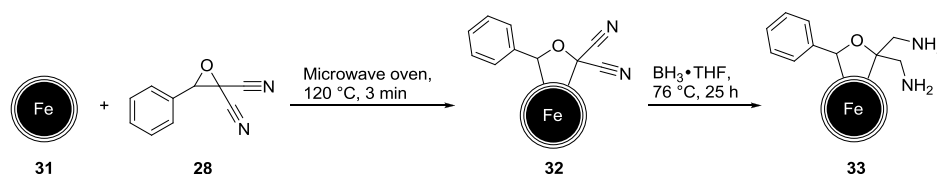
Therefore, the surface of the nanomagnets was functionalized to improve the extraction capacity, also aiming to avoid cobalt leaching and ensuring recyclability. Non-magnetic amino-functionalized materials have been reported for their extraction capability towards mercury, and especially Masri and Friedman have demonstrated the high affinity of polyamine derivatives towards Hg ions in aqueous solutions.<sup>[29]</sup> Furthermore, amino-functionalized carbon nanotubes have been successfully applied for extracting mercury(II) from water samples.<sup>[30]</sup> However, selectivity studies with these materials were either not performed or limited to binary systems. Taken these precedents as a lead, the current study focused on developing high capacity amino-polymers, such as poly(ethyleneimine) (PEI) and poly(amidoamine) (PAMAM), supported on readily recyclable magnetic nanobeads for selective  $\text{Hg}^{2+}$  removal. Furthermore Co/C-THF- $\text{NH}_2$  **30** and Fe/C-THF- $\text{NH}_2$  **33** were evaluated as magnetic scavenger for the mercury extraction.

The 1,3-diaminopropane moieties on the NPs **30** and **33** were introduced in two steps following a procedure published by Cravotto *et al.* for single-walled carbon nanotubes.<sup>[31]</sup> Epoxide **28** was opened to the corresponding ylide by microwave irradiation and attached to the conjugated  $\pi$ -system of the unmodified carbon-coated cobalt (**16**) or iron (**31**) nanoparticles (Scheme 7 and 8). In a second step, the cyano groups were reduced to amino groups by trimethylsilyl chloride (TMSCl) and sodium borohydride in THF (Scheme 7)<sup>[32,33]</sup> and  $\text{BH}_3\cdot\text{THF}$  (Scheme 8), respectively. Based on the employed amount of epoxide, a maximal theoretical nitrogen loading of 5.1 mmol per gram was calculated for **29**. The real nitrogen loading was determined to be 0.52 mmol/g, which is 10% of the theoretical value.



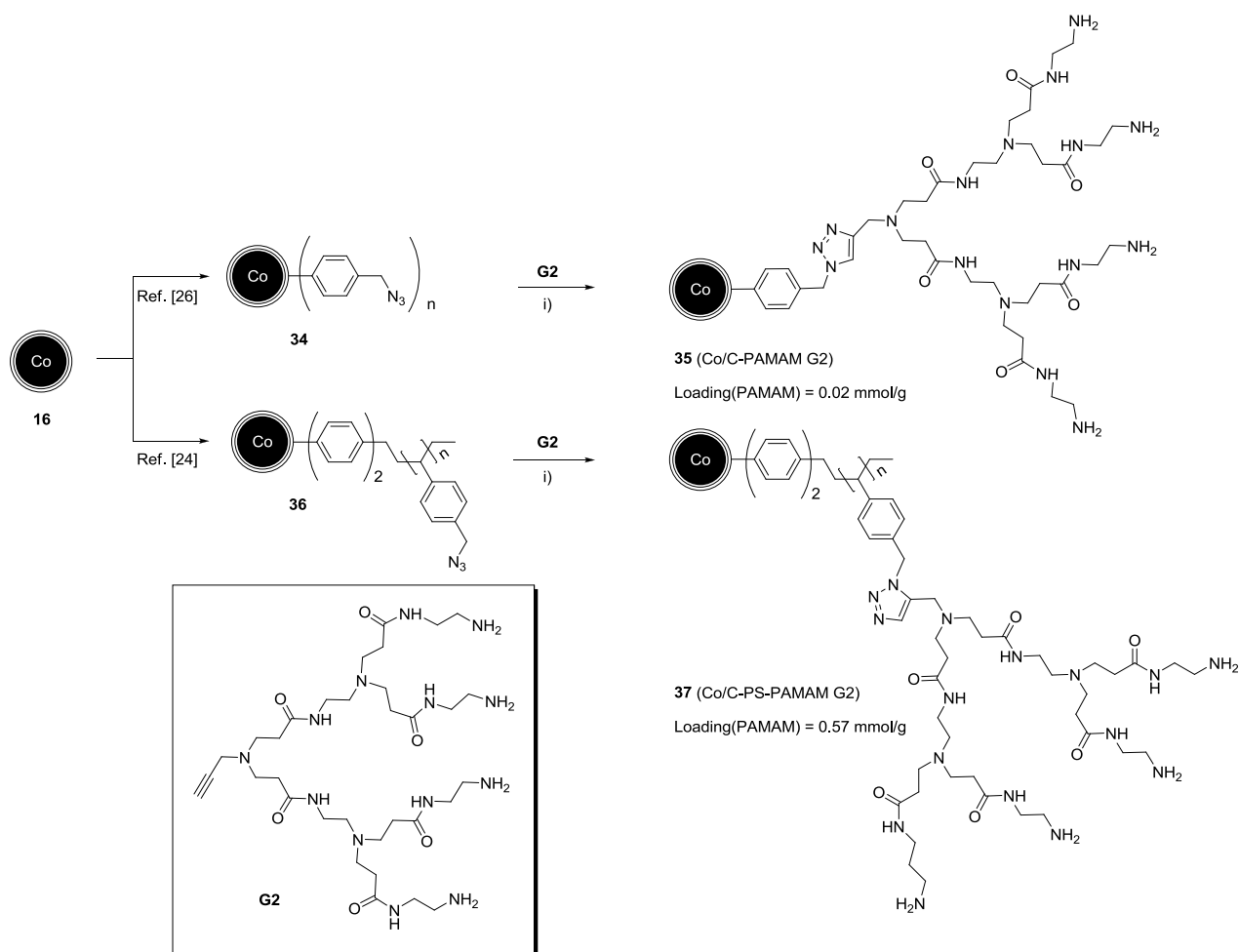
**Scheme 7.** 1,3-dipolar cycloaddition of epoxide **28** (0.76 mmol) to NPs **16** (0.3 g) followed by reduction of cyano groups to yield **30**.

In the 1,3-dipolar cycloaddition with carbon coated iron nanoparticles a larger amount of epoxide was applied, resulting in a higher theoretical nitrogen loading for **32** (11.7 mmol per gram). The real value for the nitrogen loading was determined by elemental analysis to be 1.51 mmol/g which is 13% of the theoretical maximum. Although this value seems low, it needs to be taken into consideration that the achievable degree of functionalization is limited by the accessible surface area of the nanoparticles.



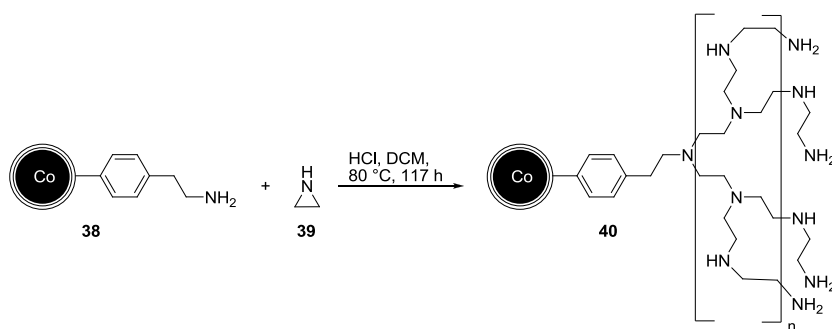
**Scheme 8.** 1,3-dipolar cycloaddition of epoxide **28** to Fe/C NPs **31** gave Fe/C-THF-CN NPs **32**. Reduction of cyano groups yielded Fe/C-THF-NH<sub>2</sub> NPs **33**.

Propargylated PAMAM dendrimer G2 having four terminal amino groups was connected in two different ways to the surface of the NPs **16** (Scheme 9): benzyl azide functionalized Co/C nanoparticles **34**<sup>[21,25]</sup> (0.1 mmol azide/ g nanomaterial) or a Wang type resin having azide end groups covalently attached to Co/C nanoparticles **36**<sup>[23]</sup> (2.4 mmol azide/ g nanomaterial), were found to be suitable platforms to accommodate PAMAM dendrimers via ligation by a copper catalyzed azide/alkyne cycloaddition using conditions previously described by the Reiser group.<sup>[21,25]</sup> The reaction was conveniently followed by monitoring the characteristic azide peak at 2100 cm<sup>-1</sup> with attenuated total reflection infrared spectroscopy (ATR-IR) spectroscopy, to give rise to **35** (0.02 mmol PAMAM/ g nanomaterial) and **37** (0.57 mmol PAMAM/ g nanomaterial), respectively. Higher magnetization values were observed for Co/C-PAMAM G2 **35** (106 emu/g) when compared to higher loaded Co/C-PS-PAMAM G2 **37** (50 emu/g), reflecting the different amounts of non-magnetic material attached to the nanobeads.



**Scheme 9.** Covalent immobilization of PAMAM dendron G2 on Co/C nanoparticles **16** via click chemistry. Reagents and conditions: i)  $\text{CuSO}_4 \cdot 5 \text{H}_2\text{O}$  (10 mol%), sodium ascorbate (30 mol%), THF/ $\text{H}_2\text{O}$  (3:1), 24 h, rt.

PEI-functionalized Co/C nanobeads were prepared starting from **38**<sup>[20]</sup> (0.15 mmol amine/ g nanomaterial) following a procedure for the functionalization of carbon nanotubes described by Liu *et al.* (Scheme 10).<sup>[34]</sup> Using 1000 equivalents of aziridine **39**, high loadings of approximately 10 mmol amine/ g nanomaterial **40** were obtained by growing the PEI polymer on the nanoparticle surface. These nanoparticles form stable dispersions in water,<sup>[33]</sup> thus avoiding agglomeration (Figure 2), which is a general problem for unmodified Co/C nanoparticles **16**. The saturation magnetization of this material was found to be still high (39 emu/g), rivaling that of low-loading magnetite particles.<sup>[35]</sup> Therefore, an easy and effective recovery by magnetic separation is still possible within seconds.



**Scheme 10.** Cationic polymerization of aziridine **39** to yield poly(ethyleneimine) functionalized nanoparticles **40** with a nitrogen loading of 10.6 mmol/g.<sup>[33]</sup>

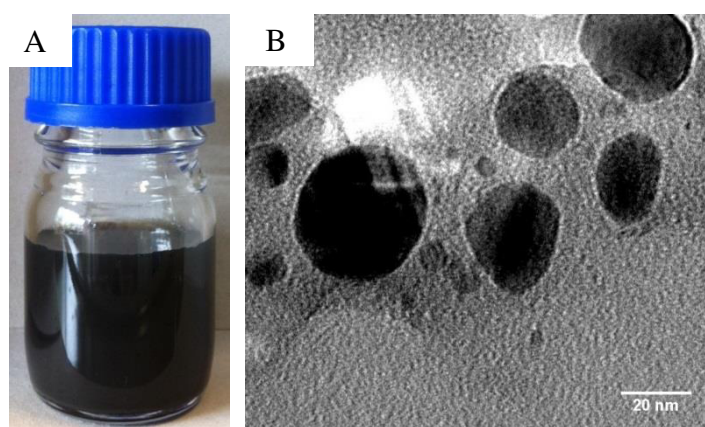


**Figure 2.** (A) Co/C-PEI nanobeads **40** dispersible in water after synthesis.<sup>[36]</sup> (B) Transmission electron microscopy (TEM) picture of PEI functionalized Co/C NPs **40**.<sup>[33]</sup> (A) reproduced from Ref. [36] and (B) reproduced from Ref. [33] with permission of The Royal Society of Chemistry.

A comparison of the extraction efficiency of all nanobeads (Figure 3) using 5 mL of an aqueous solution of HgCl<sub>2</sub> (30 ppm = 30 mg·L<sup>-1</sup>) and 5 mg of nanomaterial during 10 minutes for benchmarking purposes showed that Co/C-PAMAM G2 **35** was found to extract mercury (50%) comparable to unmodified Co/C NPs **16**, which is attributed to the low PAMAM loadings obtained during the functionalization. Improved extraction capacity was found for Co/C-PS-PAMAM G2 **37** (73%), which can be ascribed to increased loadings of terminal amino groups made possible through the additional poly(styrene) layer on the surface of the NPs<sup>[23,24,26,37]</sup>. For both materials no significant cobalt leaching was detected. Interestingly, the extraction efficiency is much better for Fe/C-THF-NH<sub>2</sub> **33**, Co/C-THF-NH<sub>2</sub> **30** and Co/C-PEI **40**. The Hg(II) removal efficiency was found to be ≥98% (reaching the detection limit [100 ppb = μg·L<sup>-1</sup>] of the inductively coupled plasma optical emission spectrometry (ICP-OES) measurement) for all three materials **30**, **33** and **40**. However, particles Fe/C-THF-NH<sub>2</sub> **33** and Co/C-THF-NH<sub>2</sub> **30** again

caused undesired iron or cobalt leaching from the nanoparticles into the solution while Co/-PEI **40** was showing no sign of cobalt leaching. The maximum extraction capacity of Co/C-PEI **40** was subsequently estimated by extracting solutions of higher mercury concentration: the scavenging of  $\text{Hg}^{2+}$  from 5 mL of a 2.9 mM solution with 5 mg nanomaterial was still possible within 10 minutes to an extent of 95%, corresponding to 550 mg  $\text{Hg}^{2+}$  extracted per gram nanomaterial **40**. This compares favorably to the results obtained for Co/C **16** (15 mg  $\text{Hg}^{2+}$  extracted/g NPs) and for previously reported magnetic mercury scavengers (5.6 – 152 mg  $\text{Hg}^{2+}$  extracted/ g nanomaterial)<sup>[4,14,38]</sup>.

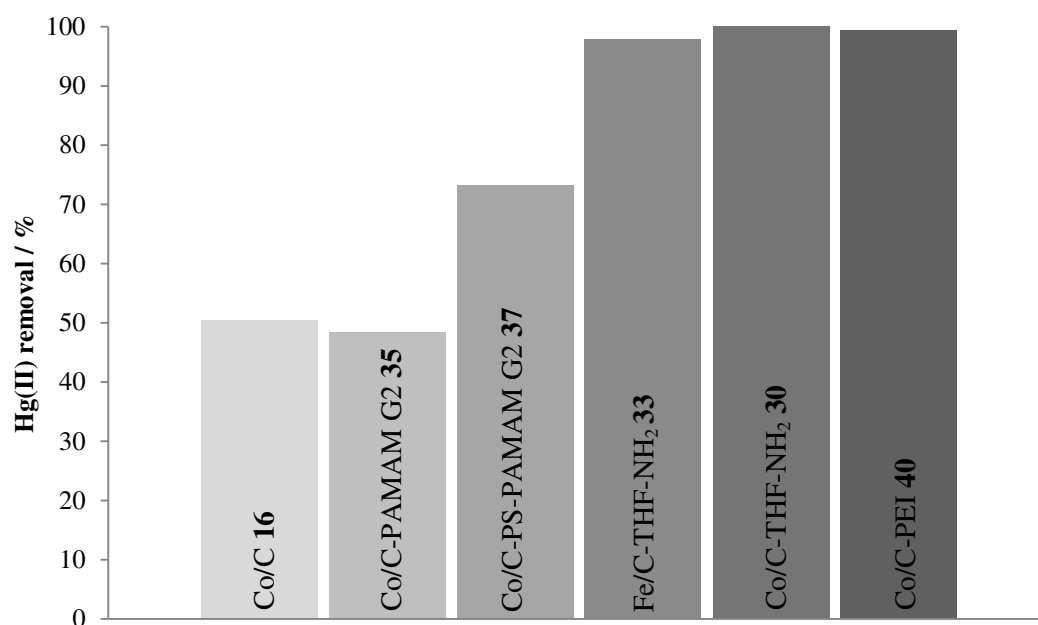


**Figure 3.** Comparison of the extraction capacity from the different nanobeads (*cf* Scheme 1, 2, 3, 4). Reaction conditions: 5 mg of NPs, 5 mL of  $\text{Hg}^{2+}$  solution (30 ppm), 10 min extraction time, solution pH 6.53.

Two control experiments were performed to ensure that Co/C-PEI NPs **40** really avoid cobalt leaching during extraction and that the absence of cobalt is not due to a complexation of Co(II) by Co/C-PEI NPs **40**. First of all, to an aqueous solution contaminated with 83 ppm Co(II), 5 mg Co/C-PEI NPs **40** were added. After an extraction time of 10 min the remaining content of Co(II) was analyzed showing that just 1.2 ppm cobalt has been complexed by the nanoparticles (Figure 4A). This study confirmed that there is no significant affinity of **40** towards cobalt. Furthermore, a selective extraction of Hg(II) in the presence of cobalt ions (83 ppm) was still possible as NPs **40** were able to extract 222 ppm mercury while no cobalt was complexed (Figure 4B).



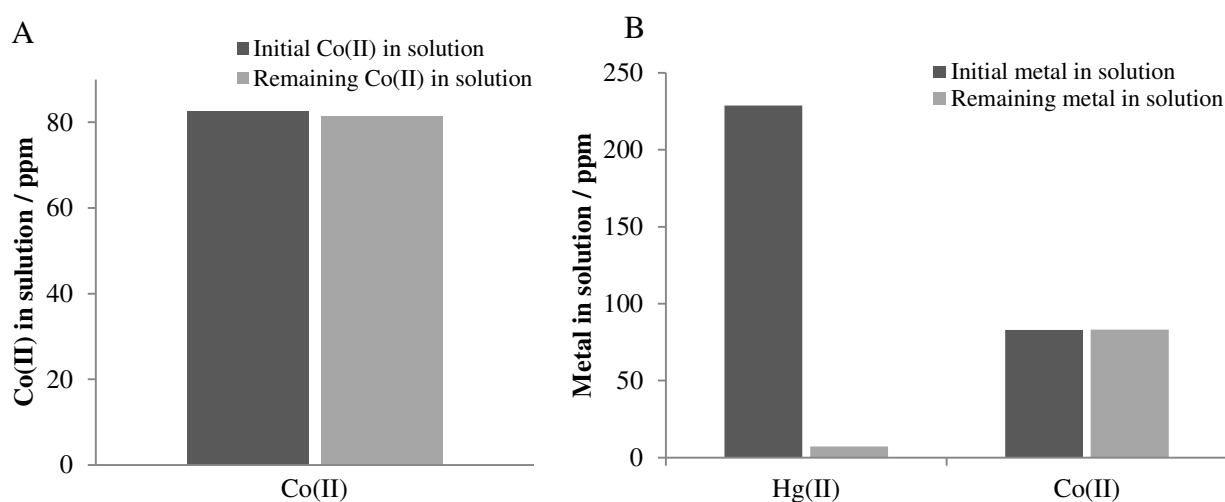


**Figure 4.** (A) Extraction using **40** in the presence of 83 ppm Co(II) and (B) in the presence of 229 ppm Hg(II) as well as 83 ppm Co(II). Conditions: 5 mg of NPs were used to decontaminate 5 mL of an aqueous sample within 10 min.

Mercury(II) could also be efficiently removed from much more diluted solutions using **40**: Starting from 100 mL of an aqueous solution containing  $1.64 \text{ mg}\cdot\text{L}^{-1}$  mercury(II) chloride, just 3 mg Co/C-PEI nanoparticles **40** were sufficient to again lower the mercury concentration to the detection limit ( $100 \text{ }\mu\text{g}\cdot\text{L}^{-1}$ ) of the ICP-OES analysis within 10 minutes (Figure 5).

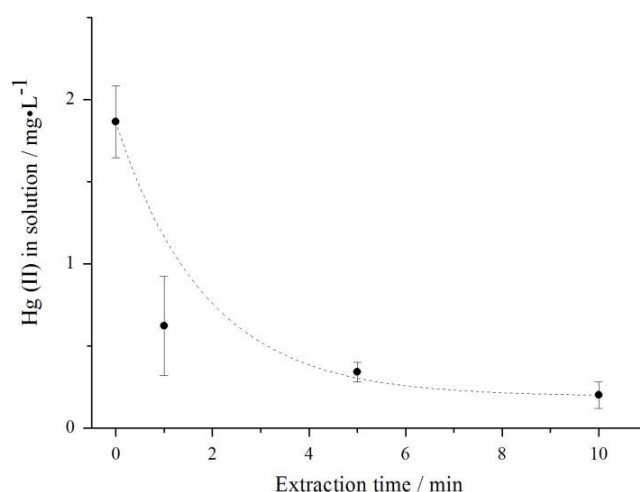
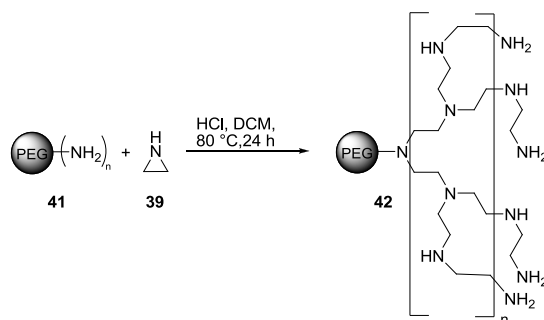


**Figure 5.** Mercury(II) extraction over time. 100 mL of an aqueous solution ( $1.64 \text{ mg}\cdot\text{L}^{-1}$ , solution pH 6.71), 3 mg Co/C-PEI nanoparticles **40**. The dashed curve represents the exponential decay fit of the data set (decay constant:  $1.8 \pm 1.2 \text{ min}^{-1}$ ). After 10 min, the detection limit ( $100 \text{ }\mu\text{g}\cdot\text{L}^{-1}$ ) of the ICP-OES analysis was reached.

To validate that the mercury uptake occurs due to a complexation of the heavy metal by the amino groups, the extraction capacity of the PEI-polymer itself was tested. A commercially available PEG-resin with terminal amino groups **41** was functionalized with PEI in the same manner (Scheme 11) as for the Co/C-phenylethylamine particles **38** described above. The so obtained PEI-resin **42** (10.9 mmol N/g resin) was used for extraction, applying identical conditions as in the previous experiments.



**Scheme 11.** Synthesis of PEI functionalized PEG resin **42** with a nitrogen loading of 10.9 mmol/g.

A similar extraction capacity for the PEI-functionalized resin **42** when compared to the Co/C-PEI nanobeads **40** was determined, while the PEG-amino resin **41** itself showed nearly no ability to extract mercury (Figure 6). These findings suggest that indeed the poly(amino) functionalities on the surface of the NPs are responsible for the removal of mercury, which is in agreement with literature reports for amino functionalized multi-wall carbon nanotubes<sup>[30]</sup>, chitosan based absorbents<sup>[38]</sup> or poly(amine) derivatives<sup>[29]</sup>.

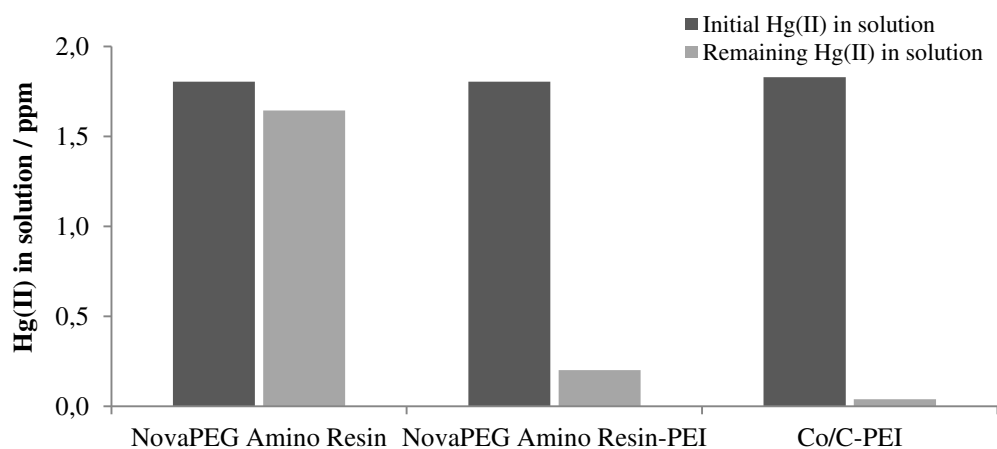


**Figure 6.** Comparison of the extraction capacity from NovaPEG amino resin **41**, NovaPEG amino resin-PEI **42** and Co/C-PEI **40**. Reaction conditions: 3 mg of NPs or resin, 100 mL of Hg<sup>2+</sup> solution (1.8 ppm), 10 min extraction time.

It is known that PEI can also chelate metals such as  $\text{Ni}^{2+}$ ,  $\text{Cu}^{2+}$ ,  $\text{Zn}^{2+}$ ,  $\text{Cd}^{2+}$  and  $\text{Pb}^{2+}$ .<sup>[39]</sup> However, to the best of our knowledge no selectivity studies using PEI for extracting mercury in the presence of other metal ions are reported. Testing the extraction of  $\text{Hg}^{2+}$  against other competitive metals when they were in solution at the same time, indeed it was found that Co/C-PEI nanomagnets **40** showed a high preference for mercury(II) (Figure 7A and B). Two experiments were performed with different extraction times, namely 10 minutes and 3 hours. No significant changes were detected between these two time points, indicating that, for these conditions, the equilibrium time for all tested metals has been reached after only 10 minutes of extraction. This result is supported by the selective extraction of mercury(II) shown also for the PEI-resin **42** (Figure 8A). Moreover, x-ray photoelectron spectroscopy (XPS) analysis on the NPs used to obtain the results in Figure 7A confirmed the preferential uptake of mercury against the other metals (see experimental section). In addition, an experiment at basic pH 8.3 was performed to evaluate the influence of the pH on the adsorption of the metals. Again, a preferential uptake of mercury was detected together with small amounts of copper(II) and lead(II) (Figure 8B).

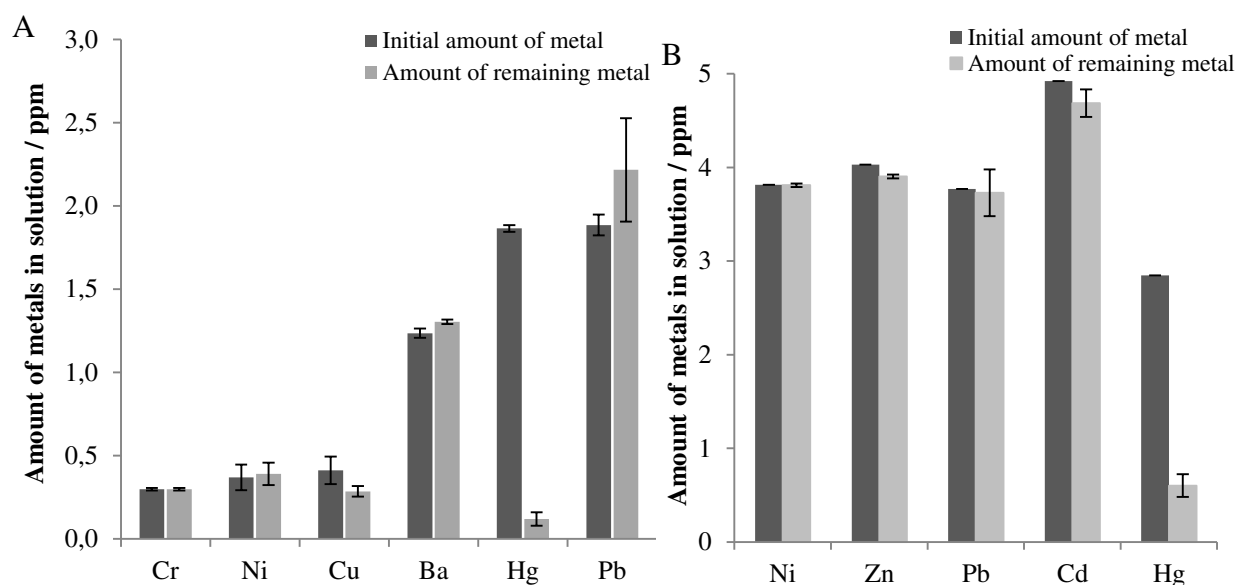


**Figure 7.** Selective extraction of  $\text{Hg}^{2+}$  using Co/C-PEI **40** in the presence of competitive metal ions. (A) 3 mg of NPs were used to decontaminate a 100 mL solution containing  $\text{Hg}^{2+}$ ,  $\text{Cu}^{2+}$ ,  $\text{Pb}^{2+}$ ,  $\text{Ni}^{2+}$ ,  $\text{Ba}^{2+}$  and  $\text{Cr}^{3+}$  in equimolar amounts (10  $\mu\text{M}$ ) within 10 min, solution pH 5.59. (B) 3 mg of NPs were used to decontaminate an aqueous 100 mL solution containing  $\text{Hg}^{2+}$ ,  $\text{Pb}^{2+}$ ,  $\text{Ni}^{2+}$ ,  $\text{Zn}^{2+}$  and  $\text{Cd}^{2+}$ , solution pH 6.16.

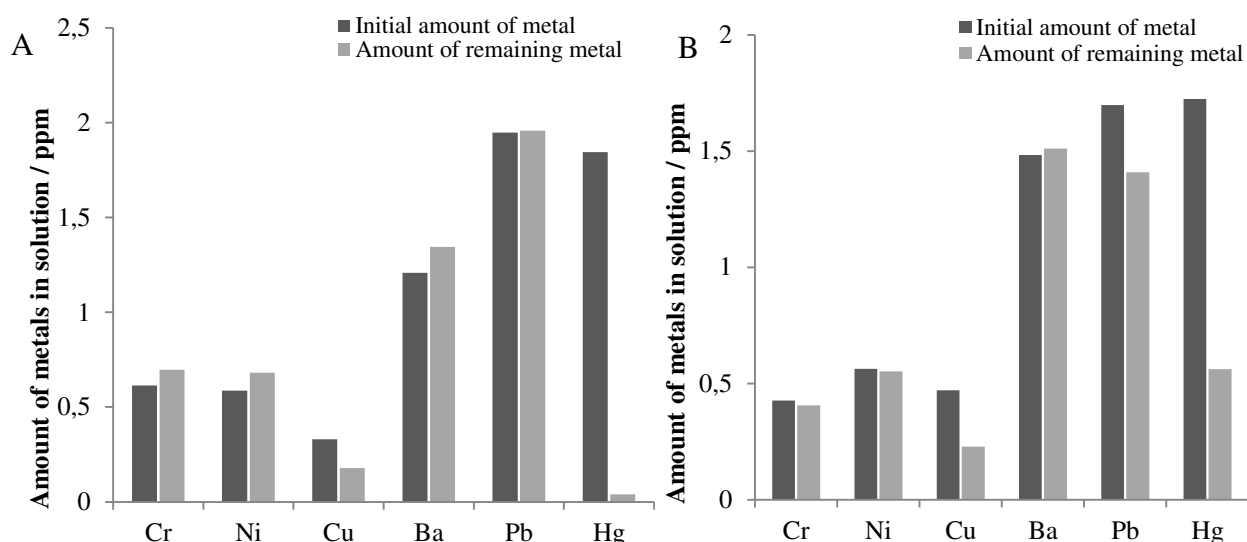


**Figure 8.** (A) Selective extraction of  $\text{Hg}^{2+}$  using NovaPEG amino resin-PEI **42** in the presence of competitive metal ions, solution pH 5.59. (B) Selective extraction of  $\text{Hg}^{2+}$  using Co/C-PEI **40** in the presence of competitive metal ions, solution pH 8.3. Reaction conditions: 3 mg of resin (A) or NPs (B) were used to decontaminate a 100 mL solution containing  $\text{Hg}^{2+}$ ,  $\text{Cu}^{2+}$ ,  $\text{Pb}^{2+}$ ,  $\text{Ni}^{2+}$ ,  $\text{Ba}^{2+}$  and  $\text{Cr}^{3+}$  in equimolar amounts (10  $\mu\text{M}$ ) within 10 min.

Having developed a scavenger that combines the advantages of using a selective adsorbent with the magnetic properties of a solid support, we tested the performance of nanobeads **40** in tap water samples. For these experiments water from the facilities of the University of Regensburg was used and artificially contaminated with  $\text{Hg}^{2+}$  (2 ppm). Especially, the water sample was analyzed with respect to the content of mercury, magnesium and iron before and after treatment with nanobeads **40**. The concentration of  $\text{Ca}^{2+}$  was also measured to be around 100 ppm, thus being present in large excess with respect to the extraction capacity of **40** used in this experiment. However, the values obtained from ICP measurements for calcium before and after extraction were somewhat erratic, which might be due to aging of the samples caused by carbon dioxide absorption. Despite the presence of those other ions that are naturally occurring in drinking water mercury was still efficiently removed (Table 1, Sample 1). As iron can occur in higher concentrations in water of different areas<sup>[40]</sup> an additional experiment was performed in the presence of an excess of iron. Still 90%  $\text{Hg}^{2+}$  was successfully extracted even if the content of iron was approximately 20 times higher than that of mercury (Table 1, Sample 2).

Table 1. Extraction results in tap water.

	Metal ions before / after extraction [ppm]		
	Hg <sup>[a]</sup>	Fe <sup>[b]</sup>	Mg <sup>[b]</sup>
Sample 1 - Regensburg drinking water spiked with Hg <sup>2+</sup>	2.2 / 0.3	≤0.1 / ≤0.1	19.1 / 19.1
Sample 2 - Regensburg drinking water spiked with Fe <sup>2+</sup> and Hg <sup>2+</sup>	2.2 / 0.2	35 / 32.5	-

Sample 1 - [a] Artificially added to the tap water samples (the source of mercury used is HgCl<sub>2</sub>). [b] Real values determined for tap water samples from the University of Regensburg. Extraction conditions: 3 mg Co/C-PEI NPs **40** were used to decontaminate 100 mL aqueous solution (pH 6.71) within 10 minutes. In addition, the sample contained approx. 100 ppm Ca<sup>2+</sup> (see text).

Sample 2 - [a] and [b] Artificially added to the tap water samples (the source of iron used is FeCl<sub>2</sub>·4 H<sub>2</sub>O). Extraction conditions: 3 mg Co/C-PEI NPs **40** were used to decontaminate 100 mL aqueous solution (pH 6.45 ) within 10 minutes.

Having proven the feasibility of the nanomagnets for extracting mercury in real water samples, a simple recycling methodology of the magnetic scavenger had to be established. More specifically mercury had to be released after extraction in order to regenerate and reuse the nanomaterial. Considering the fact that the amino groups in **40** were responsible for scavenging the mercury ions, a logical approach was the protonation of these groups using acidic conditions to reverse their complexation ability. For the release the following procedure was established: after the extraction time, the nanobeads were collected with a magnet and the aqueous decontaminated solution was completely decanted, followed by the addition of 20 mL of an acid to release the mercury(II) affording a concentrated mercury(II) solution (Figure 9).

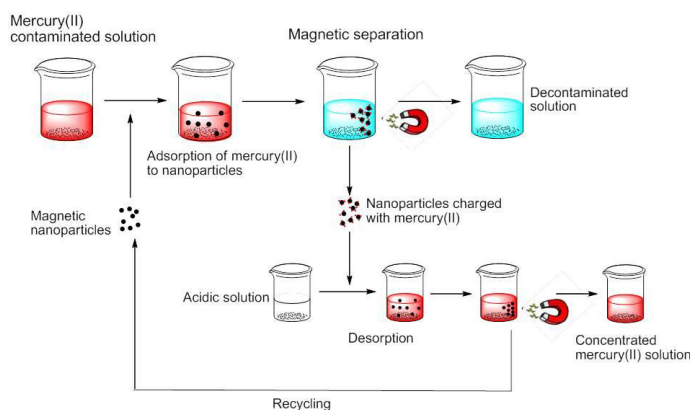
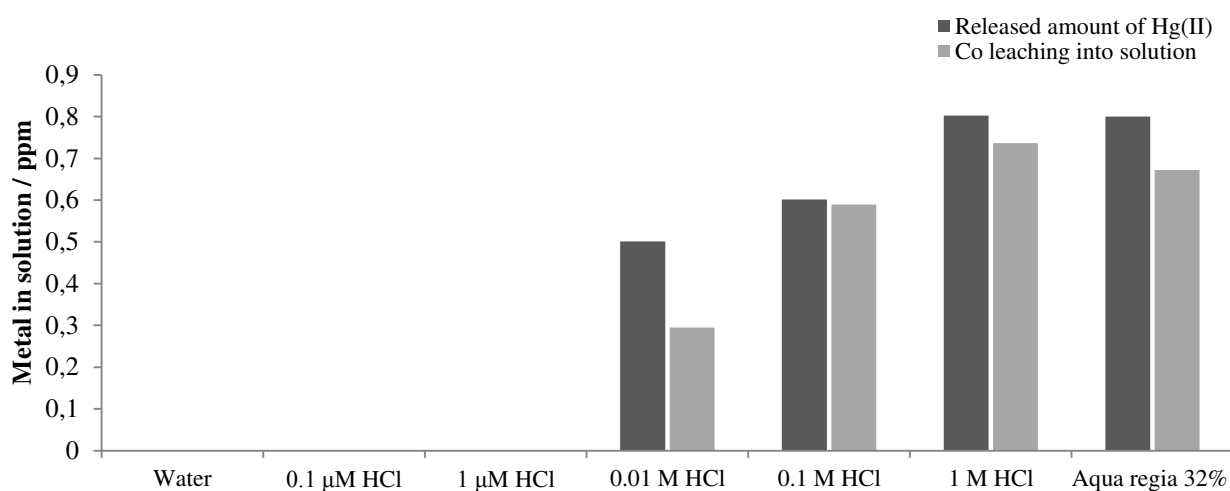


Figure 9. Recycling protocol for the extraction of mercury in tap water samples.

The best conditions for the mercury release were investigated, first of all, testing hydrochloric acid in different molarities (0.0001 – 0.1 M) as well as aqua regia (32%, (v/v)). Prior to all experiments, a typical extraction procedure was performed using 3 mg of NPs **40** in 100 mL of an aqueous Hg(II) solution (tap water, 1.8 ppm). All nanoparticles samples extracted 1.7 ppm Hg<sup>2+</sup> before they were treated with the corresponding acid for the release study. Furthermore, the cobalt leaching from the core of the nanoparticles was studied during the release process. Figure 10 shows that a treatment with water, 0.1  $\mu$ M HCl as well as 1  $\mu$ M HCl did not lead to any mercury release. Using aqua regia (32%), 1 M HCl or 0.1 M HCl led to mercury(II) release up to 50% of the extracted mercury, however, also a considerable amount of cobalt leaching could be detected. In the end, the release with 0.01 M HCl represented the best compromise between an efficient release and a minimum of cobalt leaching.



**Figure 10.** Mercury(II) release study with water, aqua regia (32%) and hydrochloric acid (different molarities). Co/C-PEI nanoparticles **40** used for the release had previously complexed 1.7 ppm Hg(II) which marks the maximum release level of Hg(II).

However, the percentage of release was still not satisfactory as more than 50% of the complexing sites remained blocked with residual mercury. Therefore, different acids (0.01 M) were tested to evaluate the best acid for the release treatment. These experiments showed that strong acids like H<sub>2</sub>SO<sub>4</sub>, HCl and HNO<sub>3</sub> were suitable for achieving high mercury release, while weak acids like acetic acid were less effective (Figure 11). It became obvious that H<sub>2</sub>SO<sub>4</sub> gave the best results with regard to release efficiency.

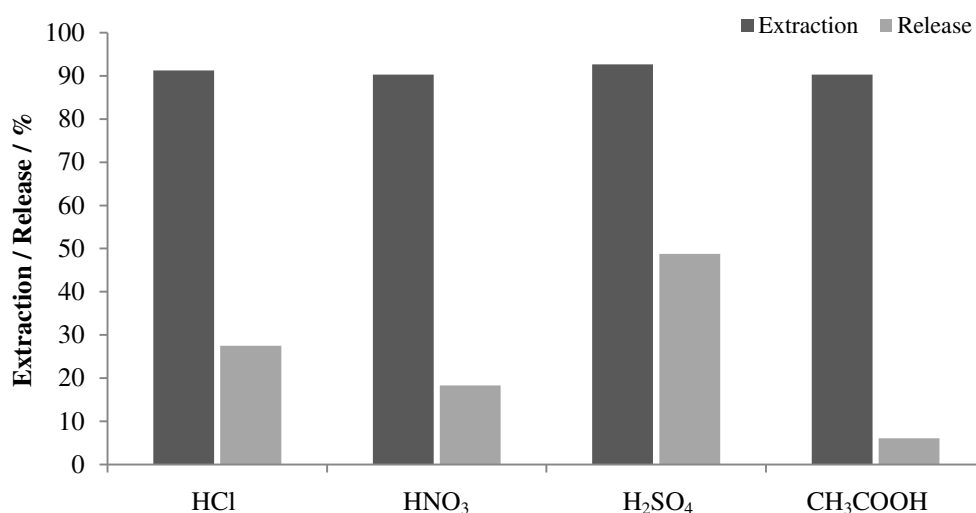


**Figure 11.** Mercury(II) release study with different acids (0.01 M). 1.7 ppm Hg(II) have been previously extracted with the NPs used for the release.

Further optimizations were performed with H<sub>2</sub>SO<sub>4</sub> solutions differing in molarity and thus in the pH. The best conditions were found to be 0.5 M H<sub>2</sub>SO<sub>4</sub>, corresponding to a pH value of approximately 0.4. Noteworthy, ICP measurements revealed that no significant cobalt leaching from the core of the nanomaterial is detected during the release of mercury.

Thus, a multicycle extraction/recycling protocol was established (Figure 9) for aqueous solutions (tap water) containing mercury. Briefly, the mercury(II) contaminated water containing the nanomagnets **40** was shaken for 10 minutes and then the NPs were recovered applying an external magnet. Subsequently, the decontaminated water was decanted and the NPs **40** were treated with H<sub>2</sub>SO<sub>4</sub> (20 mL, 0.5 M, 20 minutes) in order to release the mercury. Finally, a magnet was used once more to collect the NPs and decant the acidic solution. This was then followed by washing with a 0.5 M potassium carbonate solution and water to regenerate the amino groups of **40**, and the nanobeads were used in the next cycle.

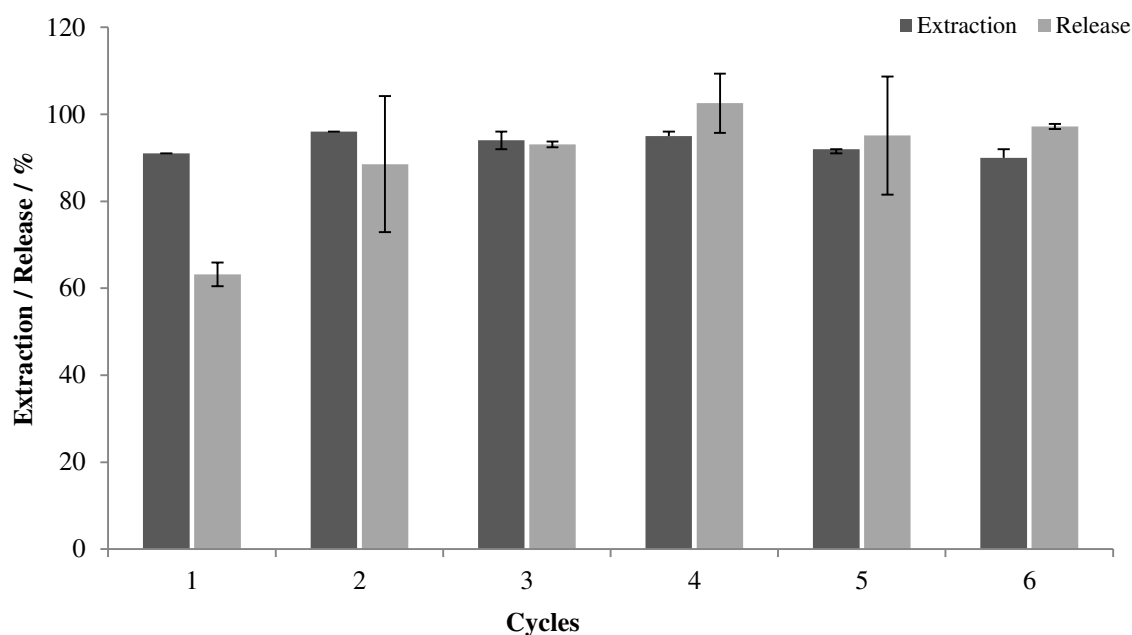


**Figure 12.** Reusability of Co/C-PEI **40** in six consecutive runs (extraction and subsequent release). Reaction conditions extraction: Co/C-PEI **40** (3 mg) were shaken in 100 mL of 2 ppm Hg(II) containing aqueous sample (pH 6.7) for 10 min. Reaction conditions release: 20 mL 0.5 M H<sub>2</sub>SO<sub>4</sub> within 20 min.

Following the scheme in Figure 9, it was demonstrated that in six consecutive cycles more than 90% of the mercury could be extracted from tap water samples (6 x 100 mL spiked with 2 ppm Hg<sup>2+</sup> each) within 10 minutes (Figure 12). Even though the release step was not complete each time, the extraction capacity remained nearly unchanged during the six runs. In some cases the release was observed to be higher than 100% as mercury from a previous incomplete release step was apparently set free in the next cycle. In addition, TEM analysis (see experimental section) proved that there were no significant changes or alterations in the appearance of the nanoparticles visible after the recycling process. These results have encouraged us to study the applicability of these magnetic scavengers in a large-scale experiment aiming to prove their use in a realistic industrial application. For this purpose a 20 L reactor was used (see Figure 13) and filled with normal Zurich drinking water artificially contaminated with 30 µg·L<sup>-1</sup> Hg(II). An even lower concentration of particles than in the previous recycling experiments was employed (3 mg/L), gratifyingly, after one hour reaction time the water was detoxified from mercury to 93%. A residual mercury content of 2 ppb (2 µg·L<sup>-1</sup>) was determined by atomic fluorescence spectroscopy (AFS), which is within the limit for drinking water according to World Health Organization.<sup>[40]</sup>



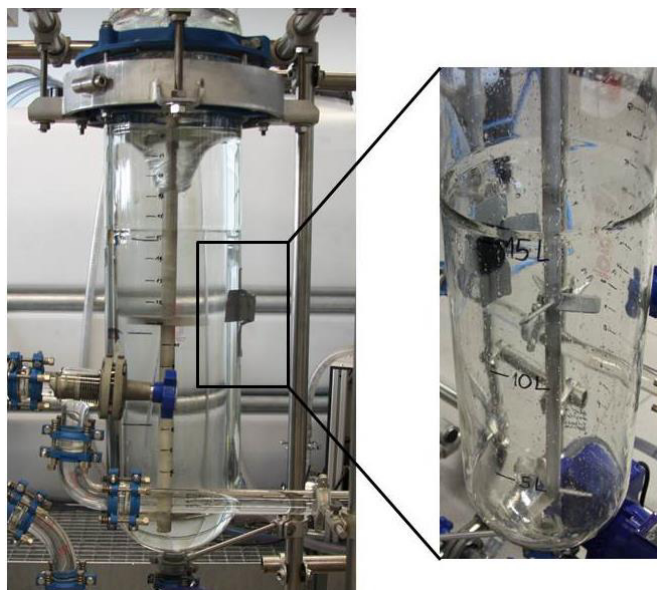


**Figure 13.** Large-scale experiment was performed in a reactor containing 20 L of an aqueous mercury solution ( $30 \mu\text{g}\cdot\text{L}^{-1}$ ). The extraction was done at rt in one hour using 3 mg NPs **40** per liter, which were recovered by an external neodymium magnet (magnification, right picture).

### 1.3 Conclusion

First of all, the suitability of Co/C nanoparticles **16** as scavenger for Hg(II) extraction was studied, however, a limited extraction capacity and poor recyclability were observed. To examine the influence of amino functionalities on the extraction capacity five different amino functionalized nanobeads were successfully synthesized and their mercury extraction efficiency was tested. Co/C-PEI NPs **40** were found to be the best material with regard to extraction capacity and selectivity while avoiding cobalt leaching from the core of the particles. After studying its applicability in real water samples a facile recycling protocol has been established for six consecutive runs. Thus, the simple and efficient scavenger developed here has proved its potential to decontaminate water samples from mercury(II) poisoning, which also might be applicable in the open environment due to the facile recovery of the magnetic support.

## 1.4 Experimental section

### Materials and methods

Reactions involving moisture and/or oxygen sensitive reagents were performed in flame dried glassware under an atmosphere of pre-dried nitrogen. Microwave reactions were performed in a CEM Discover S-Class microwave oven using pressure stable sealed 10 mL vials. NovaPEG amino resin Novabiochem® (batch number: S6625326; loading: 0.59 mmol/g) was purchased from Merck KGaA. Thin layer chromatography was performed with TLC pre-coated aluminum sheets (Merck silica gel 60 F<sub>254</sub> or Macherey-Nagel ALUGRAM® Xtra Sil G/UV<sub>254</sub>, 0.2 mm layer thickness). Visualization was accomplished with UV light ( $\lambda = 254$  nm or 366 nm) and through staining with a basic potassium permanganate solution. NMR spectra were recorded on a BRUKER Avance 400 and a BRUKER Avance 300 spectrometer. All spectra were recorded in CDCl<sub>3</sub> or commercially available deuterated solvents. Chemical shifts are reported as  $\delta$ , parts per million, calibrated to the residual solvent signal. The coupling constants  $J$  are reported in Hertz [Hz]. Splitting patterns for the spin multiplicity in the spectra are given as follows: s = singlet, m = multiplet. Attenuated total reflection infrared spectroscopy (ATR-IR) was carried out on a Biorad Excalibur FTS 3000 (equipped with a Specac Golden Gate Diamond Single Reflection ATR-System) and on a Varian FTS 1000 spectrometer. Wave numbers are reported as cm<sup>-1</sup>. Mass spectrometry was performed at the Central Analytical Department of the University of Regensburg on a Finnigan ThermoQuest TSQ 7000 and an Agilent Q-TOF 6540 UHD. Elemental microanalysis was performed by the micro analytical section of the University of Regensburg using a Vario MICRO cube or Titrino plus 848. Thermogravimetric analysis (TGA) was done on a Perkin Elmer TGA 7. Inductively coupled plasma optical emission spectrometry (ICP-OES) was measured on a SpectroFlame EOP (Spectro) in an acidic medium (32% aqua regia, v/v; detection limit for Hg<sup>2+</sup>: 0.1 mg/L = 1 ppm). Atomic fluorescence spectroscopy (AFS) was performed at Bachema AG Switzerland. Transmission electron microscopy was measured on a FEI TecnaiF30 (Department of Physics, University of Regensburg). Saturation magnetization of magnetic samples was measured using superconducting quantum interference device (SQUID) magnetometry analysis on a Quantum Design MPMS XL. X-ray photoelectron spectroscopy (XPS) analysis was performed at SuSoS (Switzerland) using a PhI5000 VersaProbe spectrometer (ULVAC-PHI, INC.) equipped with a 180° spherical capacitor energy analyzer and a multi-channel detection system with 16 channels. Spectra were acquired at a base pressure of 5·10<sup>-8</sup> Pa using a focused scanning monochromatic Al-K $\alpha$  source (1486.6 eV) with a spot size of 200  $\mu$ m. The instrument was run in the FAT analyzer mode with electrons emitted at 45° to the

surface normal. Pass energy used for survey scans was 187.85 eV and 46.95 eV for detail spectra. Charge neutralization utilizing both a cool cathode electron flood source (1.2 eV) and very low energy  $\text{Ar}^+$  – ions (10 eV) was applied throughout the analysis. Data were analyzed using the program CasaXPS [Version 2.3.12, [www.casaxps.com](http://www.casaxps.com)]. The signals were integrated following Shirley background subtraction. Sensitivity factors were calculated using published ionization cross-sections<sup>[41]</sup> corrected for attenuation, transmission-function of the instrument and source to analyzer angle. As a result, the measured amounts are given as apparent normalized atomic concentration and the accuracy under the chosen condition is approximately  $\pm 10\%$ . Nanoparticles were dispersed in an ultrasonic bath (Bandelin Sonorex RK255 H-R) and recovered with the aid of a neodymium based magnet (side length 12 mm).

### **Nanoparticle preparation**

Carbon-coated cobalt nanoparticles (Co/C, mean particle size  $\approx 25$  nm) were obtained from Turbobeats Llc, Switzerland. Before usage, the nanobeads were washed five times in a Millipore water/ $\text{HCl}_{\text{conc}}$  mixture (10/1, v/v). Residual acid was removed by washing the nanoparticles with Millipore water until the pH of the decanted solution was neutral. Finally, the particles were washed with acetone (3x) and diethyl ether (2x) and dried at 50 °C under vacuum.<sup>[19]</sup>

### **Nomenclature**

For the nanoparticles in this chapter the nomenclature is as follows: Co/C for magnetic nanoparticles with cobalt core and carbon shell and Fe/C for magnetic nanoparticles with iron core and carbon shell. Co/C-R or Fe/C-R for functionalized Co/C or Fe/C NPs where R indicates the functional group attached to the graphene-like layers: PEI for a poly(ethylenimine) shell, THF-CN for phenyltetrahydrofuran with cyano groups, THF-NH<sub>2</sub> for phenyltetrahydrofuran with amino groups, PAMAM G2 for the dendrimeric poly(amidoamine) coating of the second generation and Co/C-PS-PAMAM G2 for polystyrene coated cobalt nanoparticles with an additional dendrimeric functionalization.

### **Adsorption of mercury from aqueous solutions**

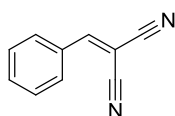
A certain amount of the specified magnetic nanoparticles was added to a known volume of an aqueous solution containing certain heavy metals (see the detailed description in the main part). The metals were present in defined concentrations and the extraction was performed at room temperature at the pH specified in the main part. The metal salts used are  $\text{HgCl}_2$ ,  $\text{BaCl}_2 \cdot 2\text{H}_2\text{O}$ ,

$\text{CuCl}_2$ ,  $\text{CrCl}_3 \cdot 6\text{H}_2\text{O}$ ,  $\text{PbCl}_2$ ,  $\text{Ni}(\text{C}_5\text{H}_7\text{O}_2)_2$ ,  $\text{Zn}(\text{ClO}_4)_2 \cdot 6\text{H}_2\text{O}$ ,  $\text{FeCl}_2 \cdot 4\text{H}_2\text{O}$  and  $\text{CdCl}_2 \cdot \text{H}_2\text{O}$ . To ensure proper dispersion of the particles in the aqueous solution, the sample was initially sonicated for one minute and then agitated using a mechanical shaker for the remaining extraction time. Afterwards, the nanoparticles were collected using an external magnet, the supernatant was decanted and filtered through a syringe filter. The solution was acidified by addition of a certain amount of aqua regia and the remaining heavy metals in solution were determined by inductively coupled plasma optical emission spectrometry (ICP-OES, measuring medium: aqua regia 32%, v/v). In case of the large scale extraction experiment, the remaining  $\text{Hg}^{2+}$  in solution was analyzed by atomic fluorescence spectroscopy (AFS) with a lower detection limit of 1  $\mu\text{g/L}$  (1 ppb).

### Desorption of mercury and re-usability of the nanoparticles

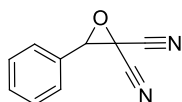
The release of the  $\text{Hg}^{2+}$  from the magnetic nanobeads was accomplished by treatment with an acidic medium (for details see chapter 1.2). The amount of nanoparticles used for the extraction (3 mg) was dispersed in 20 mL of the specified acid and then sonicated for 3 min followed by 5 min of mechanical shaking. The nanobeads were collected with a magnet, the supernatant was decanted and the particles were washed with a potassium carbonate solution (0.5 M) and water before they were re-used in the next adsorption experiment. This procedure was repeated six times to study the materials' recyclability and reused for the next cycle. The amount of desorbed  $\text{Hg}^{2+}$  in the acidic solution was determined by ICP-OES (measuring medium: aqua regia 32%, v/v) after diluting with aqua regia and filtering through a syringe filter.

### 2-Benzylidenemalononitrile (43)<sup>[42]</sup>



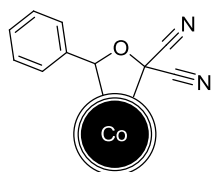
Malononitrile (2.64 g, 40.0 mmol, 1.0 equiv.) was dissolved in dist. water (160 mL) and benzaldehyde (4.1 mL, 40.0 mmol, 1.0 equiv.) were added. The resulting mixture was stirred at room temperature for 14 h, during which the product precipitated as a white solid and was filtered off (6.17 g, 40.0 mmol, 100%,  $R_f = 0.49$  (hexanes/EtOAc 5:1)).

$^1\text{H NMR}$  (300 MHz,  $\text{CDCl}_3$ ):  $\delta_{\text{H}} = 7.55 - 7.40$  (m, 2H), 7.78 (s, 1H), 7.67-7.61 (m, 1H), 7.57-7.52 (m, 2H);  $^{13}\text{C NMR}$  (75 MHz,  $\text{CDCl}_3$ ):  $\delta_{\text{C}} = 160.1, 134.8, 131.0, 130.9, 129.8, 113.8, 112.7, 83.1$ .

**3-Phenyloxirane-2,2-dicarbonitrile (28)**<sup>[42]</sup>

2-Benzylidenemalononitrile **43** (800 mg, 5.2 mmol) was dissolved in acetonitrile (2 mL) and an aqueous NaOCl solution (6 mL) was added. The resulting mixture was stirred at room temperature for 100 min. The solution was extracted with DCM (3x150 mL) and the combined organic layers were washed with sat. NaHCO<sub>3</sub> and dried over MgSO<sub>4</sub>. The solvent was evaporated and the crude product was purified by silica column chromatography (hexanes/EtOAc 9:1) yielding **28** as a slightly yellowish solid (655 mg, 3.85 mmol, 74%,  $R_f = 0.57$  (hexanes/EtOAc 5:1)).

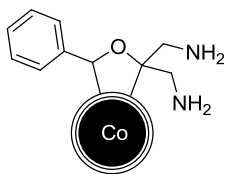
<sup>1</sup>H NMR (300 MHz, CDCl<sub>3</sub>):  $\delta_H = 7.55 - 7.40$  (m, 5H), 4.71 (s, 1H); <sup>13</sup>C NMR (75 MHz, CDCl<sub>3</sub>):  $\delta_C = 131.5, 129.2, 127.5, 126.8, 111.6, 110.1, 65.8, 41.7$ ; IR (v/cm<sup>-1</sup>): 2355, 2339, 1259, 1087, 1020, 611; LRMS (ESI):  $m/z = 170.1$  [M]<sup>+</sup>.

**5-Phenyldihydrofuran-2,2(3H)-dicarbonitrile functionalized Co/C nanoparticles (29)**<sup>[33]</sup>

In a microwave vial Co/C nanoparticles (300 mg) were mixed with 3-phenyloxirane-2,2-dicarbonitrile **28** (130 mg, 0.76 mmol). The sealed tube was heated to 120 °C in the microwave for 3 minutes. After cooling to room temperature, the particles were recovered with the aid of a magnet and washed with EtOAc (6x2 mL) and diethyl ether (3x2 mL). After evaporation of the solvent, 314 mg of the Co/C-THF-CN particles **29** were obtained.

IR (KBr,  $\tilde{\nu}/\text{cm}^{-1}$ ): 2953, 2925, 2958, 2367, 2356, 2333, 2188, 1706, 1629, 1597, 1550, 1458, 1376, 1259, 1169, 1159, 1086, 1007, 964, 788; elemental microanalysis [%]: C, 6.95; H, 0.16; N, 0.74 - loading (NH<sub>2</sub>) 0.52 mmol/g, loading (THF unit) 0.26 mmol/g.

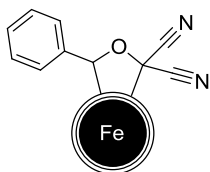
**(5-Phenyltetrahydrofuran-2,2-diyl)dimethanamine functionalized Co/C nanoparticles (30)<sup>[33]</sup>**



A Schlenk flask was charged with anhydrous THF (0.8 mL), trimethylsilyl chloride (TMSCl) (51  $\mu$ L, 0.4 mmol, 40 equiv.) and  $\text{NaBH}_4$  (7.6 mg, 0.2 mmol, 20 equiv.) under nitrogen atmosphere. The resulting solution was heated at 80  $^{\circ}\text{C}$  for 3 h. After cooling down to room temperature, 50 mg of Co/C-THF-CN nanobeads **29** (0.03 mmol nitrile groups, 1 equiv.) were added and the mixture was heated at 80  $^{\circ}\text{C}$  for 24 h. The reaction was quenched by slow addition of water and the nanoparticles were washed with water (3x8 mL), THF (3x8 mL), acetone (2x8 mL) and diethyl ether (2x8 mL). After drying under vacuum 50 mg **30** were obtained.

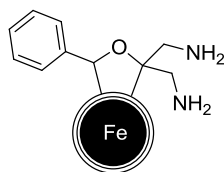
**IR** (KBr,  $\tilde{\nu}/\text{cm}^{-1}$ ): 2955, 2920, 2871, 1459, 1377, 889, 762.

**5-Phenyldihydrofuran-2,2(3*H*)-dicarbonitrile functionalized Fe/C nanoparticles (32)**



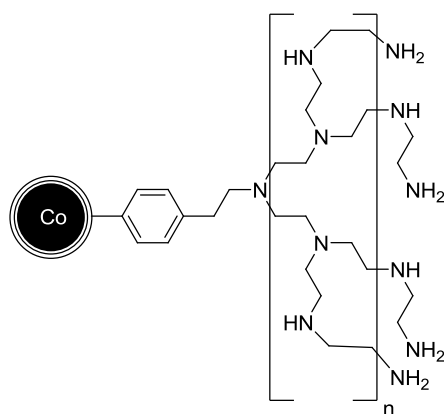
In a microwave vial 100 mg Fe/C nanoparticles were mixed with 150 mg of 3-phenyloxirane-2,2-dicarbonitrile **28** (0.88 mmol). The sealed tube was heated to 120  $^{\circ}\text{C}$  in the microwave for 3 minutes. After cooling to room temperature, the particles were recovered with an external magnet and washed with EtOAc (15x3 mL) and diethyl ether (3x2 mL). After evaporation of the solvent 116 mg of the Fe/C-THF-CN particles **32** were obtained.

**IR** (KBr,  $\tilde{\nu}/\text{cm}^{-1}$ ): 2956, 2927, 2855, 2360, 2358, 2357, 2344, 1458, 1377, 757; **elemental microanalysis** [%]: C, 14.68; H, 0.44; N, 2.13 - **loading** ( $\text{NH}_2$ ) 1.51 mmol/g, **loading** (THF unit) 0.76 mmol/g.

**(5-Phenyltetrahydrofuran-2,2-diyl)dimethanamine functionalized Fe/C nanoparticles (33)**

A Schlenk flask was loaded with 100 mg of the Fe/C-THF-CN nanobeads **32** (0.15 mmol, 1 equiv.) and  $\text{BH}_3 \cdot \text{THF}$  (1 M, 1.7 mL, 1.7 mmol, 11 equiv.) under nitrogen atmosphere. The mixture was refluxed at 76 °C for 25 h. After magnetic decantation, the particles were washed with THF (1x2 mL), water (3x3 mL) and THF (3x2 mL) and dried under vacuum resulting in 94 mg of **33**.

**IR** (KBr,  $\tilde{\nu}/\text{cm}^{-1}$ ): 3427, 1583, 1373, 999, 710.

**Poly(ethyleneimine) functionalized Co/C nanoparticle (40)**<sup>[33]</sup>

4-(2-Aminoethyl)phenyl functionalized Co/C nanoparticles **38** (945 mg, 0.104 mmol, 1.0 equiv.) in DCM (95 mL) were dispersed in an ultrasonic bath for 15 min. Under stirring, aziridine (5.4 mL, 104 mmol, 1000 equiv.) and  $\text{HCl}_{\text{conc}}$  (140  $\mu\text{L}$ ) were added to the reaction mixture before heating to 80 °C for 48 h. Afterwards, the nanoparticles were collected with the help of an external magnet and the solvent was decanted. The nanobeads were washed with DCM (2x20 mL),  $\text{H}_2\text{O}$  (3x20 mL) and diethyl ether (2x20 mL) before being dried *in vacuo* at 50 °C to give 1.0 g of PEI functionalized nanobeads.

**IR** (neat,  $\tilde{\nu}/\text{cm}^{-1}$ ): 3366, 3249, 2953, 2842, 2363, 2168, 2039, 1641, 1461, 1297, 1057, 488; **elemental microanalysis** [%]: C, 11.51; H, 1.23; N, 2.68 - **loading** (N) 1.80 mmol/g.

As the degree of polymerization was not satisfactory the whole procedure was repeated using 500 mg of Co/C-PEI (0.055 mmol based on the initial amine loading, 1 equiv.) in DCM (49 mL), 100  $\mu\text{L}$   $\text{HCl}_{\text{conc}}$  and 2.85 mL aziridine (55 mmol, 1000 equiv.). After a reaction time of 69 h

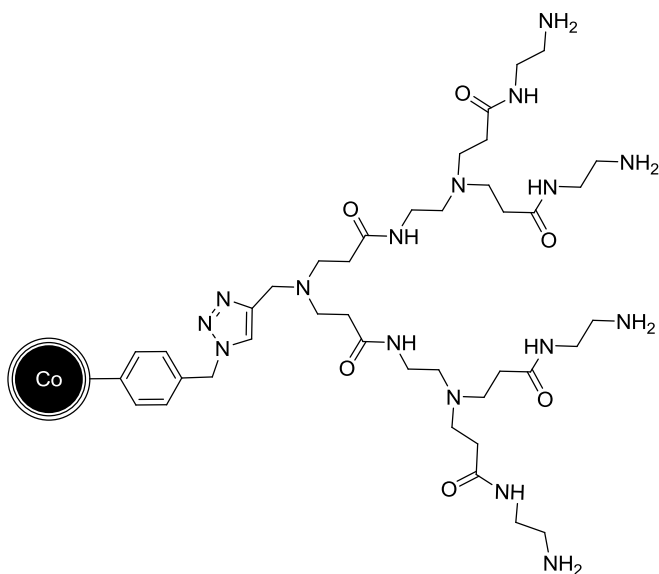
1.19 g of Co/C-PEI nanoparticles could be collected. The extent of polymerization was estimated by TGA (66wt%).

**IR** (neat,  $\tilde{\nu}/\text{cm}^{-1}$ ): 3417, 2933, 2821, 2362, 1648, 1604, 1458, 1014, 870; **elemental microanalysis** [%]: C, 30.46; H, 7.09; N, 14.97 - **loading** (N) 10.58 mmol/g.

### Synthesis of PAMAM Dendrimers

The synthesis of PAMAM dendrons was done according to a procedure described by Chu *et al.*<sup>[43]</sup> Herein, propargyl amine (1.0 equiv.) was reacted with methylacrylate (83 equiv.) under  $\text{N}_2$  atmosphere at room temperature giving rise to the dendron G0.5 (95%). Then ethylenediamine (60 equiv.) was added to the dendron (1.0 equiv.) to yield dendron G1 with two amino functional groups (98%). After repetition of these two steps, consecutive generations of the dendrons could be obtained in good yields. For every half-generation dendron purification by silica column chromatography was required. NMR and EI-MS are in accordance with the literature values.<sup>[43]</sup>

### Synthesis of magnetic Co/C-PAMAM G2 (35)

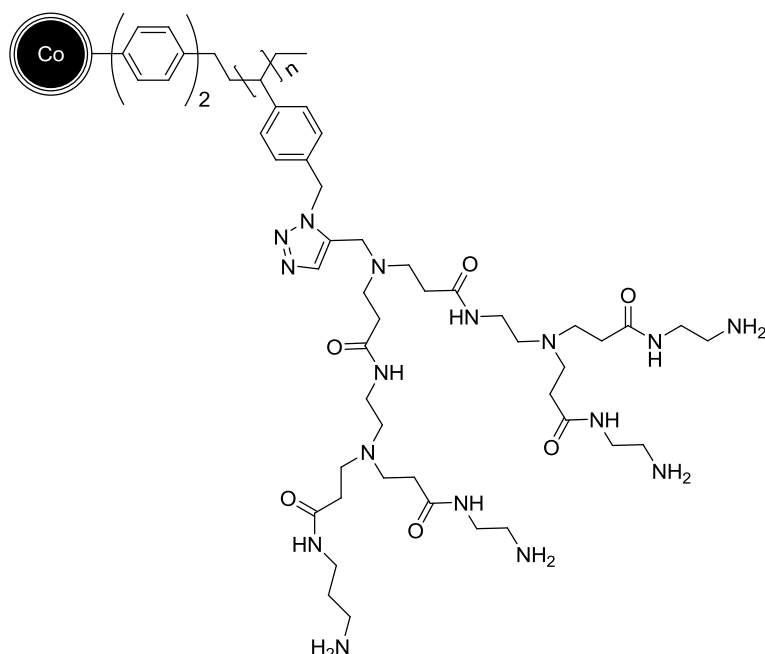


In a typical experiment, 100 mg of azide functionalized nanoparticles **34** (1.0 equiv.) and the respective PAMAM dendrons (5 equiv.) were used. The PAMAM was previously dissolved in 5 mL of a THF/ $\text{H}_2\text{O}$  3:1 mixture followed by the successive addition of Co/C-  $\text{N}_3$  nanobeads **34**, Na-ascorbate (30 mol%) and  $\text{CuSO}_4$  (10 mol%). Afterwards, the reaction mixture was sonicated for 15 minutes and stirred for 48 hours at room temperature. The magnetic nanoparticles were separated applying an external magnet and washed with acetone (5x5 mL),  $\text{H}_2\text{O}$  (5x5 mL) and acetone (3x5 mL). Drying under vacuum gave the desired nanobeads **35**.

**TGA** ( $\text{N}_2$ ): 0.02 mmol/g.



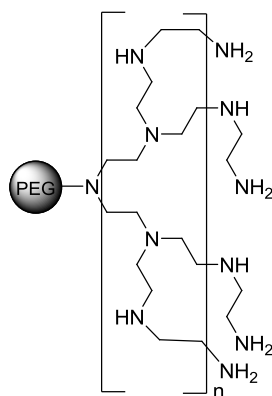
### Synthesis of magnetic Co/C-PS-PAMAM G2 (37)



In a typical experiment, 100 mg of azide functionalized nanoparticles **36** (1.0 equiv.) and the respective PAMAM dendrons (5 equiv.) were used. The PAMAM was dissolved in 5 mL of a THF/H<sub>2</sub>O 3:1 mixture followed by the successive addition of Co/C- N<sub>3</sub> nanobeads **36**, Na-ascorbate (30 mol%) and CuSO<sub>4</sub> (10 mol%). Afterwards, the reaction mixture was sonicated for 15 minutes and then stirred for 48 hours at room temperature. The magnetic nanoparticles were collected, the supernatant decanted and the particles were washed with acetone (5x5 mL), H<sub>2</sub>O (5x5 mL) and acetone (3x5 mL). In the end, the nanobeads **37** were dried under vacuum.

**TGA** (N<sub>2</sub>): 0.6 mmol; **IR** (neat,  $\tilde{\nu}$  /cm<sup>-1</sup>): 2085, 1632, 1537, 108, 1422, 1250, 1148, 1121, 1103, 1016, 808.

### NovaPEG amino resin-PEI (42)



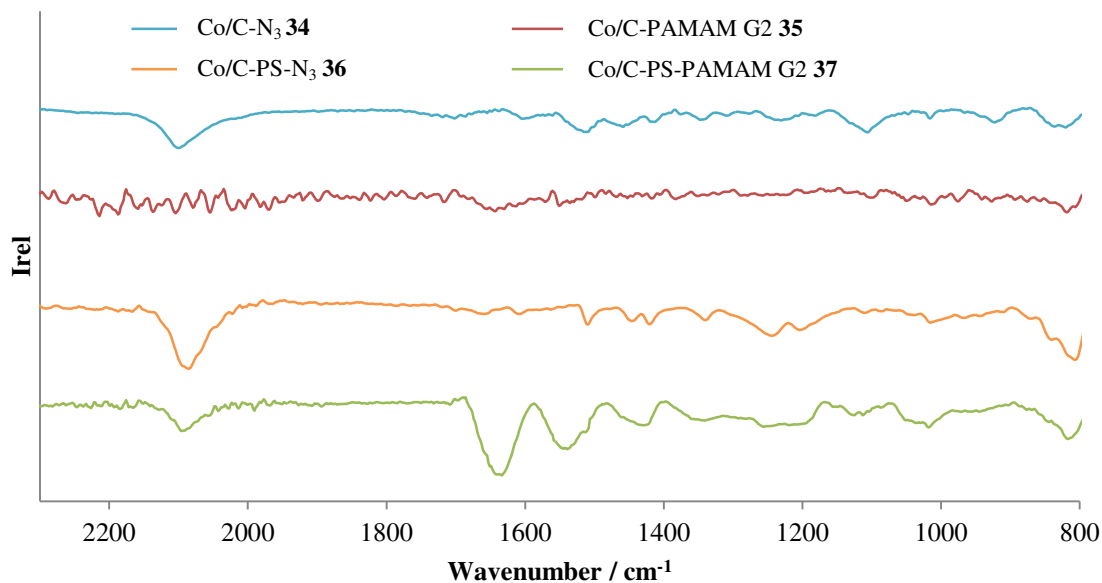
In a round-bottom flask, commercially available NovaPEG amino resin (50 mg, 0.03 mmol, 1 equiv.) was pre-swollen in DCM (5 mL) before aziridine (775  $\mu$ L, 14.9 mmol, 506 equiv.) and

HCl<sub>conc</sub> (16  $\mu$ L) were added. The mixture was stirred at 80 °C for 24 h. After cooling to room temperature, the resin was filtered off, washed with DCM (2x5 mL), H<sub>2</sub>O (2x5 mL) and DCM (3x5 mL) before being dried under vacuum at 50 °C.

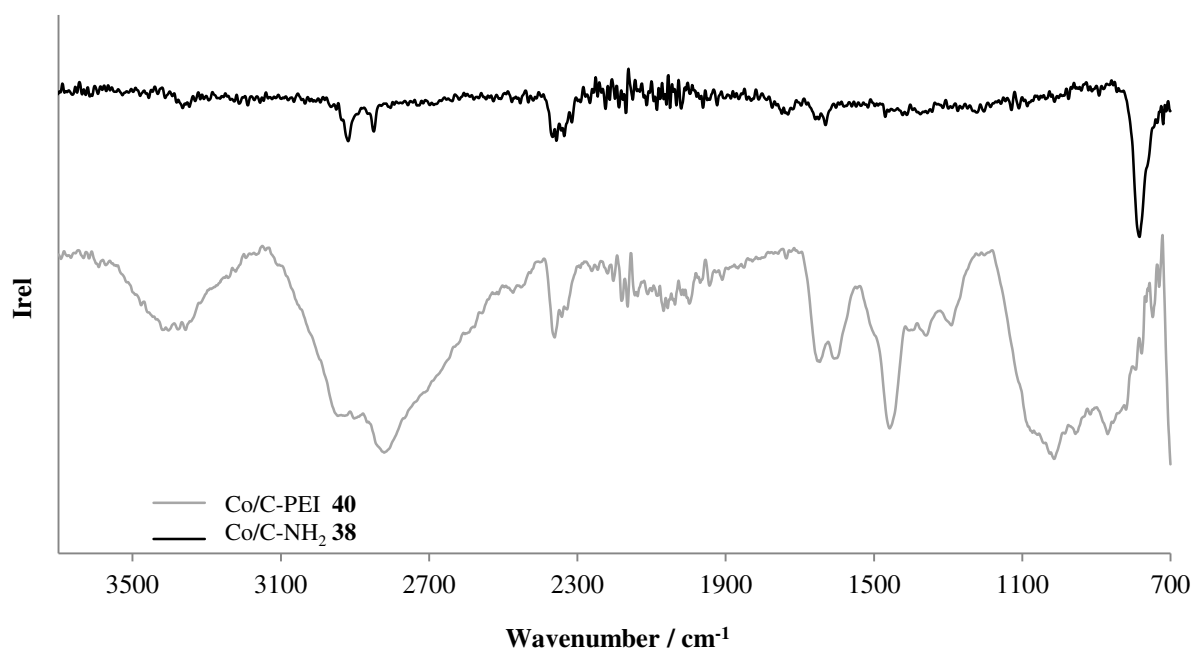
**IR** (neat,  $\tilde{\nu}$  /cm<sup>-1</sup>): 3413, 2936, 2823, 1653, 1614, 1457, 1357, 1292, 1098, 963, 853, 734, 651, 589; **TGA** (N<sub>2</sub>): 65 wt% PEI; **elemental microanalysis** [%]: C, 38.27; H, 8.18; N, 16.24 - **loading** (N) 10.94 mmol/g.

## IR spectra

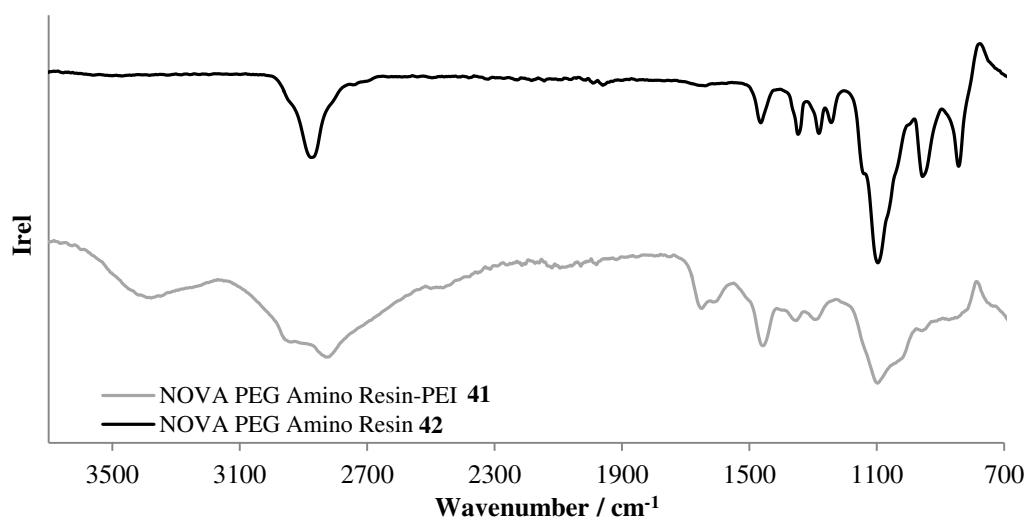
IR spectra of Co/C-N<sub>3</sub> **34** (blue), Co/C-PAMAM G2 **35** (red), Co/C-PS-N<sub>3</sub> **36** (yellow) and Co/C-PS-PAMAM G2 **37** (green).



IR spectra of 4-(2-aminoethyl)phenyl functionalized Co/C nanoparticles **38** (top) and Co/C-PEI **40** (bottom).<sup>[33]</sup>

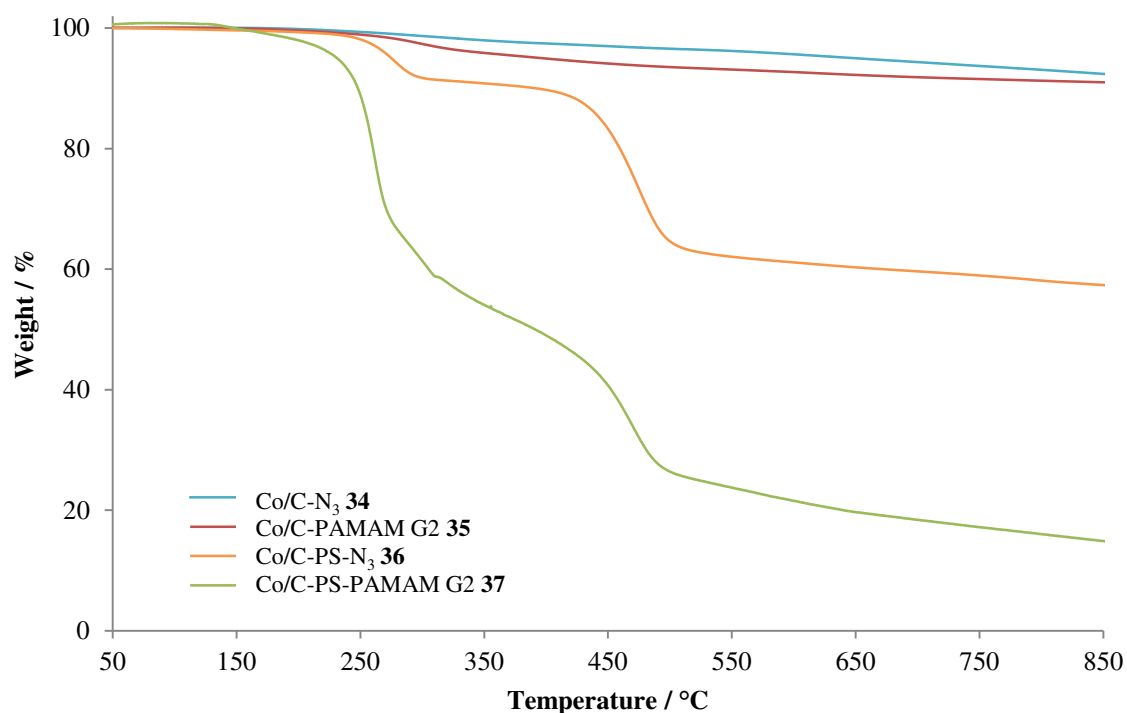


IR spectra of NOVA PEG Amino Resin **41** (top) and NOVA PEG Amino Resin-PEI **42** (bottom).

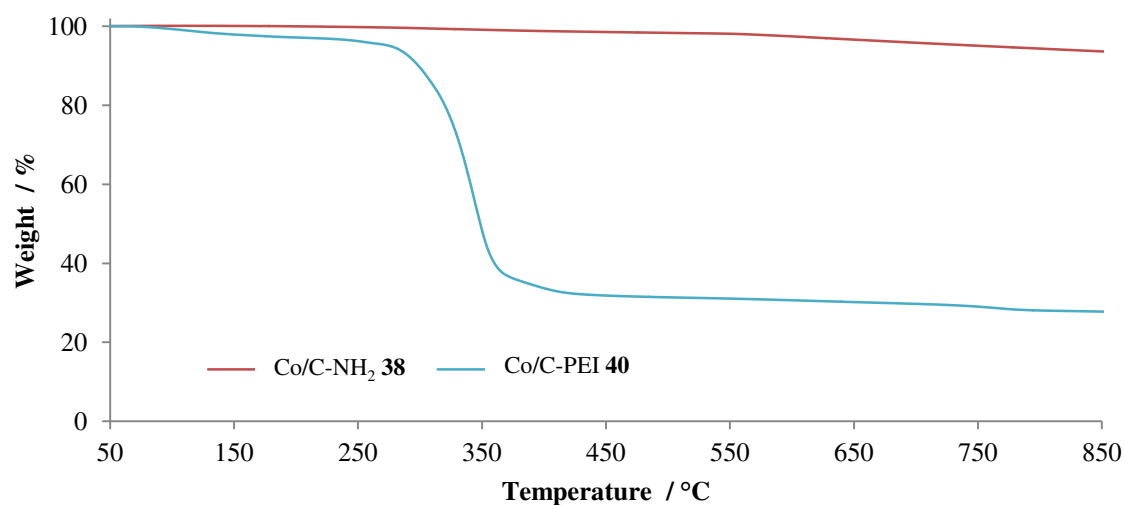


## TGA spectra

TGA spectra of the azide tagged nanoparticles **34** (blue) and **36** (yellow) and the subsequent PAMAM-clicked magnetic beads **35** (red) and **37** (green). The loadings can be estimated from the weight loss % of the materials.

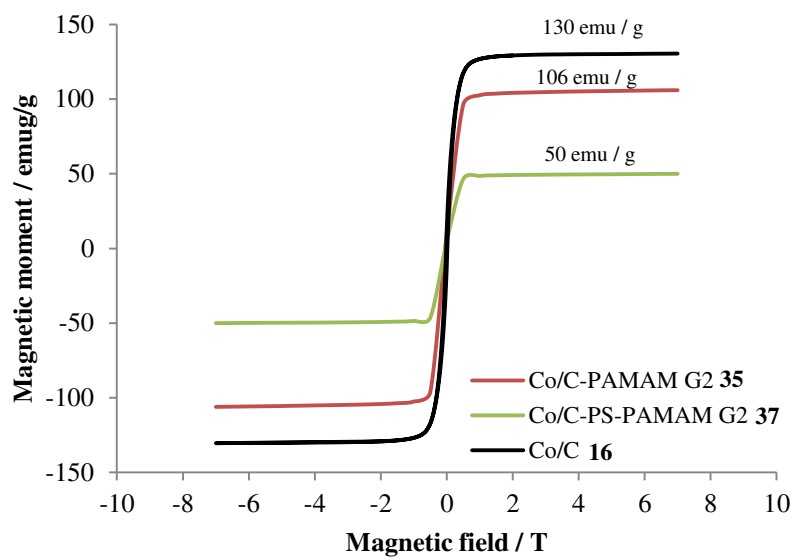


TGA analysis of the 4-(2-aminoethyl)phenyl functionalized NPs **38** (red) PEI-coated NPs **40** (blue) to estimate % of polymerization.<sup>[33]</sup>

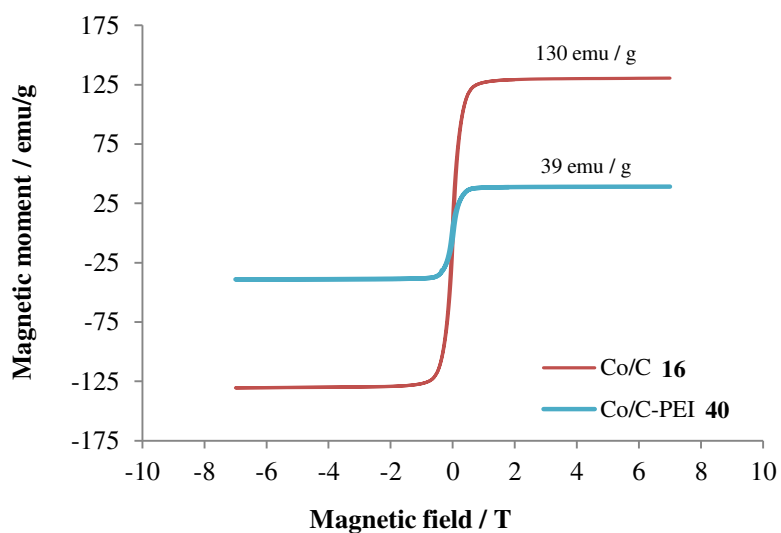


## SQUID measurements

Magnetization of the pristine Co/C **16** (black) and functionalized nanoparticles **35** (red) and **37** (green) obtained from SQUID measurements at 290 K.

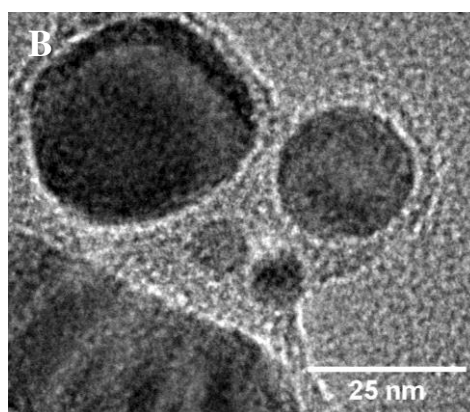
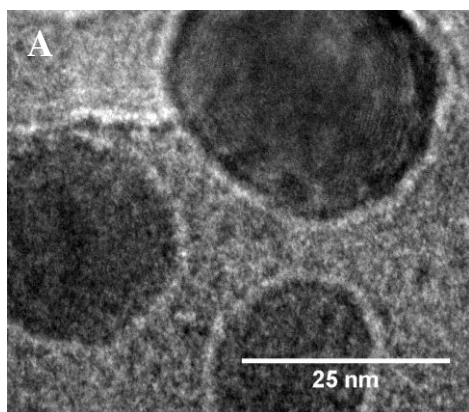


Magnetization of PEI-functionalized NPs **40** (blue) and Co/C **16** (red) obtained from SQUID measurement at 290 K.



### TEM picture

Transmission electron microscopy (TEM) pictures of Co/C-PEI NPs **40** before (A) and after recycling process (B).



## X-Ray Photoelectron Spectroscopy

XPS analysis was performed on 3 samples of Co/C nanoparticles after extraction of metals:

- Co/C **16** after the extraction of HgCl<sub>2</sub>
- Co/C-PEI **40** after the extraction of HgCl<sub>2</sub>
- Co/C-PEI **40** after the extraction of HgCl<sub>2</sub> from a mixture of different metal salts (HgCl<sub>2</sub>, BaCl<sub>2</sub>·2H<sub>2</sub>O, CuCl<sub>2</sub>, CrCl<sub>3</sub>·6H<sub>2</sub>O, PbCl<sub>2</sub>, Ni(C<sub>5</sub>H<sub>7</sub>O<sub>2</sub>)<sub>2</sub>)

Results:

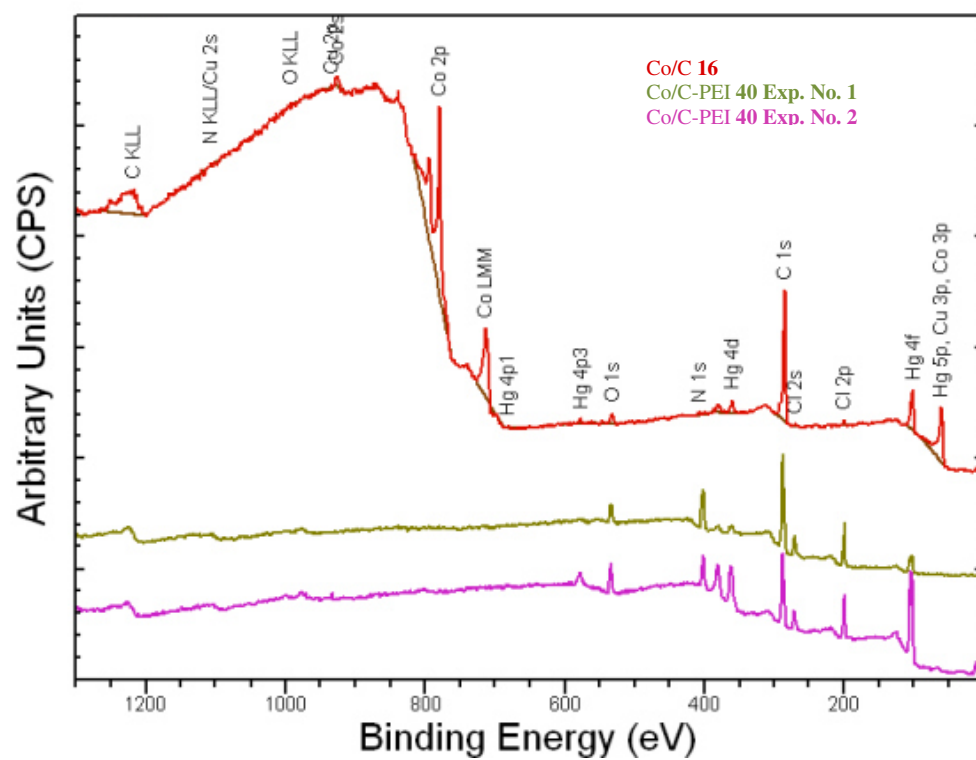
- Co/C NPs **16**: The metallic Co core of the particle can still be detected, indicating, that the C-coating is less than 10 nm thick. Mercury is oxidized with a binding energy for the Hg 4f<sub>7/2</sub> peak of 101.1 eV.
- Co/C-PEI **40**: The metallic Co core of the particle is not detected anymore on these particles. Hg is detected, also in its oxidized form (Hg 4f<sub>7/2</sub> peak of 101.5 eV).
- Co/C-PEI **40**: The metallic Co core of the particle is not detected anymore on these particles. Hg is detected (3.6 At.-%), also in its oxidized form (Hg 4f<sub>7/2</sub> peak of 101.9 eV). Additionally some Cu (0.6 At.-%) was detected. Ni, Cr, Pb and Ba could not be detected.

Table 1. Normalized At.-% of all detected elements.

At.-%	Exp. No.	Co	Hg	Cu	Ba	Pb	Cr	Ni
Co/C <b>16</b>		8.0	1.5	N/A	N/A	N/A	N/A	N/A
Co/C-PEI <b>40</b>	1	0.0	0.4	N/A	N/A	N/A	N/A	N/A
Co/C-PEI <b>40</b>	2	0.0	3.6	0.6	0.0	0.0	0.0	0.0

Survey spectra of the powder samples (binding energy is calibrated to C-C at 284.5 eV): Co/C **16** after the extraction of HgCl<sub>2</sub> (red;), Co/C-PEI **40** Exp. No. 1 after the extraction of HgCl<sub>2</sub> (green;), Co/C-PEI **40** Exp. No. 2 after the extraction of HgCl<sub>2</sub> from a mixture of different metal salts (HgCl<sub>2</sub>, BaCl<sub>2</sub>·2H<sub>2</sub>O, CuCl<sub>2</sub>, CrCl<sub>3</sub>·6H<sub>2</sub>O, PbCl<sub>2</sub>, Ni(C<sub>5</sub>H<sub>7</sub>O<sub>2</sub>)<sub>2</sub>) (pink;).



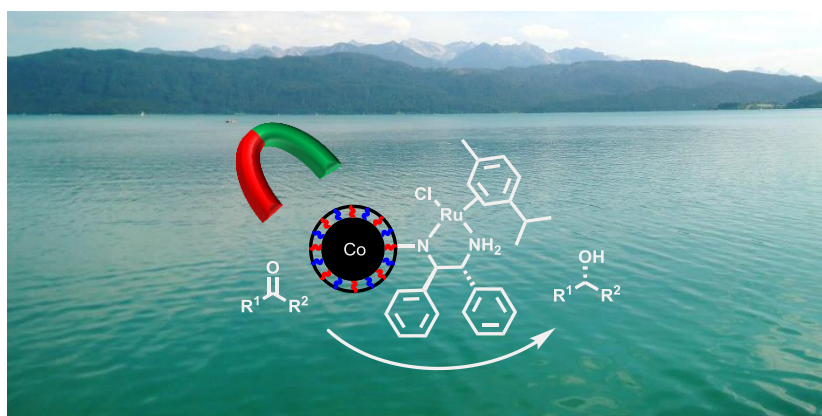


## 1.5 References

- [1] A. Farrukh, A. Akram, A. Ghaffar, S. Hanif, A. Hamid, H. Duran, B. Yameen, *ACS Appl. Mater. Interfaces* **2013**, 5, 3784–3793.
- [2] H. Parham, B. Zargar, R. Shiralipour, *J. Hazard. Mater.* **2012**, 205–206, 94–100.
- [3] M. H. Baki, F. Shemirani, *Anal. Methods* **2013**, 5, 3255–3263.
- [4] J. Zhao, B. Zhu, H. Yu, L. Yan, Q. Wei, B. Du, *J. Colloid Interface Sci.* **2013**, 389, 46–52.
- [5] Y. Zhai, S. Duan, Q. He, X. Yang, Q. Han, *Microchim. Acta* **2010**, 169, 353–360.
- [6] P. I. Girginova, A. L. Daniel-da-Silva, C. B. Lopes, P. Figueira, M. Otero, V. S. Amaral, E. Pereira, T. Trindade, *J. Colloid Interface Sci.* **2010**, 345, 234–240.
- [7] a) C. C. Freyhardt, M. Tsapatsis, R. F. Lobo, K. J. Balkus, M. E. Davis, *Nature* **1996**, 381, 295–298; b) K. Inoue, K. Yoshizuka, K. Ohto, *Anal. Chim. Acta* **1999**, 388, 209–218; c) A. K. Kushwaha, N. Gupta, M. C. Chattopadhyaya, *J. Chem. Pharm. Res.* **2011**, 807–815.
- [8] M. A. Shannon, P. W. Bohn, M. Elimelech, J. G. Georgiadis, B. J. Mariñas, A. M. Mayes, *Nature* **2008**, 452, 301–310.
- [9] A. Khan, *Sep. Sci. Technol.* **2006**, 41, 1169–1177.
- [10] S. A. Idris, S. R. Harvey, L. T. Gibson, *J. Hazard. Mater.* **2011**, 193, 171–176.
- [11] F. M. Koehler, M. Rossier, M. Waelle, E. K. Athanassiou, L. K. Limbach, R. N. Grass, D. Günther, W. J. Stark, *Chem. Commun.* **2009**, 4862–4864.
- [12] J.-f. Liu, Z.-s. Zhao, G.-b. Jiang, *Environ. Sci. Technol.* **2008**, 42, 6949–6954.
- [13] Y. Zhai, Q. He, Q. Han, S. Duan, *Microchim. Acta* **2012**, 178, 405–412.
- [14] M. K. Rofouei, A. Rezaei, M. Masteri-Farahani, H. Khani, *Anal. Methods* **2012**, 4, 959–966.
- [15] X. Shen, Q. Wang, W. Chen, Y. Pang, *Appl. Surf. Sci.* **2014**, 317, 1028–1034.
- [16] M. Faraji, Y. Yamini, A. Saleh, M. Rezaee, M. Ghambarian, R. Hassani, *Anal. Chim. Acta* **2010**, 659, 172–177.
- [17] Y. Wang, X. Luo, J. Tang, X. Hu, Q. Xu, C. Yang, *Anal. Chim. Acta* **2012**, 713, 92–96.
- [18] K. Mandel, F. Hutter, C. Gellermann, G. Sextl, *Appl. Mater. Interf.* **2012**, 4, 5633–5642.
- [19] M. Rossier, F. M. Koehler, E. K. Athanassiou, R. N. Grass, B. Aeschlimann, D. Günther, W. J. Stark, *J. Mater. Chem.* **2009**, 19, 8239–8243.
- [20] R. N. Grass, E. K. Athanassiou, W. J. Stark, *Angew. Chem. Int. Ed.* **2007**, 46, 4909–4912.
- [21] Q. M. Kainz, A. Schätz, A. Zöpfl, W. J. Stark, O. Reiser, *Chem. Mater.* **2011**, 23, 3606–3613.
- [22] a) Q. M. Kainz, R. Linhardt, R. N. Grass, G. Vilé, J. Pérez-Ramírez, W. J. Stark, O. Reiser, *Adv. Funct. Mater.* **2014**, 24, 2020–2027; b) S. Wittmann, J.-P. Majoral, R. N. Grass, W. J. Stark, O. Reiser, *Green Process Synth.* **2012**, 1, 275–279; c) S. Wittmann, A. Schätz, R. N. Grass, W. J. Stark, O. Reiser, *Angew. Chem. Int. Ed.* **2010**, 49, 1867–1870; d) Q. M. Kainz, R. Linhardt, P. K. Maity, P. R. Hanson, O. Reiser, *ChemSusChem* **2013**, 6, 721–729.
- [23] Q. M. Kainz, A. Späth, S. Weiss, T. D. Michl, A. Schätz, W. J. Stark, B. König, O. Reiser, *ChemistryOpen* **2012**, 1, 125–129.
- [24] Q. M. Kainz, M. Zeltner, M. Rossier, W. J. Stark, O. Reiser, *Chem. Eur. J.* **2013**, 19, 10038–10045.

- [25] A. Schätz, R. N. Grass, W. J. Stark, O. Reiser, *Chem. Eur. J.* **2008**, *14*, 8262–8266.
- [26] M. Rossier, A. Schaetz, E. K. Athanassiou, R. N. Grass, W. J. Stark, *Chem. Eng. J.* **2011**, *175*, 244–250.
- [27] M. Rossier, F. M. Koehler, E. K. Athanassiou, R. N. Grass, M. Waelle, K. Birbaum, D. Günther, W. J. Stark, *Ind. Eng. Chem. Res.* **2010**, *49*, 9355–9362.
- [28] B. Tawabini, S. Al-Khaldi, M. Atieh, M. Khaled, *Water Sci. Technol.* **2010**, *61*, 591–598.
- [29] M. S. Masri, M. Friedman, *Environ. Sci. Technol.* **1972**, *6*, 745–746.
- [30] M. Soleimani, M. Ghahraman Afshar, A. Sedghi, *ISRN Nanotechnology* **2013**, Article ID 674289.
- [31] S. Tagliapietra, G. Cravotto, E. Gaudino, S. Visentin, V. Mussi, *Synlett* **2012**, *23*, 1459–1462.
- [32] A. Giannis, K. Sandhoff, *Angew. Chem. Int. Ed.* **1989**, *28*, 218–220.
- [33] Q. M. Kainz, S. Fernandes, C. M. Eichenseer, F. Besostri, H. Körner, R. Müller, O. Reiser, *Faraday Discuss.* **2014**, *175*, 27–40.
- [34] Y. Liu, D.-C. Wu, W.-D. Zhang, X. Jiang, C.-B. He, T. S. Chung, S. H. Goh, K. W. Leong, *Angew. Chem. Int. Ed.* **2005**, *44*, 4782–4785.
- [35] A. K. Tucker-Schwartz, R. L. Garrell, *Chem. Eur. J.* **2010**, *16*, 12718–12726.
- [36] S. Fernandes, C. M. Eichenseer, P. Kreitmeier, J. Rewitzer, V. Zlateski, R. N. Grass, W. J. Stark, O. Reiser, *RSC Adv.* **2015**, *5*, 46430–46436.
- [37] a) M. Keller, A. Perrier, R. Linhardt, L. Travers, S. Wittmann, A.-M. Caminade, J.-P. Majoral, O. Reiser, A. Ouali, *Adv. Synth. Catal.* **2013**, *355*, 1748–1754; b) A. Schaetz, M. Zeltner, T. D. Michl, M. Rossier, R. Fuhrer, W. J. Stark, *Chem. Eur. J.* **2011**, *17*, 10566–10573.
- [38] G. Z. Kyzas, E. A. Deliyanni, *Molecules* **2013**, *18*, 6193–6214.
- [39] a) C. Bazzicalupi, A. Bianchi, C. Giorgi, P. Gratter, P. Mariani, B. Valtancoli, *Inorg. Chem.* **2013**, *52*, 2125–2137; b) M. Keller, V. Collière, O. Reiser, A.-M. Caminade, J.-P. Majoral, A. Ouali, *Angew. Chem. Int. Ed.* **2013**, *52*, 3626–3629.
- [40] *Guidelines for drinking-water quality, 2nd ed. Vol. 2. Health criteria and other supporting information.*, World Health Organization, Geneva, **1996**.
- [41] J. H. Scofield, *J. Elec. Spec. Rel. Phen.* **1976**, *8*, 129–137.
- [42] M. L. Deb, P. J. Bhuyan, *Tetrahedron Lett.* **2005**, *46*, 6453–6456.
- [43] Y.-J. Lin, B.-K. Tsai, C.-J. Tu, J. Jeng, C.-C. Chu, *Tetrahedron* **2013**, *69*, 1801–1807.

## 2 Synthesis and application of magnetic Noyori-type ruthenium catalysts for asymmetric transfer hydrogenation reactions in water<sup>i</sup>



A Noyori-type ruthenium catalyst was immobilized on magnetic platforms consisting of carbon-coated cobalt nanoparticles and different polymers. Both reactivity and enantioselectivity of these catalysts were benchmarked in the asymmetric transfer hydrogenation of acetophenone in an aqueous medium. The best catalyst, having connected the ruthenium catalyst to the nanoparticle by a poly(styrene) matrix, was characterized by infrared (IR) spectroscopy and a superconducting quantum interference device (SQUID) to determine the saturation magnetization of the magnetic material, as well as by transmission electron microscopy (TEM) and energy-dispersive X-ray spectroscopy (EDX). A variety of aryl methyl ketones could be reduced to their corresponding alcohols with good yields (81–100%) and selectivity (91–99% *ee*). Catalyst recovery and reuse was evaluated over 10 runs with ruthenium leaching into the product of <10 ppm, meeting the pharmaceutical requirements for ruthenium impurities of orally available drugs.<sup>ii</sup>

<sup>i</sup> Reprinted and adapted with permission of The American Chemical Society: C. M. Eichenseer, B. Kastl, M. A. Pericàs, P. R. Hanson, O. Reiser, *ACS Sustainable Chem. Eng.* **2016**, DOI 10.1021/acssuschemeng.6b00197. Copyright © 2016 The American Chemical Society.

<sup>ii</sup> Magnetization measurements were done by H. Körner. All other experiments and studies were performed by C. M. Eichenseer. A part of the work was done at the laboratories of M. A. Pericàs at ICIQ in Tarragona, Spain.

## 2.1 Introduction

The asymmetric transfer hydrogenation (ATH) of prochiral ketones to optically active secondary alcohols has been of great importance for decades. Besides excellent selectivities and yields that are generally obtained, the high tolerance toward a large number of solvents as well as the application of nonhazardous hydrogen sources, such as triethylamine and formic acid mixtures or *i*PrOH in an alkaline base systems, are the key advantages in this transformation. Chiral transition metal complexes based on iridium, rhodium, or ruthenium have been most widely used<sup>[1]</sup>, although more recently iron catalysts,<sup>[2–5]</sup> especially those of Morris *et al.*,<sup>[2–4]</sup> have also been shown to be very promising for ATH processes. Arguably the most successful and widely used ATH catalyst is Ru-TsDPEN **44** (ruthenium *N*-(*p*-toluenesulfonyl)-1,2-diphenylethylenediamine) developed by Noyori, Ikariya and co-workers (Figure 14).<sup>[6]</sup>

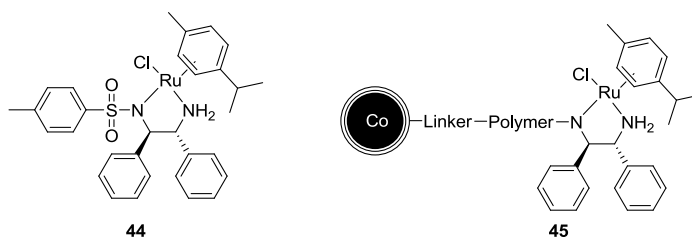


**Figure 14.** Ru-TsDPEN **44** and Noyori-type catalyst immobilized on carbon-coated cobalt nanoparticles **45**.

As ruthenium, while still being comparatively inexpensive, is more scarce than gold (4 times by weight, 2 times by mol)<sup>[7]</sup> and many of its complexes are regarded as toxic and as carcinogenic,<sup>[8]</sup> the recycling of the catalyst as well as its removal down to ppb levels from a reaction mixture is highly desirable. The recovery of a homogeneous catalyst as well as the purification of the products often requires methods like filtration, centrifugation, or extraction, but even then complete removal can be difficult. Moreover, such workup is tedious and energy-consuming, and therefore posing a great disadvantage, especially for industrial applications. Furthermore, the catalytically active ruthenium metal hydride species generated in the course of the ATH is sensitive toward air, rendering isolation even more difficult.<sup>[9]</sup> To circumvent these problems, a large number of heterogeneous variants of **44** were developed utilizing different supports such as polymers,<sup>[10,11]</sup> ionic liquids,<sup>[12]</sup> dendrimers,<sup>[13]</sup> inorganic materials (like silica or Fe<sub>3</sub>O<sub>4</sub> nanoparticles),<sup>[9,14,15,16]</sup> or organic/inorganic hybrid<sup>[17,18]</sup> materials. Yet, all of these supports suffer from several drawbacks. Anchoring a catalyst to ionic liquids or dendrimers, for

example, makes an extraction step necessary for the recycling of the catalyst. When using a heterogeneous support such as polystyrene resins, unsatisfactory swelling properties limit the choice of solvents possible for a reaction, generally ruling out water. Moreover, their low mechanical robustness does not allow agitation of a reaction mixture by conventional stirring.

Magnetic nanoparticles are increasingly recognized as promising platforms for catalysts<sup>[19]</sup> and have also been developed in combination with ruthenium nanoparticles for non-stereoselective transfer hydrogenations.<sup>[20]</sup> The obvious advantage of these kind of materials is their facile manipulation by external magnets that allows facile agitation or decantation from the reaction solution. Among those, carbon-coated cobalt nanoparticles (20–50 nm) developed by Stark *et al.*<sup>[21]</sup> have been shown to be promising starting points for the synthesis of magnetic catalysts.<sup>[22]</sup> Due to their facile preparation in bulk, high mechanical robustness, surface to volume ratio and stability against temperature (up to 160 °C) as well as pH (4–11), they are superior against other types of materials. Additionally, their advantages are the availability of several methods for the functionalization of their carbon surface and their high magnetization (130 emu/g); the latter being especially significant when nonmagnetic polymers are grown on their surface, thus greatly reducing the overall magnetization.

Herein, the development of magnetic ATH catalysts of type **45** is described, immobilized on iron oxide nanoparticles as well as on organic/inorganic hybrids consisting of carbon-coated cobalt nanoparticles (Co/C) and different organic polymers, aiming at a recoverable and reusable system which allows the asymmetric transfer hydrogenation (ATH) of aromatic ketones while not requiring further addition of surfactants.

## 2.2 Results and discussion

For preliminary studies, two different types of nanomaterial were functionalized with a Noyori-type ruthenium catalyst. As a first approach, iron oxide nanoparticles were synthesized by thermal decomposition of Fe(III)acetylacetonate in the presence of oleic acid and oleylamine as surfactants.<sup>[23,24]</sup> This procedure gave spherical, well-defined and monodisperse NPs **49** with a small diameter (Figure 15 A and B) which should then be functionalized with 3-(trimethoxysilyl)propane-1-thiol **46**.

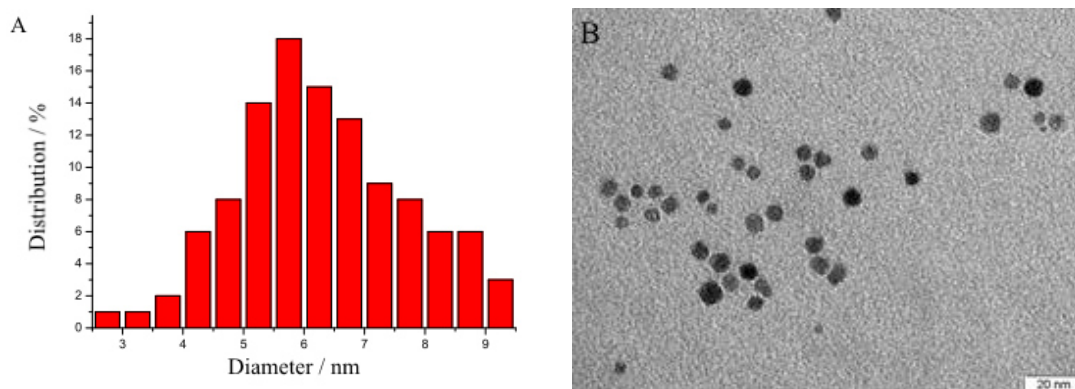
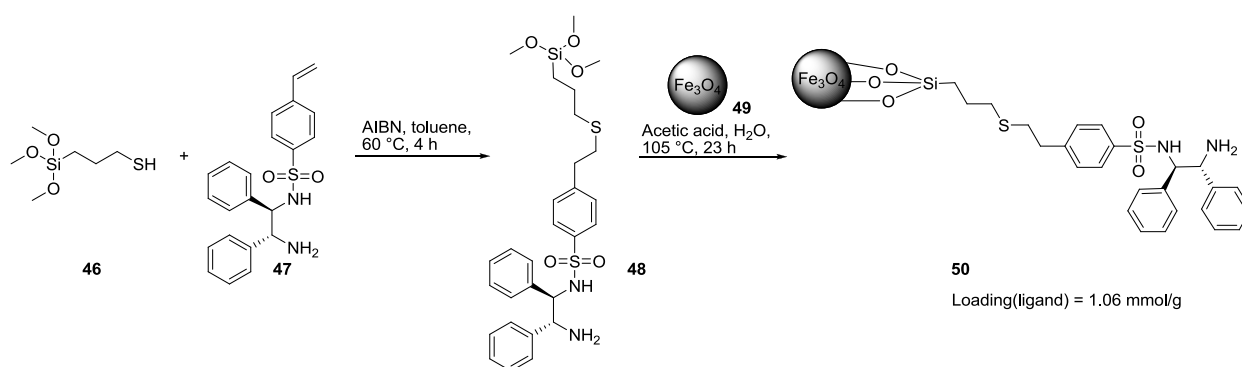


**Figure 15.** (A) Size distribution of magnetic Fe<sub>3</sub>O<sub>4</sub> nanoparticles **49** determined by TEM. (B) TEM picture of Fe<sub>3</sub>O<sub>4</sub> NPs **49**.

However, the thiol moiety of **46** might be unstable under the reaction conditions. This is why **46** was first coupled in a thiol-ene reaction with chiral 1,2-diamine ligand **47** to give diamine **48** which was then reacted *in situ* with the Fe<sub>3</sub>O<sub>4</sub> nanoparticles (NPs) **49** (Scheme 12). Characterization by elemental analysis revealed a loading of 1.06 mmol ligand per gram particles, which is equal to 18% of the maximal theoretical value, calculated based on the employed amount of diamine **48** (5.9 mmol/g).

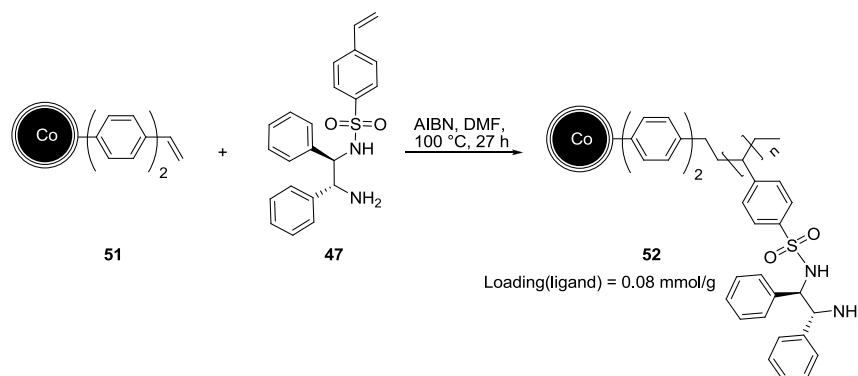


**Scheme 12.** Immobilization of ligand **47** on magnetic NPs **49**.

Furthermore, the Noyori-type ruthenium catalyst should be immobilized on magnetic carbon-coated cobalt nanoparticles by radical polymerization between NPs **51** and chiral 1,2-diamine ligand **47** (ratio 1:30) giving **52** (Scheme 13). The loading was determined by elemental analysis to be 0.08 mmol diamine ligand per gram of nanoparticles. Unfortunately, the polymerization yield on the NPs was very low (2% of the maximal theoretical loading), as



monomer **47** preferably formed a homopolymer under the applied reaction conditions. Since this ineffective polymerization reaction is not a desirable route, another strategy had to be developed.



**Scheme 13.** Radical polymerization between NPs **51** and chiral 1,2-diamine **47** (ratio 1:30) yielding the immobilized ligand **52**.

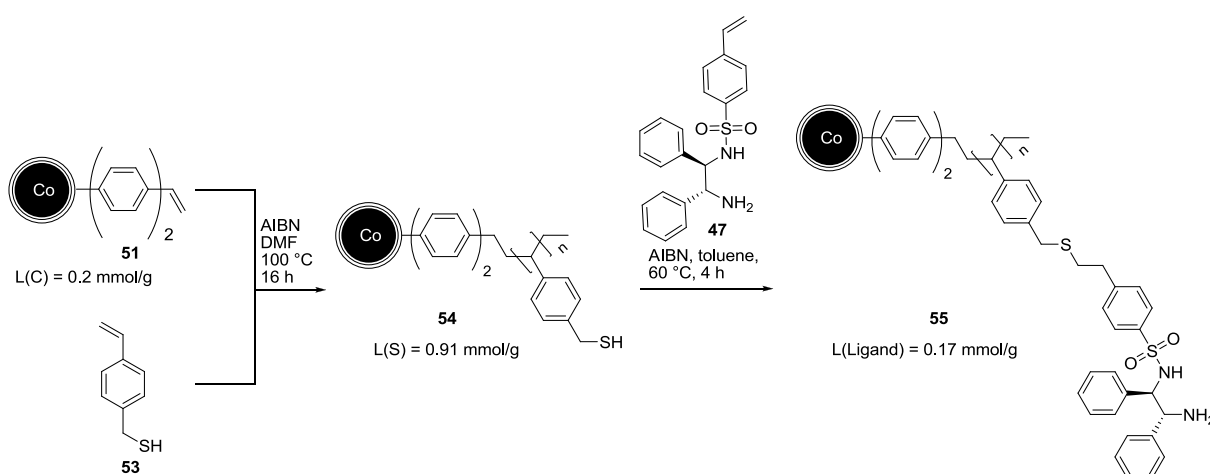
The immobilized ligands **50** and **52** were tested in the ATH of acetophenone following the reaction conditions published by Pericàs *et al.*<sup>[10]</sup> The catalyst was formed *in situ* by complexing the immobilized ligands **50** and **52** with ruthenium, giving the active catalysts **Ru-50** and **Ru-52**. In addition to 0.6 mol% of catalyst **Ru-50** and **Ru-52**, a 5:2 mixture of formic acid and triethylamine was required as hydrogen source. The reaction time was set to 24 h, after which yield and enantioselectivity of the product were determined by chiral GC analysis with *n*-dodecane as internal standard. Catalyst **Ru-50** gave the product in 82% yield with 96% *ee*, although the NPs formed a stable dispersion in DCM. This means they could not be collected anymore with an external magnet rendering a potential recycling process impossible. In contrary, catalyst **Ru-52** could be collected within seconds with a magnet, however, the catalyst's activity is lower compared to **Ru-50** as the product was formed in a yield of 63% with 90% *ee*. Luckily, the enantiomeric excess was in both cases high ( $\geq 90\%$ ). All in all, catalyst **Ru-50** showed a higher activity but it was not recyclable while the activity of catalyst **Ru-52** required optimization. Based on these findings, carbon-coated cobalt nanoparticles seem to be the better support for the immobilization of a Noyori-type ruthenium catalyst. In the following, it will be focused on different functionalization strategies of Co/C in order to improve the catalyst's activity. Furthermore, the reaction conditions were changed hereafter to avoid DCM as solvent. In contrast to DCM, water is an environmentally friendly, non-toxic and inexpensive solvent. On the one hand, its application in catalysis has a positive ecological and economic impact and on the other hand, it is known to accelerate ATH reactions.<sup>[25]</sup> A catalytic system for the ATH of aromatic ketones in water is developed, which does not require further addition of surfactants.



### Preparation of magnetically retrievable catalysts on carbon-coated cobalt nanobeads

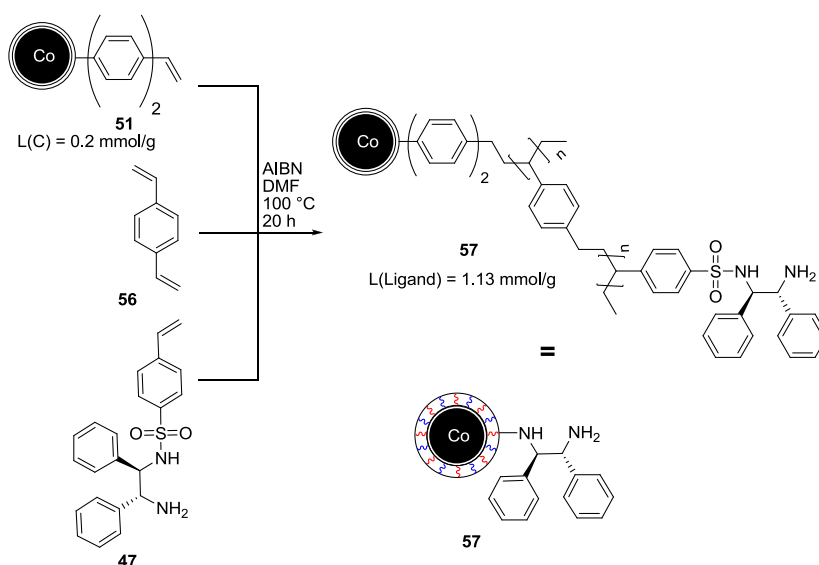
Different routes for the immobilization of the Noyori-type complex **45** varying the polymer and the linker connection with carbon-coated cobalt nanobeads were studied. In all cases, the chiral (1*R*,2*R*)-1,2-diphenylethane-1,2-diamine ligands with the core structure **44** were covalently anchored to the particles. Subsequently, the active catalyst was prepared *in situ* by complexation of the immobilized ligand with  $[\text{RuCl}_2(p\text{-cymene})]_2$ , followed by the addition of the reagents and substrate for the ATH.

In order to grow polystyrene-type polymers onto the carbon-coated nanobeads (Scheme 14–16), diphenyl vinyl functionalized nanoparticles **51** were synthesized following a reported procedure.<sup>[26]</sup> Subsequently, **51** was further functionalized in a radical polymerization<sup>[27]</sup> using (4-vinylphenyl)methanethiol **53** as a monomer, leading to magnetic poly(benzylthiol) nanoparticles **54**. Finally, the vinyl substituted chiral (1*R*,2*R*)-1,2-diphenylethane-1,2-diamine **47** was attached *via* a thiol–ene reaction (Scheme 14).<sup>[28]</sup> By microelemental analysis, a loading of 0.17 mmol diamine per gram of nanomaterial **55** was determined, which means that 19% of the thiol groups in **54** were successfully substituted.



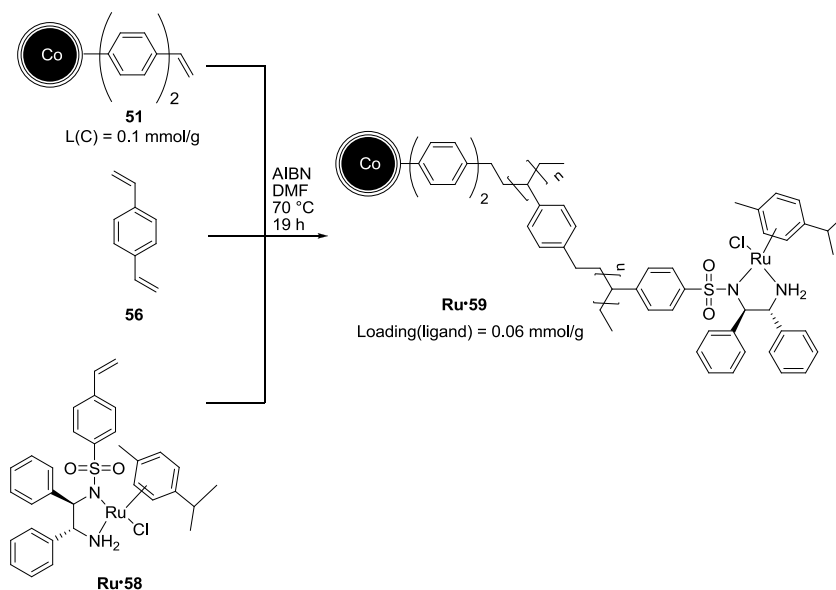
**Scheme 14.** Synthesis of immobilized ligand **55** by radical polymerization followed by thiol–ene reaction with 1.5 equivalents of diamine **47**.

Alternatively, a copolymerization between **51**, vinyl substituted (1*R*,2*R*)-1,2-diphenylethane-1,2-diamine ligand **47**, and divinylbenzene (DVB) **56**, which acted as the polymerization linker, in a ratio of 1:50:50 was performed to give Co/C nanoparticles **57** (Scheme 15). Again, the loading of the ligand was determined by elemental analysis: compared to nanomaterial **55**, a six times higher value of 1.13 mmol 1,2-diamine per gram was found.



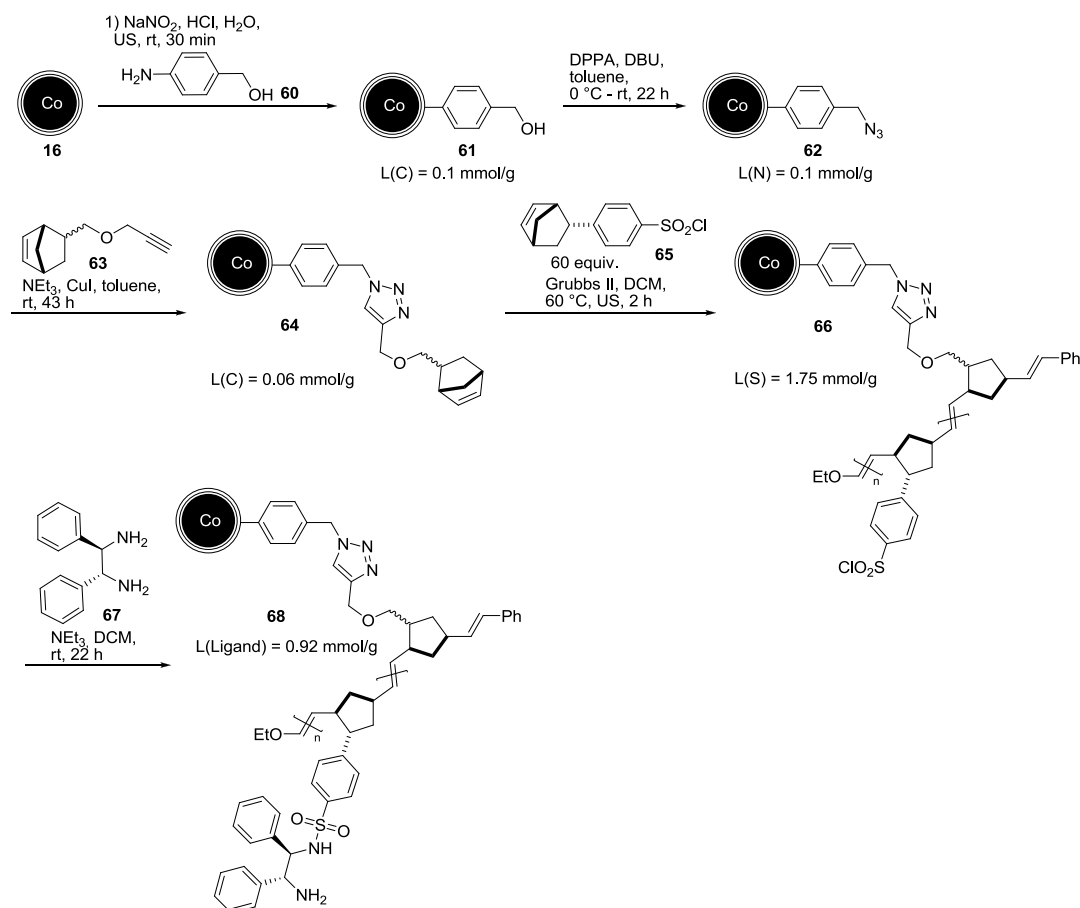
**Scheme 15.** Synthesis of immobilized ligand **57** by radical copolymerization between NPs **51**, DVB **56** and chiral 1,2-diamine ligand **47** (ratio 1:50:50).

The copolymerization approach was repeated with different monomers. Using nanoparticles **51**, the chiral 1,2-diamine ligand ruthenium complex **Ru-58** and DVB **56** in a ratio of 1:19:50, NPs **Ru-59** (Scheme 16) were synthesized. Noteworthy, the reaction temperature was lowered to  $70^\circ\text{C}$  as the Ru-complex **Ru-58** is labile at elevated temperatures. As before, the loading was determined by elemental analysis revealing that just  $0.06 \text{ mmol}$  ligand per gram of NPs had been attached. This low value demonstrated the polymerization with the 1,2-diamine ligand **47** was working more efficiently than with the vinyl substituted ruthenium complex **Ru-58** which might be due to altered electronic properties of **Ru-58** compared to the free ligand **47** and therefore, a different behavior in radical polymerization reactions. This finding confirmed that it is preparatively more sensible to form the ruthenium complex after attachment on the nanoparticles and directly prior to the reaction.



**Scheme 16.** Synthesis of immobilized ruthenium complex **Ru-59** by copolymerization between **51**, DVB **56** and diamine ruthenium complex **Ru-58** (ratio 1:50:19).

The third approach focused on a ring-opening metathesis polymerization (ROMP; Scheme 17). As the key component, norbornene tagged nanobeads **64** were synthesized following an adapted procedure from Hanson and Reiser *et al.*<sup>[29]</sup> Importantly, the conversion of benzyl alcohol **61** to the corresponding azide **62** could be conducted more conveniently using DPPA (diphenyl phosphorazidate<sup>[30]</sup>)/DBU rather than hazardous  $\text{HN}_3$  as reported previously. Arming **64** with a Grubbs-II metathesis catalyst, norbornyl tagged sulfonyl chloride **65** (60 equivalents) was ligated in a ROM polymerization to give rise to a magnetic gel **66** with free benzyl sulfonyl chloride moieties. Coupling of the chiral 1,2-diamine **67** under basic conditions led to the desired immobilized chiral ligand **68**, for which a loading of  $0.92 \text{ mmol}$  diamine ligand per gram of particles was determined by elemental analysis.



**Scheme 17.** Synthesis of immobilized ligand **68** by ROM polymerization.

### Comparison of catalytic activity

Having these immobilized ligands **55** (0.17 mmol/g), **57** (1.13 mmol/g), and **68** (0.92 mmol/g) as well as the immobilized catalyst **Ru-59** (0.06 mmol/g) in hand, the catalytic activity of the corresponding ruthenium complexes was evaluated (Figure 16). In a model reaction, acetophenone was used as substrate for the asymmetric transfer hydrogenation in water applying 1 mol% of the ruthenium complexes **Ru-55**, **Ru-57**, **Ru-59**, and **Ru-68**, which were prepared *in situ* by treating **55**, **57**, and **68** with  $[\text{RuCl}_2(p\text{-cymene})]_2$ , whereas **Ru-59** was already the active ruthenium complex. As hydrogen source a nonhazardous and safe mixture of triethylamine and formic acid was applied. Aiming for a fast and efficient process, the temperature was initially set at  $40^\circ\text{C}$ , and the reaction was stopped after three hours by collecting the catalyst with an external magnet and decanting the reaction solution, followed by chiral GC analysis with *n*-dodecane as an internal standard. While all catalysts displayed high enantioselectivities ( $\geq 94\% ee$ ), catalyst **Ru-68**, having connected the ruthenium catalyst to the nanoparticle by a

ROMP polymer, is the least active (Figure 16), which might be due to its poor dispersibility in water. Catalyst **Ru•59** gave the product also in poor yield (38%) which is probably caused by deactivation of the pre-formed ruthenium complex. In contrast, catalyst **Ru•55** and **Ru•57**, having a poly(styrene) matrix, displayed about twice the activity. Since in **Ru•57** a 10-fold higher loading can be achieved compared to **Ru•55**, this magnetic material is considered the best catalyst and was therefore further characterized and evaluated.

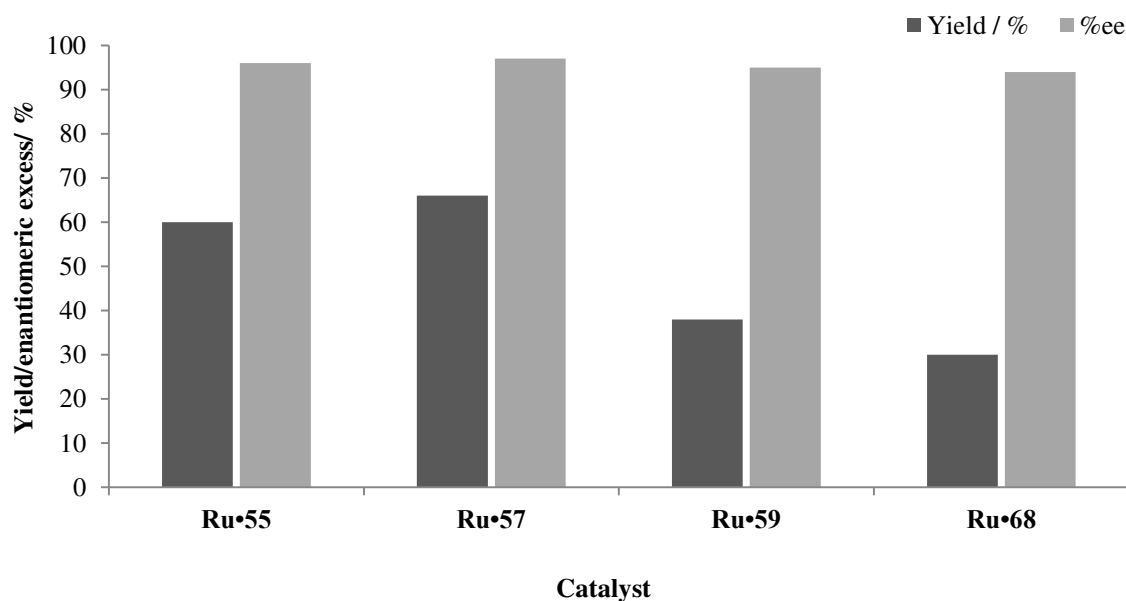


**Figure 16.** Comparison of different catalysts in the asymmetric transfer hydrogenation. Conditions: 1 mol% active catalyst, 1 mmol acetophenone, formic acid/triethylamine 3.3/2.7 mmol, water, 3 h, 40 °C.

### Characterization of the magnetic ligand **57** and catalyst **Ru•57**

The attenuated total reflectance (ATR) infrared (IR) spectrum for the immobilized ligand **57** (Figure 17, bottom) is similar to that of the nonimmobilized ligand **47** and especially shows the characteristic vibrations for SO<sub>2</sub>N groups at 1150 and 1300 cm<sup>-1</sup>, revealing the successful anchoring of the ligand to the nanoparticles.

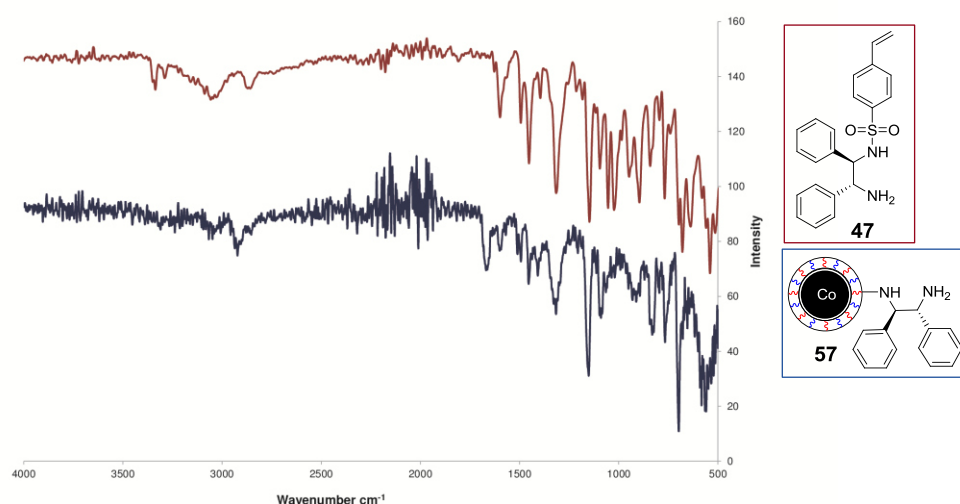


**Figure 17.** IR spectra of free ligand **47** (top, in red) and immobilized ligand **57** (bottom, in blue).

For **57**, a magnetization of 30 emu/g was measured *via* a superconducting quantum interference device (SQUID). This is lower than that of unfunctionalized carbon-coated cobalt nanoparticles **16** (130 emu/g, Figure 18, red), attesting to the successful attachment of the polymer, which shields the magnetic core and therefore reduces its magnetization. Nevertheless, magnetization of **57** is much higher than that of analogous polymer embedded nanoparticles based on magnetite and allows its fast collection with the help of an external magnet.

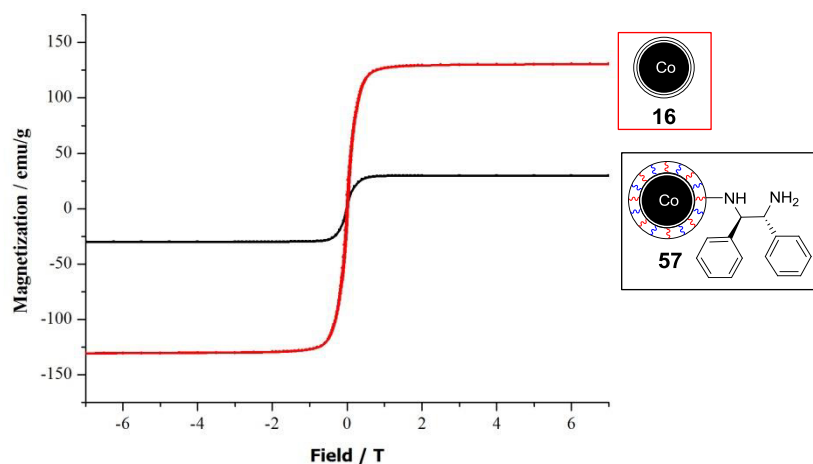


**Figure 18.** Saturation magnetization at 290 K of naked Co/C nanoparticles **16** (red) and diamine ligand immobilized on Co/C **57** (black).

For the transfer hydrogenations performed with nanoparticles **57**, the active ruthenium catalyst **Ru·57** was prepared *in situ via* complexation. On account of characterization, the catalyst was also isolated by treating **57** with  $[\text{RuCl}_2(p\text{-cymene})]_2$  (0.01 mmol Ru, 0.83 equiv.) followed by collecting **Ru·57** with the aid of a magnet. ICP-OES analysis showed 80% incorporation of Ru (0.008 mmol). TEM analysis (Figure 19 A) of the nanoparticles **Ru·57** revealed that the magnetic nanobeads (visible as black dots) are incorporated into the polymer (greyish diffuse structure). Energy-dispersive X-ray spectroscopy (EDX) allowed the visualization of the major elements present, showing an even distribution of ruthenium across the polymer network (Figure 19 B and D), while the magnetic cobalt particles serve as the anchor point for the polymer matrix (Figure 19 B and C).

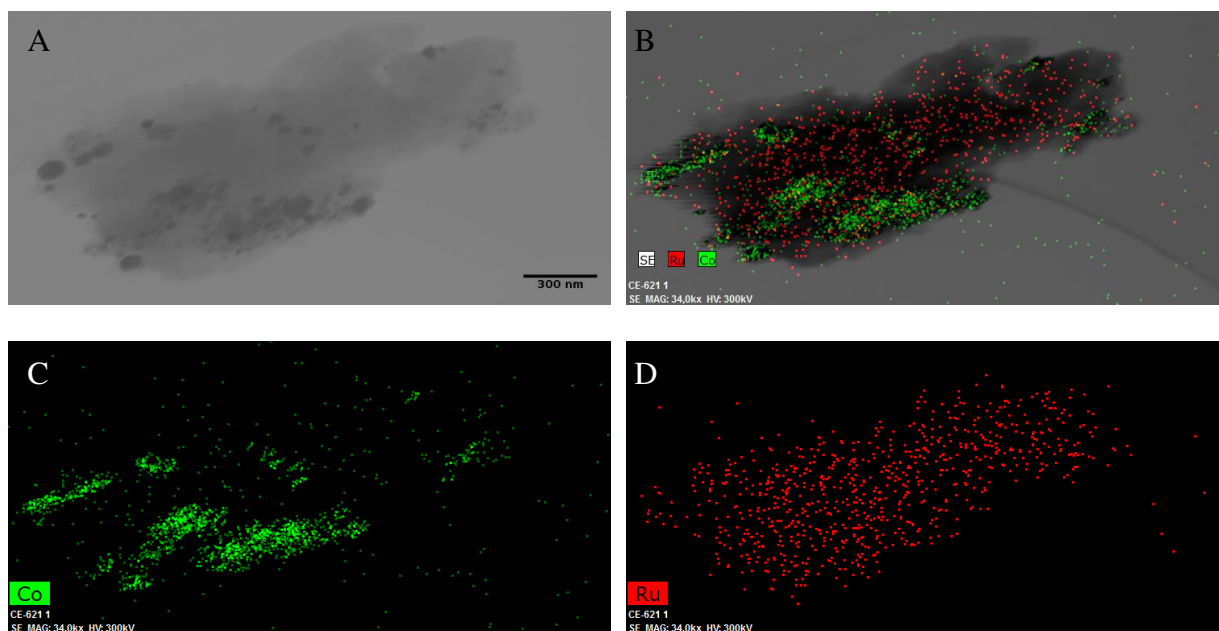
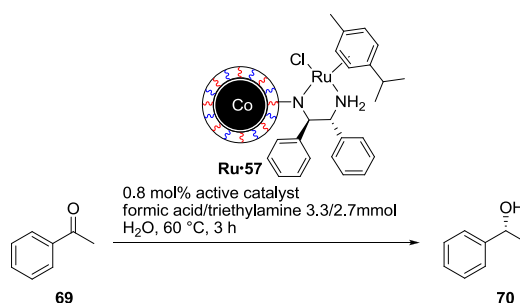


**Figure 19.** (A) TEM picture of Co/C in a polymeric network (catalyst **Ru·57**). (B) Element mapping by EDX for ruthenium (red) and cobalt (green). (C) Element mapping for Co. (D) Element mapping for Ru.

### Catalytic Performance in the asymmetric transfer hydrogenation

Next, we explored the scope and limitation of catalyst **Ru·57** in asymmetric transfer hydrogenations. Gratifyingly, increasing the reaction temperature from 40 °C to 60 °C only resulted in a slight drop of enantioselectivity (from 97 to 94% *ee*) but significantly accelerated the reaction. Thus, using 0.8 mol% of catalyst **Ru·57**, the asymmetric transfer hydrogenation of

acetophenone **69** in water was complete within three hours and 1-phenyl ethanol **70** could be isolated in 99% yield with 94% *ee* (Scheme 18).

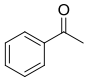
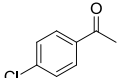
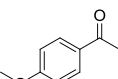
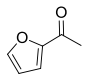
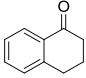
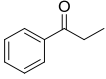
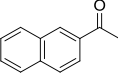
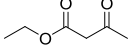


**Scheme 18.** ATH of acetophenone **69** using catalyst **Ru-57**.

Under these reaction conditions, different aromatic ketones were tested (Table 2). In all cases, the corresponding alcohols were obtained in high yields and enantioselectivities. Electron-rich (Table 2, entries 3–4), electron-neutral (Table 2, entries 1 and 5–7) as well as electron-poor (Table 2, entry 2) acetophenones can be employed with equally good results. Substitution of the phenyl moiety by furyl (Table 2, entry 4) or naphthyl (entry 7) as well as replacing methyl by other alkyl substituents (entries 5, 6) were also well tolerated. The nonaromatic substrate ethyl 3-oxobutanoate (entry 8) could be isolated in 63% yield after just 30 min, however, the enantiomeric excess is quite low with only 10% indicating that the interaction of this substrate, which is comparatively small, with the chiral catalyst **Ru-57** is relatively weak.



**Table 2.** Asymmetric transfer hydrogenation of substituted ketones with catalyst **Ru-57** in water.

Entry	Substrate	Yield <sup>[a]</sup> [%]	Enantiomeric excess <sup>[a]</sup> [%]
1		100	94
2		100	92
3		90 <sup>[b]</sup>	94
4		91	99
5		98	92
6		81	91
7		100	95
8 <sup>[c]</sup>		63 <sup>[b]</sup>	10 <sup>[d]</sup>

<sup>[a]</sup> Determined by chiral GC analysis using an internal standard.<sup>[b]</sup> Isolated yield.<sup>[c]</sup> Reaction time is just 30 min.<sup>[d]</sup> Determined by chiral GC analysis after derivatization by acetylation.

Catalyst **Ru-57** can be recovered quantitatively by a fast and efficient magnetic decantation while the product remains in the aqueous solution. The latter can be isolated by extraction with diethyl ether, yielding the pure product without the need for further purification. Recyclability of catalyst **Ru-57** was tested in 10 sequential runs, showing consistently high enantioselectivities, whereas a gradual decrease in yield was observed after the sixth run (Figure 20). On the basis of ICP-OES measurements, Ru leaching into the aqueous phase was low and varied between 15 and 100 ppm (over 10 runs 6% of the initially employed Ru leached into the aqueous phase). Therefore, it can be concluded that a deactivation of the catalyst is responsible for the decrease in activity. After extracting the aqueous phase with ether and isolating the products by concentration of the organic phase, ruthenium contamination of the product between 0.8 and 3.3 ppm was measured, being beyond the threshold of 10 ppm that is recommended as contamination in oral drugs according to the European Medicines Agency.<sup>[31]</sup> It should be

stressed that all of these measurements were done without any chromatographic workup in the course of the reaction, which would have reduced the ruthenium level even further.

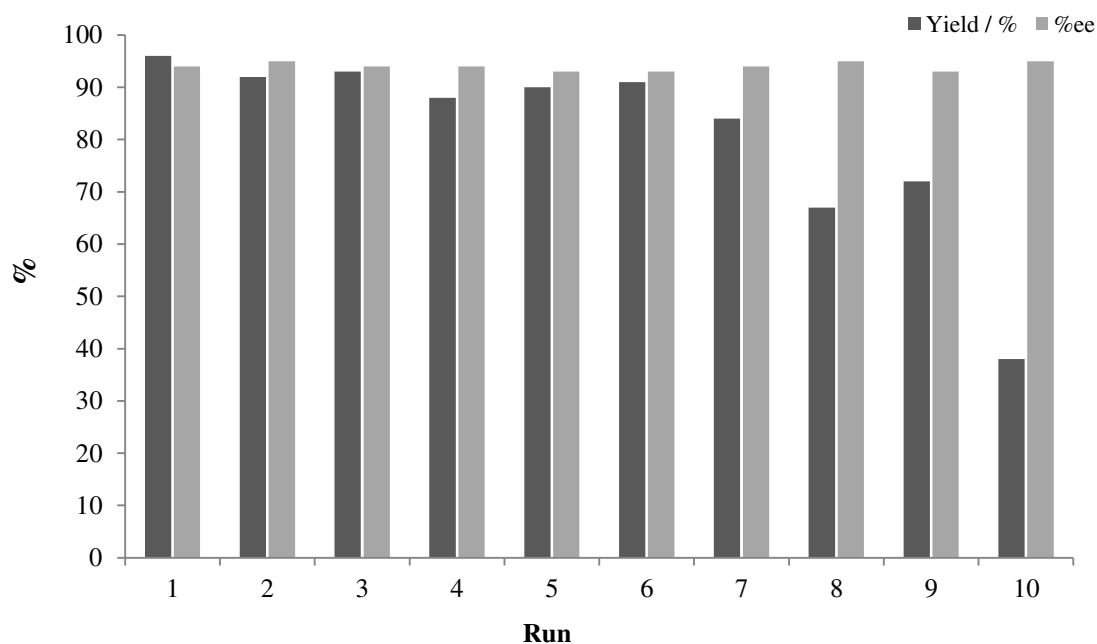


**Figure 20.** Recycling of catalyst **Ru-57** in the asymmetric transfer hydrogenation of acetophenone **69**. Conditions: 1 mmol acetophenone, 0.8 mol% catalyst **Ru-57**, formic acid/triethylamine 3.3/2.7 mmol, water, 60 °C, 3 h.

## 2.3 Conclusion

In conclusion, a Noyori-type catalyst has been successfully immobilized on carbon-coated cobalt nanoparticles. Three different polymer matrices that served as a bridge between the magnetic nanoparticles and the ruthenium catalyst were evaluated. Best results with respect to loading and activity were found when the ruthenium catalyst possessing a vinyl group in the organic ligand framework was attached *via* copolymerization with divinylbenzene to vinylbenzene functionalized carbon-coated cobalt nanoparticles. The resulting catalyst showed high activity and selectivity in the asymmetric transfer hydrogenation of various ketones and could be recovered and directly reused without further reactivation treatment in ten consecutive runs, taking advantage of the magnetic properties of the material. The catalyses could be carried out in water as an environmentally friendly solvent; notably, no further additives like a detergent have to be employed, contrasting other immobilized catalysts that are reported for applications in aqueous media.<sup>[9,14,16,32,33]</sup> Finally, formic acid/triethylamine as nonhazardous hydrogen source and ruthenium as a comparatively inexpensive metal, as opposed to rhodium that was previously

often utilized in magnetic nanoparticle supported transfer hydrogenation catalysts,<sup>[16,17,33]</sup> can be readily applied.

## 2.4 Experimental section

### Materials and methods

Reactions with moisture and oxygen sensitive reagents were performed in flame dried glassware under an atmosphere of pre-dried nitrogen or argon. Heavy-wall glass tubes or heavy-wall Schlenk flasks are borosilicate glass tubes which are stable up to 5 bar. Column chromatography was performed with silica gel (Merck, Geduran 60, 0.063–0.200 mm particles size). Thin layer chromatography was performed with TLC pre-coated aluminum sheets (Merck silica gel 60 F<sub>254</sub> or Macherey-Nagel ALUGRAM<sup>®</sup> Xtra Sil G/UV<sub>254</sub>, 0.2 mm layer thickness). Visualization was accomplished with UV light ( $\lambda = 254$  nm or 366 nm) and stained with Vanillin/sulfuric acid or basic potassium permanganate. NMR spectra were recorded on BRUKER Avance 400 and BRUKER Avance 300 spectrometer. All spectra were recorded in CDCl<sub>3</sub> or commercially available deuterated solvents. Chemical shifts are reported as  $\delta$ , parts per million, calibrated to the signal of the solvent. The coupling constants  $J$  are reported in Hertz (Hz). Splitting patterns for the spin multiplicity in the spectra are given as follows: s = singlet, bs = broad singlet, d = doublet, t = triplet, q = quartet, dd = doublet of a doublet, ddd = doublet of a doublet of a doublet, dt = doublet of a triplet, qd = quartet of a doublet, m = multiplet. Attenuated total reflection infrared spectroscopy (ATR-IR) was carried out on a Varian FTS 1000 spectrometer (equipped with a Specac Golden Gate Diamond Single Reflection ATR-System), a Cary 630 FT-IR (Agilent Technologies), a Bruker Optics FT-IR Alpha spectrometer, a Varian 800 FT-IR Scimitar Series or a Thermo Nicolet 5700 FTIR spectrometer. Solid as well as liquid compounds were measured neat or as KBr pellets and wave numbers are reported as cm<sup>-1</sup>. Mass spectrometry was performed using a Finnigan ThermoQuest TSQ 7000 at the Central Analytical Laboratory (University of Regensburg). Chiral gas chromatography was performed on a Fisons GC 8000. CP-Chirasil-Dex CB (25 m x 0.25 mm, 0.25  $\mu$ m film, injection temperature 250 °C, detector temperature 250 °C, P = 100 kPa He gas) was used as chiral stationary phase. Furthermore, chiral gas chromatography was measured on an Agilent 6890N Series equipped with a Chiraldex G-TA column (30 m x 0.25 mm, 0.12  $\mu$ m). The optical rotation of optically active compounds was measured in the specified solvent on an Anton Paar MCP 500 at 589 nm (sodium-*d*-line) in a 1 dm measuring cell. Samples for the inductively coupled plasma optical emission spectrometry (ICP-OES) were measured on a SpectroFlame EOP (Spectro) in an acidic medium (aqua regia 32% (v/v)). Elemental microanalysis was performed by the micro analytical section of the University of Regensburg using a Vario MICRO cube or Titrino plus 848 and by MEDEC Ltd. For transmission electron microscopy an FEI TecnaiF30 was used, for element mapping a

Bruker QUANTAX-EDX was utilized (Department of Physics, University of Regensburg). Furthermore, TEM images were recorded using a JEOL JEM 1011 operating at an acceleration voltage of 100 kV and equipped with an SIS Megaview III CCD camera (Microscopy Units, Universitat Rovira i Virgili, Tarragona, Spain). The saturation magnetization of magnetic samples was measured by superconducting quantum interference device (SQUID) magnetometry analysis on an MPMS XL from Quantum Design. Nanoparticles were dispersed in an ultrasonic bath (Bandelin Sonorex RK255 H-R) and recovered with the aid of a neodymium based magnet (side length 12 mm).

### Nanoparticle preparation

Carbon-coated cobalt nanoparticles (Co/C, mean particle size  $\approx 25$  nm) were obtained from Turbobeats Llc, Switzerland. Before usage the nanobeads were washed five times in a Millipore water/HCl<sub>conc</sub> mixture (10/1). To remove any residual acid the nanoparticles were washed with Millipore water until the pH of the decanted solution was neutral. Finally, the particles were washed with acetone (3x) and diethyl ether (2x) and dried at 50 °C under vacuum.<sup>[34]</sup>

### Nomenclature

For the nanoparticles in this chapter the nomenclature is as follows: Co/C for magnetic carbon-coated cobalt nanoparticles with cobalt core and graphene-like shells, Co/C-diamine for Co/C nanobeads functionalized with the chiral 1,2-diamine, Co/C-Copolymerization-diamine for nanobeads which were functionalized by copolymerization bearing the chiral 1,2-diamine moieties on the surface, Co/C-thiol-ene-diamine for particles which were functionalized with the chiral 1,2-diamine *via* thiol-ene reaction and Co/C-ROMP-diamine for Co/C nanobeads with the chiral 1,2-diamine on the surface which was introduced by ring-opening-metathesis polymerization.

### Fe<sub>3</sub>O<sub>4</sub> nanoparticles (49)<sup>[23]</sup>

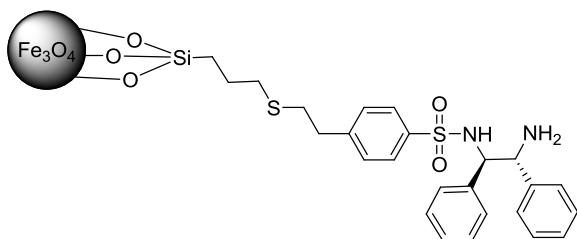


A two-neck flask was charged with iron(III)acetylacetonate (1.8 g, 5 mmol, 1 equiv.), 1,2-dodecanediol (5.6 g, 25 mmol, 5 equiv.) and oleic acid (4.7 g, 15 mmol, 3 equiv.). Subsequently, oleylamine (7 mL, 15 mmol, 3 equiv.) and dibenzyl ether (20 mL) were added and the mixture was heated to 260 °C for 3 h. Afterwards, the reaction was allowed to warm to room

temperature. MeOH was added to precipitate the nanoparticles which were collected with the help of a magnet. The supernatant solution was decanted and the particles were washed with MeOH (4x20 mL) and acetone (3x20 mL). Drying under vacuum (30 °C, 20 h) gave 480 mg of the desired Fe<sub>3</sub>O<sub>4</sub> nanoparticles.

**IR** (KBr,  $\tilde{\nu}/\text{cm}^{-1}$ ): 3440, 2962, 2920, 2848, 1648, 1407, 1065, 606; **elemental microanalysis** [%]: C, 14.06; H, 2.47; N, 0; Si, 1.49.

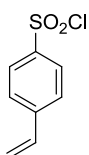
***N*-((1*R*,2*R*)-2-amino-1,2-diphenylethyl)-4-(2-(3-silylpropylthio)ethyl)benzenesulfonamide functionalized Fe<sub>3</sub>O<sub>4</sub> nanoparticles (**50**)**



(*R,R*)-1,2-diamine ligand (352 mg, 0.929 mmol, 1.05 equiv.) was dissolved in degassed toluene (3.75 mL) under argon atmosphere. Subsequently, 3-(trimethoxysilyl)propane-1-thiol (164  $\mu\text{L}$ , 0.885 mmol, 1 equiv.) and AIBN (4.6 mg, 0.028 mol, 4 mol%) were added and the resulting solution was stirred at 60 °C for 4 h. After cooling down to room temperature, Fe<sub>3</sub>O<sub>4</sub> nanoparticles (150 mg) as well as acetic acid (19  $\mu\text{L}$ , 0.33 mmol) and Millipore water (26  $\mu\text{L}$ , 1.45 mmol) were added. The slurry was stirred at 105 °C for 23 h. Afterwards, the nanobeads were collected magnetically, the supernatant was decanted and the particles were washed with diethyl ether (3x3 mL), DCM (1x3 mL) and diethyl ether (1x3 mL). Drying *in vacuo* yielded 500 mg NPs **50**.

**IR** (KBr,  $\tilde{\nu}/\text{cm}^{-1}$ ): 3451, 2922, 2852, 1660, 1597, 1550, 1494, 1450, 1407, 1327, 1249, 1158, 1091, 1057, 764, 700, 673, 657, 642, 628, 612, 598, 583; **elemental microanalysis** [%]: C, 39.25; H, 3.80; N, 2.96; Si, 4.10; S, 9.62 - **loading** (N) 1.06 mmol/g.

**4-Vinylbenzene-1-sulfonyl chloride (**71**)**<sup>[35]</sup>

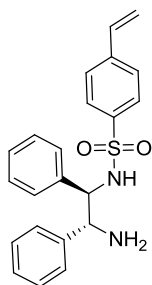


In a Schlenk flask, sodium 4-vinylbenzenesulfonate (8.34 g, 38.8 mmol, 1.0 equiv.) was suspended in anhydrous DMF (38 mL) under nitrogen atmosphere and cooled to 0 °C. After

dropwise addition of thionyl chloride (16.0 mL, 26.22 g, 220.4 mmol, 5.7 equiv.) at 0 °C the mixture was allowed to warm to room temperature and stirred for 24 h. The solution was poured into ice and extracted with diethyl ether. The organic layers were washed with brine, dried over MgSO<sub>4</sub>, filtered and evaporated. The crude product was purified by column chromatography eluting with DCM to yield the product as clear, colorless oil (4.33 g, 21.3 mmol, 55%).

$R_f$  = 0.98 (DCM);  $^1\text{H NMR}$  (300 MHz, CDCl<sub>3</sub>):  $\delta_{\text{H}}$  = 8.06 – 7.91 (m, 2H), 7.70 – 7.49 (m, 2H), 6.79 (dd,  $J$  = 17.6, 10.9 Hz, 1H), 5.97 (d,  $J$  = 17.6 Hz, 1H), 5.54 (d,  $J$  = 10.9 Hz, 1H);  $^{13}\text{C NMR}$  (75 MHz, CDCl<sub>3</sub>):  $\delta_{\text{C}}$  = 144.6, 143.1, 134.9, 127.6, 127.3, 119.5;  $\text{IR}$  (neat,  $\tilde{\nu}/\text{cm}^{-1}$ ): 3091, 3072, 3058, 1591, 1398, 1371, 1291, 1189, 1168, 1118, 1082, 1029, 988, 927, 843, 792, 738, 646, 557, 542.

***N*-((1*R*,2*R*)-2-amino-1,2-diphenylethyl)-4-vinylbenzenesulfonamide (47)**<sup>[36,37]</sup>

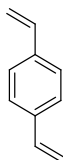


(1*R*,2*R*)-1,2-diphenylethane-1,2-diamine **67** (2.00 g, 9.43 mmol, 1.0 equiv.) was dissolved in anhydrous DCM (8 mL) and triethylamine (7.45 mL, 5.44 g, 53.7 mmol, 5.7 equiv.) under nitrogen atmosphere. The mixture was stirred for 20 min at room temperature before a solution of 4-vinylbenzene-1-sulfonyl chloride **71** (2.12 g, 10.6 mmol, 1.1 equiv.) in anhydrous DCM (6 mL) was added dropwise. The resulting mixture was stirred for 22 h at room temperature. After washing with sat. NaHCO<sub>3</sub> solution, the aqueous phase was extracted with DCM. The combined organic layers were dried over MgSO<sub>4</sub>, filtered and evaporated to yield 3.43 g of the crude product. Purification by column chromatography (hexanes/EtOAc 1:1) gave the product as white solid (2.60 g, 6.88 mmol, 73%).

$R_f$  = 0.10 (hexanes/EtOAc 1:1);  $[\alpha]_D^{20}$  - 39.7 ( $c$  = 1.0, CHCl<sub>3</sub>) (*R*) (lit. value<sup>[37]</sup>  $[\alpha]_D^{20}$  - 36.7 ( $c$  = 1.0, CHCl<sub>3</sub>) 96% *ee* (*R*));  $^1\text{H NMR}$  (300 MHz, DMSO-*d*<sub>6</sub>):  $\delta_{\text{H}}$  = 7.43 – 7.28 (m, 4H), 7.14 – 7.02 (m, 5H), 7.01 – 6.87 (m, 5H), 6.69 (dd,  $J$  = 17.7, 11.0 Hz, 1H), 5.88 (dd,  $J$  = 17.7, 0.6 Hz, 1H), 5.36 (d,  $J$  = 11.5 Hz, 1H), 4.32 (d,  $J$  = 7.4 Hz, 1H), 4.06 (bs, 2H), 3.94 (d,  $J$  = 7.4 Hz, 1H);  $^{13}\text{C NMR}$  (75 MHz, DMSO-*d*<sub>6</sub>):  $\delta_{\text{C}}$  = 142.6, 140.3, 140.1, 139.8, 135.5, 127.6, 127.4, 127.4, 127.3, 126.6, 126.5, 126.4, 126.1, 117.1, 64.9, 60.7;  $\text{IR}$  (neat,  $\tilde{\nu}/\text{cm}^{-1}$ ): 3336, 3290, 3052, 2871,

1627, 1598, 1494, 1452, 1395, 1315, 1214, 1148, 1095, 1054, 1023, 948, 896, 841, 768, 697, 679, 638; **LRMS** (ESI):  $m/z = 379.1489$   $[M+H]^+$ .

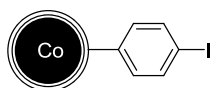
### 1,4-Divinylbenzene (**56**)<sup>[38]</sup>



In a Schlenk flask, methyltriphenylphosphonium bromide (12.79 g, 35.7 mmol, 2.4 equiv.) and KO<sup>t</sup>Bu (4.85 g, 43.2 mmol, 2.9 equiv.) were dissolved in anhydrous THF (20 mL). After cooling to 0 °C a solution of terephthalaldehyde (2.00 g, 14.9 mmol, 1 equiv.) in THF (20 mL) was added dropwise. The reaction solution was allowed to warm to rt and stirred further for 2 h. Afterwards, the mixture was poured into a separating funnel filled with 80 mL dest. water. The phases were separated and the aqueous phase was extracted with diethyl ether. The combined organic layers were dried over MgSO<sub>4</sub>, filtered and concentrated under vacuum. The byproduct triphenylphosphine oxid was precipitated by pouring the concentrated reaction solution into 60 mL hexanes and filtering off the precipitated solid before the solution was concentrated again. Further purification was accomplished by column chromatography eluting with pure hexanes. The desired product was isolated as white crystals (1.194 g, 9.17 mmol, 62%).

$R_f = 0.80$  (hexanes);  $^1\text{H NMR}$  (400 MHz, CDCl<sub>3</sub>):  $\delta_H = 7.39$  (s, 4H), 6.72 (dd,  $J = 17.6, 10.9$  Hz, 2H), 5.76 (d,  $J = 17.6$  Hz, 2H), 5.25 (d,  $J = 10.9$  Hz, 2H);  $^{13}\text{C NMR}$  (101 MHz, CDCl<sub>3</sub>):  $\delta_C = 137.3, 136.6, 126.5, 113.9$ .

### Iodo-phenyl functionalized Co/C nanoparticles (**72**)<sup>[26]</sup>



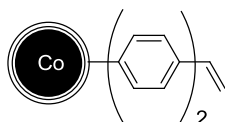
A round bottom flask was charged with Co/C nanobeads (500 mg), 4-iodoaniline (110 mg, 0.5 mmol), HCl<sub>conc</sub> (0.5 mL) and H<sub>2</sub>O (6.5 mL). The mixture was sonicated for 15 min before being cooled in an ice bath. Dropwise addition of a pre-cooled solution of NaNO<sub>2</sub> (52 mg, 0.75 mmol) in H<sub>2</sub>O (6.5 mL) led to the *in situ* generation of the diazonium species. The slurry was stirred another 30 min at 0 °C followed by further 30 min sonication to ensure complete addition. The particles were collected with the help of an external magnet and the supernatant was decanted. The nanobeads were washed with 1 M NaOH solution (4x10 mL), H<sub>2</sub>O



(4x10 mL), acetone (3x10 mL) and diethyl ether (2x10 mL) before being dried *in vacuo*, yielding 496 mg of **72**.

**IR** (KBr,  $\tilde{\nu}/\text{cm}^{-1}$ ): 3435, 2922, 2852, 1737, 1650, 1635, 1559, 1542, 1457, 1384; **elemental microanalysis** [%]: C, 8.08; H, 0.13; N, 0.1 - **loading** (C) 0.13 mmol/g.

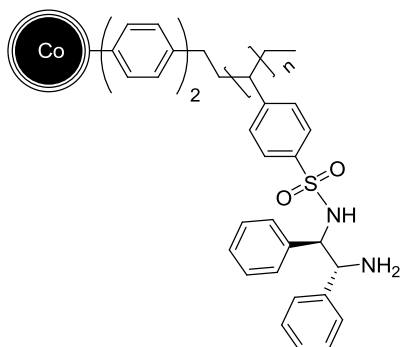
### Diphenyl-vinyl functionalized Co/C nanoparticles (**51**)<sup>[26]</sup>



Iodo-phenyl functionalized nanobeads **72** (485 mg, 0.063 mmol, 1 equiv.), 4-vinylphenylboronic acid (109 mg, 0.74 mmol, 11.7 equiv.),  $\text{Pd}(\text{OAc})_2$  (8.3 mg, 0.037 mmol, 0.6 equiv.), triphenylphosphine (27 mg, 0.1 mmol, 11.6 equiv.) and  $\text{Na}_2\text{CO}_3$  (86 mg, 0.81 mmol, 12.9 equiv.) were added to a Schlenk flask under nitrogen atmosphere. After addition of degassed  $\text{H}_2\text{O}$  (3.0 mL) and degassed *i*PrOH (3.0 mL) the mixture was refluxed at 95 °C for 16 h. Afterwards, the mixture was allowed to cool to room temperature before the particles were collected with a magnet. The supernatant was decanted and the nanobeads were washed with  $\text{H}_2\text{O}$  (3x6 mL), MeOH (2x6 mL), EtOAc (2x6 mL), pentane (1x6 mL) and acetone (3x6 mL). Drying *in vacuo* gave 477 mg of the particles **51**.

**IR** (KBr,  $\tilde{\nu}/\text{cm}^{-1}$ ): 3432, 2923, 2854, 1737, 1637, 1460, 1376; **elemental microanalysis** [%]: C, 10.65; H, 0.36; N, 0.06 - **loading** (C) 0.27 mmol/g.

### Poly(*N*-((1*R*,2*R*)-2-amino-1,2-diphenylethyl)benzenesulfonamide)styrene functionalized Co/C nanoparticles (**52**)

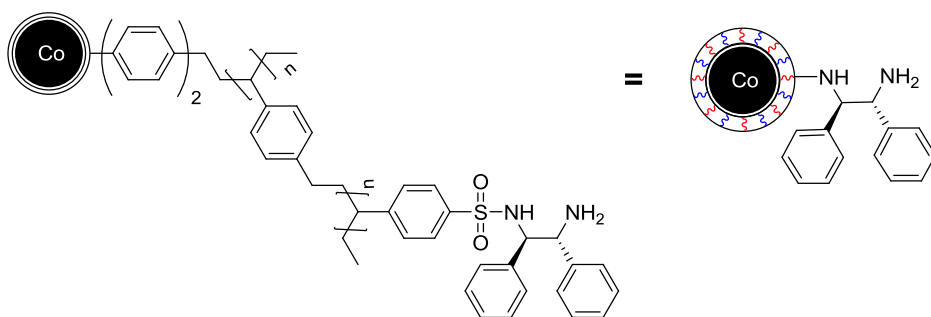


Diphenyl-vinyl functionalized Co/C nanoparticles **51** (172 mg, 0.02 mmol, 1 equiv.) and (1*R*,2*R*)-diamino ligand **47** (227 mg, 0.6 mmol, 30 equiv.) were dispersed in anhydrous DMF (2.8 mL) under nitrogen atmosphere. The resulting mixture was degassed by four consecutive cycles of freeze-pump-thaw. A solution of AIBN (9.6 mg, 0.06 mmol, 10 mol%) in degassed

anhydrous DMF (0.1 mL) was added and the mixture was stirred at 100 °C for 21 h. Upon cooling to rt, the nanobeads were collected, the solvent was decanted and the particles were washed with DMF (2x3 mL), H<sub>2</sub>O (4x3 mL), diethyl ether (4x3 mL) and DCM (4x3 mL), followed by drying at 50 °C under vacuum to give 169 mg of nanobeads **52**.

**IR** (KBr,  $\tilde{\nu}/\text{cm}^{-1}$ ): 3444, 2921, 2846, 1653, 1646, 1635, 1624, 1617, 1558, 1541, 1506, 1458, 1318, 1156, 1094, 1002, 825, 758, 700, 668, 582; **elemental microanalysis** [%]: C, 10.48; H, 0.37; N, 0.23; S, 0.28 - **loading** (ligand) 0.08 mmol/g.

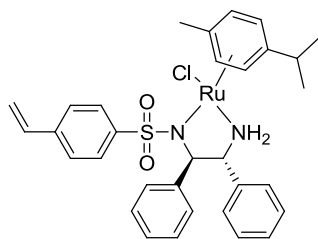
**Poly(*N*-((1*R*,2*R*)-2-amino-1,2-diphenylethyl)benzenesulfonamide)styrene functionalized Co/C nanoparticles (**57**)**



A flame dried heavy-wall Schlenk flask was charged with diphenyl-vinyl functionalized Co/C nanoparticles **51** (150 mg, 0.0405 mmol, 1 equiv.), divinylbenzene (264 mg, 2.025 mmol, 50 equiv.), 1,2-diamine ligand **47** (766 mg, 2.025 mmol, 50 equiv.) and degassed anhydrous DMF (2.5 mL) under nitrogen atmosphere. Subsequently, a solution of AIBN (20 mg, 0.12 mmol, 3 mol% of combined monomers) in degassed anhydrous DMF (0.4 mL) was added to the reaction flask. The resulting mixture was heated to 100 °C for 20 h. After cooling down, the particles were collected with an external magnet and the supernatant was decanted. The nanobeads were washed thoroughly with DMF (15x3 mL), H<sub>2</sub>O (4x3 mL) and diethyl ether (5x3 mL) and dried *in vacuo*, yielding 565 mg of the desired 1,2-diamine functionalized particles **57**.

**SQUID** (emu/g) 29.85; **IR** (KBr,  $\tilde{\nu}/\text{cm}^{-1}$ ): 3309, 3047, 2920, 1658, 1591, 1496, 1490, 1452, 1406, 1317, 1149, 1082, 1064, 912, 893, 823, 767, 696, 582, 559; **elemental microanalysis** [%]: C, 55.80; H, 4.96; N, 5.20; S, 3.63 - **loading** (ligand) 1.13 mmol/g.

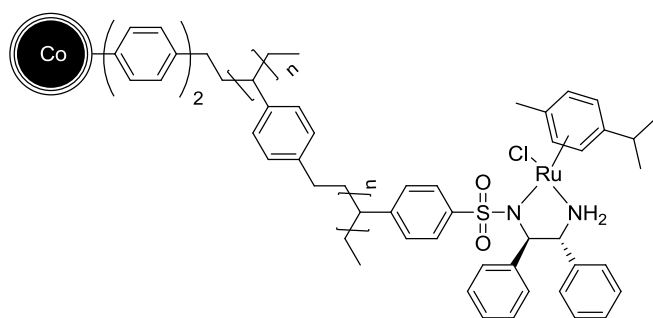
**[RuCl(*p*-cymene){NH<sub>2</sub>CH(Ph)CH(Ph)NSO<sub>2</sub>C<sub>8</sub>H<sub>7</sub>}] (Ru·58)<sup>[39]</sup>**



*N*-((1*R*,2*R*)-2-amino-1,2-diphenylethyl)-4-vinylbenzenesulfonamide (**47**) (75.7 mg, 0.2 mmol, 2.0 equiv.) was dissolved in anhydrous DCM (6 mL) under nitrogen atmosphere. KO<sup>t</sup>Bu (24.7 mg, 0.22 mmol, 2.2 equiv.) was added and the mixture was stirred 15 min at rt before addition of [RuCl<sub>2</sub>(*p*-cymene)]<sub>2</sub> (61.2 mg, 0.1 mmol, 1.0 equiv.). Subsequently, the solution was stirred at rt for 21 h. Filtration and evaporation gave the crude product, which was purified by recrystallization from DCM/hexanes to yield the pure product as brown powder (68.8 mg, 0.11 mmol, 53%).

<sup>1</sup>H NMR (300 MHz, CDCl<sub>3</sub>): δ<sub>H</sub> = 7.07 – 6.30 (m, 16H), 5.84 (s, 1H), 5.91 – 5.58 (m, 4H), 5.22 (d, *J* = 10.9 Hz, 1H), 3.74 (d, *J* = 9.9 Hz, 1H), 3.67 – 3.53 (m, 1H), 3.45 (bs, 1H), 3.12 (m, 1H), 2.36 (s, 3H), 1.38 (d, *J* = 5.7 Hz, 6H); IR (neat,  $\tilde{\nu}/\text{cm}^{-1}$ ): 3273, 3213, 2963, 1495, 1394, 1260, 1126, 1081, 1018, 910, 798; LRMS (ESI): *m/z* = 649.1274 [M+H]<sup>+</sup>, 613.1471 [M-Cl]<sup>+</sup>.

**Poly(*N*-((1*R*,2*R*)-2-amino-1,2-diphenylethyl)benzenesulfonamide)styrene - Ru-complex functionalized Co/C nanoparticles (Ru·59)**

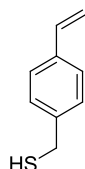


A heavy-wall Schlenk tube was charged with diphenyl-vinyl functionalized Co/C nanoparticles **51** (30 mg, 4.5 μmol, 1 equiv.), divinyl benzene (29 mg, 0.23 mmol, 50 equiv.), Ru-1,2-diamine complex **Ru·58** (55 mg, 0.085 mmol, 19 equiv.) and degassed anhydrous DMF (1 mL) under nitrogen atmosphere. Subsequently, a solution of AIBN (1.5 mg, 9.3 μmol, 3 mol% of combined monomers) in DMF (0.2 mL) was added to the reaction vessel. The resulting mixture was heated to 70 °C for 19 h. After cooling to rt, the particles were collected with an external magnet, the supernatant was decanted and the nanobeads were washed thoroughly with DMF (5x3 mL), H<sub>2</sub>O

(4x3 mL) and diethyl ether (5x3 mL). The particles were dried *in vacuo*, yielding 32 mg of **Ru-59**.

**SQUID** (emu/g) 82.28; **IR** (KBr,  $\tilde{\nu}/\text{cm}^{-1}$ ): 3443, 2918, 2850, 1637, 1560, 1542, 1508, 1458, 1385, 1420, 1116; **elemental microanalysis** [%]: C, 14.84; H, 0.64; N, 0.18; S, 0.18 - **loading** (ligand) 0.06 mmol/g.

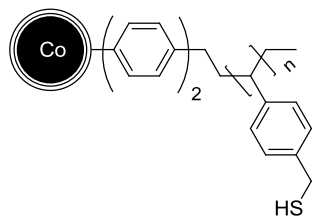
#### (4-Vinylphenyl)methanethiol (**53**)<sup>[40]</sup>



4-Vinylbenzylchloride (5.044 g, 33.0 mmol, 1.0 equiv.), thiourea (2.64 g, 34.7 mmol, 1.05 equiv.) and *tert*-butylcatechol (66 mg, 0.40 mmol, 1.2 mol%) were dissolved in MeOH (10 mL). The resulting mixture was stirred at 47 °C overnight. Subsequently, the solution was cooled to 0 °C with an ice bath and diethyl ether (6 mL) was added, which led to the precipitation of a white solid that was filtered off. The solid was dissolved in Millipore H<sub>2</sub>O (63 mL), the insoluble parts were filtered off before dropwise addition of 32% NH<sub>3</sub> solution (aqueous, 2 mL). A pink-colored solid precipitated which was isolated and washed with cold water. The crude product was purified by vacuum distillation (1.2 mbar, 86 °C) while the condensate was cooled in a CO<sub>2(s)</sub>/acetone mixture. The product was isolated as clear oil (0.9 g, 6 mmol, 20%).

**<sup>1</sup>H NMR** (300 MHz, CDCl<sub>3</sub>):  $\delta_{\text{H}}$  = 7.37 (d,  $J$  = 8.2 Hz, 2H), 7.28 (d,  $J$  = 8.2 Hz, 2H), 6.70 (dd,  $J$  = 17.6, 10.9 Hz, 1H), 5.73 (dd,  $J$  = 17.6, 0.7 Hz, 1H), 5.24 (dd,  $J$  = 10.8, 0.6 Hz, 1H), 3.74 (d,  $J$  = 7.5 Hz, 2H), 1.75 (t,  $J$  = 7.5 Hz, 1H); **<sup>13</sup>C NMR** (75 MHz, CDCl<sub>3</sub>):  $\delta_{\text{C}}$  = 140.9, 136.6, 136.5, 128.4, 126.7, 114.0, 28.9.

#### Poly(benzyl mercaptan)styrene functionalized Co/C nanoparticles (**54**)

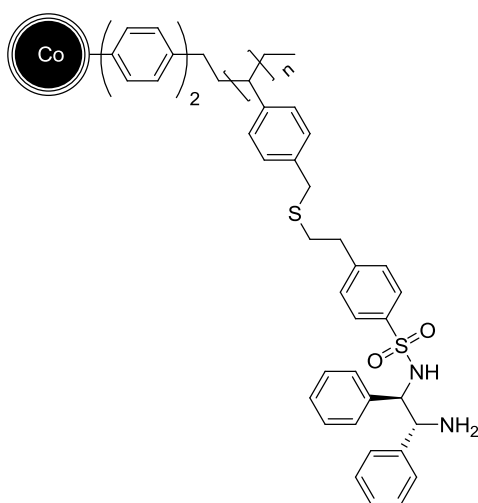


A heavy-wall Schlenk tube was charged with diphenyl-vinyl functionalized Co/C nanoparticles **51** (92 mg, 0.025 mmol, 1 equiv.), 4-vinylbenzyl thiol **53** (374 mg, 2.49 mmol, 100 equiv.) and

degassed anhydrous DMF (1.7 mL). Subsequently, a solution of AIBN (12 mg, 0.075 mmol, 3 mol%) in DMF (0.2 mL) was added to the reaction vessel. The resulting mixture was heated to 100 °C for 20 h. After cooling to rt, the particles were collected with an external magnet, and the supernatant was decanted. The nanobeads were washed with DMF (2x3 mL), H<sub>2</sub>O (3x3 mL) and diethyl ether (4x3 mL) and dried *in vacuo*, yielding 101 mg of **54**.

**SQUID** (emu/g) 80.24; **IR** (KBr,  $\tilde{\nu}/\text{cm}^{-1}$ ): 2928, 2853, 2358, 1461, 784, 632; **elemental microanalysis** [%]: C, 19.12; H, 1.19; N, 0; S, 2.92 - **loading** (S) 0.91 mmol/g.

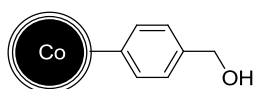
**Poly(*N*-((1*R*,2*R*)-2-amino-1,2-diphenylethyl)-4-(2-(benzylthio)ethyl)benzenesulfonamide)-styrene functionalized Co/C nanoparticles (**55**)**



A heavy-wall Schlenk tube was charged with nanoparticles **54** (36 mg, 0.033 mmol, 1.0 equiv.), a solution of 1,2-diamine ligand **47** (19 mg, 0.043 mmol, 1.5 equiv.) in degassed anhydrous toluene (1 mL) and AIBN (0.2 mg, 1.5  $\mu\text{mol}$ , 3 mol%). The resulting mixture was stirred at 60 °C for 6 h. After magnetic decantation, the nanobeads were washed with toluene (1x1 mL) and diethyl ether (4x1 mL) before being dried *in vacuo* to yield 39 mg of **55**.

**IR** (KBr,  $\tilde{\nu}/\text{cm}^{-1}$ ): 3442, 2918, 2850, 1636, 1559, 1541, 1507, 1457, 1385, 1314, 1155, 1090, 821, 699; **elemental microanalysis** [%]: C, 21.61; H, 1.49; N, 0.61; S, 3.12 - **loading** (ligand) 0.17 mmol/g.

**Benzyl-alcohol functionalized Co/C nanoparticles (**61**)**<sup>[41]</sup>

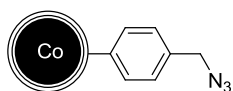


A round bottom flask was charged with Co/C nanobeads **16** (500 mg), 4-aminobenzyl alcohol (62 mg, 0.5 mmol), HCl<sub>conc</sub> (0.5 mL) and H<sub>2</sub>O (6.5 mL). The mixture was sonicated for 15 min

and cooled in an ice bath. A cooled solution of  $\text{NaNO}_2$  (52 mg, 0.75 mmol) in  $\text{H}_2\text{O}$  (6.5 mL) was added dropwise. The slurry was stirred for another 30 min at 0 °C, followed by sonication for further 30 min to ensure complete addition. After magnetic decantation the nanobeads were washed with 1 M NaOH solution (4x10 mL),  $\text{H}_2\text{O}$  (4x10 mL) and diethyl ether (4x10 mL) before being dried *in vacuo*, yielding 495 mg of nanobeads **61**.

**IR** (KBr,  $\tilde{\nu}/\text{cm}^{-1}$ ): 3433, 2918, 2848, 1637, 1560, 1384, 1103, 813; **elemental microanalysis** [%]: C, 10.64; H, 0.17; N, 0.1 - **loading** 0.10 mmol/g.

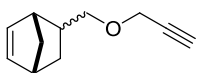
### Benzyl-azide functionalized Co/C nanobeads (**62**)<sup>[41,42]</sup>



Under nitrogen atmosphere benzyl-alcohol functionalized Co/C nanoparticles **61** (150 mg, 0.015 mmol, 1.0 equiv.) were dispersed in degassed anhydrous toluene (2 mL). Subsequently, diphenylphosphoryl azide (DPPA) (5  $\mu\text{L}$ , 6 mg, 0.023 mmol, 1.5 equiv.) was added. After addition of DBU (4  $\mu\text{L}$ , 4 mg, 0.023 mmol, 0.5 equiv.) at 0 °C the reaction mixture was stirred at 0 °C for 30 min followed by 22 h at room temperature. The nanobeads were collected and the solvent was decanted. Subsequently, the particles were washed with  $\text{H}_2\text{O}$  (3x2 mL), 5% HCl solution (1x2 mL), water (3x2 mL) and diethyl ether (2x2 mL) and dried under vacuum, yielding 154 mg of azide functionalized nanobeads **62**.

**SQUID** (emu/g) 104.38; **IR** (KBr,  $\tilde{\nu}/\text{cm}^{-1}$ ): 3430, 2918, 2848, 2088, 1637, 1590, 1319, 1204, 1165, 1089, 944, 911, 813, 723, 688; **elemental microanalysis** [%]: C, 12.24; H, 0.42; N, 0.69 - **loading** (N) 0.16 mmol/g.

### 5-((Prop-2-ynyloxy)methyl)bicyclo[2.2.1]hept-2-ene (**63**)<sup>[43]</sup>



Under nitrogen atmosphere a Schlenk flask was charged with 5-norbornene-2-methanol (2.00 g, 1.61 mmol, 1.0 equiv.) and anhydrous DMF (10 mL). The solution was cooled to 0 °C and NaH (60 wt% in mineral oil, 1.03 g, 25.8 mmol, 1.6 equiv.) in anhydrous DMF (3.3 mL) was added. Subsequently, the resulting mixture was stirred at 0 °C for 25 min before dropwise addition of propargyl bromide (2.68 g, 22.5 mmol, 1.4 equiv.). The reaction was allowed to warm to room temperature and stirred for 24 h. After quenching the reaction with water (10 mL), the phases were separated and the aqueous phase was extracted with EtOAc (3x10 mL). The combined

organic layers were washed with H<sub>2</sub>O, dried over MgSO<sub>4</sub>, filtered and concentrated *in vacuo*. The crude product was purified by column chromatography (hexanes/EtOAc 19:1 → 9:1). The pure product could be isolated as a white solid (784 mg, 4.8 mmol, 30%, *exolendo* 2:1, obtained as *ende/exo* mixture).

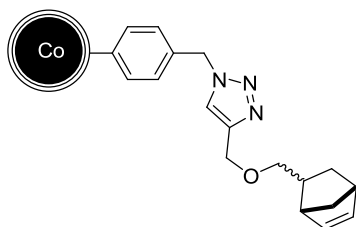
*Exo*-adduct:

$R_f = 0.56$  (hexanes/EtOAc 9:1); <sup>1</sup>H NMR (300 MHz, CDCl<sub>3</sub>): 6.13 (dd,  $J = 5.7, 3.1$  Hz, 1H), 5.95 (dd,  $J = 5.7, 2.9$  Hz, 1H), 4.10 (d,  $J = 2.4$  Hz, 2H), 3.29 – 3.08 (m, 2H), 2.91 (s, 1H), 2.80 (s, 1H), 2.40 (t,  $J = 2.4$  Hz, 1H), 2.39 – 2.28 (m, 1H), 1.82 (ddd,  $J = 11.7, 9.2, 3.8$  Hz, 1H), 1.43 (ddd,  $J = 8.2, 4.1, 2.0$  Hz, 1H), 1.34 – 1.29 (m, 1H), 0.51 (ddd,  $J = 11.6, 4.4, 2.6$  Hz, 1H).

*Endo*-adduct:

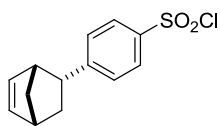
$R_f = 0.56$  (hexanes/EtOAc 9:1); <sup>1</sup>H NMR (300 MHz, CDCl<sub>3</sub>): 6.09 (d,  $J = 2.9$  Hz, 1H), 6.06 (d,  $J = 2.8$  Hz, 1H), 4.16 (d,  $J = 2.4$  Hz, 2H), 3.64 – 3.36 (m, 2H), 2.80 (s, 1H), 2.75 (s, 1H), 2.42 (t,  $J = 2.4$  Hz, 1H), 1.74 – 1.65 (m, 1H), 1.30 – 1.28 (m, 1H), 1.25 – 1.24 (m, 1H), 1.23 – 1.21 (m, 1H), 1.13 (ddd,  $J = 11.7, 4.4, 3.6$  Hz, 1H).

**1-Benzyl-4-(((1*R*,4*R*)-bicyclo[2.2.1]hept-5-en-2-ylmethoxy)methyl)-1*H*-1,2,3-triazole functionalized Co/C nanoparticles (**64**)<sup>[29]</sup>**



In a heavy-wall Schlenk tube, benzyl-azide tagged nanoparticles **62** (135 mg, 0.022 mmol, 1 equiv.) were sonicated in degassed anhydrous toluene (0.8 mL) for 10 min. Subsequently, (1*R*,4*R*)-5-((prop-2-ynyloxy)methyl)bicyclo[2.2.1]hept-2-ene **63** (71 mg, 0.44 mmol, 20 equiv.), triethylamine (9  $\mu$ L, 0.066 mmol, 3 equiv.) and CuI (3 mg, 0.017 mmol, 0.75 equiv.) were added and the resulting slurry was stirred at room temperature for 43 hours. After magnetic decantation, the nanobeads were washed thoroughly with toluene (6x2 mL) before being dried under vacuum to yield norbornene tagged particles **64** (140.0 mg).

IR (KBr,  $\tilde{\nu}/\text{cm}^{-1}$ ): 3429, 2926, 2872, 2075, 1637, 1560, 1508, 1458, 1384, 1320, 1207, 1165, 1090, 1022, 910; elemental microanalysis [%]: C, 13.04; H, 0.49; N, 0.45 - loading (C) 0.06 mmol/g.

**4-(Bicyclo[2.2.1]hept-5-en-2-yl)benzene-1-sulfonyl chloride (65)**<sup>[44]</sup>

4-Vinylbenzene-1-sulfonyl chloride (1.00 g, 4.93 mmol, 1 equiv.) was dissolved in anhydrous toluene (2.3 mL) before freshly cracked cyclopentadiene (1.2 mL, 14.5 mmol, 3 equiv.) was added. The reaction solution was refluxed at 120 °C for 5.5 h. After cooling to rt, the solvent was decanted and the black residue was extracted with EtOAc (5x5 mL). The combined organic layers were evaporated to give the crude product as brown oil. Purification by successive column chromatography (hexanes, hexanes/EtOAc 97:3, hexanes/EtOAc 9:1) yielded the product as slightly yellow solid (281.4 mg, 1.05 mmol, 21%, *endo/exo* 1/0.14, obtained as *endo/exo* mixture).

Major *endo*-isomer:

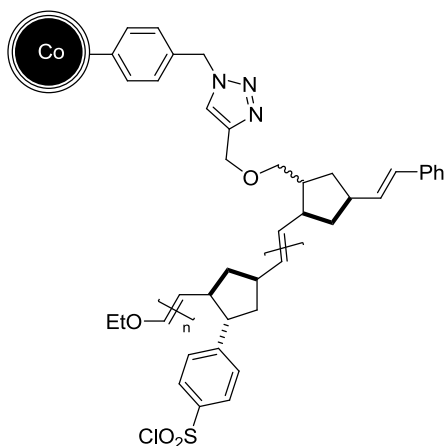
$R_f$  = 0.79 (hexanes/EtOAc 5:1);  $^1\text{H NMR}$  (400 MHz,  $\text{CDCl}_3$ ):  $\delta_{\text{H}}$  = 7.91 – 7.84 (m, 2H), 7.36 (d,  $J$  = 8.3 Hz, 2H), 6.32 (dd,  $J$  = 5.7, 3.1 Hz, 1H), 5.76 (dd,  $J$  = 5.7, 2.8 Hz, 1H), 3.53 – 3.42 (m, 1H), 3.12 (bs, 1H), 3.03 (bs, 1H), 2.32 – 2.22 (m, 1H), 1.56 (dd,  $J$  = 4.2, 1.9 Hz, 1H), 1.52 (bs, 1H), 1.33 (ddd,  $J$  = 12.0, 4.6, 2.5 Hz, 1H).

Minor *exo*-isomer:

$R_f$  = 0.79 (hexanes/EtOAc 5:1);  $^1\text{H NMR}$  (400 MHz,  $\text{CDCl}_3$ ):  $\delta_{\text{H}}$  = 7.98 – 7.92 (m, 2H), 7.52 – 7.47 (m, 2H), 6.27 (dd,  $J$  = 5.7, 3.2 Hz, 1H), 6.22 (dd,  $J$  = 5.6, 2.8 Hz, 1H), 3.03 (bs, 1H), 2.97 (bs, 1H), 2.84 – 2.77 (m, 1H), 2.31 – 2.23 (m, 1H), 1.59 (dd,  $J$  = 4.2, 1.9 Hz, 1H), 1.50 (bs, 1H), 1.33 (ddd,  $J$  = 12.0, 4.6, 2.5 Hz, 1H).



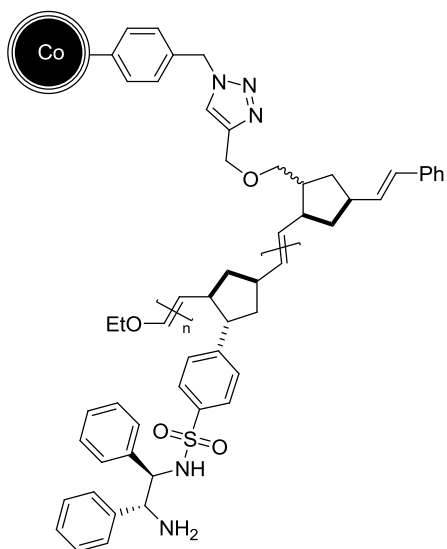
**4-(4-((*E*)-2-(2-(((1-benzyl-1*H*-1,2,3-triazol-4-yl)methoxy)methyl)-4-styrylcyclopentyl)vinyl)-2-((*E*)-2-ethoxyvinyl)cyclopentyl)benzene-1-sulfonyl chloride functionalized Co/C nanoparticles (**66**)**



In a heavy-wall Schlenk tube, norbornene functionalized nanobeads **64** (120 mg, 7.2  $\mu\text{mol}$ , 1 equiv.) in degassed DCM (1.5 mL) were sonicated at 60  $^{\circ}\text{C}$  for 15 min. After addition of a solution of Grubbs-II catalyst (6 mg, 7.2  $\mu\text{mol}$ , 1 equiv.) in degassed DCM (0.6 mL), the mixture was sonicated for another 30 min at 60  $^{\circ}\text{C}$ . 4-((1*R*,2*R*,4*R*)-bicyclo[2.2.1]hept-5-en-2-yl)benzene-1-sulfonyl chloride **65** (116 mg, 0.43 mmol, 60 equiv.) in degassed DCM (1.5 mL) was added followed by sonication at 60  $^{\circ}\text{C}$  for 1.5 h. After magnetic decantation the particles were washed with DCM (4x4 mL) before the addition of a 1:1 mixture of DCM and ethyl vinyl ether (1.5 mL). After 20 min sonication at room temperature the particles were collected with a magnet, washed with DCM (3x2 mL) and dried under vacuum, yielding 197 mg of the magnetic gel with benzyl sulfonyl chloride moieties **66**.

**SQUID** (emu/g) 93.87; **IR** (neat,  $\tilde{\nu}/\text{cm}^{-1}$ ): 2922, 2362, 2324, 1590, 1370, 1362, 1165, 1148, 1104, 1030; **elemental microanalysis** [%]: C, 35.34; H, 2.65; N, 0.18; S, 5.60 - **loading** (S) 1.75 mmol/g.

***N*-((1*R*,2*R*)-2-amino-1,2-diphenylethyl)-4-(4-((*E*)-2-(2-(((1-benzyl-1*H*-1,2,3-triazol-4-yl)methoxy)methyl)-4-styrylcyclopentyl)vinyl)-2-((*E*)-2-ethoxyvinyl)cyclopentyl)benzenesulfonamide functionalized Co/C nanoparticles (**68**)**



(1*R*,2*R*)-1,2-diphenylethane-1,2-diamine **67** (56 mg, 0.266 mmol, 1 equiv.) was dissolved in anhydrous DCM (8 mL) and triethylamine (210  $\mu$ L, 1.52 mmol, 5.7 equiv.) under nitrogen atmosphere. The resulting mixture was stirred for 20 min at rt before sulfonyl chloride functionalized nanoparticles **66** (170 mg, 0.298 mmol, 1.12 equiv.) were added. After 23 h at rt, the magnetic particles were collected, washed with DCM (4x8 mL) and dried *in vacuo* to yield 209 mg nanoparticles **68**.

**SQUID** (emu/g) 46.60; **IR** (neat,  $\tilde{\nu}/\text{cm}^{-1}$ ): 3746, 2362, 2324, 1766, 1751, 1738, 1716, 1373, 1359, 1374, 1234, 1209, 918; **elemental microanalysis** [%]: C, 42.93; H, 3.52; N, 2.76; S, 4.06 - **loading** (ligand) 0.92 mmol/g.

#### **General procedure A: Catalyst screening for asymmetric transfer hydrogenation in water using catalyst **55**, **57**, **68**<sup>[45]</sup>**

Under nitrogen atmosphere, the immobilized ligand **55** (10 mg, 1.7  $\mu$ mol, 1 equiv.), **57** (10.6 mg, 0.012 mmol, 1 equiv.) or **68** (13 mg, 0.012 mmol, 1 equiv.), [RuCl<sub>2</sub>(*p*-cymene)]<sub>2</sub> (for **55** 0.4 mg, 0.7  $\mu$ mol, for **57** and **68** 2.9 mg, 0.010 mmol, 0.83 equiv., leading to 1 mol% active catalyst) and 0.6 mL degassed anhydrous DCM were introduced into a heavy-wall Schlenk flask. The mixture was stirred at 40 °C for 1 h. Subsequently, the particles were collected, the solvent was decanted and the particles were washed with degassed DCM. To the active catalyst was added degassed H<sub>2</sub>O (0.6 mL) acetophenone (1 equiv.), formic acid (3.3 equiv.), triethylamine (2.7 equiv.) and *n*-dodecane as internal GC standard (0.5 equiv.). The resulting solution was heated to 40 °C for 3 h

before cooling down to rt. The solvent was decanted and the NPs were washed with diethyl ether (3x1 mL). The phases of the combined solutions were separated and the aqueous layer was extracted with diethyl ether (4x3 mL). The combined organic layers were dried over  $\text{MgSO}_4$ , filtered and evaporated. Yield and enantiomeric excess were determined by chiral GC analysis.

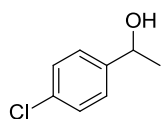
### Asymmetric transfer hydrogenation with catalyst **Ru-59**<sup>[45]</sup>

Under nitrogen atmosphere a heavy-wall Schlenk flask was charged with catalyst **Ru-59** (20 mg, 1  $\mu\text{mol}$ , 1 mol%), degassed  $\text{H}_2\text{O}$  (1 mL), acetophenone (12  $\mu\text{L}$ , 0.1 mmol, 1 equiv.), formic acid (13  $\mu\text{L}$ , 0.33 mmol, 3.3 equiv.), triethylamine (38  $\mu\text{L}$ , 0.27 mmol, 2.7 equiv.) and *n*-dodecane as internal GC standard (11  $\mu\text{L}$ , 0.05 mmol, 0.5 equiv.). The resulting mixture was stirred at 40 °C for 3 h. After cooling to rt, the solvent was decanted and the NPs were washed with diethyl ether (3x1 mL). Upon separation of the phases, the aqueous layer was extracted with diethyl ether (4x3 mL). The combined organic layers were dried over  $\text{MgSO}_4$ , filtered and concentrated *in vacuo*. Yield and enantiomeric excess were determined by chiral GC analysis.

### General procedure B: Racemic reduction of ketones

In a round-bottom flask, the specified ketone (1 equiv.) was dissolved in EtOH (1 M) before cooling to 0 °C. Subsequently,  $\text{NaBH}_4$  (1 equiv.) was added and the resulting mixture was allowed to warm to rt. The progress of the reaction was monitored by TLC (hexanes/EtOAc 5:1). After completion, the unreacted  $\text{NaBH}_4$  was quenched by slow addition of distilled water and sat.  $\text{NH}_4\text{Cl}$  solution. The phases were separated and the aqueous phase was extracted with EtOAc (3x). The combined organic layers were washed with brine, dried over  $\text{MgSO}_4$ , filtered and evaporated to yield the crude product. If necessary, the crude product was purified by column chromatography (hexanes/EtOAc).

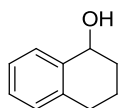
### 1-(4-Chlorophenyl)ethanol (**73**)



Following GP-B, 1-(4-chlorophenyl)ethanone (1.0 mL, 1.19 g, 7.71 mmol, 1 equiv.) and  $\text{NaBH}_4$  (292 mg, 7.71 mmol, 1 equiv.) were used to obtain product **73** as clear oil (1.18 g, 7.54 mmol, 98%).

$R_f = 0.14$  (hexanes/EtOAc 5:1);  $^1\text{H NMR}$  (300 MHz,  $\text{CDCl}_3$ ):  $\delta_{\text{H}} = 7.30$  (s, 4H), 4.86 (q,  $J = 6.4$  Hz, 1H), 2.13 (s, 1H), 1.46 (dd,  $J = 6.5, 0.5$  Hz, 3H);  $^{13}\text{C NMR}$  (75 MHz,  $\text{CDCl}_3$ ):  $\delta_{\text{C}} = 144.4, 133.2, 128.7, 126.9, 69.9, 25.4$ .

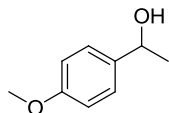
### 1,2,3,4-Tetrahydronaphthalen-1-ol (**74**)



Following GP-B, 1-tetralone (1.0 mL, 1.10 g, 7.3 mmol, 1 equiv.) and  $\text{NaBH}_4$  (284 mg, 7.5 mmol, 1.03 equiv.) were used to obtain alcohol **74** as red-brownish oil (1.06 g, 7.15 mmol, 98%).

$R_f = 0.26$  (hexanes/EtOAc 5:1);  $^1\text{H NMR}$  (300 MHz,  $\text{CDCl}_3$ ):  $\delta_{\text{H}} = 7.47 - 7.41$  (m, 1H), 7.25 – 7.16 (m, 2H), 7.14 – 7.08 (m, 1H), 4.78 (t,  $J = 4.9$  Hz, 1H), 2.93 – 2.65 (m, 2H), 2.05 – 1.72 (m, 5H);  $^{13}\text{C NMR}$  (75 MHz,  $\text{CDCl}_3$ ):  $\delta_{\text{C}} = 138.8, 137.2, 129.1, 128.7, 127.6, 126.2, 68.2, 32.3, 29.3, 18.8$ .

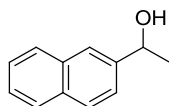
### 1-(4-Methoxyphenyl)ethanol (**75**)



Following GP-B, 1-(4-methoxyphenyl)ethanone (1.00 g, 6.66 mmol, 1 equiv.) and  $\text{NaBH}_4$  (252 mg, 6.66 mmol, 1 equiv.) were used to obtain product **75** as clear oil (0.94 g, 6.15 mmol, 92%).

$R_f = 0.13$  (hexanes/EtOAc 5:1);  $^1\text{H NMR}$  (300 MHz,  $\text{CDCl}_3$ ):  $\delta_{\text{H}} = 7.33 - 7.27$  (m, 2H), 6.93 – 6.82 (m, 2H), 4.85 (q,  $J = 6.4$  Hz, 1H), 3.80 (s, 3H), 1.86 (s, 1H), 1.47 (d,  $J = 6.4$  Hz, 3H);  $^{13}\text{C NMR}$  (75 MHz,  $\text{CDCl}_3$ ):  $\delta_{\text{C}} = 159.1, 138.1, 126.8, 113.9, 70.1, 55.4, 25.1$ .

### 1-(Naphthalen-2-yl)ethanol (**76**)

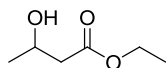


Following GP-B, 2-acetylnaphthalene (1.00 g, 5.88 mmol, 1 equiv.) and  $\text{NaBH}_4$  (222 mg, 5.88 mmol, 1 equiv.) were used to obtain product **76** as white solid (1.00 g, 5.80 mmol, 99%).

$R_f = 0.25$  (hexanes/EtOAc 5:1);  $^1\text{H NMR}$  (400 MHz,  $\text{CDCl}_3$ ):  $\delta_{\text{H}} = 7.89 - 7.77$  (m, 4H), 7.55 – 7.43 (m, 3H), 5.07 (q,  $J = 6.5$  Hz, 1H), 1.97 (s, 1H), 1.59 (d,  $J = 6.5$  Hz, 3H);  $^{13}\text{C NMR}$  (101

MHz, CDCl<sub>3</sub>):  $\delta_C$  = 143.3, 133.5, 133.1, 128.4, 128.1, 127.8, 126.3, 125.9, 124.0, 123.9, 70.7, 25.3.

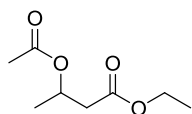
### Ethyl 3-hydroxybutanoate (**77**)



Following GP-B, ethyl 3-oxobutanoate (1.0 mL, 1.03 g, 7.9 mmol, 1 equiv.) and NaBH<sub>4</sub> (299 mg, 7.9 mmol, 1 equiv.) were used to obtain product **77** as clear oil (623 mg, 4.71 mmol, 60%).

$R_f$  = 0.47 (hexanes/EtOAc 2:1); <sup>1</sup>H NMR (300 MHz, CDCl<sub>3</sub>):  $\delta_H$  = 4.26 – 4.08 (m, 3H), 2.72 (bs, 1H), 2.45 (qd,  $J$  = 16.5, 6.1 Hz, 2H), 1.25 (dt,  $J$  = 8.1, 4.4 Hz, 6H); <sup>13</sup>C NMR (75 MHz, CDCl<sub>3</sub>):  $\delta_C$  = 173.2, 64.4, 60.8, 42.8, 22.5, 14.3.

### Derivatization of ethyl 3-hydroxybutanoate (**77**) to ethyl 3-acetoxybutanoate (**78**) for GC analysis<sup>[46]</sup>



In a round-bottom flask, ethyl 3-hydroxybutanoate **77** (100 mg, 0.76 mmol, 1 equiv.) was dissolved in DCM (4.6 mL). Subsequently, triethylamine (534  $\mu$ L, 384.5 mg, 3.8 mmol, 5 equiv.) and acetic anhydride (359  $\mu$ L, 387.9 mg, 3.8 mmol, 5 equiv.) were added and the resulting solution was stirred for 18 h at room temperature and then for 18 h at 50 °C. After addition of water the phases were separated and the aqueous phase was extracted with DCM (3x5 mL) before the combined organic layers were washed with brine. Drying over MgSO<sub>4</sub>, filtering and evaporating under reduced pressure gave the crude product which was purified by column chromatography (hexanes:EtOAc 5:1) to give **78** (100 mg, 0.57 mmol, 75%,  $R_f$  = 0.82 (hexanes/EtOAc 2:1)).

<sup>1</sup>H NMR (300 MHz, CDCl<sub>3</sub>):  $\delta_H$  = 5.35 – 5.17 (m, 1H), 4.13 (q,  $J$  = 7.0 Hz, 2H), 2.55 (ddd,  $J$  = 21.2, 15.5, 6.6 Hz, 2H), 2.01 (s, 3H), 1.25 (ddd,  $J$  = 13.7, 10.0, 5.7 Hz, 6H); <sup>13</sup>C NMR (75 MHz, CDCl<sub>3</sub>):  $\delta_C$  = 170.4 (2C), 67.5, 60.7, 41.0, 21.3, 20.0, 14.3.

**General procedure C: Asymmetric transfer hydrogenation in water with catalyst Ru-57 – Substrate screening and recycling tests<sup>[45]</sup>**

A heavy-wall Schlenk flask was charged with **57** (10.6 mg, 0.012 mmol, 1 equiv.), [RuCl<sub>2</sub>(*p*-cymene)]<sub>2</sub> (2.9 mg, 0.010 mmol, 0.83 equiv., leading to max. 1 mol% active catalyst) and degassed anhydrous DCM (0.6 mL) under nitrogen atmosphere. The resulting mixture was heated at 40 °C for 1 h. Subsequently, the nanoparticles were collected with the aid of an external magnet, the solvent was decanted and the particles were washed with degassed DCM (3x 1 mL) to remove any free ruthenium species. ICP-OES analysis showed that 0.008 mmol of Ru was incorporated into the immobilized ligand leading to 0.008 mmol of active catalyst (0.8 mol%). Afterwards, degassed Millipore water (0.6 mL) was added as well as the substrate (1.0 mmol, 1 equiv.), formic acid (125 µL, 3.3 mmol, 3.3 equiv.), triethylamine (376 µL, 2.7 mmol, 2.7 equiv.) and *n*-dodecane as internal standard (114 µL, 0.5 mmol, 0.5 equiv.). The reaction was stirred at 60 °C for 3 h. Subsequently, the particles were collected with the help of a magnet and the solvent was decanted into a separating funnel. The particles were washed with degassed diethyl ether (3x1 mL), combining the decanted solution and the washing solutions in the separating funnel. For the recycling procedure, the recovered catalyst was subjected to the next run by directly adding fresh reagents. The decanted solution was diluted by addition of water and the phases were separated. The aqueous phase was extracted with diethyl ether (4x3 mL), the combined organic layers were dried over MgSO<sub>4</sub>, filtered and concentrated *in vacuo*. Yield and enantiomeric excess were determined by chiral GC analysis. Afterwards, the corresponding products were isolated from unreacted starting material and the internal standard by column chromatography (not in recycling procedure) eluting with hexanes/EtOAc.

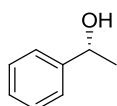
**Analysis of Ru leaching during recycling**

The ruthenium leaching was determined in the aqueous phase, as well as in the organic phase. After each run, the aqueous phase of the extraction was completely evaporated and the residue was dissolved in a defined amount of aqua regia 32% (v/v), filtered through a syringe filter and analyzed by ICP-OES. Calibration was done with freshly prepared ruthenium standard solutions. The same procedure was used for the organic phase, however, after determination of the yield and *ee* through chiral GC analysis.

### Analysis of non-complexed Ru

The decanted DCM from the Ru complexation as well as the washing solutions were fully evaporated. The residue was dissolved in a certain amount of aqua regia 32% (v/v), filtered through a syringe filter and subjected to ICP-OES. Calibration was done with freshly prepared Ruthenium standard solutions.

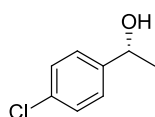
#### (*R*)-1-phenylethanol (**70**)



Following GP-C, acetophenone **69** (116  $\mu$ L, 120 mg) was used as substrate to obtain 121 mg of product **70** as clear, colorless oil (GC yield 100%, 99% isolated) with 94% *ee*.

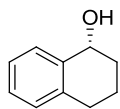
$R_f$  = 0.63 (hexanes/EtOAc 2:1);  $[\alpha]_D^{20}$  +50.3 ( $c$  = 1.0,  $\text{CHCl}_3$ ) 94% *ee* (*R*) (lit. value<sup>[47]</sup>  $[\alpha]_D^{20}$  +54.9 ( $c$  = 1.0,  $\text{CHCl}_3$ ) 96% *ee* (*R*)); **chiral GC analysis** (CP-Chirasil-Dex CB, column temperature 125 °C)  $t_r(\text{standard})$  = 4.91 min,  $t_r(R)$  = 7.43 min,  $t_r(S)$  = 8.39 min;  **$^1\text{H}$  NMR** (300 MHz,  $\text{CDCl}_3$ ):  $\delta_{\text{H}}$  = 7.41 – 7.26 (m, 5H), 4.91 (q,  $J$  = 6.5 Hz, 1H), 2.04 (bs, 1H), 1.51 (d,  $J$  = 6.5 Hz, 3H);  **$^{13}\text{C}$  NMR** (75 MHz,  $\text{CDCl}_3$ ):  $\delta_{\text{C}}$  = 145.9, 128.6, 127.6, 125.5, 70.5, 25.3.

#### (*R*)-1-(4-chlorophenyl)ethanol (**79**)



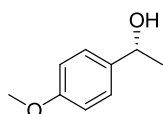
Following GP-C, 1-(4-chlorophenyl)ethanone (130  $\mu$ L, 154 mg) was used as substrate to obtain 153 mg of product **79** as clear, colorless oil (GC yield 100%, 98% isolated) with 92% *ee*.

$R_f$  = 0.14 (hexanes/EtOAc 5:1);  $[\alpha]_D^{20}$  +41.9 ( $c$  = 1.0,  $\text{CHCl}_3$ ) 92% *ee* (*R*) (lit. value<sup>[48]</sup>  $[\alpha]_D^{20}$  +43.5 ( $c$  = 1.0,  $\text{CHCl}_3$ ) 96% *ee* (*R*)); **chiral GC analysis** (CP-Chirasil-Dex CB, column temperature 145 °C)  $t_r(\text{standard})$  = 3.21 min,  $t_r(R)$  = 9.97 min,  $t_r(S)$  = 11.23 min;  **$^1\text{H}$  NMR** (300 MHz,  $\text{CDCl}_3$ ):  $\delta_{\text{H}}$  = 7.30 (s, 4H), 4.86 (q,  $J$  = 6.4 Hz, 1H), 2.13 (s, 1H), 1.46 (dd,  $J$  = 6.5, 0.5 Hz, 3H);  **$^{13}\text{C}$  NMR** (75 MHz,  $\text{CDCl}_3$ ):  $\delta_{\text{C}}$  = 144.4, 133.2, 128.7, 126.9, 69.9, 25.4.

**(R)-1,2,3,4-tetrahydronaphthalen-1-ol (80)**

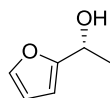
Following GP-C, 1-tetralone (133  $\mu$ L, 146 mg) was used as substrate to obtain 127 mg of product **80** as red-brownish oil (GC yield 98%, 87% isolated, 0.87 mmol) with 92% *ee*.

$R_f$  = 0.26 (hexanes/EtOAc 5:1);  $[\alpha]_D^{20}$  -30.1 ( $c$  = 1.0,  $\text{CHCl}_3$ ) 92% *ee* (*R*) (lit. value<sup>[47]</sup>  $[\alpha]_D^{20}$  -30.5 ( $c$  = 1.0,  $\text{CHCl}_3$ ) 97% *ee* (*R*)); **chiral GC analysis** (CP-Chirasil-Dex CB) column temperature 155  $^{\circ}\text{C}$  for determining the yield:  $t_r(\text{standard})$  = 2.77 min,  $t_r(\text{keton})$  = 7.16 min,  $t_r(\text{product})$  = 9.09 min; column temperature 135  $^{\circ}\text{C}$  for separation of the enantiomers after evaporation and dilution:  $t_r(\text{standard})$  = 3.94 min,  $t_r(\text{keton})$  = 14.38 min,  $t_r(S)$  = 21.33 min,  $t_r(R)$  = 21.60 min;  **$^1\text{H}$  NMR** (300 MHz,  $\text{CDCl}_3$ ):  $\delta_{\text{H}}$  = 7.47 – 7.41 (m, 1H), 7.25 – 7.16 (m, 2H), 7.14 – 7.08 (m, 1H), 4.78 (t,  $J$  = 4.9 Hz, 1H), 2.93 – 2.65 (m, 2H), 2.05 – 1.72 (m, 5H);  **$^{13}\text{C}$  NMR** (75 MHz,  $\text{CDCl}_3$ ):  $\delta_{\text{C}}$  = 138.8, 137.2, 129.1, 128.7, 127.6, 126.2, 68.2, 32.3, 29.3, 18.8.

**(R)-1-(4-methoxyphenyl)ethanol (81)**

Following GP-C, 1-(4-methoxyphenyl)ethanone (150 mg) was used as substrate to obtain 138 mg of product **81** as clear, colorless oil (90% isolated, 0.90 mmol,) with 94% *ee*.

$R_f$  = 0.13 (hexanes/EtOAc 5:1),  $[\alpha]_D^{20}$  +48.2 ( $c$  = 1.0,  $\text{CHCl}_3$ ) 94% *ee* (*R*) (lit. value<sup>[48]</sup>  $[\alpha]_D^{20}$  +56.8 ( $c$  = 1.0,  $\text{CHCl}_3$ ) 95% *ee* (*R*)); **chiral GC analysis** (CP-Chirasil-Dex CB, column temperature 130  $^{\circ}\text{C}$ )  $t_r(\text{standard})$  = 4.40 min,  $t_r(\text{keton})$  = 14.87 min,  $t_r(R)$  = 19.30 min,  $t_r(S)$  = 21.70 min;  **$^1\text{H}$  NMR** (300 MHz,  $\text{CDCl}_3$ ):  $\delta_{\text{H}}$  = 7.33 – 7.27 (m, 2H), 6.93 – 6.82 (m, 2H), 4.85 (q,  $J$  = 6.4 Hz, 1H), 3.80 (s, 3H), 1.86 (s, 1H), 1.47 (d,  $J$  = 6.4 Hz, 3H);  **$^{13}\text{C}$  NMR** (75 MHz,  $\text{CDCl}_3$ ):  $\delta_{\text{C}}$  = 159.1, 138.1, 126.8, 113.9, 70.1, 55.4, 25.1.

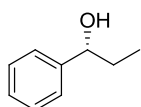
**(R)-1-(furan-2-yl)ethanol (82)**

Following GP-C, 2-acetylfuran (110 mg) was used as substrate to obtain 97 mg of product **82** as yellowish oil (GC yield 91%, 86% isolated, 0.86 mmol) with 99% *ee*.



$R_f = 0.25$  (hexanes/EtOAc 5:1);  $[\alpha]_D^{20} +17.4$  ( $c = 1.0$ ,  $\text{CHCl}_3$ ) 99% *ee* (*R*) (lit. value<sup>[49]</sup>  $[\alpha]_D^{20} +17.3$  ( $c = 1.0$ ,  $\text{CHCl}_3$ ) 98% *ee* (*R*)); **chiral GC analysis** (CP-Chirasil-Dex CB, column temperature 75 °C, progress rate 10 °C/min, final column temperature 125 °C for 5 min)  $t_r(S) = 20.57$  min,  $t_r(R) = 23.46$  min,  $t_r(\text{standard}) = 34.05$  min;  $^1\text{H NMR}$  (300 MHz,  $\text{CDCl}_3$ ):  $\delta_H = 7.37$  (dd,  $J = 1.8$ , 0.8 Hz, 1H), 6.32 (dd,  $J = 3.2$ , 1.8 Hz, 1H), 6.22 (d,  $J = 3.2$  Hz, 1H), 4.88 (q,  $J = 6.6$  Hz, 1H), 2.09 (bs, 1H), 1.54 (d,  $J = 6.6$  Hz, 3H);  $^{13}\text{C NMR}$  (75 MHz,  $\text{CDCl}_3$ ):  $\delta_C = 157.7$ , 142.0, 110.3, 105.3, 63.7, 21.4.

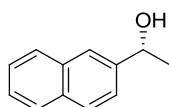
### (*R*)-1-phenylpropan-1-ol (**83**)



Following GP-C, 1-phenylpropan-1-one (133  $\mu\text{L}$ , 134 mg) was used as substrate to obtain 114 mg of product **83** as clear, colorless oil (GC yield 81%, 84% isolated, 0.84 mmol) with 91% *ee*.

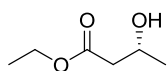
$R_f = 0.34$  (hexanes/EtOAc 5:1);  $[\alpha]_D^{20} +38.6$  ( $c = 1.0$ ,  $\text{CHCl}_3$ ) 91% *ee* (*R*) (lit. value<sup>[48]</sup>  $[\alpha]_D^{20} +44.5$  ( $c = 1.0$ ,  $\text{CHCl}_3$ ) 97% *ee* (*R*)); **chiral GC analysis** (CP-Chirasil-Dex CB, column temperature 115 °C)  $t_r(\text{standard}) = 6.85$  min,  $t_r(\text{keton}) = 9.03$  min,  $t_r(R) = 19.30$  min,  $t_r(S) = 21.59$  min;  $^1\text{H NMR}$  (300 MHz,  $\text{CDCl}_3$ ):  $\delta_H = 7.40 - 7.22$  (m, 5H), 4.72 – 4.46 (m, 1H), 2.01 (bs, 1H), 1.80 (ddd,  $J = 14.2$ , 10.9, 9.9 Hz, 2H), 0.92 (t,  $J = 7.4$  Hz, 3H);  $^{13}\text{C NMR}$  (75 MHz,  $\text{CDCl}_3$ ):  $\delta_C = 144.7$ , 128.5, 127.6, 126.1, 76.2, 32.0, 10.3.

### (*R*)-1-(naphthalen-2-yl)ethanol (**84**)



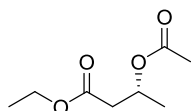
Following GP-C, 2-acetylnaphthalene (170 mg) was used as substrate to obtain 171 mg of product **84** as a white solid (GC yield 100%, 99% isolated, 0.99 mmol) with 95% *ee*.

$R_f = 0.25$  (hexanes/EtOAc 5:1);  $[\alpha]_D^{20} +49.0$  ( $c = 1.0$ ,  $\text{CHCl}_3$ ) 95% *ee* (*R*) (lit. value<sup>[48]</sup>  $[\alpha]_D^{20} +48.9$  ( $c = 1.0$ ,  $\text{CHCl}_3$ ) 95% *ee* (*R*)); **chiral GC analysis** (CP-Chirasil-Dex CB, column temperature 150 °C)  $t_r(\text{standard}) = 2.97$  min,  $t_r(\text{keton}) = 20.87$  min,  $t_r(R) = 32.71$  min,  $t_r(S) = 35.64$  min;  $^1\text{H NMR}$  (400 MHz,  $\text{CDCl}_3$ ):  $\delta_H = 7.89 - 7.77$  (m, 4H), 7.55 – 7.43 (m, 3H), 5.07 (q,  $J = 6.5$  Hz, 1H), 1.97 (s, 1H), 1.59 (d,  $J = 6.5$  Hz, 3H);  $^{13}\text{C NMR}$  (101 MHz,  $\text{CDCl}_3$ ):  $\delta_C = 143.3$ , 133.5, 133.1, 128.4, 128.1, 127.8, 126.3, 125.9, 124.0, 123.9, 70.7, 25.3.

**(*R*)-ethyl 3-hydroxybutanoate (**85**)**

Following GP-C, ethyl 3-oxobutanoate (126  $\mu$ L, 130 mg) was used as substrate to obtain **84** pure product **85** as a clear, colorless oil (63% isolated yield, 0.39 mmol) after 30 min. Enantiomeric excess was determined after converting the compound to (*R*)-ethyl 3-acetoxybutanoate **86**.

$R_f$  = 0.47 (hexanes/EtOAc 2:1);  $^1\text{H NMR}$  (300 MHz,  $\text{CDCl}_3$ ):  $\delta_{\text{H}}$  = 4.26 – 4.08 (m, 3H), 2.72 (bs, 1H), 2.45 (qd,  $J$  = 16.5, 6.1 Hz, 2H), 1.25 (dt,  $J$  = 8.1, 4.4 Hz, 6H);  $^{13}\text{C NMR}$  (75 MHz,  $\text{CDCl}_3$ ):  $\delta_{\text{C}}$  = 173.2, 64.4, 60.8, 42.8, 22.5, 14.3.

**(*R*)-ethyl 3-acetoxybutanoate (**86**)<sup>[46]</sup>**

In a round-bottom flask, (*R*)-ethyl 3-hydroxybutanoate **85** (64 mg, 0.49 mmol, 1 equiv.) was dissolved in DCM (3 mL). Subsequently, triethylamine (342  $\mu$ L, 248 mg, 2.45 mmol, 5 equiv.) and acetic anhydride (232  $\mu$ L, 250 mg, 2.45 mmol, 5 equiv.) were added and the resulting solution was stirred at room temperature for 24 h. After addition of water, the phases were separated and the aqueous phase was extracted with DCM (3x3 mL) before the combined organic layers were washed with brine. Drying over  $\text{MgSO}_4$ , filtering and evaporating under reduced pressure gave the crude product which was purified by column chromatography (hexanes:EtOAc 5:1) to yield **86** as clear, colorless oil (77 mg, 0.44 mmol, 90%,). Chiral GC analysis showed 10% *ee*.

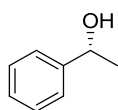
$R_f$  = 0.82 (hexanes/EtOAc 2:1); **chiral GC analysis** (CP-Chirasil-Dex CB, column temperature 110  $^{\circ}\text{C}$ )  $t_{\text{r}}(\text{S})$  = 6.57 min,  $t_{\text{r}}(\text{R})$  = 6.84 min;  $^1\text{H NMR}$  (300 MHz,  $\text{CDCl}_3$ ):  $\delta_{\text{H}}$  = 5.35 – 5.17 (m, 1H), 4.13 (q,  $J$  = 7.0 Hz, 2H), 2.55 (ddd,  $J$  = 21.2, 15.5, 6.6 Hz, 2H), 2.01 (s, 3H), 1.25 (ddd,  $J$  = 13.7, 10.0, 5.7 Hz, 6H);  $^{13}\text{C NMR}$  (75 MHz,  $\text{CDCl}_3$ ):  $\delta_{\text{C}}$  = 170.4 (2C), 67.5, 60.7, 41.0, 21.3, 20.0, 14.3.

**General Procedure D: Asymmetric transfer hydrogenation in DCM<sup>[10]</sup>**

The nanoparticles bearing the immobilized ligand **50** (30 mg, 32  $\mu$ mol, 1 mol%) or **52** (30 mg, 2.4  $\mu$ mol, 1 mol%),  $[\text{RuCl}_2(\text{p-cymene})]_2$  (for **50** 6.7 mg, for **52** 0.5 mg, 0.6 mol%) and DCM (1.0 mL) were introduced to a Schlenk flask under nitrogen atmosphere. The resulting mixture

was degassed by three consecutive cycles of freeze-pump-thaw and heated to 40 °C for 1 h. Subsequently, acetophenone (1 equiv.), formic acid (5 equiv.) and triethylamine (2 equiv.) as well as *n*-dodecane (0.5 equiv.) as GC standard were added. The reaction solution was stirred at 40 °C for 24 h. After cooling down to rt, the nanobeads were collected, the solvent was decanted and the particles were washed with DCM (2x2 mL). The combined organic layers were washed with sat. NaHCO<sub>3</sub> solution (4 mL), dried over MgSO<sub>4</sub>, filtered and concentrated *in vacuo*. Yield and enantiomeric excess were determined by chiral GC analysis.

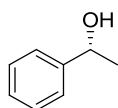
#### (*R*)-1-phenylethanol (**70**) with catalyst Ru-50



Following GP-C, acetophenone (386  $\mu$ L, 397 mg) was used as substrate to obtain product **70** as clear, colorless oil (GC yield 82%) with 96% *ee*.

$R_f$  = 0.63 (hexanes/EtOAc 2:1); **chiral GC analysis** (CP-Chirasil-Dex CB, column temperature 120 °C)  $t_r$ (acetophenone) = 4.78 min,  $t_r$ (standard) = 5.32 min,  $t_r$ (*R*) = 8.20 min,  $t_r$ (*S*) = 9.24 min; **<sup>1</sup>H NMR** (300 MHz, CDCl<sub>3</sub>):  $\delta_H$  = 7.41 – 7.26 (m, 5H), 4.91 (q, *J* = 6.5 Hz, 1H), 2.04 (bs, 1H), 1.51 (d, *J* = 6.5 Hz, 3H); **<sup>13</sup>C NMR** (75 MHz, CDCl<sub>3</sub>):  $\delta_C$  = 145.9, 128.6, 127.6, 125.5, 70.5, 25.3.

#### (*R*)-1-phenylethanol (**70**) with catalyst Ru-52



Following GP-C, acetophenone (29  $\mu$ L, 30 mg) was used as substrate to obtain product **70** as clear, colorless oil (GC yield 63%) with 90% *ee*.

$R_f$  = 0.63 (hexanes/EtOAc 2:1); **chiral GC analysis** (CP-Chirasil-Dex CB, column temperature 125 °C)  $t_r$ (acetophenone) = 4.79 min,  $t_r$ (standard) = 5.34 min,  $t_r$ (*R*) = 8.34 min,  $t_r$ (*S*) = 9.27 min; **<sup>1</sup>H NMR** (300 MHz, CDCl<sub>3</sub>):  $\delta_H$  = 7.41 – 7.26 (m, 5H), 4.91 (q, *J* = 6.5 Hz, 1H), 2.04 (bs, 1H), 1.51 (d, *J* = 6.5 Hz, 3H); **<sup>13</sup>C NMR** (75 MHz, CDCl<sub>3</sub>):  $\delta_C$  = 145.9, 128.6, 127.6, 125.5, 70.5, 25.3.

**ICP-OES measurement**

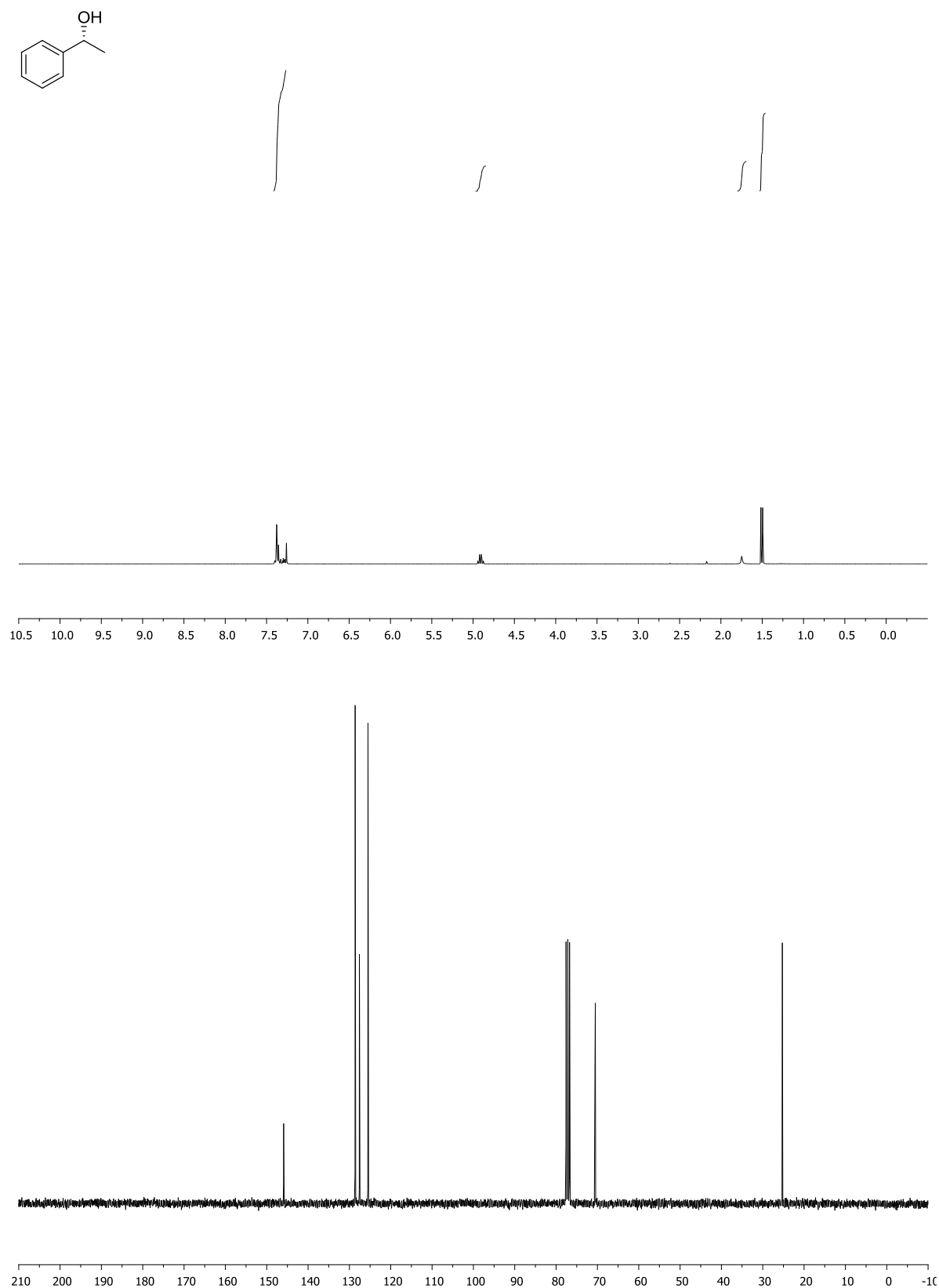
Results from ICP-OES measurements for Ru complexation of **Ru-57** and leaching in aqueous phase of recyclability test (run 1-10) and exemplarily in org. phase of run 1, 5 and 10. Amount of complexed ruthenium before run 1 was 8  $\mu\text{mol}$  Ru.

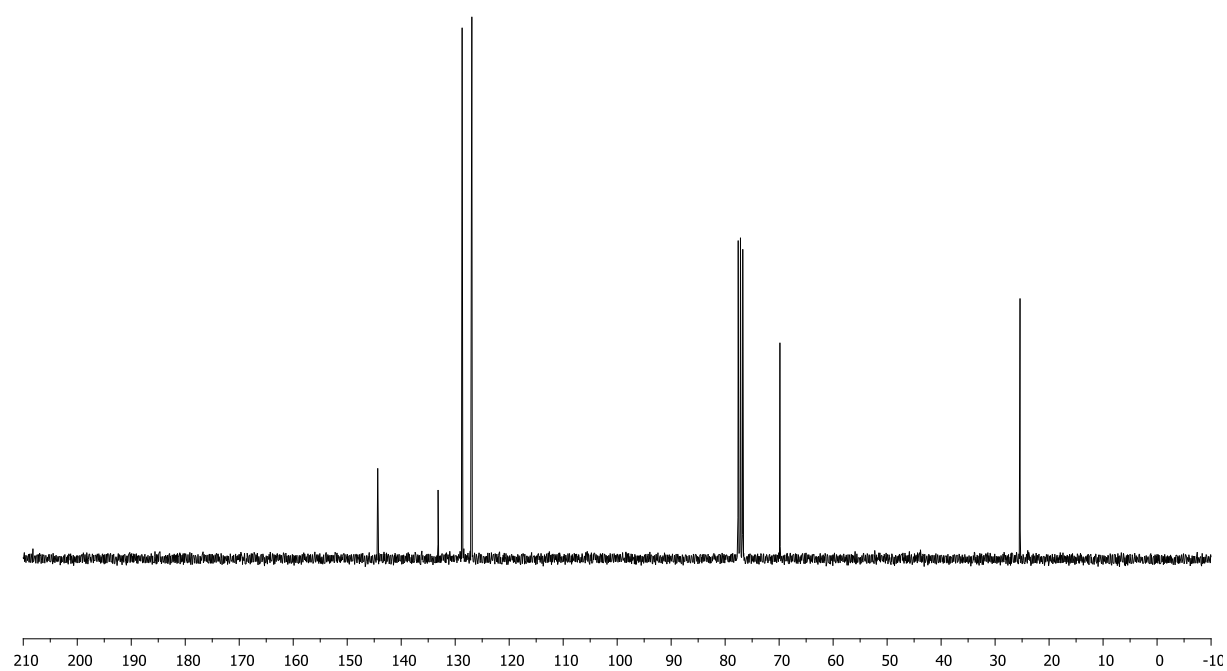
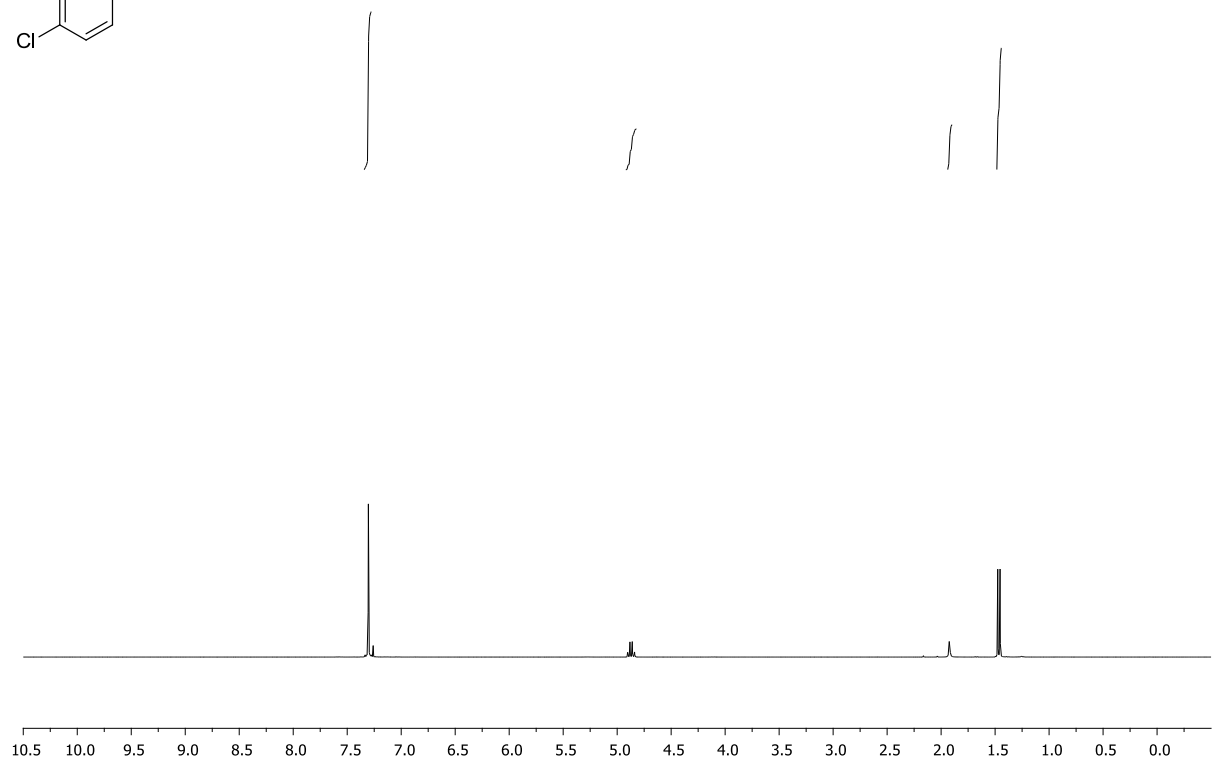
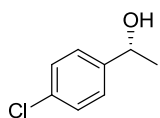
				$\mu\text{g Ru} / \text{g Phenyl-ethanol}$
Sample name	Ru / $\mu\text{mol}$	Ru leaching in % of complexed Ru	Ru leaching / $\mu\text{g}$	Ru measured / ppm
Run1	0.13	1.56	12.7	104.0
Run2	0.09	1.09	8.8	72.2
Run3	0.05	0.64	5.2	42.4
Run4	0.03	0.35	2.8	23.1
Run5	0.04	0.44	3.6	29.5
Run6	0.04	0.45	3.7	30.0
Run7	0.03	0.33	2.7	22.1
Run8	0.02	0.25	2.1	16.9
Run9	0.02	0.27	2.2	17.6
Run10	0.02	0.24	1.9	15.6
Run1 org. phase	0.004	0.05	0.4	3.3
Run5 org. phase	0.003	0.03	0.3	2.1
Run10 org phase	0.001	0.01	0.1	0.8

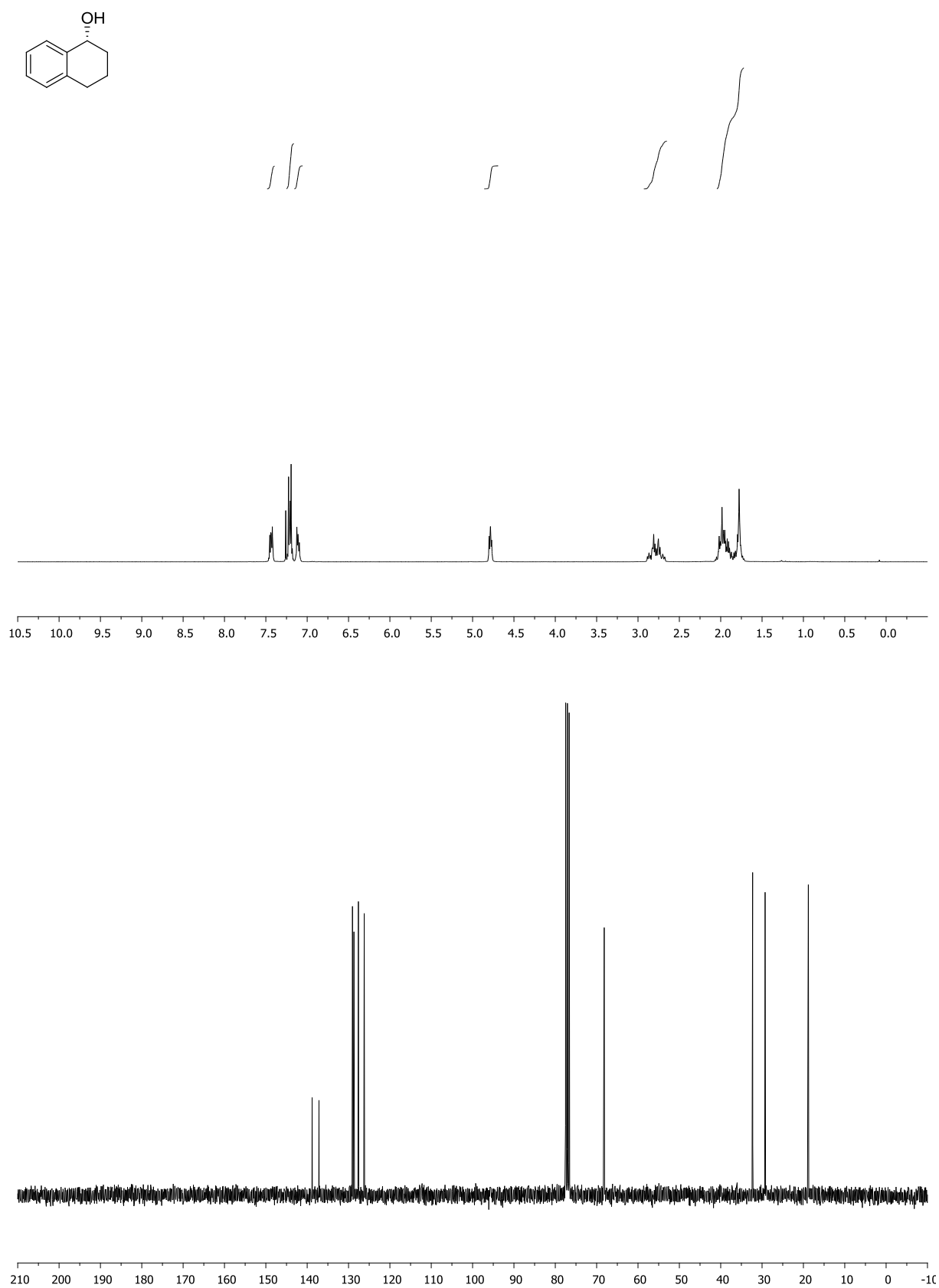
**NMR spectra**

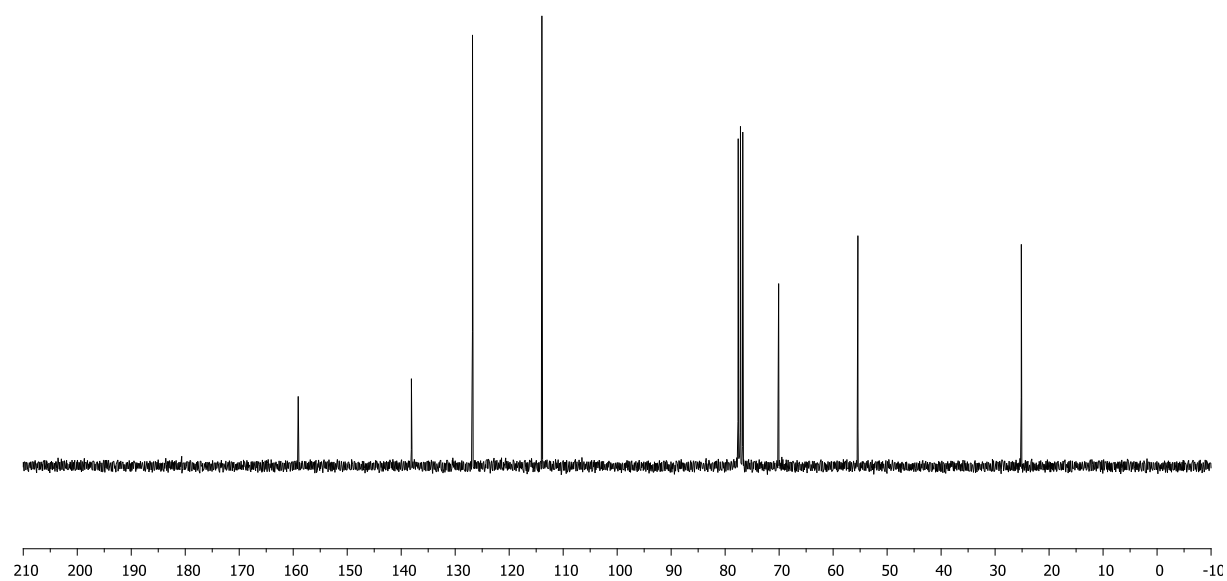
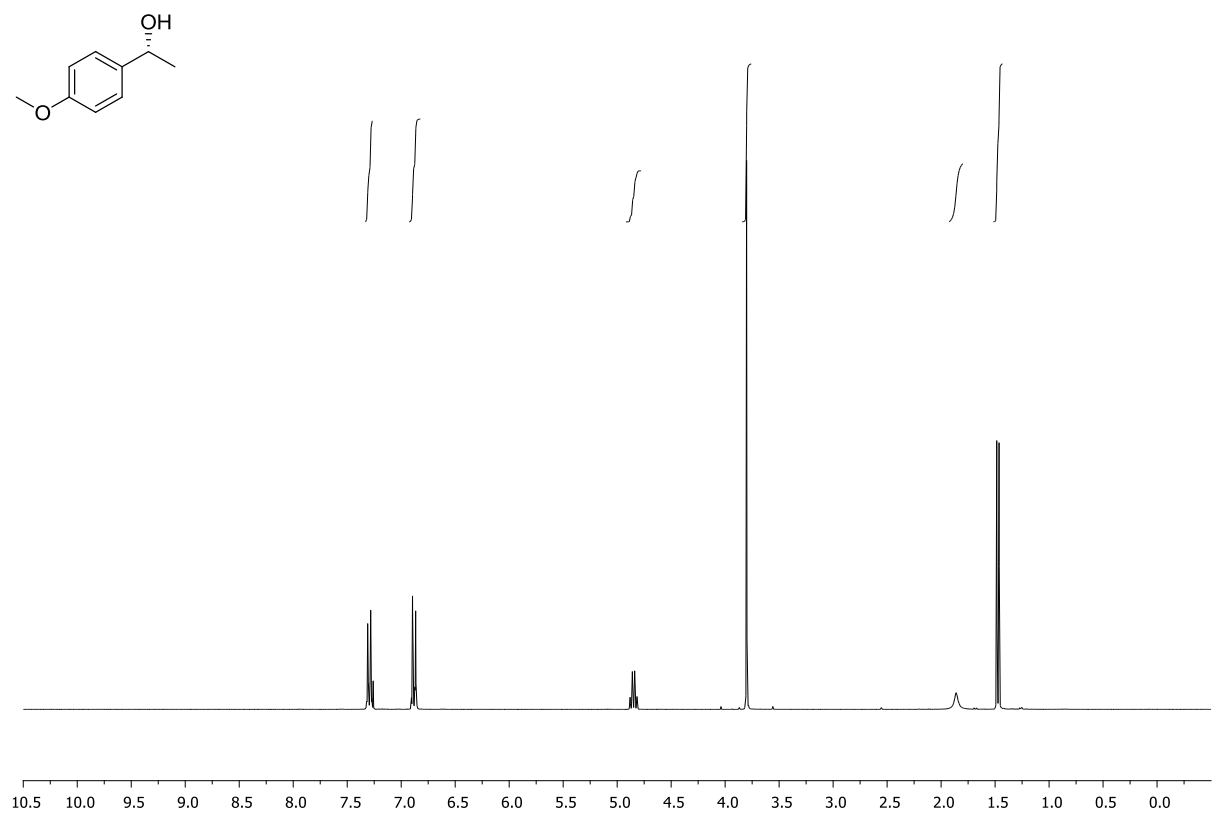
(*R*)-1-phenylethanol (**70**)

CDCl<sub>3</sub>, 300 MHz

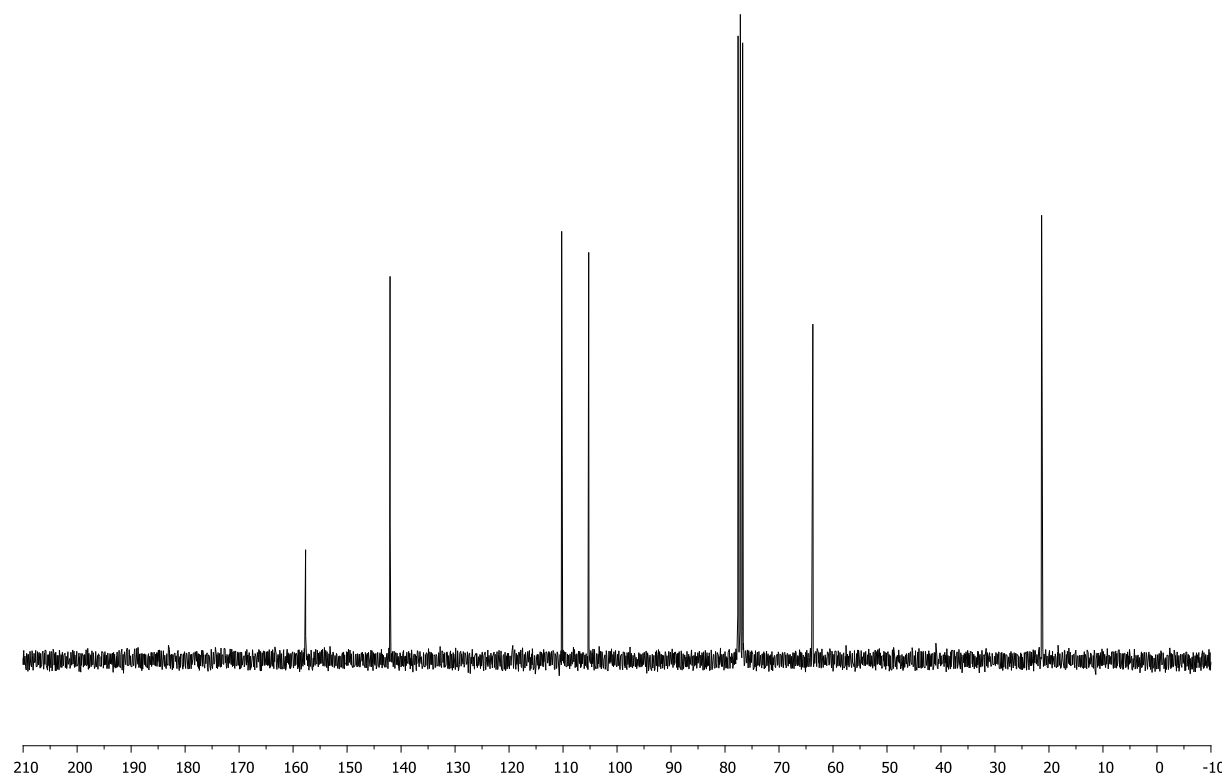
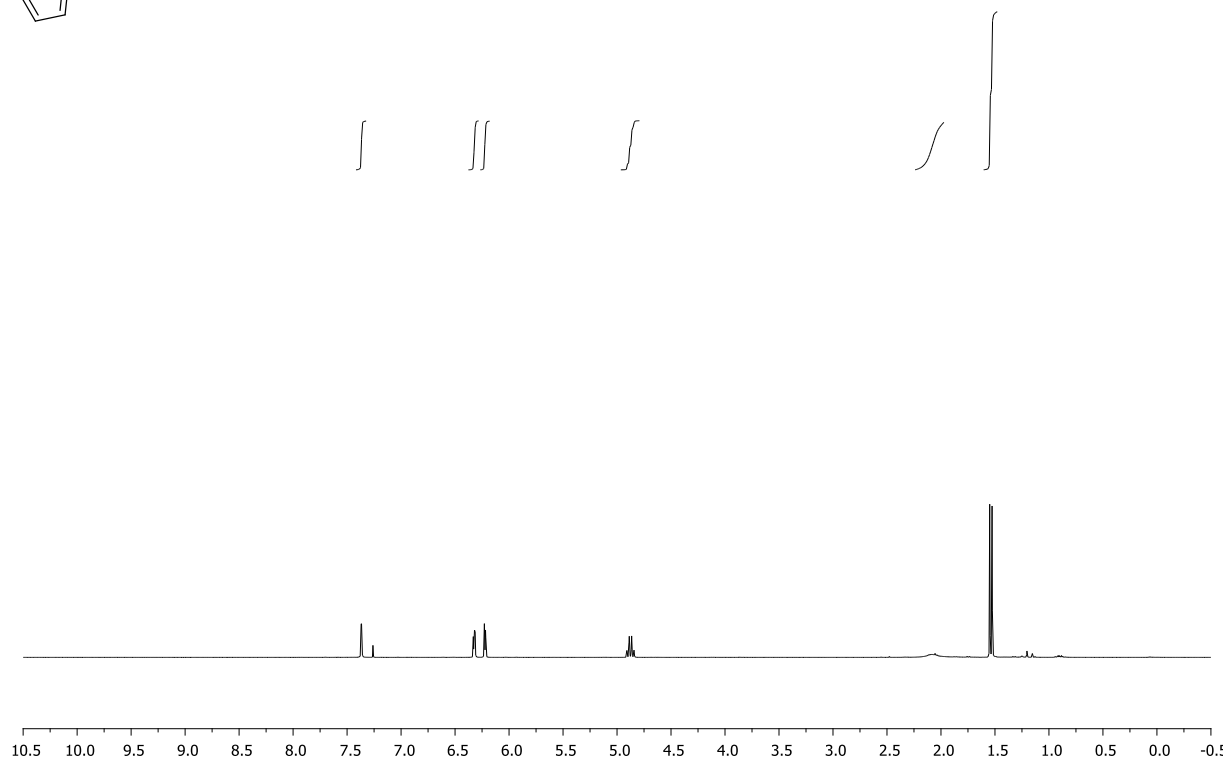
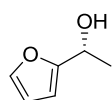


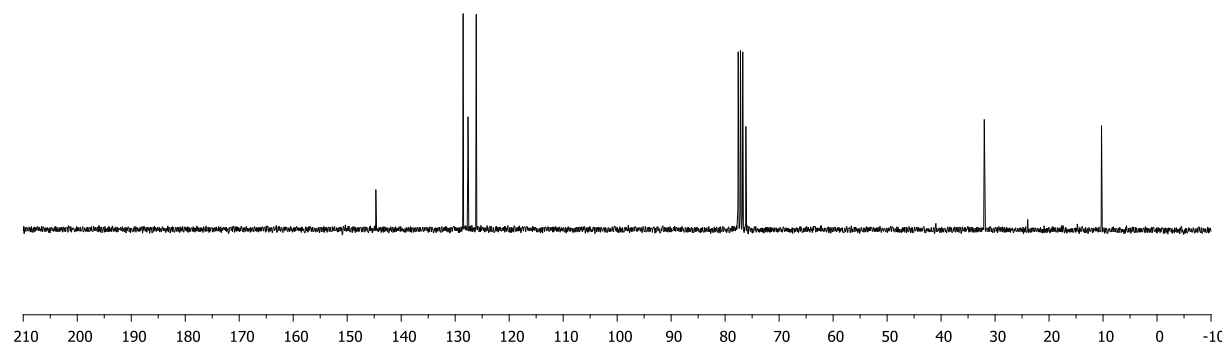
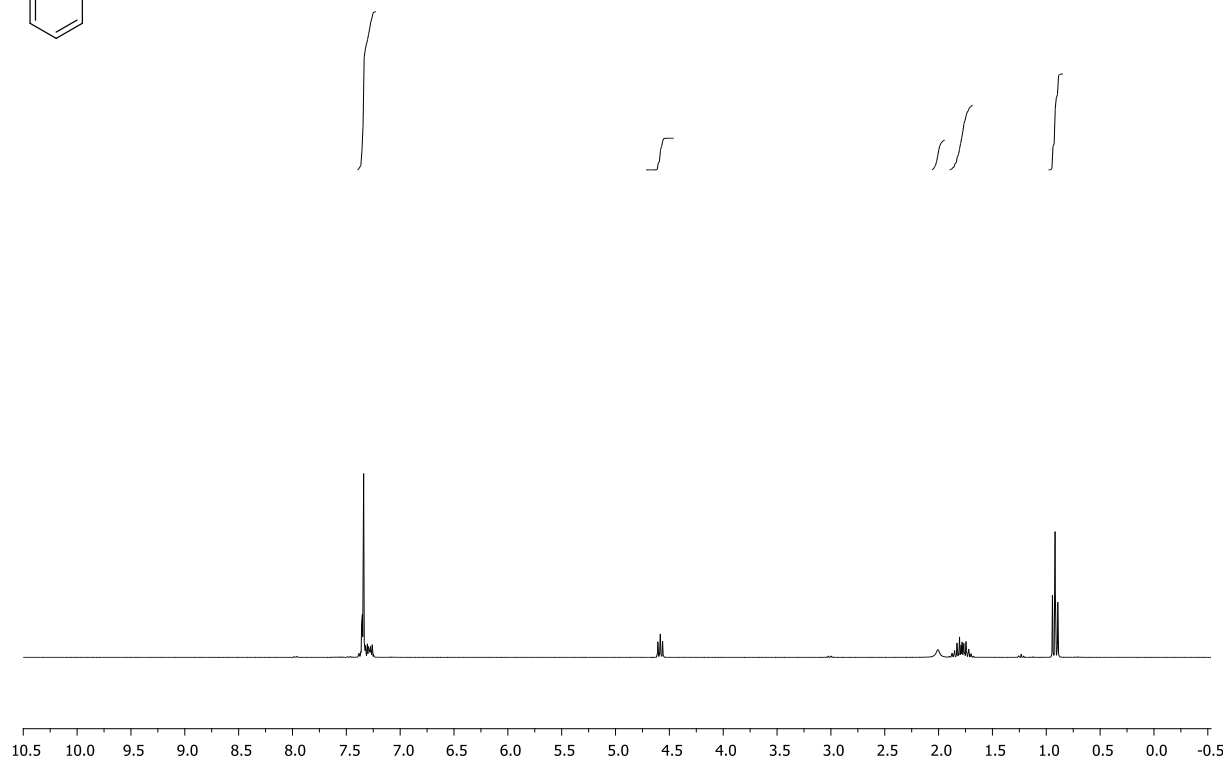
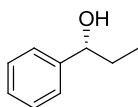
*(R)*-1-(4-chlorophenyl)ethanol (**79**)CDCl<sub>3</sub>, 300 MHz

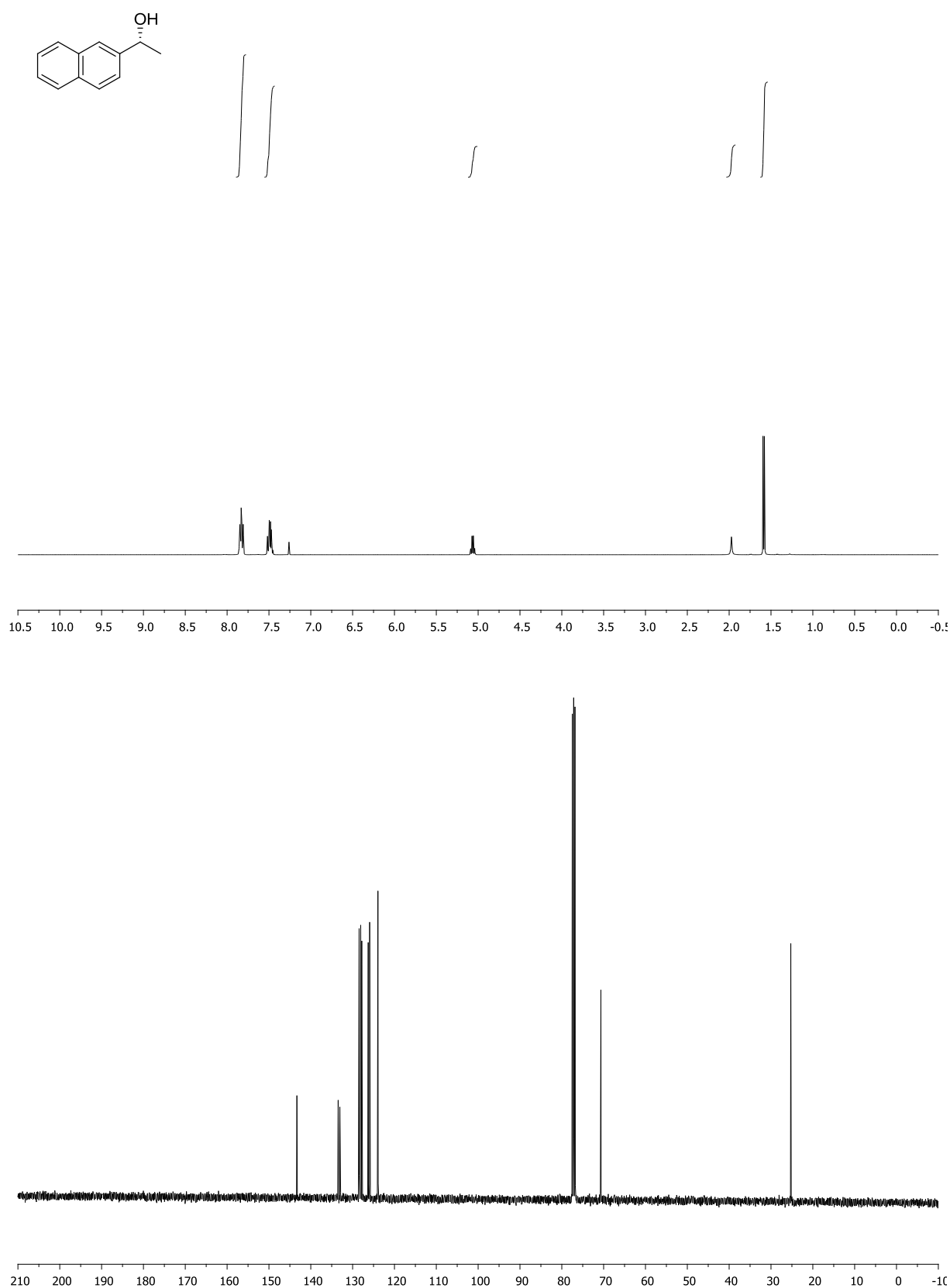
*(R)*-1,2,3,4-tetrahydronaphthalen-1-ol (**80**)CDCl<sub>3</sub>, 300 MHz

*(R)*-1-(4-methoxyphenyl)ethanol (**81**)CDCl<sub>3</sub>, 300 MHz



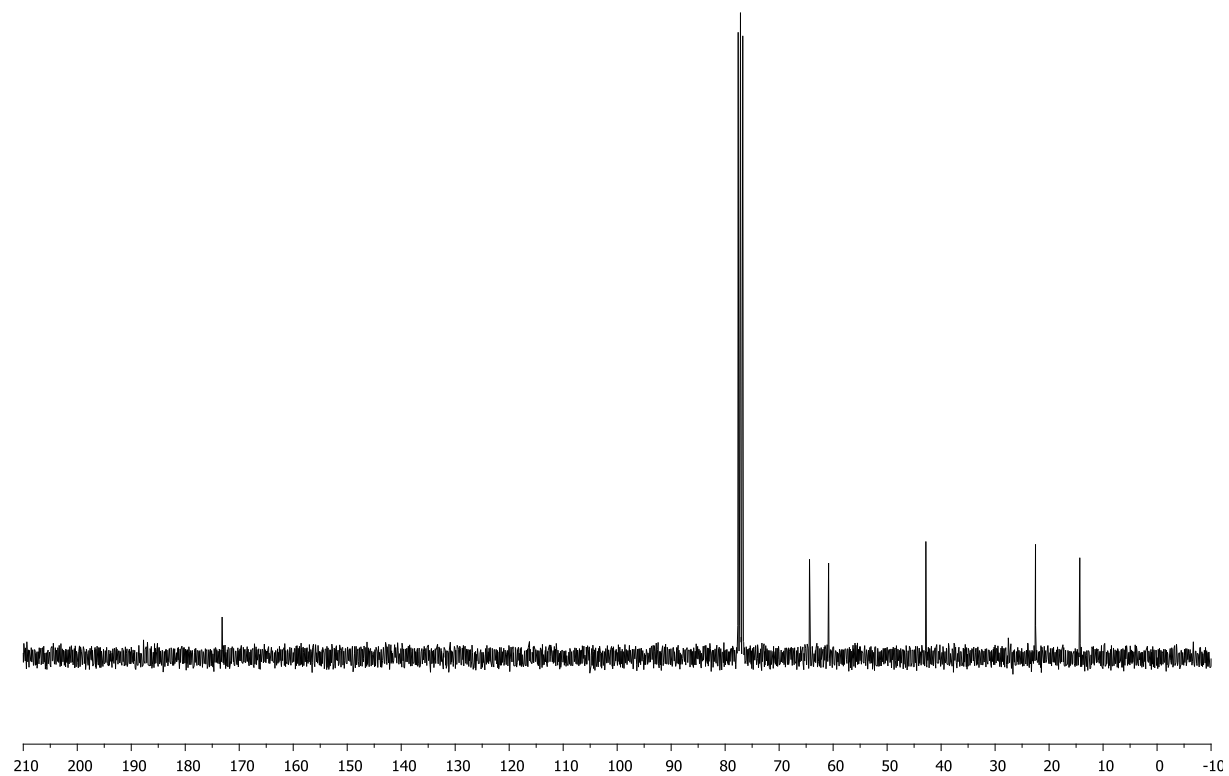
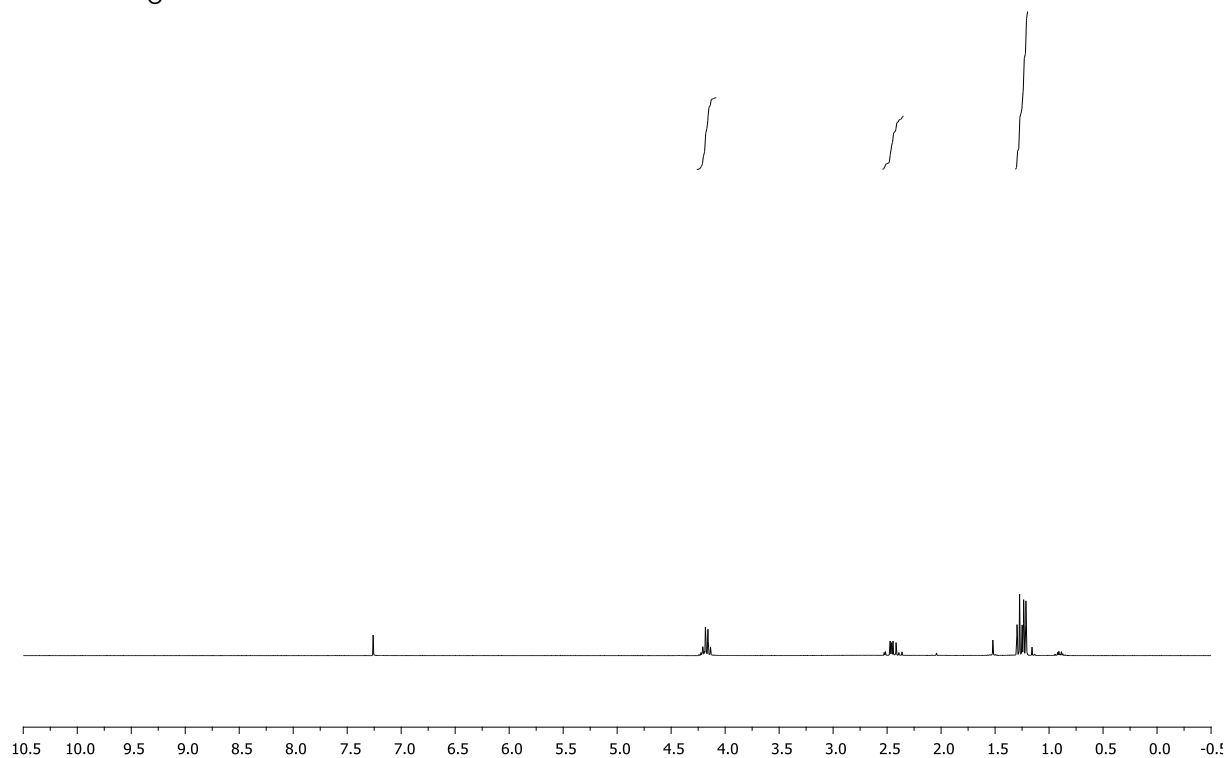
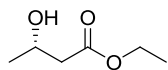
*(R)*-1-(furan-2-yl)ethanol (**82**)CDCl<sub>3</sub>, 300 MHz

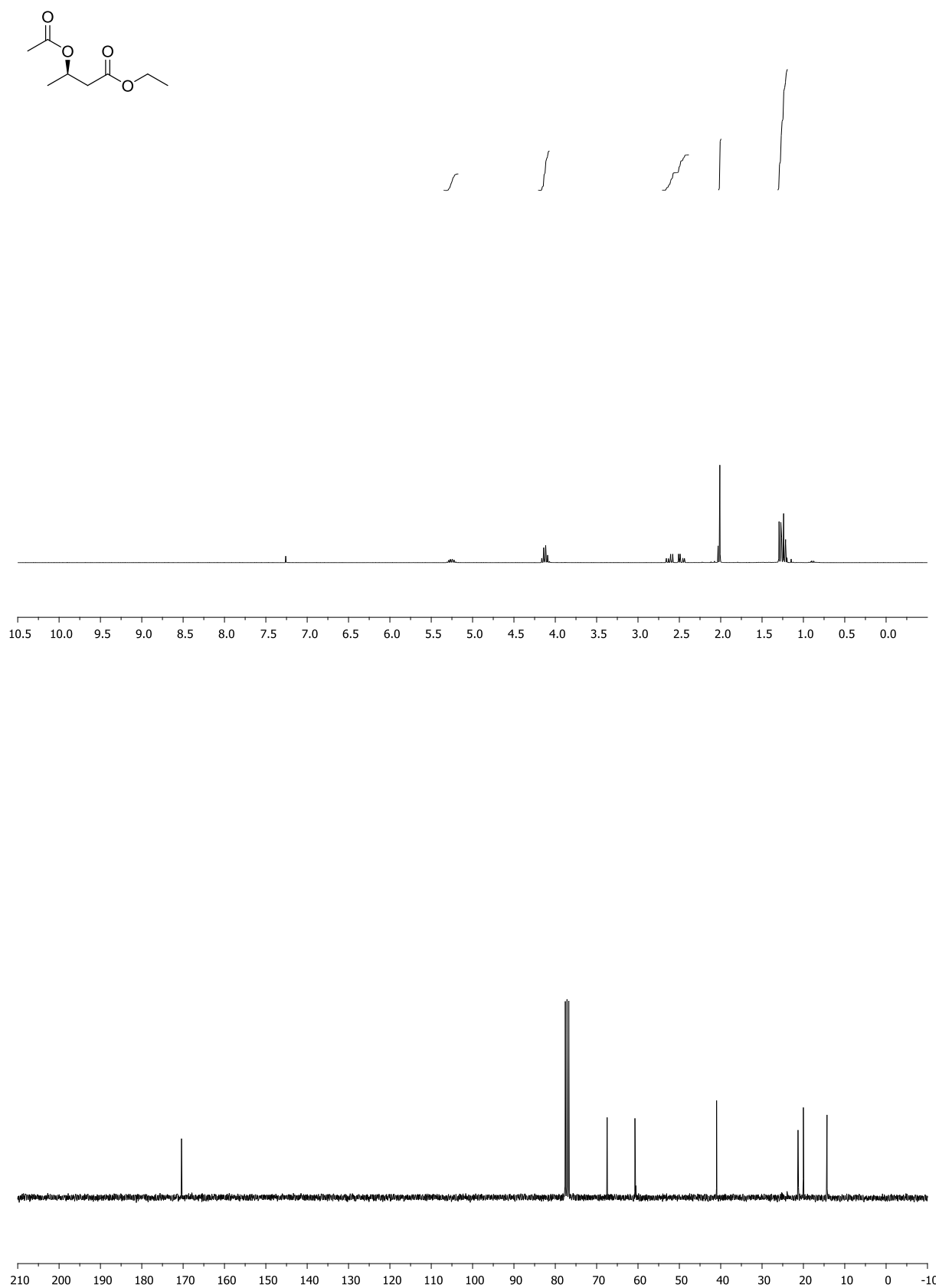
*(R)*-1-phenylpropan-1-ol (**83**)CDCl<sub>3</sub>, 300 MHz

*(R)*-1-(naphthalen-2-yl)ethanol (**84**)CDCl<sub>3</sub>, 400 MHz

(*R*)-ethyl 3-hydroxybutanoate (**85**)

CDCl<sub>3</sub>, 300 MHz

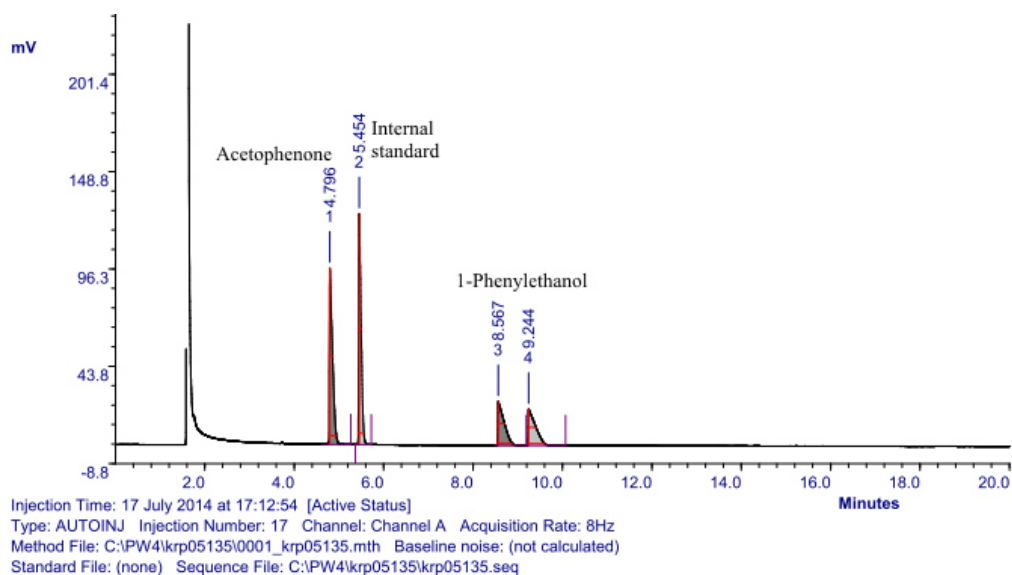


*(R)*-ethyl 3-acetoxybutanoate (**86**)CDCl<sub>3</sub>, 300 MHz

## Chiral GC spectra

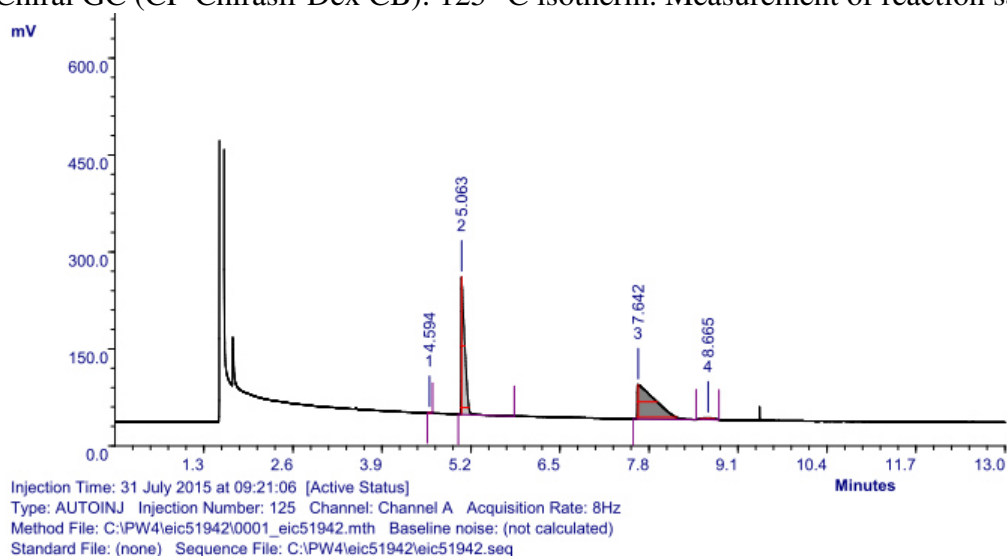
*(R)*-1-phenylethanol (**70**)

Chiral GC (CP-Chirasil-Dex CB): 125 °C isotherm. Calibration with standard, starting material and racemic product.



Peak	RT	Area	%Ar	Conc. (Ar)	Height	M	Units	Name
1	4.796	433.627	32.48	Not Calculated	95.202	0		
2	5.454	451.461	33.81	Not Calculated	124.625	0		
3	8.567	226.391	16.96	Not Calculated	23.621	0		
4	9.244	223.755	16.76	Not Calculated	19.500	0		

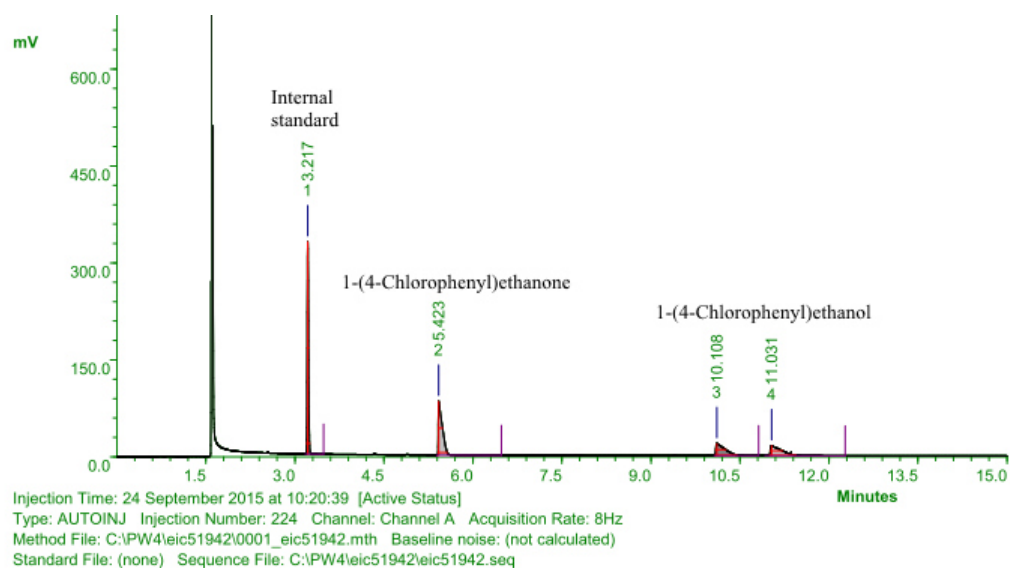
Chiral GC (CP-Chirasil-Dex CB): 125 °C isotherm. Measurement of reaction sample.



Peak	RT	Area	%Ar	Conc. (Ar)	Height	M	Units	Name
1	4.594	1.713	0.10	Not Calculated	0.762	1		
2	5.063	772.229	43.81	Not Calculated	212.793	0		
3	7.642	959.126	54.42	Not Calculated	53.054	0		
4	8.665	29.461	1.67	Not Calculated	2.501	1		

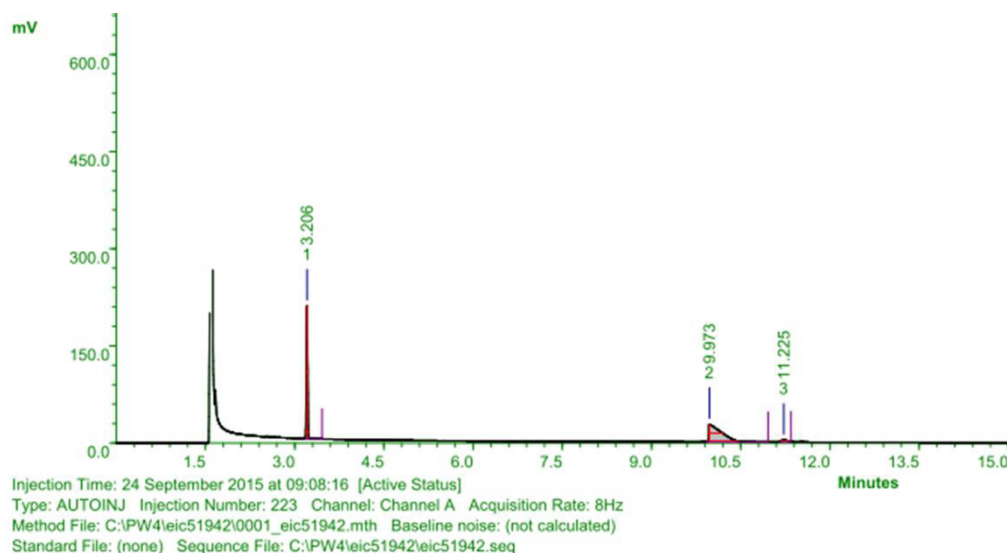
**(*R*)-1-(4-chlorophenyl)ethanol (79)**

Chiral GC (CP-Chirasil-Dex CB): 145 °C isotherm. Calibration with standard, starting material and racemic product.



Peak	RT	Area	%Ar	Conc.(Ar)	Height	M	Units	Name
1	3.217	501.201	38.50	Not Calculated	328.499	0		
2	5.423	393.069	30.20	Not Calculated	83.447	0		
3	10.108	202.604	15.56	Not Calculated	18.893	0		
4	11.031	204.808	15.73	Not Calculated	15.393	0		

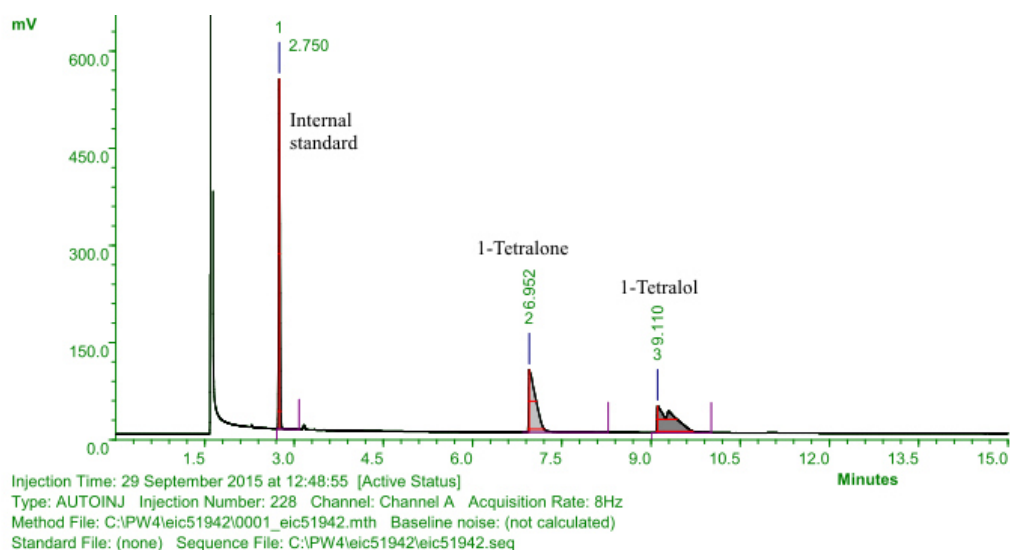
Chiral GC (CP-Chirasil-Dex CB): 145 °C isotherm. Measurement of reaction sample.



Peak	RT	Area	%Ar	Conc.(Ar)	Height	M	Units	Name
1	3.206	319.187	42.83	Not Calculated	205.130	0		
2	9.973	408.574	54.83	Not Calculated	27.219	1		
3	11.225	17.446	2.34	Not Calculated	2.600	1		

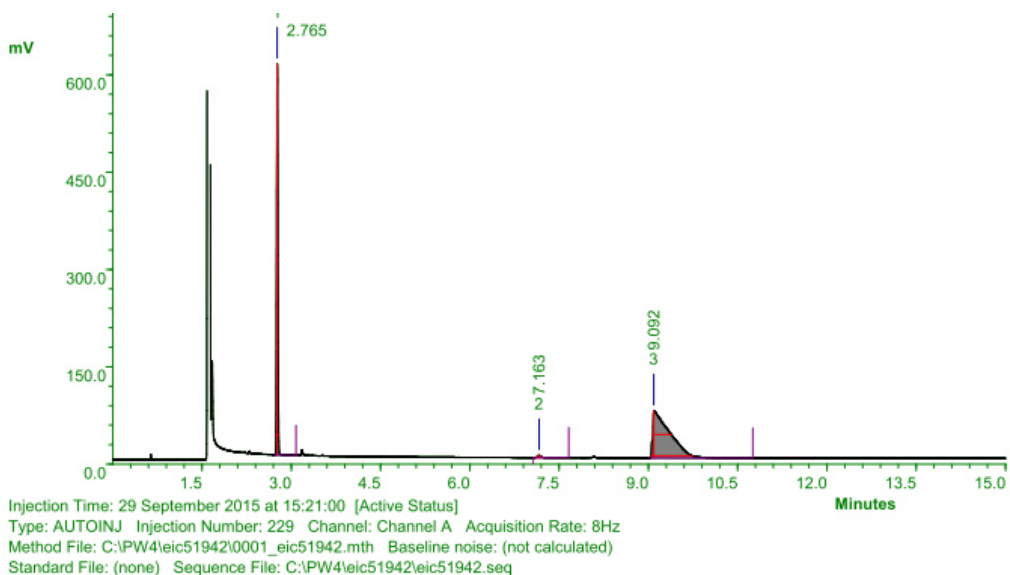
*(R)*-1,2,3,4-tetrahydronaphthalen-1-ol (**80**)

Chiral GC (CP-Chirasil-Dex CB): 155 °C isotherm. Calibration with standard, starting material and racemic product.



Peak	RT	Area	%Ar	Conc. (Ar)	Height	M	Units	Name
1	2.750	859.852	35.12	Not Calculated	540.488	0		
2	6.952	811.665	33.15	Not Calculated	96.440	0		
3	9.110	776.688	31.72	Not Calculated	41.279	1		

Chiral GC (CP-Chirasil-Dex CB) for yield: 155 °C isotherm. Measurement of reaction sample.

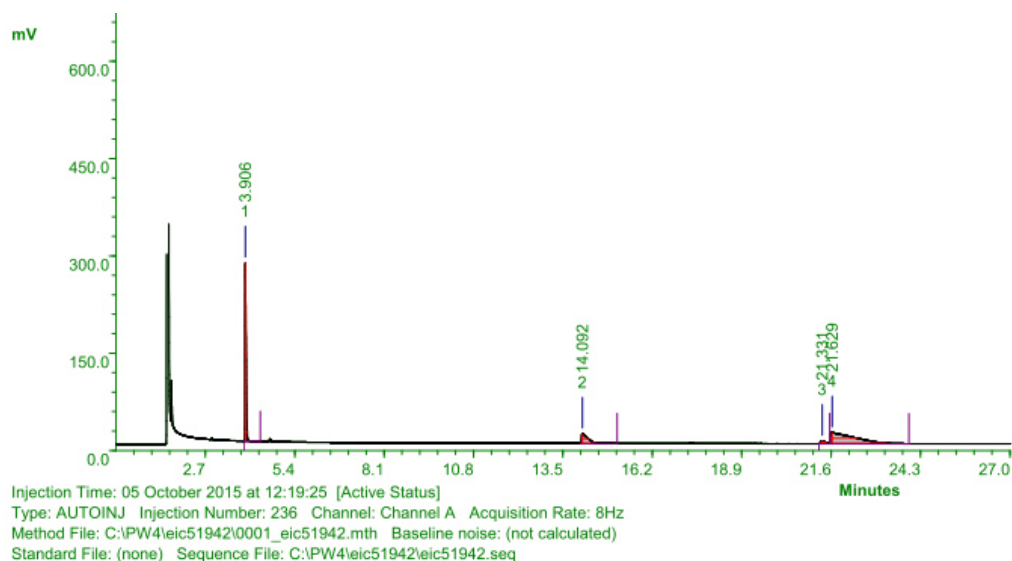


Peak	RT	Area	%Ar	Conc. (Ar)	Height	M	Units	Name
1	2.765	830.876	36.10	Not Calculated	602.524	0		
2	7.163	13.406	0.58	Not Calculated	3.330	0		
3	9.092	1457.121	63.31	Not Calculated	72.633	0		



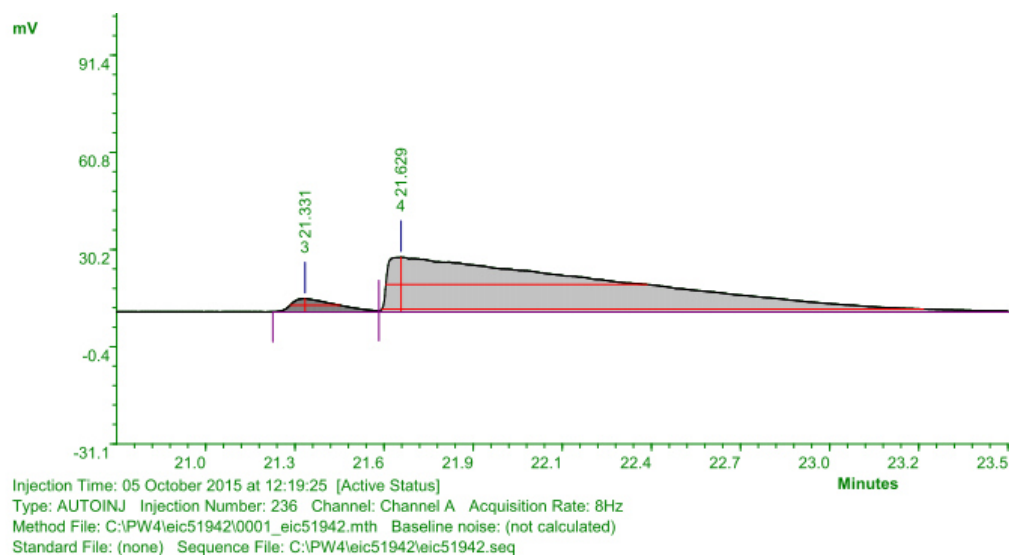
Chiral GC (CP-Chirasil-Dex CB) for determining enantiomeric excess: 135 °C isotherm.

Measurement of reaction sample after evaporation.



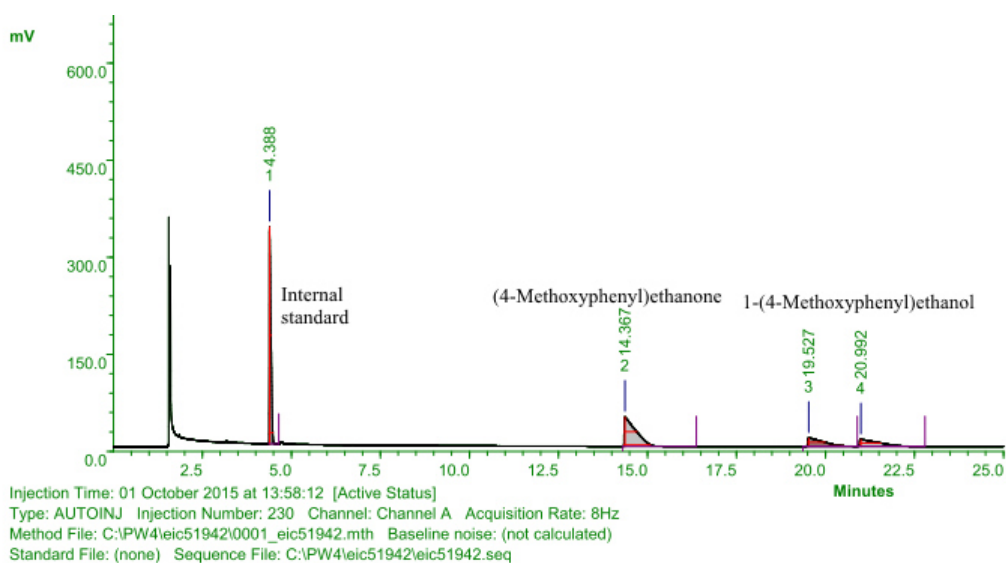
Peak	RT	Area	%Ar	Conc. (Ar)	Height	M	Units	Name
1	3.906	646.834	37.05	Not Calculated	274.751	0		
2	14.092	195.175	11.18	Not Calculated	14.627	0		
3	21.331	39.783	2.28	Not Calculated	4.121	0		
4	21.629	864.155	49.49	Not Calculated	17.167	0		

ZOOM into measurement of reaction sample after evaporation.



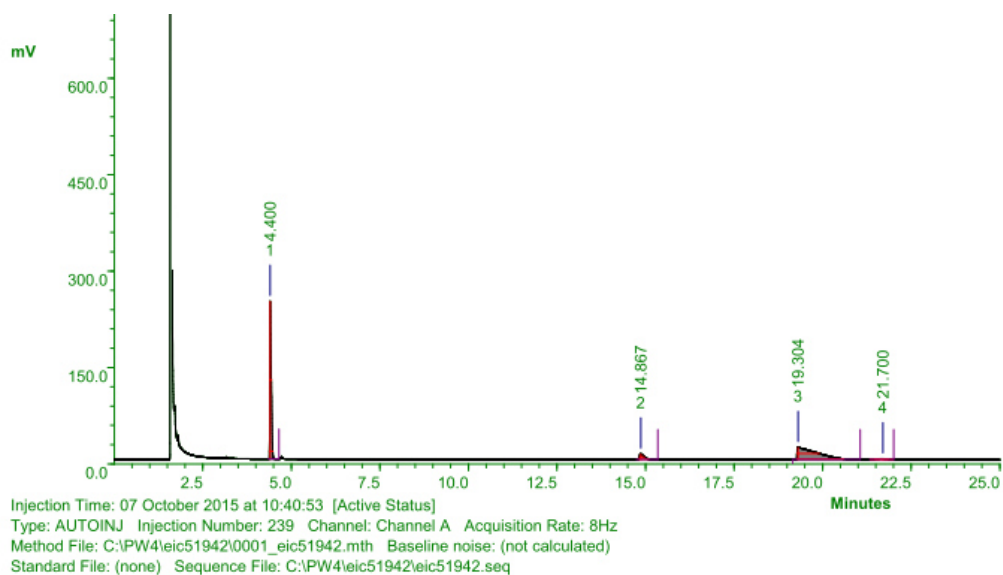
*(R)*-1-(4-methoxyphenyl)ethanol (**81**)

Chiral GC (CP-Chirasil-Dex CB): 130 °C isotherm. Calibration with standard, starting material and racemic product.



Peak	RT	Area	%Ar	Conc. (Ar)	Height	M	Units	Name
1	4.388	1006.008	36.09	Not Calculated	335.273	0		
2	14.367	1003.026	35.99	Not Calculated	45.190	0		
3	19.527	391.834	14.06	Not Calculated	12.887	0		
4	20.992	386.428	13.86	Not Calculated	10.433	0		

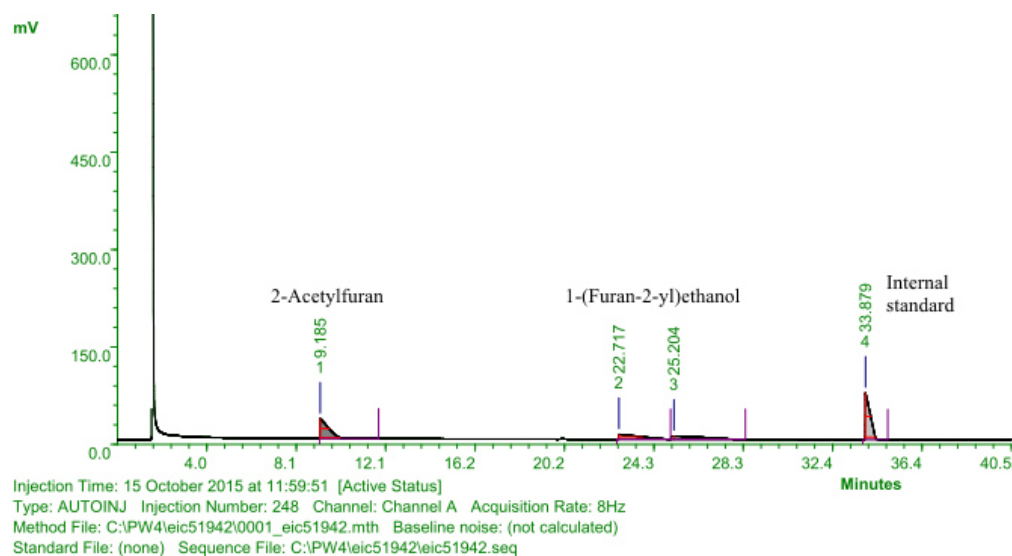
Chiral GC (CP-Chirasil-Dex CB): 130 °C isotherm. Measurement of reaction sample.



Peak	RT	Area	%Ar	Conc. (Ar)	Height	M	Units	Name
1	4.400	641.524	43.50	Not Calculated	245.467	0		
2	14.867	76.757	5.20	Not Calculated	8.638	0		
3	19.304	735.158	49.85	Not Calculated	18.805	1		
4	21.700	21.435	1.45	Not Calculated	0.924	1		

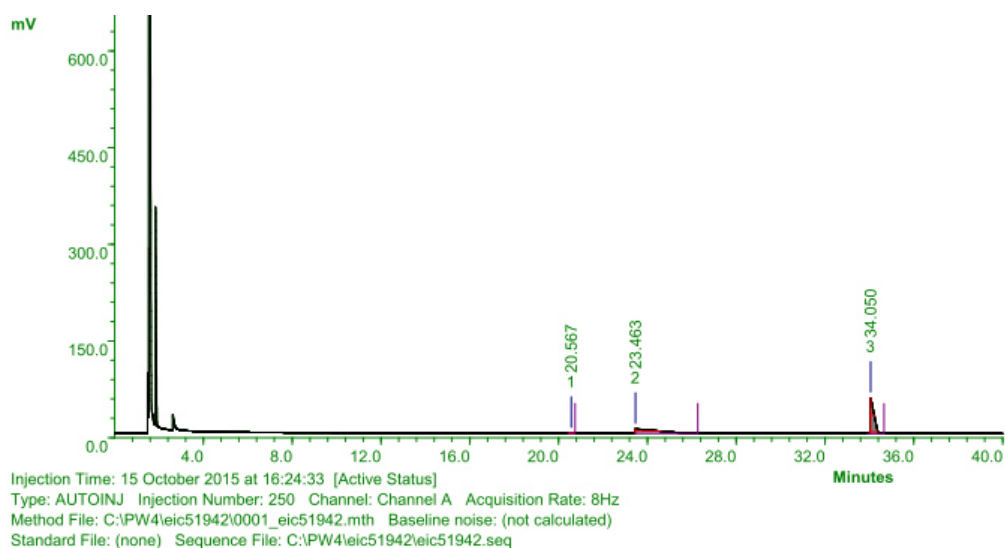
**(R)-1-(furan-2-yl)ethanol (82)**

Chiral GC (CP-Chirasil-Dex CB): 75 °C, progress rate 10 °C/min, final column temperature = 125 °C for 5 min. Calibration with standard, starting material and racemic product.



Peak	RT	Area	%Ar	Conc. (Ar)	Height	M	Units	Name
1	9.185	814.642	27.84	Not Calculated	30.001	0		
2	22.717	496.290	16.96	Not Calculated	7.577	0		
3	25.204	496.894	16.98	Not Calculated	5.047	0		
4	33.879	1117.848	38.21	Not Calculated	71.410	0		

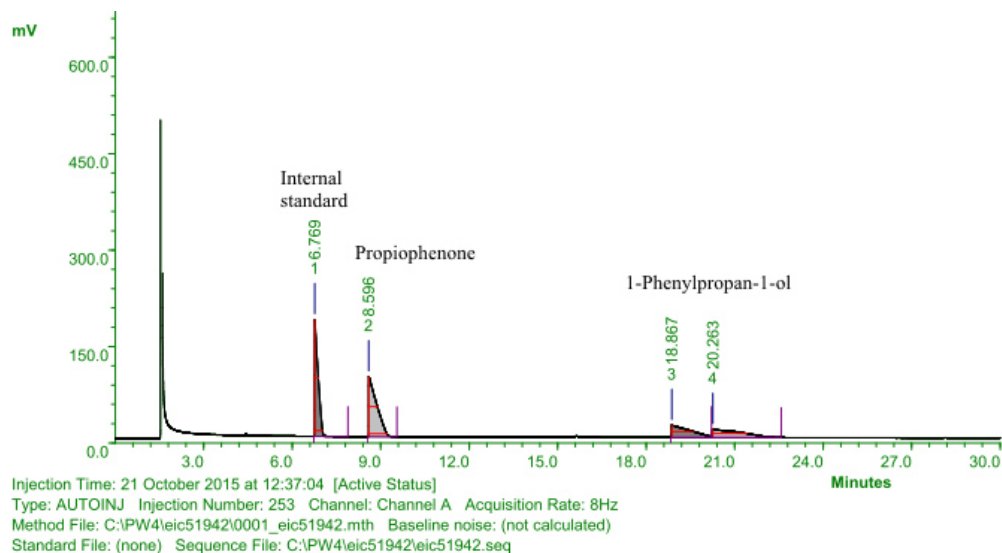
Chiral GC (CP-Chirasil-Dex CB): 75 °C, progress rate 10 °C/min, final column temperature = 125 °C for 5 min. Measurement of reaction sample.



Peak	RT	Area	%Ar	Conc. (Ar)	Height	M	Units	Name
1	20.567	3.003	0.26	Not Calculated	0.348	1		
2	23.463	482.656	42.25	Not Calculated	6.688	0		
3	34.050	656.653	57.48	Not Calculated	55.283	0		

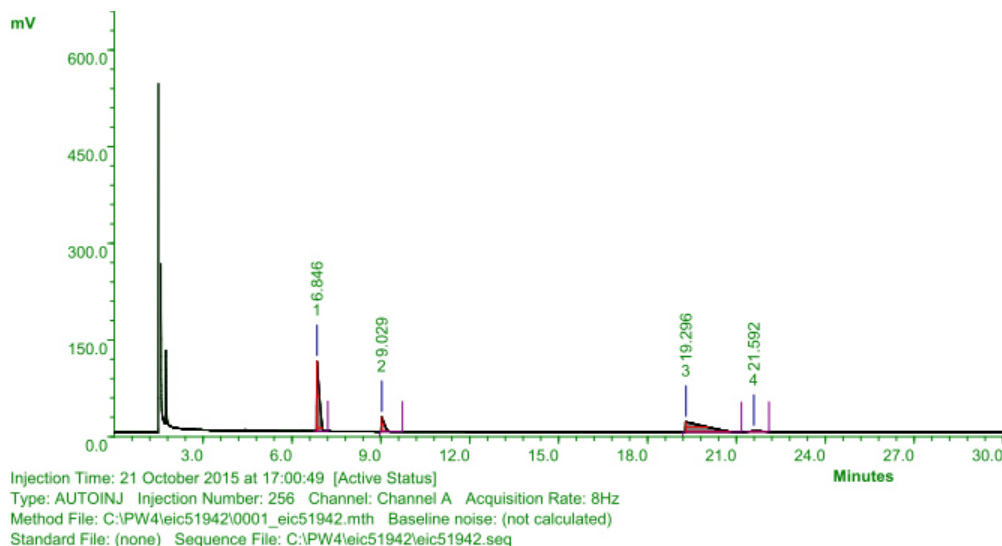
*(R)*-1-phenylpropan-1-ol (**83**)

Chiral GC (CP-Chirasil-Dex CB): 115 °C isotherm. Calibration with standard, starting material and racemic product.



Peak	RT	Area	%Ar	Conc. (Ar)	Height	M	Units	Name
1	6.769	1446.295	29.40	Not Calculated	181.869	0		
2	8.596	1764.924	35.88	Not Calculated	93.335	1		
3	18.867	843.187	17.14	Not Calculated	19.073	0		
4	20.263	864.488	17.57	Not Calculated	12.586	0		

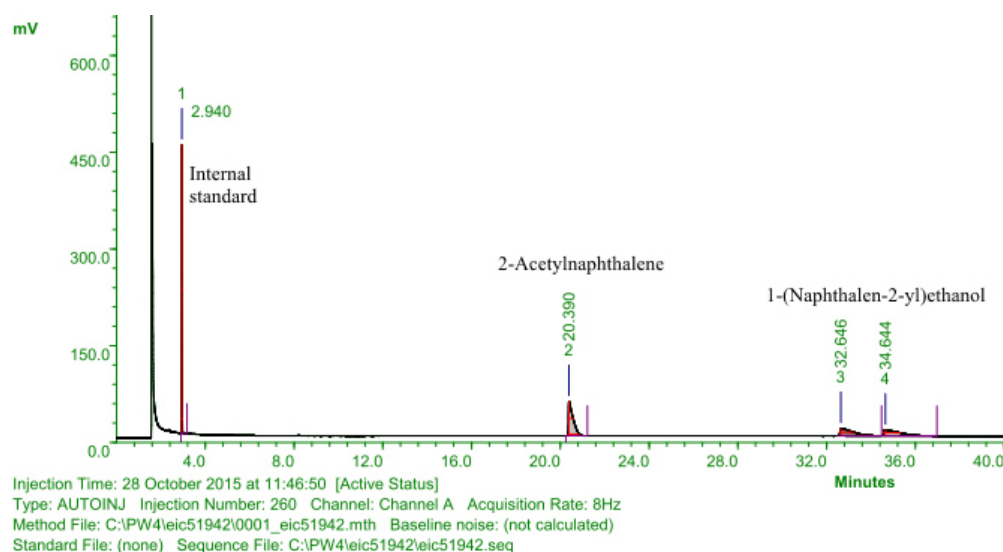
Chiral GC (CP-Chirasil-Dex CB): 115 °C isotherm. Measurement of reaction sample.



Peak	RT	Area	%Ar	Conc. (Ar)	Height	M	Units	Name
1	6.846	650.134	41.59	Not Calculated	108.406	1		
2	9.029	153.117	9.80	Not Calculated	22.099	0		
3	19.296	725.080	46.38	Not Calculated	15.737	0		
4	21.592	34.861	2.23	Not Calculated	1.039	1		

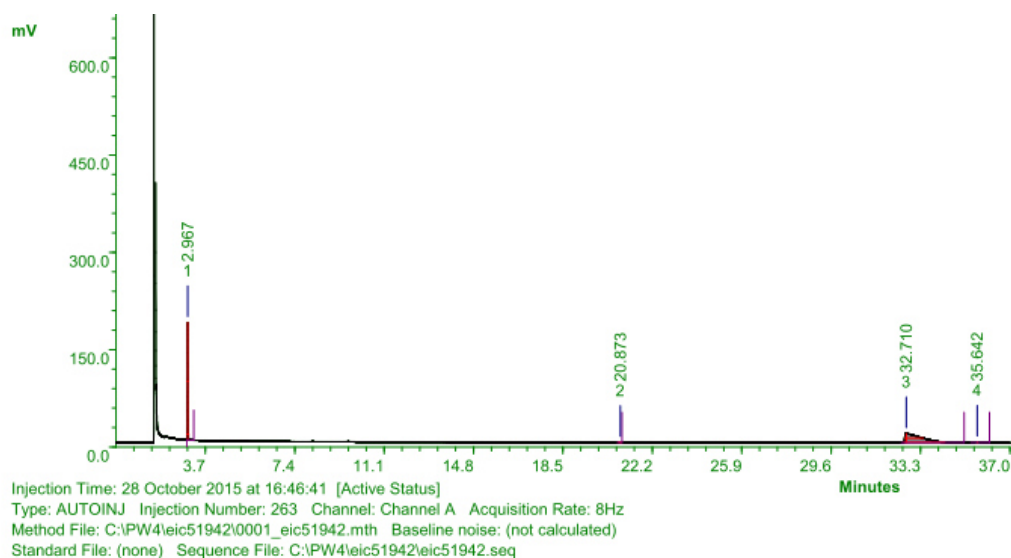
**(R)-1-(naphthalen-2-yl)ethanol (84)**

Chiral GC (CP-Chirasil-Dex CB): 150 °C isotherm. Calibration with standard, starting material and racemic product.



Peak	RT	Area	%Ar	Conc. (Ar)	Height	M	Units	Name
1	2.940	705.665	29.43	Not Calculated	446.985	0		
2	20.390	780.311	32.54	Not Calculated	53.358	0		
3	32.646	455.465	19.00	Not Calculated	11.645	0		
4	34.644	456.273	19.03	Not Calculated	9.327	0		

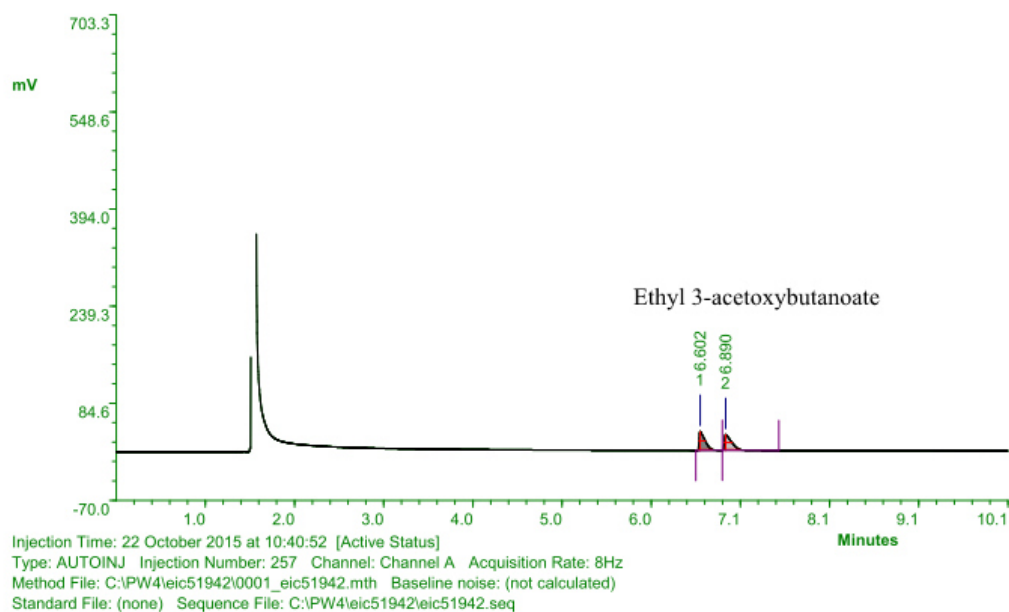
Chiral GC (CP-Chirasil-Dex CB): 150 °C isotherm. Measurement of reaction sample.



Peak	RT	Area	%Ar	Conc. (Ar)	Height	M	Units	Name
1	2.967	273.938	28.44	Not Calculated	181.206	0		
2	20.873	0.703	0.07	Not Calculated	0.107	1		
3	32.710	672.614	69.82	Not Calculated	13.952	1		
4	35.642	16.078	1.67	Not Calculated	0.678	1		

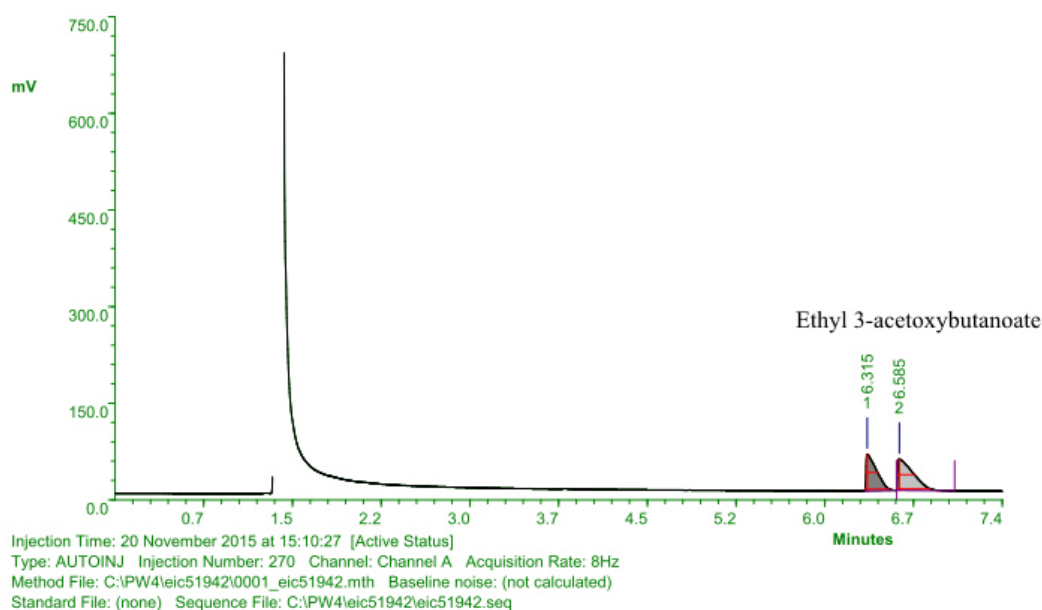
(*R*)-ethyl 3-acetoxybutanoate (**86**)

Chiral GC (CP-Chirasil-Dex CB): 110 °C isotherm. Calibration with racemic product **78**.



Peak	RT	Area	%Ar	Conc.(Ar)	Height	M	Units	Name
1	6.602	137.289	49.60	Not Calculated	30.029	0		
2	6.890	139.488	50.40	Not Calculated	24.890	0		

Chiral GC (CP-Chirasil-Dex CB) for enantiomeric excess: 110 °C isotherm. Measurement of reaction sample.



Peak	RT	Area	%Ar	Conc.(Ar)	Height	M	Units	Name
1	6.315	349.264	45.07	Not Calculated	57.341	1		
2	6.585	425.739	54.93	Not Calculated	48.347	1		

## 2.5 References

- [1] D. Wang, D. Astruc, *Chem. Rev.* **2015**, *115*, 6621–6686.
- [2] W. Zuo, S. Tauer, D. E. Prokopchuk, R. H. Morris, *Organometallics* **2014**, *33*, 5791–5801.
- [3] W. Zuo, A. J. Lough, Y. F. Li, R. H. Morris, *Science* **2013**, *342*, 1080–1083.
- [4] J. F. Sonnenberg, N. Coombs, P. A. Dube, R. H. Morris, *J. Am. Chem. Soc.* **2012**, *134*, 5893–5899.
- [5] A. Naik, T. Maji, O. Reiser, *Chem. Commun.* **2010**, *46*, 4475–4477.
- [6] a) S. Hashiguchi, A. Fujii, J. Takehara, T. Ikariya, R. Noyori, *J. Am. Chem. Soc.* **1995**, *117*, 7562–7563; b) A. Fujii, S. Hashiguchi, N. Uematsu, T. Ikariya, R. Noyori, *J. Am. Chem. Soc.* **1996**, *118*, 2521–2522; c) K.-J. Haack, S. Hashiguchi, A. Fujii, T. Ikariya, R. Noyori, *Angew. Chem. Int. Ed.* **1997**, *36*, 285–288.
- [7] [www.chemicool.com/elements](http://www.chemicool.com/elements).
- [8] A. Léonard in *Handbook on Toxicity of Inorganic Compounds* (Eds.: H. G. Seiler, H. Sigel, A. Sigel, A. Townshend), Dekker, New York, **1988**.
- [9] J. Li, Y. Zhang, D. Han, Q. Gao, C. Li, *J. Mol. Catal. A: Chem.* **2009**, *298*, 31–35.
- [10] R. Marcos, C. Jimeno, M. A. Pericàs, *Adv. Synth. Catal.* **2011**, *353*, 1345–1352.
- [11] a) C. Saluzzo, T. Lamouille, D. Hérault, M. Lemaire, *Bioorg. Med. Chem. Lett.* **2002**, *12*, 1841–1844; b) K. Polborn, K. Severin, *Eur. J. Inorg. Chem.* **2000**, 1687–1692; c) Y. Arakawa, A. Chiba, N. Haraguchi, S. Itsuno, *Adv. Synth. Catal.* **2008**, *350*, 2295–2304; d) W. Shan, F. Meng, Y. Wu, F. Mao, X. Li, *J. Organomet. Chem.* **2011**, *696*, 1687–1690; e) J. Liu, Y. Zhou, Y. Wu, X. Li, Chan, Albert S. C., *Tetrahedron: Asymmetry* **2008**, *19*, 832–837.
- [12] a) V. I. Pârvulescu, C. Hardacre, *Chem. Rev.* **2007**, *107*, 2615–2665; b) T. J. Geldbach, P. J. Dyson, *J. Am. Chem. Soc.* **2004**, *126*, 8114–8115; c) I. Kawasaki, K. Tsunoda, T. Tsuji, T. Yamaguchi, H. Shibuta, N. Uchida, M. Yamashita, S. Ohta, *Chem. Commun.* **2005**, 2134–2136.
- [13] a) W. Liu, X. Cui, L. Cun, J. Zhu, J. Deng, *Tetrahedron: Asymmetry* **2005**, *16*, 2525–2530; b) Y.-C. Chen, T.-F. Wu, L. Jiang, J.-G. Deng, H. Liu, J. Zhu, Y.-Z. Jiang, *J. Org. Chem.* **2005**, *70*, 1006–1010; c) W. Wang, Q. Wang, *Chem. Commun.* **2010**, *46*, 4616–4618.
- [14] A. Zoabi, S. Omar, R. Abu-Reziq, *Eur. J. Inorg. Chem.* **2015**, *2015*, 2101–2109.
- [15] a) R. Liu, T. Cheng, L. Kong, C. Chen, G. Liu, H. Li, *J. Catal.* **2013**, *307*, 55–61; b) Z. Weng, S. Muratsugu, N. Ishiguro, S.-i. Ohkoshi, M. Tada, *Dalton Trans.* **2011**, *40*, 2338–2347; c) L. Wu, Y.-M. He, Q.-H. Fan, *Adv. Synth. Catal.* **2011**, *353*, 2915–2919.
- [16] Y. Sun, G. Liu, H. Gu, T. Huang, Y. Zhang, H. Li, *Chem. Commun.* **2011**, *47*, 2583–2585.
- [17] X. Gao, R. Liu, D. Zhang, M. Wu, T. Cheng, G. Liu, *Chem. Eur. J.* **2014**, *20*, 1515–1519.
- [18] a) J. Huang, F. Zhang, H. Li, *Appl. Catal. A: Gen.* **2012**, *431–432*, 95–103; b) W. Xiao, R. Jin, T. Cheng, D. Xia, H. Yao, F. Gao, B. Deng, G. Liu, *Chem. Commun.* **2012**, *48*, 11898–11900.
- [19] a) D. Wang, D. Astruc, *Chem. Rev.* **2014**, *114*, 6949–6985; b) Q. M. Kainz, O. Reiser, *Acc. Chem. Res.* **2014**, *47*, 667–677; c) R. B. Nasir Baig, M. N. Nadagouda, R. S. Varma, *Coord. Chem. Rev.* **2015**, *287*, 137–156; d) L. M. Rossi, Costa, Natalia J. S., F. P. Silva, R. Wojcieszak, *Green Chem.* **2014**, *16*, 2906–2933; e) R. Dalpozzo, *Green Chem.* **2015**; f) M. B. Gawande, S. N. Shelke, R. Zboril, R. S. Varma, *Acc. Chem. Res.* **2014**, *47*, 1338–1348; g) M. B. Gawande, Y. Monga, R. Zboril, R. K. Sharma, *Coord. Chem. Rev.* **2015**, *288*, 118–143.
- [20] B. Baruwati, V. Polshettiwar, R. S. Varma, *Tetrahedron Lett.* **2009**, *50*, 1215–1218.
- [21] R. N. Grass, E. K. Athanassiou, W. J. Stark, *Angew. Chem. Int. Ed.* **2007**, *46*, 4909–4912.

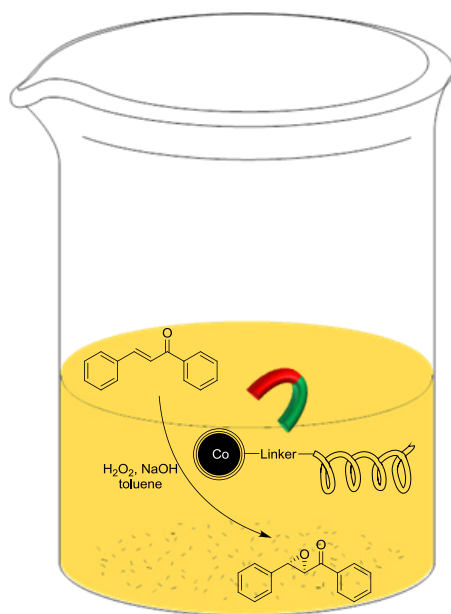


- [22] a) Q. M. Kainz, R. Linhardt, R. N. Grass, G. Vilé, J. Pérez-Ramírez, W. J. Stark, O. Reiser, *Adv. Funct. Mater.* **2014**, *24*, 2020–2027; b) R. Linhardt, Q. M. Kainz, R. N. Grass, W. J. Stark, O. Reiser, *RSC Adv.* **2014**, *4*, 8541–8549; c) S. Wittmann, J.-P. Majoral, R. N. Grass, W. J. Stark, O. Reiser, *Green Process Synth.* **2012**, *1*, 275–279; d) S. Wittmann, A. Schätz, R. N. Grass, W. J. Stark, O. Reiser, *Angew. Chem. Int. Ed.* **2010**, *49*, 1867–1870; e) A. Schätz, T. R. Long, R. N. Grass, W. J. Stark, P. R. Hanson, O. Reiser, *Adv. Funct. Mater.* **2010**, *20*, 4323–4328; f) A. Schätz, R. N. Grass, Q. Kainz, W. J. Stark, O. Reiser, *Chem. Mater.* **2010**, *22*, 305–310; g) S. Wittmann, A. Schätz, R. N. Grass, W. J. Stark, O. Reiser, *Angew. Chem. Int. Ed.* **2010**, *49*, 1867–1870.
- [23] P. Riente, C. Mendoza, M. A. Pericás, *J. Mater. Chem.* **2011**, *21*, 7350–7355.
- [24] a) S. Sun, H. Zeng, *J. Am. Chem. Soc.* **2002**, *124*, 8204–8205; b) S. Sun, H. Zeng, D. B. Robinson, S. Raoux, P. M. Rice, S. X. Wang, G. Li, *J. Am. Chem. Soc.* **2004**, *126*, 273–279.
- [25] a) X. Wu, X. Li, W. Hems, F. King, J. Xiao, *Org. Biomol. Chem.* **2004**, *2*, 1818–1821; b) X. Wu, X. Li, A. Zanotti-Gerosa, A. Pettman, J. Liu, A. J. Mills, J. Xiao, *Chem. Eur. J.* **2008**, *14*, 2209–2222; c) X. Wu, J. Liu, D. Di Tommaso, J. A. Iggo, C. R. A. Catlow, J. Bacsá, J. Xiao, *Chem. Eur. J.* **2008**, *14*, 7699–7715; d) X. Wu, J. Xiao, *Chem. Commun.* **2007**, 2449–2466; e) X. Li, X. Wu, W. Chen, F. E. Hancock, F. King, J. Xiao, *Org. Lett.* **2004**, *6*, 3321–3324; f) D. S. Matharu, D. J. Morris, G. J. Clarkson, M. Wills, *Chem. Commun.* **2006**, 3232–3234.
- [26] C. G. Tan, R. N. Grass, *Chem. Commun.* **2008**, 4297–4299.
- [27] A. Schätz, M. Zeltner, T. D. Michl, M. Rossier, R. Fuhrer, W. J. Stark, *Chem. Eur. J.* **2011**, *17*, 10566–10573.
- [28] K. Hayashi, K. Ono, H. Suzuki, M. Sawada, M. Moriya, W. Sakamoto, T. Yogo, *Chem. Mater.* **2010**, *22*, 3768–3772.
- [29] A. Schätz, T. R. Long, R. N. Grass, W. J. Stark, P. R. Hanson, O. Reiser, *Adv. Funct. Mater.* **2010**, *20*, 4323–4328.
- [30] B. Lal, B. N. Pramanik, M. S. Manhas, A. K. Bose, *Tetrahedron Lett.* **1977**, *18*, 1977–1980.
- [31] European Medicines Agency, *Guideline on the Specification Limits for Residues of Metal Catalysts or Metal Reagents*, London, **2008**.
- [32] a) N. Haraguchi, K. Tsuru, Y. Arakawa, S. Itsuno, *Org. Biomol. Chem.* **2009**, *7*, 69–75; b) P. N. Liu, J. G. Deng, Y. Q. Tu, S. H. Wang, *Chem. Commun.* **2004**, 2070–2071.
- [33] G. Liu, H. Gu, Y. Sun, J. Long, Y. Xu, H. Li, *Adv. Synth. Catal.* **2011**, *353*, 1317–1324.
- [34] M. Rossier, F. M. Koehler, E. K. Athanassiou, R. N. Grass, B. Aeschlimann, D. Günther, W. J. Stark, *J. Mater. Chem.* **2009**, *19*, 8239–8243.
- [35] A. del Prado, N. Briz, R. Navarro, M. Pérez, A. Gallardo, H. Reinecke, *Macromolecules* **2012**, *45*, 2648–2653.
- [36] X. Xu, R. Wang, J. Wan, X. Ma, J. Peng, *RSC Adv.* **2013**, *3*, 6747.
- [37] Y. Arakawa, A. Chiba, N. Haraguchi, S. Itsuno, *Adv. Synth. Catal.* **2008**, *350*, 2295–2304.
- [38] S. Tanaka, M. Matsumoto, R. Goseki, T. Ishizone, A. Hirao, *Macromolecules* **2013**, *46*, 146–154.
- [39] Y. Yang, Z. Weng, S. Muratsugu, N. Ishiguro, S.-i. Ohkoshi, M. Tada, *Chem. Eur. J.* **2012**, *18*, 1142–1153.
- [40] S. J. Nelson, Jr., *U.S. Patent* **1966**, 3260748.
- [41] A. Schätz, R. N. Grass, W. J. Stark, O. Reiser, *Chem. Eur. J.* **2008**, *14*, 8262–8266.
- [42] B. Lal, B. N. Pramanik, M. S. Manhas, A. K. Bose, *Tetrahedron Lett.* **1977**, *18*, 1977–1980.
- [43] M. Hong, J.-Y. Liu, B.-X. Li, Y.-S. Li, *Macromolecules* **2011**, *44*, 5659–5665.



- [44] a) A. M. Harned, H. S. He, P. H. Toy, D. L. Flynn, P. R. Hanson, *J. Am. Chem. Soc.* **2005**, *127*, 52–53; b) A. M. Harned, W. M. Sherrill, D. L. Flynn, P. R. Hanson, *Tetrahedron* **2005**, *61*, 12093–12099.
- [45] X. Wu, X. Li, F. King, J. Xiao, *Angew. Chem. Int. Ed.* **2005**, *44*, 3407–3411.
- [46] L. L. Machado, F. J. Q. Monte, de Oliveira, Maria da Conceição F., M. C. de Mattos, T. L. Lemos, V. Gotor-Fernández, G. de Gonzalo, V. Gotor, *J. Mol. Catal., B: Enzym.* **2008**, *54*, 130–133.
- [47] R. Soni, T. H. Hall, B. P. Mitchell, M. R. Owen, M. Wills, *J. Org. Chem.* **2015**, *80*, 6784–6793.
- [48] W.-P. Liu, M.-L. Yuan, X.-H. Yang, K. Li, J.-H. Xie, Q.-L. Zhou, *Chem. Commun.* **2015**, *51*, 6123–6125.
- [49] T. Touge, T. Hakamata, H. Nara, T. Kobayashi, N. Sayo, T. Saito, Y. Kayaki, T. Ikariya, *J. Am. Chem. Soc.* **2011**, *133*, 14960–14963.

### 3 Juliá-Colonna epoxidation catalyzed by poly(*L*-leucine) functionalized magnetic nanoparticles



In a direct polymerization of *L*-leucine-*N*-carboxyanhydride (*L*-leucine-NCA) with amino functionalized nanobeads as initiators poly(*L*-leucine) catalysts were immobilized on carbon-coated cobalt and iron nanoparticles. The amino groups were introduced by different routes and the influence of the linker between the poly(*L*-leucine) and the magnetic core was studied with regard to the polymerization behavior as well as the catalyst activity. Different conditions for the catalyst preparation and the asymmetric epoxidation of (*E*)-chalcone as model substrate were investigated and compared. The  $\text{H}_2\text{O}_2$ /PTC protocol in combination with magnetic poly(*L*-leucine), having connected the catalyst to the nanoparticle by a tetrahydrofuran unit, was identified as the best option. Applying this catalyst, the influence of elevated temperatures, the catalyst ratio and reaction times were studied. In the end, the recyclability of the catalyst was tested in two runs.<sup>i</sup>

<sup>i</sup> Magnetization measurements were performed by H. Körner. TEM was done by Prof. J. Zweck. All other experiments were carried out by C. M. Eichenseer.

### 3.1 Introduction

Juliá and Colonna<sup>[1]</sup> reported in 1980 an enantioselective version of the achiral Weitz-Scheffer epoxidation of  $\alpha,\beta$ -unsaturated ketones using a simple poly(amino acid) catalyst. The transformation was highly enantioselective for electron-deficient substrates. The original Juliá and Colonna conditions consist of a triphasic system comprising an aqueous alkaline hydrogen peroxide phase, an organic phase, which is not miscible with water and contains the substrate, as well as the insoluble polymeric catalyst. Kelly and Roberts<sup>[2]</sup> studied the mechanism of the epoxidation and reported a two-step procedure: the fast and reversible addition of hydroperoxide and subsequently, the intramolecular nucleophilic elimination of the hydroxide. Most often poly(leucine) with a typical chain length of 30 amino acids is used as catalyst. It belongs to the amino acids which most likely adapt an  $\alpha$ -helical conformation in solution. As this is significant for the catalyst's activity it accounts for the preferential application of poly(leucine).<sup>[2,3]</sup> Over the years, the catalyst preparation as well as the reaction conditions were improved by a number of researchers, not only to broaden the substrate scope but also to reduce the reaction time dramatically.<sup>[3,4,5,6]</sup>

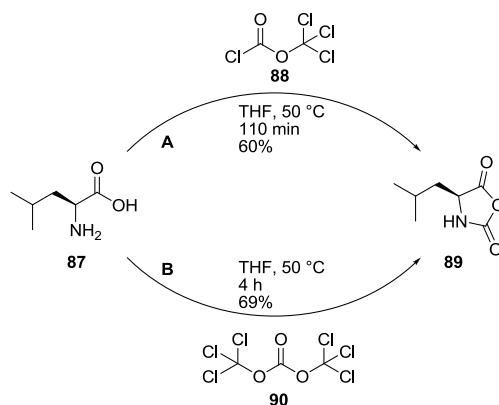
Milizter *et al.*<sup>[6]</sup> reported the application of a phase transfer catalyst (PTC) which can accelerate the reaction greatly yielding the product in good enantioselectivities. Subsequently, Gerlach and Geller were able to show an upscaling of the catalyst preparation as well as the asymmetric epoxidation, performing the reaction on a one hundred gram substrate level. The epoxy ketone could be isolated in good yield and high optical purity.<sup>[7]</sup> Roberts *et al.* developed two variants for a biphasic Juliá-Colonna epoxidation.<sup>[8,9]</sup> The first protocol reported the transformation in a non-aqueous medium. The substrate was dissolved in THF to which DBU and anhydrous urea- $\text{H}_2\text{O}_2$  were added while the insoluble catalyst represents the second phase.<sup>[8]</sup> Alternatively, the reaction can be performed in a homogeneous mixture of water and DME which contains the substrate as well as sodium percarbonate, acting as oxidant and base. Once again the second phase consists of the insoluble catalyst.<sup>[9]</sup> Disadvantageous, the poly(amino acid) catalyst becomes gel- or paste-like during the reaction regardless of the applied protocol, hindering simple filtration. Therefore, a trend towards heterogeneous variants developed. At the beginning, the covalent anchoring of the catalyst to organic polymers like poly(styrene) was investigated.<sup>[10]</sup> Later on, the noncovalent adsorption on silica was tested.<sup>[3,11]</sup> This modification both facilitated the catalyst separation by filtration and led to an acceleration of the reaction. Further improvement with regard to recyclability could be achieved by the covalent attachment of the catalyst to silica gel.<sup>[12]</sup> The Si-O-Si bond used for anchoring the poly(amino acid) was stable over 10 runs with just minor loss of activity while the recovery of the catalyst was

simplified. However, until now, there is no report about poly(amino acid) catalysts for the Juliá-Colonna epoxidation immobilized on magnetic nanoparticles.

Herein, the synthesis of five different amino functionalized magnetic carbon-coated cobalt nanoparticles and their application as initiator in the polymerization with *L*-leucine-NCA is described. The resulting poly(*L*-leucine) covalently attached to the magnetic nanoparticles was studied as catalyst for the asymmetric epoxidation of (*E*)-chalcone under various conditions.

### 3.2 Results and discussion

Leucine-*N*-carboxyanhydride (leucine-NCA) is a cyclic derivative of leucine which is widely used as monomer for the preparation of peptides.<sup>[13]</sup> For a long time the cyclization with phosgene has been the preferred method thanks to the short and efficient reaction. Though, the gaseous compound is highly toxic and difficult to handle. Therefore, alternative phosgene sources were tested and methods employing liquid diphosgene or solid triphosgene were developed. In this work, the phosgenation of *L*-leucine **87** was performed on the one hand with diphosgene<sup>[14]</sup> **88** (Scheme 19 A) and on the other hand with triphosgene<sup>[13]</sup> **90** (Scheme 19 B). In both reactions the product could be obtained in good yields, however, triphosgene **90** as phosgene source was safer as well as more convenient to handle and gave the product in better yield (69%). This is why in the following triphosgene **90** was utilized for the synthesis of *L*-leucine-NCA **89**.

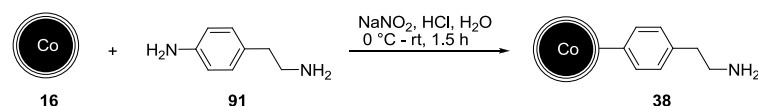


**Scheme 19.** (A) Synthesis of leucine-NCA **89** with diphosgene **88**. (B) Synthesis of leucine-NCA **89** with triphosgene **90**.

Following the immobilization strategy of Tang *et al.*,<sup>[12]</sup> poly(*L*-leucine) should be grafted on the solid support *via* polymerization of *L*-leucine-NCA **89** initiated by amino groups.

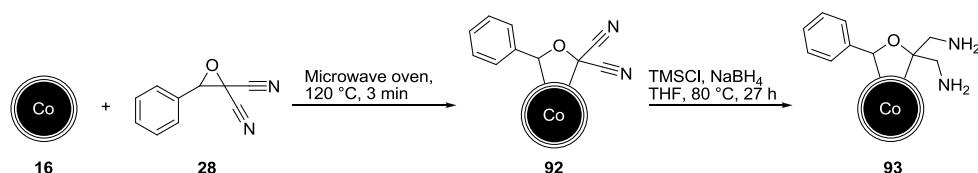
Therefore, magnetic nanoparticles should be functionalized with amino moieties. It was envisioned to design different amino functionalized nanoparticles which vary in the way the functional group is attached to the core of the particle. It should then be investigated which influence the type of connection has on the polymerization behavior as well as on the catalytic activity.

By using well-established diazonium chemistry<sup>[15,16]</sup> 4-(2-aminoethyl)aniline **91** was anchored to Co/C NPs **16** (Scheme 20) yielding NPs **38**. After just 1.5 h the amino functionalized nanobeads could be collected and the nitrogen loading was determined by elemental analysis to be 0.18 mmol per gram nanoparticles, which is 18% of the maximal theoretical nitrogen loading of 1.0 mmol per gram based on the employed amount of **91**.



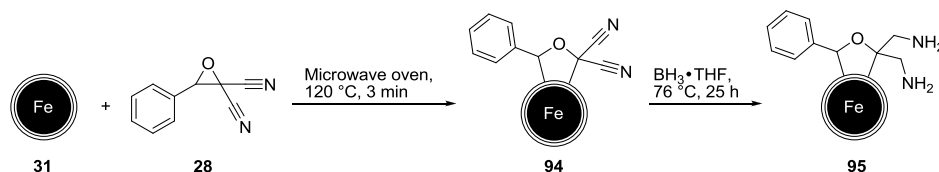
**Scheme 20.** Functionalization of NPs **16** (1.0 g) with 4-(2-aminoethyl)aniline **91** (1.0 mmol) by diazonium chemistry.

In a second approach, tetrahydrofuran units bearing two amino moieties were bound to the surface of the nanoparticles *via* microwave-induced opening of epoxide **28** and 1,3-dipolar cycloaddition of the corresponding ylide to the graphene-like shell of **16**. A subsequent reduction of the cyano groups with *in situ* generated  $\text{BH}_3 \cdot \text{THF}$  led to the amino functionalized material **93** (Scheme 21).<sup>[17,18]</sup> According to the applied amount of monomer, a theoretical nitrogen loading of 5.9 mmol per gram was the maximum which could have been obtained. Elemental analysis confirmed a real nitrogen loading of 0.82 mmol/g, which is high in comparison to the values typically obtained by diazonium chemistry but represents just 14% of the maximal theoretical loading.



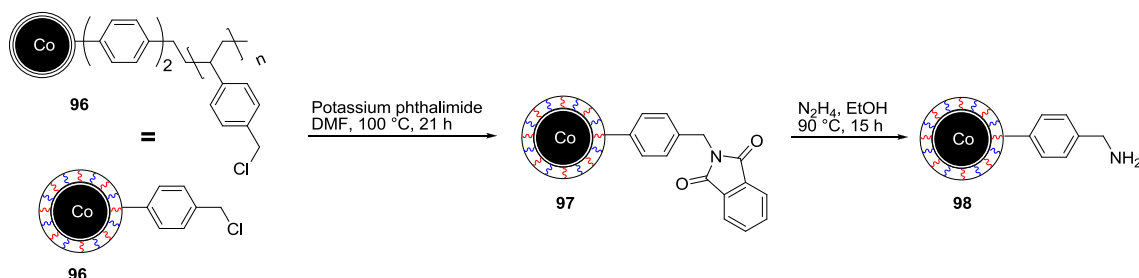
**Scheme 21.** Functionalization of Co/C NPs **16** (0.1 g) by 1,3-dipolar cycloaddition of epoxide **28** (0.59 mmol) and subsequent reduction.

The same functionalization strategy as shown in Scheme 21 was performed with carbon-coated iron nanoparticles **31** leading to cyano moieties attached to NPs **94** which were reduced with commercially available  $\text{BH}_3 \cdot \text{THF}$  to yield NPs **95** (Scheme 22). In this experiment, a higher amount of epoxide monomer was employed leading to a maximal theoretical nitrogen loading of 11.7 mmol per gram. A real nitrogen loading of 1.67 mmol per gram could be determined by elemental analysis, representing 14% of the theoretical loading.



**Scheme 22.** Functionalization of Fe/C NPs **31** (0.15 g) by 1,3-dipolar cycloaddition of epoxide **28** (0.88 mmol) and subsequent reduction.

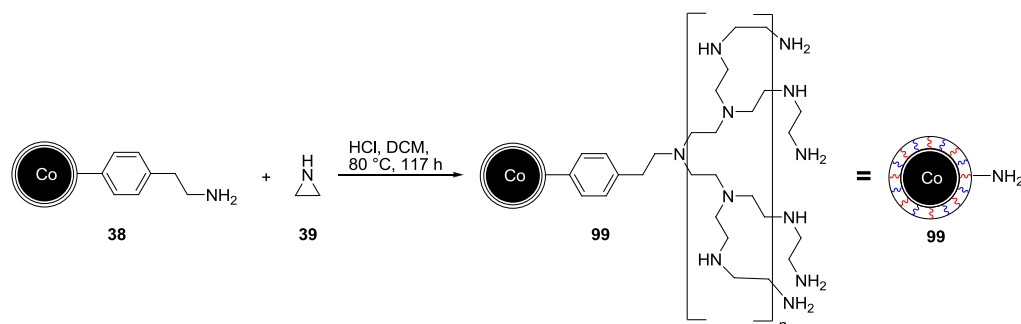
Co/C-PS-Cl NPs **96** having a poly(styrene) shell with terminal benzyl chloride moieties anchored to the surface of the nanobeads could be transformed to the amino functionalized nanobeads **98** *via* Gabriel synthesis. In the presence of potassium phthalimide, NPs **96** were heated in anhydrous DMF to form the intermediate **97**. Afterwards, a suspension of **97** in a hydrazine/EtOH mixture was refluxed to yield Co/C-PS-NH<sub>2</sub> **98** with a nitrogen loading of 2.7 mmol per gram (Scheme 23). This high nitrogen loading was rendered possible by the additional polymer grafted on the particles resulting in a bigger surface area and therefore more available functional groups.



**Scheme 23.** Gabriel synthesis of Co/C-PS-NH<sub>2</sub> **98**.

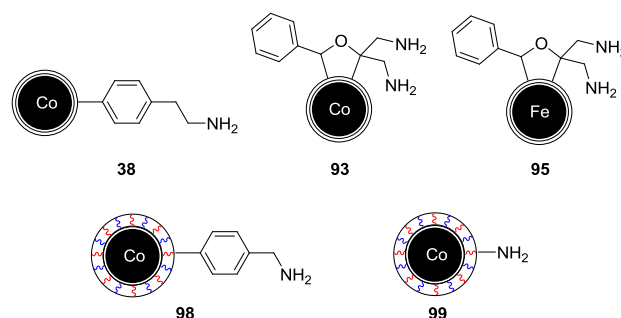
Adapting a procedure reported by Liu *et al.*,<sup>[19]</sup> a poly(ethyleneimine) shell should be attached to the surface of the amino functionalized NPs **38** to increase both the nitrogen loading and the dispersibility. Co/C-PEI NPs **99** were synthesized *via* cationic polymerization of

aziridine **39** with a catalytic amount of HCl within 117 h (Scheme 24).<sup>[16]</sup> An excellent nitrogen loading of 3.0 mmol per gram confirmed the successful growth of a PEI layer on the nanoparticles.



**Scheme 24.** Polymerization of aziridine **39** to yield Co/C-PEI NPs **99** with a nitrogen loading of 3.0 mmol per gram.

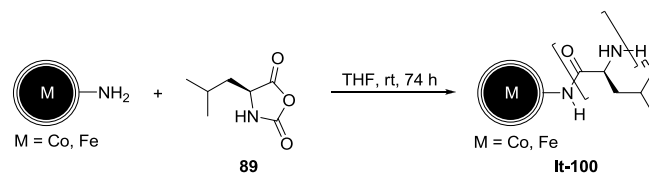
With different amino functionalized NPs **38**, **93**, **95**, **98** and **99** (Figure 21) in hand, they were studied as initiators in the polymerization with *L*-leucine-NCA **89** (33 equivalents) in THF at room temperature.<sup>[12,20]</sup> This low-temperature (lt) polymerization reaction was performed in the same manner with all five amino functionalized materials. The results hereof are summarized in Table 3.

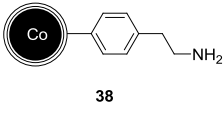
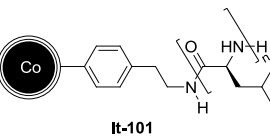
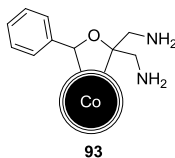
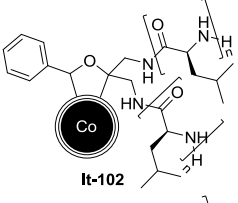
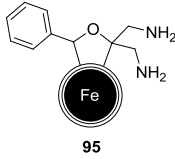
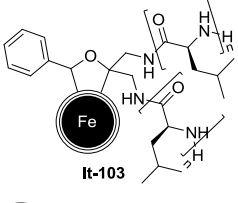
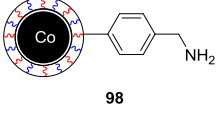
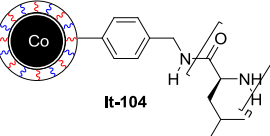
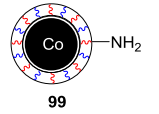
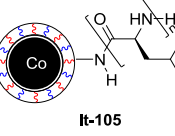


**Figure 21.** Different amino functionalized nanoparticles.

The resulting materials were characterized by elemental analysis to determine the loading of leucine. Furthermore, superconducting quantum interference device (SQUID) magnetometry analysis was used to measure the remaining magnetization of the particles. This value correlates to how well the magnetic core is shielded by the polymer giving an insight on the polymeric layer's dimension.

**Table 3.** Summarized results of low *It*-polymerization reaction with amino functionalized NPs **38**, **93**, **95**, **98** and **99** and *L*-leucine-NCA **89** (33 equiv.) at rt yielding magnetic poly(*L*-leucine) catalysts comparable to **It-100**.



Entry	Starting material	Loading (N) [mmol/g]	Product	Loading (Leucine) [mmol/g]	Magnetization [emu/g]
1	 <b>38</b>	0.18	 <b>It-101</b>	3.1	80.9
2	 <b>93</b>	0.82	 <b>It-102</b>	1.5	100.4
3	 <b>95</b>	1.7	 <b>It-103</b>	3.7	19.6
4	 <b>98</b>	2.7	 <b>It-104</b>	3.3	22.9
5	 <b>99</b>	3.0	 <b>It-105</b>	2.3	59.2

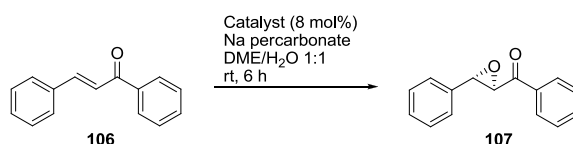
Due to the high values for the leucine loading, it could be deduced that the synthesis of magnetic poly(*L*-leucine) catalyst **It-100** was successful in all cases. Low loaded amino NPs **38** resulted in high loaded NPs **It-101** with a saturation magnetization of 90 emu/g (Table 3, entry 1). This value was still close to the saturation magnetization of unfunctionalized Co/C NPs **16** (130 emu/g) indicating that the extent of the grafted polymer was limited. In agreement, **It-102** having a lower leucine loading showed an even higher magnetization (100 emu/g) suggesting a thinner polymer layer than in **It-101** (Table 3, entry 2). The high loaded amino materials **98** and



**99** yielded the poly(*L*-leucine) catalysts **lt-104** and **lt-105** with likewise high leucine loadings (3.3 and 2.3 mmol/g, respectively). As **98** and **99** already featured a polymer attached to the magnetic core, the poly(amino acid) coating represented a second layer and therefore decreased the saturation magnetization even further (23 and 59 emu/g, see Table 3, entries 4–5). Nevertheless, magnetization of **lt-104** and **lt-105** was still high enough for a fast and efficient collection with the help of a magnet.

The thus obtained catalysts were studied in the Juliá-Colonna epoxidation with regard to their activity and enantioselectivity. In a model reaction, (*E*)-chalcone **106** was epoxidized using 8 mol% of the corresponding poly(*L*-leucine) catalyst with sodium percarbonate as oxidant and base (Table 4).<sup>[12]</sup> The resulting system was biphasic consisting of the semi-heterogeneous catalyst and a homogeneous solvent mixture of water and DME. After six hours at rt, the product **107** and the remaining starting material **106** were isolated and the results achieved with the different catalysts **lt-101**, **lt-102**, **lt-103**, **lt-104** and **lt-105** were compared. Unfortunately, all catalysts displayed poor enantioselectivity but with catalysts **lt-103**, **lt-104** and **lt-105** the product was formed in good yields (Table 4). Among all, **lt-104** was the best catalyst as it showed the highest selectivity while still being active (54%, 29% *ee*). Therefore, this catalyst was used for further optimization studies.

**Table 4.** Conditions and results for the epoxidation of (*E*)-chalcone **106** with the percarbonate protocol. Reaction conditions: 8 mol% catalyst, sodium percarbonate, DME/H<sub>2</sub>O 1:1, rt 6 h.



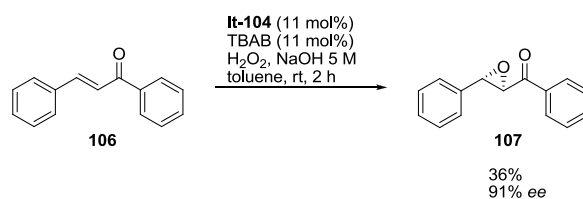
Entry	Catalyst	Yield [%] <sup>[a]</sup>	<i>ee</i> [%] <sup>[b]</sup>
1	<b>lt-101</b>	29	9
2	<b>lt-102</b>	37	3
3	<b>lt-103</b>	65	10
4	<b>lt-104</b>	54	29
5	<b>lt-105</b>	75	8
6	No catalyst	65	0

<sup>[b]</sup> Isolated yield.

<sup>[b]</sup> Determined by chiral HPLC analysis.

According to Roberts *et al.*<sup>[3]</sup> the untreated poly(amino acid) catalyst was found to be ineffective under the biphasic conditions, unlike under the original Juliá-Colonna triphasic conditions. An activation procedure which consisted of stirring the catalyst in a mixture of toluene and aqueous NaOH was required to enable an efficient catalysis. It was suspected that also poly(*L*-leucine) immobilized on Co/C NPs might need an activating treatment. However, pre-activated catalyst **It-104** gave the product in a lower yield (18% compared to 54%) while the enantiomeric excess of 25% remained as low as for the non-activated catalyst.

After discovering that the activation procedure did not work, the reaction conditions were switched to the original triphasic protocol which consisted of an organic phase containing the substrate, an aqueous phase with the oxidant as well as the semi-heterogeneous catalyst.<sup>[21]</sup> Additionally, a phase transfer catalyst (PTC) was applied which facilitated the interaction between the phases and significantly accelerated the epoxidation as Militzer *et al.*<sup>[6]</sup> previously reported. Catalyst **It-104** was tested under the new triphasic reaction conditions (Scheme 25). Luckily, the catalyst showed an improved enantioselectivity, yielding the product **107** with 91% *ee* but the isolated yield dropped to 36% compared to 54% in the percarbonate protocol. This might be caused by the reduced reaction time (two hours instead of six hours), though, it needs to be stated that while the reaction time was shortened, the catalyst loading was increased (11 mol% in comparison to 8 mol% in the percarbonate method). All in all, the results from the triphasic conditions with an additional PTC were encouraging, so in the following the investigations were continued using the H<sub>2</sub>O<sub>2</sub>/PTC protocol.



**Scheme 25.** Epoxidation of (*E*)-chalcone **106** with the H<sub>2</sub>O<sub>2</sub> protocol.

Nevertheless, a way to accelerate the catalysis had to be found in order to develop a synthetically useful process. Roberts *et al.*<sup>[3]</sup> described a significantly higher activity of the catalyst when the polymerization was performed at elevated temperatures. Therefore, we set out to investigate the influence of the high temperature (ht) polymerization on the activity of the magnetic nanoparticle supported poly(*L*-leucine) catalysts (Table 5). The amino functionalized NPs **38**, **93**, **95**, **98** and **99** were once more used as initiators in the polymerization with *L*-leucine-NCA **89**. The reaction was successfully carried out in DME at 90 °C yielding high

loaded poly(*L*-leucine) functionalized NPs **ht-101**, **ht-102**, **ht-103**, **ht-104** and **ht-105**. The results hereof are summarized in Table 5. As described before, all magnetic nanomaterials were characterized by elemental analysis for the determination of the leucine loading. Furthermore, the saturation magnetization of **ht-101**, **ht-102** and **ht-104** was measured to evaluate the degree of polymerization. While the high magnetization of **ht-101** indicated the limited formation of a polymer, the low values obtained for **ht-102** and **ht-104** suggested the growth of a large polymer layer on the surface.

**Table 5.** Summarized results of ht-polymerization reaction with amino functionalized NPs **38**, **93**, **95**, **98** and **99** and *L*-leucine-NCA **89** (32 equiv.) at 90 °C yielding magnetic poly(*L*-leucine) catalysts based on the model of **ht-100**.

Reaction scheme:  $\text{M-NH}_2 + \text{89} \xrightarrow{\text{DME, 90 } ^\circ\text{C, 18 h}} \text{ht-100}$  (M = Co, Fe)

Entry	Starting material	Loading (N) [mmol/g]	Product	Loading (Leucine) [mmol/g]	Magnetization [emu/g]
1	 <b>38</b>	0.18	 <b>ht-101</b>	2.9	80.4
2	 <b>93</b>	0.60	 <b>ht-102</b>	6.6	31.0
3	 <b>95</b>	0.83	 <b>ht-103</b>	4.1	n.d.
4	 <b>98</b>	2.7	 <b>ht-104</b>	4.8	13.0
5	 <b>99</b>	1.7	 <b>ht-105</b>	5.8	n.d.

Exemplary for all nanoparticles, a transmission electron microscopy (TEM) picture of **ht-104** was recorded to explore the assembly of the nanoparticles further. In Figure 22 a spherical structure is visible which represents the core of the nanoparticles. At the bottom left of the core the superlattice planes of the cobalt are depicted. Additionally, it can be seen that the magnetic nanoparticle is embedded in a grey structure which is most likely the polymer layer attached to the particles.

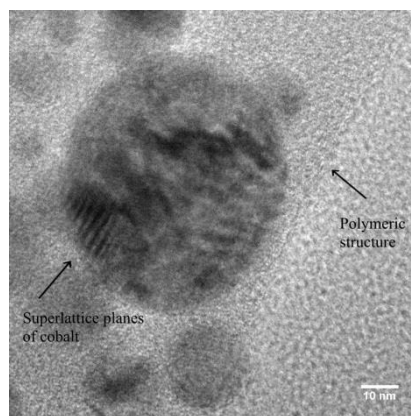


**Figure 22.** TEM picture of **ht-104**.

The catalysts synthesized by high temperature polymerization were expected to be more active than the low temperature catalysts. Therefore, their reactivity was investigated in both the percarbonate and the  $\text{H}_2\text{O}_2$ /PTC protocol to choose the most suitable reaction conditions for the respective catalysts. Ht-catalyst **ht-104** was selected for the initial comparison of the two protocols as it is structurally similar to catalyst **lt-104** which turned out to be the most active catalyst before. **ht-104** showed poor enantioselectivity (22% *ee*) in the percarbonate method while the yield was moderate after six hours with 8 mol% catalyst (51%). Using the  $\text{H}_2\text{O}_2$ /PTC protocol, **ht-104** catalyzed the epoxidation of (*E*)-chalcone with 89% *ee*. After six hours, the product could be obtained in 33% yield which was again lower than in the percarbonate protocol in spite of the higher amount of catalyst (11 mol%). It can be concluded that the  $\text{H}_2\text{O}_2$ /PTC method developed by Militzer and co-workers<sup>[6]</sup> was more suitable for magnetic Co/C-poly(*L*-leucine) catalysts with regard to enantioselectivity. For this reason, the activity of the remaining ht-catalysts **ht-101**, **ht-102**, **ht-103** and **ht-105** in the epoxidation of (*E*)-chalcone was evaluated using the  $\text{H}_2\text{O}_2$ /PTC protocol (Table 6). All catalyst gave the product with good to excellent enantiomeric excess (89-92% *ee*) while the yield ranged from 10-43%. Catalyst **ht-105** showed the best results in terms of yield and enantiomeric excess but the catalyst formed a very stable dispersion in the reaction solution and could not be magnetically collected after the reaction

(Table 6, entry 5). In contrast, **ht-103** could be easily recovered while still yielding the product with good selectivity (91% *ee*, Table 6, entry 3). The synthesis of the poly(*L*-leucine) functionalized NPs **ht-103** is accomplished conveniently in just three steps. Since combining an easy preparation and a good enantioselectivity in the epoxidation, this catalyst was the most promising one and was chosen for the further optimization work.

**Table 6.** Results for the epoxidation of (*E*)-chalcone **106** with H<sub>2</sub>O<sub>2</sub>/PTC protocol. Reaction conditions: 11 mol% catalyst, 11 mol% TBAB, H<sub>2</sub>O<sub>2</sub>, NaOH (5 M), toluene, rt, 2 h.

Entry	Catalyst	Yield [%] <sup>[a]</sup>	<i>ee</i> [%] <sup>[b]</sup>
1	<b>ht-101</b>	10	n.d.
2	<b>ht-102</b>	22	89
3	<b>ht-103</b>	25	91
4	<b>ht-104</b>	21	89
5	<b>ht-105</b>	43	92

<sup>[a]</sup> Determined by NMR spectroscopy using an internal standard.

<sup>[b]</sup> Determined by chiral HPLC analysis.

Several optimization studies were performed to increase the yield of epoxide **107** obtained with magnetic Co/C-poly(*L*-leucine) catalyst **ht-103**. First of all, the amount of catalyst was increased from 11 mol% to 25 mol%. The yield, though, did not even double (41% compared to 25%) while the enantioselectivity remained at a very good level (91% *ee*). Therefore, the higher catalyst amount could not significantly improve the reaction. In a next approach to accelerate the reaction, the temperature was increased from room temperature to 50 °C but both yield and enantiomeric excess dropped under these reaction conditions.

According to Ottolina *et al.*<sup>[22]</sup> the poly(amino acid) catalyst behaves comparable to an enzyme-like catalyst. This means that high chalcone concentrations lead to inhibition of the reaction while low concentrations act accelerating. This is why the activity of the catalyst was studied in a more diluted system. The concentration of (*E*)-chalcone **106** was lowered to 110 mM and the aqueous phase containing the oxidant was diluted while all other reaction parameters remained unchanged. However, a test reaction with catalyst **ht-103** showed no major improvements in activity after two hours reaction time. The epoxide **107** was formed in 30% yield with an enantiomeric excess of 92%.

Despite all efforts, the reaction proceeded too slowly. So in a next step, the influence of the solvent should be evaluated. As can be seen from Table 7 the best result with regard to enantioselectivity was reached in the original mixture of toluene and H<sub>2</sub>O (Table 7, entry 1). Using mixtures of THF/H<sub>2</sub>O or DCM/MeOH/H<sub>2</sub>O with a PTC led to good yields but with no stereocontrol which is most likely due to the failure of the poly(*L*-leucine) chains to adapt an  $\alpha$ -helical conformation (entry 2 and 6). To sum up, using a combination of toluene and H<sub>2</sub>O as solvent system was still the best option. Therefore, recyclability investigations of the catalyst were conducted using these reaction conditions.

**Table 7.** Solvent screening for asymmetric epoxidation of (*E*)-chalcone **106** using poly(*L*-leucine) functionalized NPs **ht-103**. Reaction conditions: 11 mol% catalyst, 11 mol% TBAB, H<sub>2</sub>O<sub>2</sub>, NaOH (5 M), solvent mixture, rt, 2 h.<sup>ii</sup>

Entry	Solvent	PTC	Yield [%] <sup>[a]</sup>	<i>ee</i> [%] <sup>[b]</sup>
1	H <sub>2</sub> O/toluene	Yes	25	91
2	H <sub>2</sub> O/THF	Yes	60	0
3	H <sub>2</sub> O/THF	No	29	9
4	H <sub>2</sub> O/acetonitrile	Yes	0	n.d.
5	H <sub>2</sub> O/acetonitrile	No	0	n.d.
6	H <sub>2</sub> O/DCM/MeOH	Yes	58	3
7	H <sub>2</sub> O/DCM/MeOH	No	36	1
8	H <sub>2</sub> O/EtOH/toluene	Yes	23	0
9	H <sub>2</sub> O/EtOH/toluene	No	31	0

<sup>[a]</sup> Isolated yield.

<sup>[b]</sup> Determined by chiral HPLC analysis.

For the recycling procedure, the catalyst **ht-103** was magnetically collected after the first run and after decantation of the reaction solution the catalyst was directly subjected to a second run by adding fresh reagents. Unfortunately, a drop in yield from 25% in the first run to 15% in the second run was detected (Figure 23). Additionally, the enantioselectivity suffered in the second run as the product was formed with an enantiomeric excess of 82% *ee* compared to 91% in the first run implying a further deactivation of the catalyst and making a reuse unattractive.

<sup>ii</sup> Results are partially taken from the Bachelor thesis of C. Markl (supervised by C. M. Eichenseer).

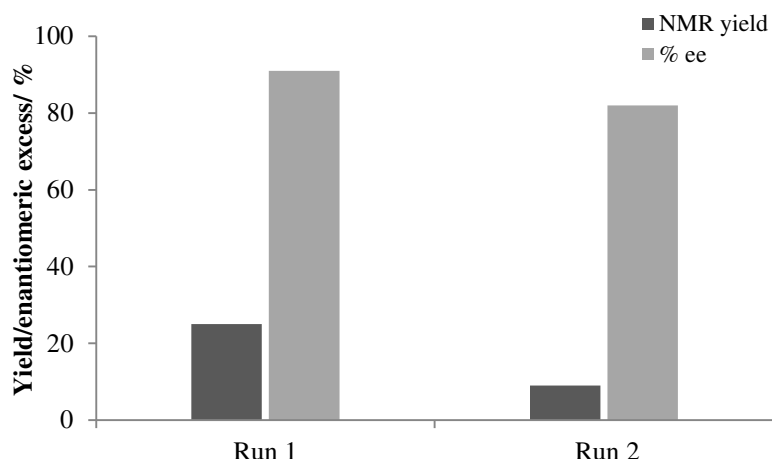
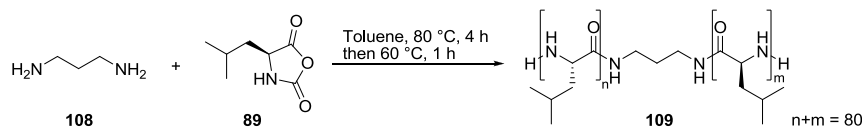


**Figure 23.** Recycling of catalyst **ht-103** in the asymmetric epoxidation of (*E*)-chalcone **106**. Reaction conditions: 11 mol% catalyst, 11 mol% TBAB, H<sub>2</sub>O<sub>2</sub>, NaOH (5 M), toluene, rt, 2 h.

As all optimization efforts seemed fruitless, the influence of the solid support on the reaction should be studied. A solely polymeric catalyst poly(*L*-leucine) **109** was prepared according to a procedure published by Gerlach and Geller<sup>[7]</sup> using 1,3-diaminopropane **108** as initiator and *L*-leucine-NCA **89** as monomer in the polymerization (Scheme 26). After four hours at 80 °C the polymeric catalyst was precipitated with MeOH and further heated at 60 °C for one hour. When applied in the epoxidation of (*E*)-chalcone **106** using the H<sub>2</sub>O<sub>2</sub>/PTC protocol, catalyst **109** showed a comparable enantioselectivity (92%) while its reactivity was clearly higher than with the magnetic nanoparticle supported catalysts as the corresponding epoxide **107** could be isolated in 77% yield. Therefore, it can be concluded that the magnetic nanoparticles as the support for the catalyst had a negative influence on the activity of the poly(*L*-leucine) resulting in low yields.



**Scheme 26.** Synthesis of poly(*L*-leucine) **109** by polymerization of *L*-leucine-NCA **89** (80 equiv.) with 1,3-diaminopropane **108** as initiator.

### 3.3 Conclusion

In summary, five different amino functionalized nanoparticles have been successfully synthesized. All of them were applied in the polymerization with *L*-leucine-NCA at low and high temperatures conditions to functionalize the magnetic carbon-coated cobalt and iron nanoparticles with poly(*L*-leucine) chains. The resulting catalysts were characterized by elemental analysis and superconducting quantum interference device (SQUID) magnetometry analysis. The reactivity and enantioselectivity were studied in the asymmetric epoxidation of (*E*)-chalcone applying different reaction conditions. The percarbonate protocol gave the chalcone oxide in good yields but with low enantiomeric excess. In contrast, the product was formed in good enantioselectivities with all catalysts using the H<sub>2</sub>O<sub>2</sub>/PTC method but the yields were relatively low. Nevertheless, catalyst **ht-103** was identified as the best and was used for further optimization studies. Though, the effort to increase the yield of chalcone oxide by raising the reaction temperature, prolonging the reaction time or increasing the amount of catalyst failed. Furthermore, a solvent screening did not show an improvement of the activity. Finally, the magnetic poly(*L*-leucine) catalyst **ht-103** could also not be reused in more than one run without a drop in yield and enantioselectivity. Overall, the chalcone oxide **107** could be synthesized in 25% yield and 91% *ee* within two hours using catalyst **ht-103** and H<sub>2</sub>O<sub>2</sub>/PTC reaction conditions.



## 3.4 Experimental section

### Materials and methods

Reactions with moisture and oxygen sensitive reagents were carried out in flame dried glassware under an atmosphere of pre-dried nitrogen. Microwave reactions were performed in the CEM Discover S-Class microwave oven using special pressure stable sealed 10 mL or 35 mL vials. Heavy-wall glass tubes or heavy-wall Schlenk flasks are borosilicate glass tubes with heavy walls that are stable up to 5 bar. Column chromatography was performed with silica gel (Merck, Geduran 60, 0.063-0.200 mm particles size). Thin layer chromatography was performed with TLC pre-coated aluminum sheets (Merck or Macherey-Nagel Silica gel 60 F254, 0.2 mm layer thickness). Visualization was accomplished with UV light ( $\lambda = 254$  nm or 366 nm) and stained with Vanillin/sulfuric acid or basic potassium permanganate. NMR spectra were recorded on BRUKER Avance 400 and BRUKER Avance 300 spectrometer. All spectra were recorded in  $\text{CDCl}_3$  or commercially available deuterated solvents. Chemical shifts are reported as  $\delta$ , parts per million, calibrated to the signal of the solvent. The coupling constants  $J$  are reported in Hertz (Hz). Splitting patterns for the spin multiplicity in the spectra are given as follows: s = singlet, d = doublet, t = triplet, q = quartet, dd = doublet of a doublet, ddd = doublet of a doublet of a doublet, dt = doublet of a triplet, m = multiplet. Attenuated total reflection infrared spectroscopy (ATR-IR) was carried out on a Varian FTS 1000 spectrometer (equipped with a Specac Golden Gate Diamond Single Reflection ATR-System), a Cary 630 FT-IR (Agilent Technologies) or a Varian 800 FT-IR Scimitar Series. Wave numbers are reported as  $\text{cm}^{-1}$ . Chiral HPLC analysis was performed on a Varian 920-LC using a Phenomenex Lux Cellulose-2 column. The optical rotation of optically active compounds was measured in the specified solvent on an Anton Paar MCP 500 at 589 nm (sodium-*d*-line) in a 1 dm measuring cell. Elemental microanalysis was performed by the micro analytical section of the University of Regensburg using a Vario MICRO cube. For transmission electron microscopy a FEI TecnaiF30 was used (Department of Physics, University of Regensburg). The saturation magnetization of magnetic samples was measured by superconducting quantum interference device (SQUID) magnetometry analysis on a MPMS XL from Quantum Design. Nanoparticles were dispersed in an ultrasonic bath (Bandelin Sonorex RK255 H-R) and recovered with the aid of a neodymium based magnet (side length 12 mm).

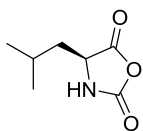
## Nanoparticle preparation

Carbon-coated cobalt nanoparticles (Co/C, mean particle size  $\approx 25$  nm) were obtained from Turbobeeds Llc, Switzerland. Before usage the nanobeads were washed five times in a Millipore water/HCl<sub>conc</sub> mixture (10/1). To remove any residual acid the nanoparticles were washed with Millipore water until the pH of the decanted solution was neutral. Finally, the particles were washed with acetone (3x) and diethyl ether (2x) and dried at 50 °C under vacuum.<sup>[23]</sup>

## Nomenclature

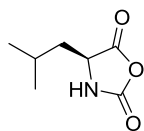
For the nanoparticles in this chapter the nomenclature is as follows: Co/C for magnetic carbon-coated cobalt nanoparticles with cobalt core and graphene-like shells, Fe/C for magnetic carbon-coated iron nanoparticles with iron core and graphene-like shells, Co/C-PEI for Co/C nanoparticles with a poly(ethylenimine) shell, Co/C-THF-R and Fe/C-THF-R for Co/C or Fe/C nanobeads, where R indicates the important functional groups: THF-CN for phenyltetrahydrofuran with cyano groups and THF-NH<sub>2</sub> for phenyltetrahydrofuran with amino groups. Co/C-NH<sub>2</sub> for nanobeads with 4-(2-aminoethyl)phenyl groups on the surface, Co/C-PS-R for nanobeads, where R indicates the functional group in the polymeric network: Cl for benzyl chloride and NH<sub>2</sub> for benzylamine.

### (S)-4-Isobutyloxazolidine-2,5-dione (**89**)<sup>[14,24]</sup>



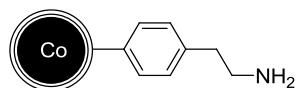
In a two-neck Schlenk flask *L*-leucine (2.62 g, 20 mmol, 1.0 equiv.) was suspended in anhydrous THF (18 mL) under nitrogen atmosphere. Subsequently, diphosgene (1.8 mL, 15 mmol, 0.75 equiv.) was slowly added and the resulting mixture was heated to 50 °C for 110 min. After cooling down to room temperature the solvent was evaporated under reduced pressure to give a white solid. The crude product was dissolved in anhydrous toluene (18 mL) followed by evaporation to remove last traces of HCl. Subsequently, the solid was dissolved in anhydrous toluene (6 mL), heated to 65 °C, precipitated with pentane in an ice bath and filtered off yielding **89** as white solid (1.88 g, 12.0 mmol, 60%).

<sup>1</sup>H NMR (300 MHz, MeOD):  $\delta_{\text{H}}$  = 4.42 (dd,  $J$  = 8.7, 5.2 Hz, 1H), 1.82 (ddd,  $J$  = 13.0, 8.1, 6.5 Hz, 1H), 1.74 – 1.58 (m, 2H), 0.98 (dd,  $J$  = 6.6, 4.7 Hz, 6H); <sup>13</sup>C NMR (75 MHz, CDCl<sub>3</sub>):  $\delta_{\text{C}}$  = 170.0, 153.0, 56.2, 40.8, 25.0, 22.7, 21.5.

**(S)-4-Isobutyloxazolidine-2,5-dione (89)**<sup>[13]</sup>

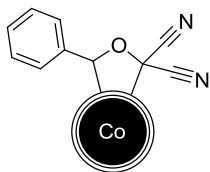
*L*-leucine (3.00 g, 22.9 mmol, 1.0 equiv.) and anhydrous THF (40 mL) were introduced to a Schlenk flask and the mixture was heated to 50 °C before triphosgene (1.22 g, 4.1 mmol, 0.18 equiv.) was added and heating was continued for four hours. Subsequently, the insoluble material was filtered off, the solution was concentrated under vacuum and the residue was dissolved in THF under reflux before the product was precipitated with hexanes in the cold. The precipitate was filtered off and dried under vacuum to yield **89** as white solid (1.33 g, 8.5 mmol, 69%).

$[\alpha]_D^{20}$  -38.0 (*c* 1.0, CHCl<sub>3</sub>) (*L*) (lit. value<sup>[13]</sup>  $[\alpha]_D^{20}$  -37.4 (*c* 1.0, CHCl<sub>3</sub>) (*L*)); <sup>1</sup>H NMR (300 MHz, MeOD):  $\delta_H$  = 4.42 (dd, *J* = 8.7, 5.2 Hz, 1H), 1.82 (ddd, *J* = 13.0, 8.1, 6.5 Hz, 1H), 1.74 – 1.58 (m, 2H), 0.98 (dd, *J* = 6.6, 4.7 Hz, 6H); <sup>13</sup>C NMR (75 MHz, CDCl<sub>3</sub>):  $\delta_C$  = 170.0, 153.0, 56.2, 40.8, 25.0, 22.7, 21.5.

**4-(2-Aminoethyl)phenyl functionalized Co/C nanoparticles (38)**<sup>[18]</sup>

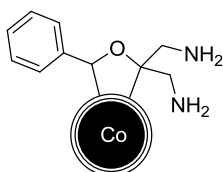
A round bottom flask was loaded with Co/C nanobeads (1.0 g), 4-(2-aminoethyl)aniline (132  $\mu$ L, 136 mg, 1.0 mmol), HCl<sub>conc</sub> (1.0 mL) and H<sub>2</sub>O (13 mL). The mixture was sonicated for 15 min before a solution of NaNO<sub>2</sub> (103 mg, 1.5 mmol) in H<sub>2</sub>O (13 mL) was added at 0 °C. The slurry was stirred another 30 min at 0 °C followed by sonication for further 30 min. After magnetic decantation the nanobeads were washed with 1 M NaOH solution (3x10 mL), H<sub>2</sub>O (3x10 mL) and diethyl ether (2x10 mL) before being dried *in vacuo* yielding 1.09 g of **38**.

**IR** (neat,  $\tilde{\nu}/\text{cm}^{-1}$ ): 3421, 2917, 2849, 1624, 1547, 1384, 1095, 1022, 825; **elemental microanalysis** [%]: C, 8.84; H, 0.26; N, 0.23 - **loading** 0.18 mmol/g.

**5-Phenyldihydrofuran-2,2(3*H*)-dicarbonitrile functionalized Co/C nanoparticles (**92**)<sup>[18]</sup>**

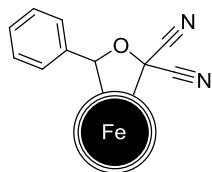
In a microwave vial Co/C nanoparticles (200 mg) were mixed with 3-phenyloxirane-2,2-dicarbonitrile **28** (100 mg, 0.59 mmol). The sealed tube was heated to 120 °C in the microwave for 3 minutes. After cooling to room temperature, the particles were recovered with the aid of a magnet and washed with EtOAc (6x2 mL) and DEE (3x2 mL). After evaporation of the solvent, 203 mg of the Co/C-THF-CN particles were obtained.

**IR** (KBr,  $\tilde{\nu}/\text{cm}^{-1}$ ): 2953, 2925, 2958, 2367, 2356, 2333, 2188, 1706, 1629, 1597, 1550, 1458, 1376, 1259, 1169, 1159, 1086, 1007, 964, 788; **elemental microanalysis** [%]: C, 10.72; H, 0.25; N, 1.15 - **loading** (NH<sub>2</sub>) 0.82 mmol/g, **loading** (tetrahydrofuran unit) 0.41 mmol/g.

**(5-Phenyltetrahydrofuran-2,2-diyl)dimethanamine functionalized Co/C nanoparticles (**93**)<sup>[18]</sup>**

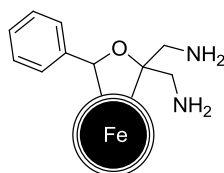
A Schlenk flask was charged with anhydrous THF (8.5 mL), trimethylsilyl chloride (TMSCl) (320  $\mu\text{L}$ , 2.6 mmol, 19.5 equiv.) and NaBH<sub>4</sub> (97 mg, 2.6 mmol, 19.5 equiv.) under nitrogen atmosphere. The resulting solution was heated at 80 °C for 4 h. After cooling down to room temperature, of Co/C-THF-CN nanobeads **92** (160 mg, 0.13 mmol, 1 equiv.) were added and the mixture was heated at 80 °C for 24 h. The reaction was quenched by slow addition of water and the nanoparticles were washed with water (3x8 mL), THF (3x8 mL), acetone (2x8 mL) and DEE (2x8 mL). After drying under vacuum 157 mg **93** were obtained.

**IR** (KBr,  $\tilde{\nu}/\text{cm}^{-1}$ ): 2955, 2920, 2871, 1459, 1377, 889, 762.

**5-Phenyldihydrofuran-2,2(3*H*)-dicarbonitrile functionalized Fe/C nanoparticles (94)**

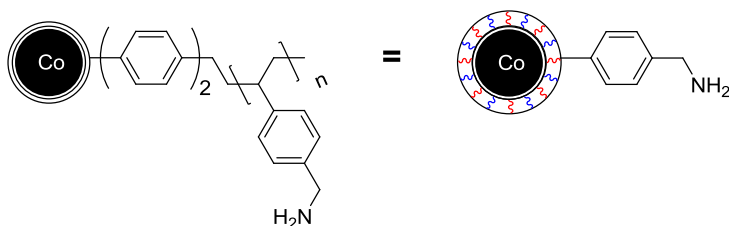
In a microwave vial Fe/C nanoparticles (150 mg) were mixed with 3-phenyloxirane-2,2-dicarbonitrile **28** (150 mg, 0.88 mmol). The sealed tube was heated to 120 °C in the microwave for 3 minutes. After cooling to room temperature, the particles were recovered with an external magnet and washed with EtOAc (15x3 mL) and DEE (3x2 mL). After evaporation of the solvent 173 mg of the Fe/C-THF-CN particles were obtained.

**IR** (KBr,  $\tilde{\nu}/\text{cm}^{-1}$ ): 2956, 2927, 2855, 2360, 2358, 2357, 2344, 1458, 1377, 757; **elemental microanalysis** [%]: C, 16.55; H, 0.46; N, 2.35 - **loading** (NH<sub>2</sub>) 1.67 mmol/g, **loading** (tetrahydrofuran unit) 0.83 mmol/g.

**(5-Phenyltetrahydrofuran-2,2-diyl)dimethanamine functionalized Fe/C nanoparticles (95)**

A Schlenk flask was loaded with anhydrous THF (8.5 mL), TMSCl (310  $\mu\text{L}$ , 2.4 mmol, 9.7 equiv.) and NaBH<sub>4</sub> (92 mg, 2.4 mmol, 9.7 equiv.) under nitrogen atmosphere. The resulting solution was heated at 80 °C for 3 h. After cooling down to room temperature Fe/C-THF-CN nanobeads **94** (150 mg, 0.25 mmol, 1 equiv.) were added and the reaction mixture was heated at 80 °C for 23 h. Afterwards, the reaction was slowly quenched with water and the nanoparticles were washed with water (3x3 mL), THF (3x2 mL) and diethyl ether (2x3 mL) before being dried under vacuum yielding 137 mg of **95**.

**IR** (KBr,  $\tilde{\nu}/\text{cm}^{-1}$ ): 3427, 1583, 1373, 999, 710.

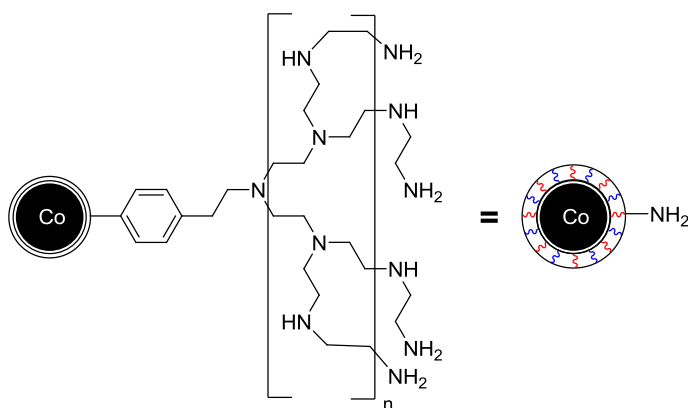
**Poly(benzylamine) styrene functionalized Co/C nanoparticles (98)**<sup>[25]</sup>

Co/C-PS-Cl nanoparticles **96** (500 mg, 1.3 mmol, 1.0 equiv.) were dispersed in anhydrous DMF (20 mL) under nitrogen atmosphere. Potassium phthalimide (5.3 g, 29 mmol, 22 equiv.) was added to the stirring solution and the mixture was heated to 100 °C for 21 h. After cooling to room temperature, the nanoparticles were recovered with the aid of a magnet, washed with water (4x20 mL), methanol (3x20 mL), acetone (2x20 mL) and DCM (2x20 mL) and dried yielding 487 mg of the intermediate **97**.

**IR** (neat,  $\tilde{\nu}/\text{cm}^{-1}$ ): 3005, 2914, 2845, 1768, 1703, 1606, 1508, 1466, 1425, 1388, 1333, 1323, 1155, 1082, 1009, 951, 933, 804, 709.

Hydrazine-Monohydrate (7.1 mL, 151 mmol, 115 equiv.) and EtOH (32 mL) was added to the nanoparticles **97** (477 mg). The resulting mixture was refluxed at 90 °C for 15 h. After cooling to room temperature the nanobeads were isolated by magnetic decantation, washed with water (4x10 mL), methanol (3x10 mL) and DCM (3x10 mL) and dried to yield 420 mg of Co/C-PS-NH<sub>2</sub> **98**.

**IR** (neat,  $\tilde{\nu}/\text{cm}^{-1}$ ): 3282, 3005, 2909, 2848, 1560, 1508, 1331, 1014, 812; **elemental microanalysis** [%]: C, 34.29; H, 3.05; N, 3.80; Cl, 0.62 - **loading** (N) 2.7 mmol/g.

**Poly(ethyleneimine) functionalized Co/C nanoparticle (99)**<sup>[18]</sup>

4-(2-Aminoethyl)phenyl functionalized Co/C nanoparticles **38** (139 mg, 0.22 mmol, 1.0 equiv.) in DCM (15 mL) were dispersed in an ultrasonic bath for 15 min. Under stirring, aziridine (1.1 mL, 22 mmol, 1000 equiv.) and HCl<sub>conc</sub> (30  $\mu\text{L}$ ) were added to the reaction mixture before

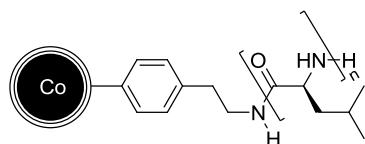
heating to 80 °C for 74 h. Afterwards, the nanoparticles were collected with the help of an external magnet and the solvent was decanted. The nanobeads were washed with DCM (2x20 mL), H<sub>2</sub>O (3x20 mL) and DEE (2x20 mL) before being dried *in vacuo* at 50 °C to give 147 mg of PEI functionalized nanobeads **99**.

**IR** (neat,  $\tilde{\nu}/\text{cm}^{-1}$ ): 3376, 2941, 2828, 2366, 2164, 2040, 1612, 1454, 1358, 1294, 1203, 1146, 1073, 1027, 893, 758, 696, 595; **elemental microanalysis** [%]: C, 14.31; H, 2.09; N, 4.36 - **loading** (N) 3.0 mmol/g.

### General procedure A: Room temperature synthesis of poly(*L*-leucine) functionalized Co/C nanoparticles<sup>[12]</sup>

A heavy-wall Schlenk tube was charged with amine functionalized nanobeads (1 equiv.) and anhydrous THF. The mixture was sonicated for 10 min before (*S*)-4-isobutyloxazolidine-2,5-dione (33 equiv.) in anhydrous THF was added. The resulting slurry was stirred at rt for 74 h. After magnetic decantation, the nanoparticles were washed with MeOH (3x) and diethyl ether (3x) and dried under vacuum.

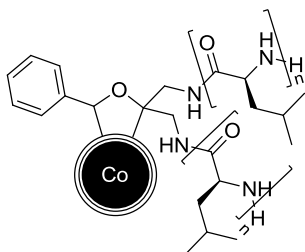
### Phenylethanamine-poly(*L*-leucine) functionalized Co/C nanoparticles (**It-101**)



According to GP-A, Co/C-NH<sub>2</sub> nanoparticles **38** (50 mg, 9  $\mu\text{mol}$ , 1 equiv.) in anhydrous THF (1 mL) and (*S*)-4-isobutyloxazolidine-2,5-dione (47 mg, 0.3 mmol, 33 equiv.) in anhydrous THF (1.5 mL) were used. 78 mg of nanobeads **It-101** could be isolated.

**SQUID** (emu/g) 80.88; **IR** (neat,  $\tilde{\nu}/\text{cm}^{-1}$ ): 3276, 2954, 2923, 2867, 1742, 1651, 1545, 1464, 1376, 1165, 785, 700, 631; **elemental microanalysis** [%]: C, 28.57; H, 3.62; N, 4.57 - **loading** (poly(*L*-leucine)) 3.10 mmol/g.

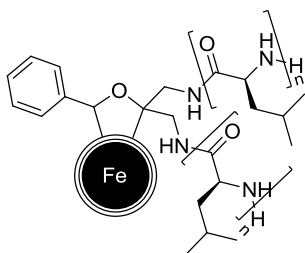
**(5-Phenyltetrahydrofuran-2,2-diyl)dimethanamine-poly(*L*-leucine) functionalized Co/C nanoparticles (It-102)**



According to GP-A, Co/C-THF-NH<sub>2</sub> nanoparticles **93** (50 mg, 41 μmol, 1 equiv.) in anhydrous THF (1 mL) and (*S*)-4-isobutyloxazolidine-2,5-dione (213 mg, 1.4 mmol, 33 equiv.) in anhydrous THF (1 mL) were used. 57 mg of **It-102** could be isolated.

**SQUID** (emu/g) 100.41; **IR** (neat,  $\tilde{\nu}/\text{cm}^{-1}$ ): 2955, 2922, 2870, 2852, 1737, 1714, 1630, 1462, 1378, 890, 632; **elemental microanalysis** [%]: C, 18.51; H, 2.00; N, 2.49 - **loading** (poly(*L*-leucine)) 1.48 mmol/g.

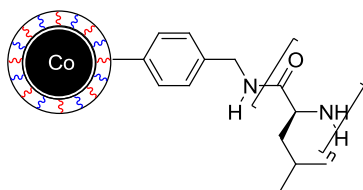
**(5-Phenyltetrahydrofuran-2,2-diyl)dimethanamine-poly(*L*-leucine) functionalized Fe/C nanoparticles (It-103)**



According to GP-A, Fe/C-THF-NH<sub>2</sub> nanoparticles **95** (50 mg, 50 μmol, 1 equiv.) in anhydrous THF (1 mL) and (*S*)-4-isobutyloxazolidine-2,5-dione (259 mg, 1.7 mmol, 33 equiv.) in anhydrous THF (1.5 mL) were used. 194 mg of nanobeads **It-103** could be isolated.

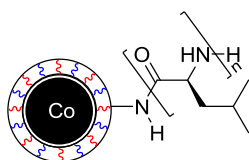
**SQUID** (emu/g) 19.64; **IR** (neat,  $\tilde{\nu}/\text{cm}^{-1}$ ): 3282, 2956, 2871, 1648, 1536, 1467, 1386, 1366, 1315, 1290, 1256, 1218, 1166, 1126, 1032, 922, 866, 696; **elemental microanalysis** [%]: C, 49.51; H, 7.03; N, 9.30 - **loading** (poly(*L*-leucine)) 3.70 mmol/g.



**Poly(benzylamine) styrene-poly(*L*-leucine) functionalized Co/C nanoparticles (It-104)**

According to GP-A, Co/C-PS-NH<sub>2</sub> nanoparticles **98** (50 mg, 0.14 mmol, 1 equiv.) in anhydrous THF (1 mL) and (*S*)-4-isobutyloxazolidine-2,5-dione (700 mg, 4.5 mmol, 33 equiv.) in anhydrous THF (1 mL) were used. 77 mg of **It-104** could be isolated.

**SQUID** (emu/g) 22.89; **IR** (neat,  $\tilde{\nu}/\text{cm}^{-1}$ ): 3286, 2955, 2923, 2870, 1652, 1544, 1462, 1377, 694; **elemental microanalysis** [%]: C, 49.83; H, 7.10; N, 8.41 - **loading** (poly(*L*-leucine)) 3.30 mmol/g.

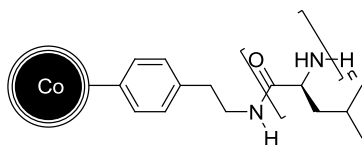
**Poly(ethyleneimine)-poly(*L*-leucine) functionalized Co/C nanoparticles (It-105)**

According to GP-A, Co/C-PEI nanoparticles **99** (50 mg, 0.15 mmol, 1 equiv.) in anhydrous THF (1 mL) and (*S*)-4-isobutyloxazolidine-2,5-dione (700 mg, 4.9 mmol, 33 equiv.) in anhydrous THF (2.5 mL) were used. 80 mg of nanobeads **It-105** could be isolated.

**SQUID** (emu/g) 59.22; **IR** (neat,  $\tilde{\nu}/\text{cm}^{-1}$ ): 3287, 2953, 2869, 1651, 1631, 1538, 1468, 1367, 1165, 700, 607; **elemental microanalysis** [%]: C, 35.48; H, 5.47; N, 7.53 - **loading** (poly(*L*-leucine)) 2.26 mmol/g.

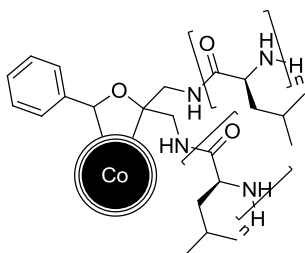
**General procedure B: High temperature synthesis of poly(*L*-leucine) functionalized Co/C nanoparticles<sup>[3]</sup>**

A heavy-wall Schlenk flask was loaded with amine functionalized nanobeads (1 equiv.), (*S*)-4-isobutyloxazolidine-2,5-dione (32 equiv.) and DME (5 mmol/L) under nitrogen atmosphere. The reaction mixture was heated to 90 °C for 18 h, after which the nanoparticles were collected with a magnet and the supernatant was decanted. After washing with MeOH (3x5 mL) and diethyl ether (3x5 mL) the particles were dried under vacuum.

**Phenylethanamine-poly(*L*-leucine) functionalized Co/C nanoparticles (ht-101)**

According to GP-B, Co/C-NH<sub>2</sub> nanoparticles **38** (50 mg, 9 μmol, 1 equiv.), (*S*)-4-isobutyloxazolidine-2,5-dione (45 mg, 0.29 mmol, 32 equiv.) and DME (1.8 mL) were used. 69 mg of **ht-101** could be isolated.

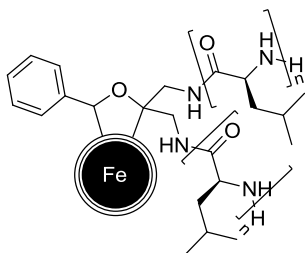
**SQUID** (emu/g) 80.44; **IR** (neat,  $\tilde{\nu}/\text{cm}^{-1}$ ): 3251, 2952, 2920, 2854, 1637, 1526, 1438, 1350; **elemental microanalysis** [%]: C, 27.37; H, 3.49; N, 4.34 - **loading** (poly(*L*-leucine)) 2.93 mmol/g.

**(5-Phenyltetrahydrofuran-2,2-diyl)dimethanamine-poly(*L*-leucine) functionalized Co/C nanoparticles (ht-102)**

According to GP-B, Co/C-THF-NH<sub>2</sub> nanoparticles **93** (50 mg, 30 μmol, 1 equiv.), (*S*)-4-isobutyloxazolidine-2,5-dione (150 mg, 0.96 mmol, 32 equiv.) and DME (6 mL) were used. 94 mg of nanobeads **ht-102** could be isolated.

**SQUID** (emu/g) 30.96; **IR** (neat,  $\tilde{\nu}/\text{cm}^{-1}$ ): 3278, 2955, 2926, 2871, 1648, 1530, 1464, 1445, 1365, 1288, 1254, 1220, 1164, 1125; **elemental microanalysis** [%]: C, 53.39; H, 8.29; N, 10.11 - **loading** (poly(*L*-leucine)) 6.62 mmol/g.

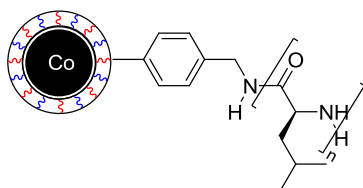
**(5-Phenyltetrahydrofuran-2,2-diyl)dimethanamine-poly(*L*-leucine) functionalized Fe/C nanoparticles (ht-103)**



According to GP-B, Fe/C-THF-NH<sub>2</sub> nanoparticles **95** (50 mg, 42 μmol, 1 equiv.), (*S*)-4-isobutyloxazolidine-2,5-dione (208 mg, 1.3 mmol, 32 equiv.) and DME (8.3 mL) were used. 146 mg of **ht-103** could be isolated.

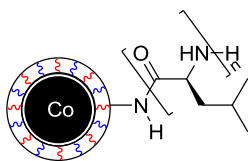
**IR** (neat,  $\tilde{\nu}/\text{cm}^{-1}$ ): 3278, 2955, 2924, 2869, 1628, 1540, 1524, 1469, 1367, 1278, 1258, 1250, 1244, 1154, 860, 776; **elemental microanalysis** [%]: C, 45.22; H, 6.19; N, 8.02 – **loading** (poly(*L*-leucine)) 4.05 mmol/g.

**Poly(benzylamine) styrene-poly(*L*-leucine) functionalized Co/C nanoparticles (ht-104)**



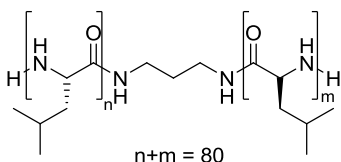
According to GP-B, Co/C-PS-NH<sub>2</sub> nanoparticles **98** (50 mg, 0.14 mmol, 1 equiv.), (*S*)-4-isobutyloxazolidine-2,5-dione (677 mg, 4.3 mmol, 32 equiv.) and DME (26.9 mL) were used. 133 mg of nanobeads **ht-104** could be isolated.

**SQUID** (emu/g) 12.99; **IR** (neat,  $\tilde{\nu}/\text{cm}^{-1}$ ): 3293, 2957, 2871, 1647, 1533, 1468, 1366, 1291, 1256, 1219, 1169, 1126, 870; **elemental microanalysis** [%]: C, 57.65; H, 8.09; N, 10.52 – **loading** (poly(*L*-leucine)) 4.80 mmol/g.

**Poly(ethyleneimine)-poly(*L*-leucine) functionalized Co/C nanoparticles (ht-105)**

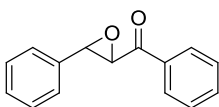
According to GP-B, Co/C-PEI nanoparticles **99** (41 mg, 69  $\mu\text{mol}$ , 1 equiv.), (*S*)-4-isobutyloxazolidine-2,5-dione (344 mg, 2.2 mmol, 32 equiv.) and DME (13.8 mL) were used. 39 mg of **ht-105** could be isolated.

**IR** (neat,  $\tilde{\nu}/\text{cm}^{-1}$ ): 3263, 3088, 2956, 2872, 1627, 1539, 1469, 1439, 1387, 1369, 1280, 1259, 1214, 1165, 1124, 1098, 1043, 1018, 870, 793, 718; **elemental microanalysis** [%]: C, 58.93; H, 8.89; N, 10.69 - **loading** (poly(*L*-leucine)) 5.80 mmol/g.

**Poly(*L*-leucine) (PII) (109)<sup>[4]</sup>**

Under nitrogen atmosphere (*S*)-4-isobutyloxazolidine-2,5-dione (1.32 g, 8.4 mmol, 80 equiv.) was dissolved in anhydrous toluene (20 mL). Upon addition of propane-1,3-diamine (8  $\mu\text{L}$ , 7.4 mg, 0.10 mmol, 1 equiv.) the mixture was heated to 80  $^{\circ}\text{C}$ . After 4 h the reaction solution was allowed to cool to 60  $^{\circ}\text{C}$  before MeOH (13 mL) was added. The heating at 60  $^{\circ}\text{C}$  was continued for 1 h followed by cooling down to room temperature. The polymer precipitated overnight, was filtered off and dried *in vacuo* yielding 654 mg of **109**.

**IR** (neat,  $\tilde{\nu}/\text{cm}^{-1}$ ): 3273, 2956, 2870, 1651, 1536, 1387, 1286, 1260, 1219, 1167, 872, 783; **elemental microanalysis** [%]: C, 61.65; H, 9.14; N, 12.03 - **loading** (poly(*L*-leucine)) 8.60 mmol/g.

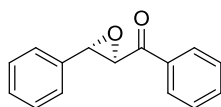
**Phenyl(3-phenyloxiran-2-yl)methanone (110)<sup>[26]</sup>**

(*E*)-chalcone (208 mg, 1.0 mmol) was dissolved in acetonitrile (0.5 mL) before NaOCl (2 mL) were added. The resulting mixture was stirred for 21 h at rt. After separation of the phases the aqueous phase was extracted with EtOAc (4x2 mL). The combined organic layers were washed

with a sat. NaCl solution, dried over  $\text{MgSO}_4$ , filtered and evaporated under reduced pressure. The crude product was purified by column chromatography (hexanes/EtOAc 30:1) yielding of the pure product as white solid (146 mg, 0.65 mmol, 65%).

$R_f$  = 0.48 (hexanes/EtOAc 5:1);  $^1\text{H NMR}$  (300 MHz,  $\text{CDCl}_3$ ):  $\delta_{\text{H}}$  = 8.01 (dd,  $J$  = 8.3, 1.2 Hz, 2H), 7.67 – 7.33 (m, 8H), 4.31 (d,  $J$  = 1.9 Hz, 1H), 4.08 (d,  $J$  = 1.8 Hz, 1H);  $^{13}\text{C NMR}$  (101 MHz,  $\text{CDCl}_3$ ):  $\delta_{\text{C}}$  = 193.1, 135.5, 134.0 (2C), 129.1, 128.9, 128.8, 128.4, 125.8, 61.1, 59.4.

**General procedure C: Asymmetric epoxidation of (E)-chalcone 106 with sodium percarbonate catalyzed by heterogeneous poly(*L*-leucine) catalysts<sup>[12]</sup>**



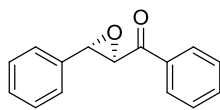
In a heavy-wall glass tube, (*E*)-chalcone (104 mg, 0.5 mmol, 1 equiv.) was dissolved in DME (1 mL) followed by the addition of  $\text{H}_2\text{O}$  (1 mL). Under stirring, sodium percarbonate (239 mg, 0.76 mmol, 1.52 equiv.) and 8 mol% catalyst **It-104** (12 mg, 40  $\mu\text{mol}$ ) were added to the solution. The mixture was stirred for 6 h at rt. After magnetic decantation the nanobeads were washed with EtOAc (2x2 mL) and the washing solutions were combined the previously decanted solution. For recycling experiments the magnetic nanocatalyst was directly subjected to the next run by adding new reagents. The solvent was evaporated and the product was purified by column chromatography eluting with a mixture of hexanes and EtOAc (30:1). The product could be isolated as white solid (60 mg, 0.27 mmol, 54%) with 29% *ee*.

$R_f$  = 0.48 (hexanes/EtOAc 5:1); **chiral HPLC analysis** (Phenomenex Lux Cellulose-2, *n*heptane/*i*PrOH 99:1, 1.0 mL/min, 254 nm):  $t_r$  = 32.09 min,  $t_r$  = 38.17 min;  $^1\text{H NMR}$  (300 MHz,  $\text{CDCl}_3$ ):  $\delta_{\text{H}}$  = 8.01 (dd,  $J$  = 8.3, 1.2 Hz, 2H), 7.67 – 7.33 (m, 8H), 4.31 (d,  $J$  = 1.9 Hz, 1H), 4.08 (d,  $J$  = 1.8 Hz, 1H);  $^{13}\text{C NMR}$  (101 MHz,  $\text{CDCl}_3$ ):  $\delta_{\text{C}}$  = 193.1, 135.5, 134.0 (2C), 129.1, 128.9, 128.8, 128.4, 125.8, 61.1, 59.4.

**General procedure D: Pre-activation of magnetic heterogeneous poly(*L*-leucine) catalyst<sup>[3]</sup>**

To the heterogeneous catalyst (1 equiv.) in toluene (80 mmol/L), a NaOH solution (4 M, 4.8 equiv.) was added. The resulting mixture was stirred for 24 h at rt. After magnetic decantation the nanoparticles were washed with  $\text{H}_2\text{O}$  (4x2 mL).

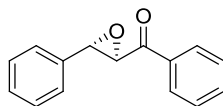
**General procedure E: Asymmetric epoxidation of (*E*)-chalcone 106 with H<sub>2</sub>O<sub>2</sub> catalyzed by heterogeneous poly(*L*-leucine) catalysts<sup>[6]</sup>**



A heavy-wall glass tube was charged with (*E*)-chalcone (83 mg, 0.4 mmol, 1.0 equiv.), 11 mol% tetra-*n*-butylammonium bromide (TBAB) (14 mg, 44  $\mu$ mol), 11 mol% catalyst **ht-103** (11 mg, 44  $\mu$ mol) and toluene (1.33 mL). After addition of a 5 M NaOH solution (0.34 mL, 1.68 mmol, 4.2 equiv.) and H<sub>2</sub>O<sub>2</sub> (30%, 1.2 mL, 11 mmol, 28.5 equiv.), the reaction vessel was closed and the mixture stirred for 2 h at rt. Subsequently, the solution was diluted with EtOAc (1.7 mL) and slowly poured into of a cold aqueous NaHSO<sub>3</sub> solution (20% w/w, 6.7 mL) to quench any residual peroxide. For the recycling experiments the magnetic nanocatalyst was directly subjected to the next run by addition of new reagents. The phases were separated, the aqueous phase was extracted with EtOAc (3x3 mL) and the combined organic layers were dried over MgSO<sub>4</sub> followed by filtering and evaporation of the solvent. The yield of the product was determined by NMR spectroscopy with an internal standard (25% with 91% *ee*).

$R_f$  = 0.48 (hexanes/EtOAc 5:1); **chiral HPLC analysis** (Phenomenex Lux Cellulose-2, *n*-heptane/*i*PrOH 99:1, 1.0 mL/min, 254 nm):  $t_r$  = 32.09 min,  $t_r$  = 38.17 min; **<sup>1</sup>H NMR** (300 MHz, CDCl<sub>3</sub>):  $\delta_H$  = 8.01 (dd,  $J$  = 8.3, 1.2 Hz, 2H), 7.67 – 7.33 (m, 8H), 4.31 (d,  $J$  = 1.9 Hz, 1H), 4.08 (d,  $J$  = 1.8 Hz, 1H); **<sup>13</sup>C NMR** (101 MHz, CDCl<sub>3</sub>):  $\delta_C$  = 193.1, 135.5, 134.0 (2C), 129.1, 128.9, 128.8, 128.4, 125.8, 61.1, 59.4.

**Diluted conditions for asymmetric epoxidation of (*E*)-chalcone 106 with H<sub>2</sub>O<sub>2</sub> catalyzed by heterogeneous poly(*L*-leucine) catalyst **ht-103**<sup>[6]</sup>**



A round-bottom flask was charged with (*E*)-chalcone (83 mg, 0.4 mmol, 1.0 equiv.), 11 mol% TBAB (14 mg, 44  $\mu$ mol), 11 mol% catalyst **ht-103** (11 mg, 44  $\mu$ mol), H<sub>2</sub>O (4.9 mL) and toluene (3.6 mL). After addition of a 5 M NaOH solution (0.3 mL, 1.7 mmol, 4.2 equiv.) and H<sub>2</sub>O<sub>2</sub> (1.2 mL, 11 mmol, 28.5 equiv.) the reaction was stirred for 2 h at rt. Subsequently, the solution was diluted with EtOAc (1.7 mL) and slowly poured into of a cold aqueous NaHSO<sub>3</sub> solution (20% w/w, 6.7 mL). The phases were separated, the aqueous phase was extracted with EtOAc (3x5 mL) and the combined organic layers were dried over MgSO<sub>4</sub>. The solvent was evaporated

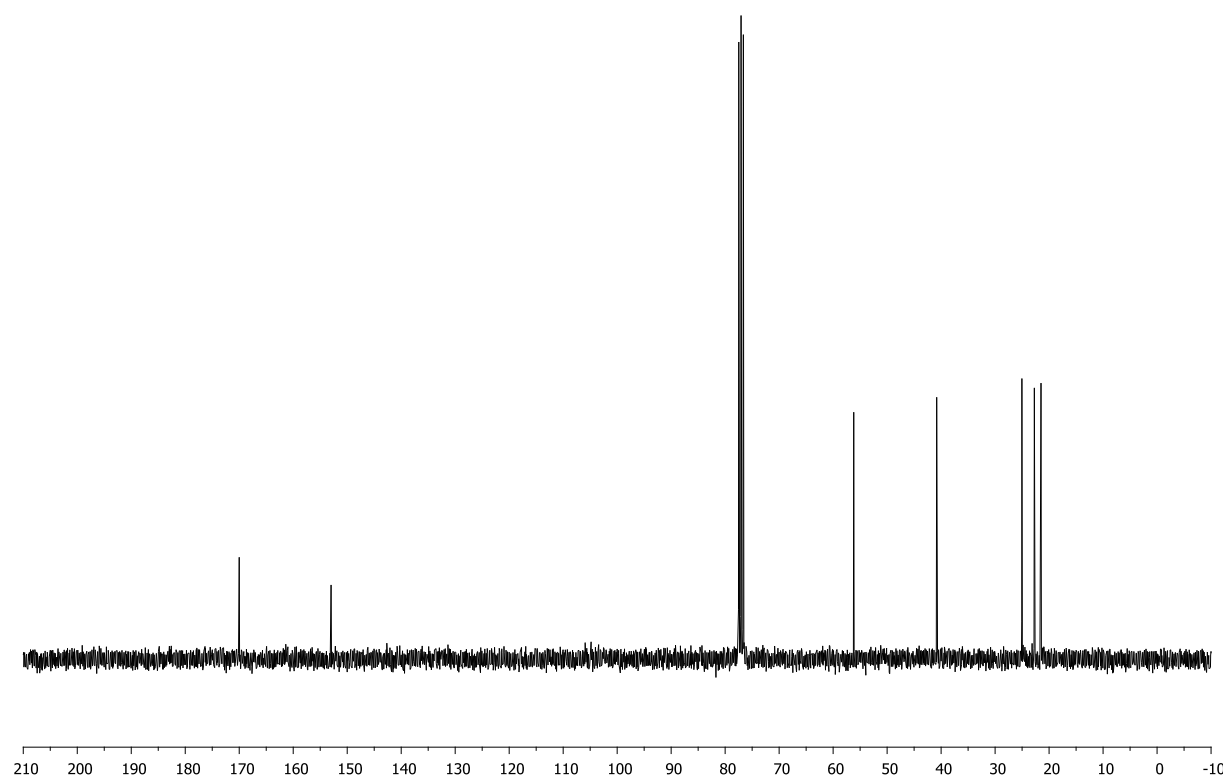
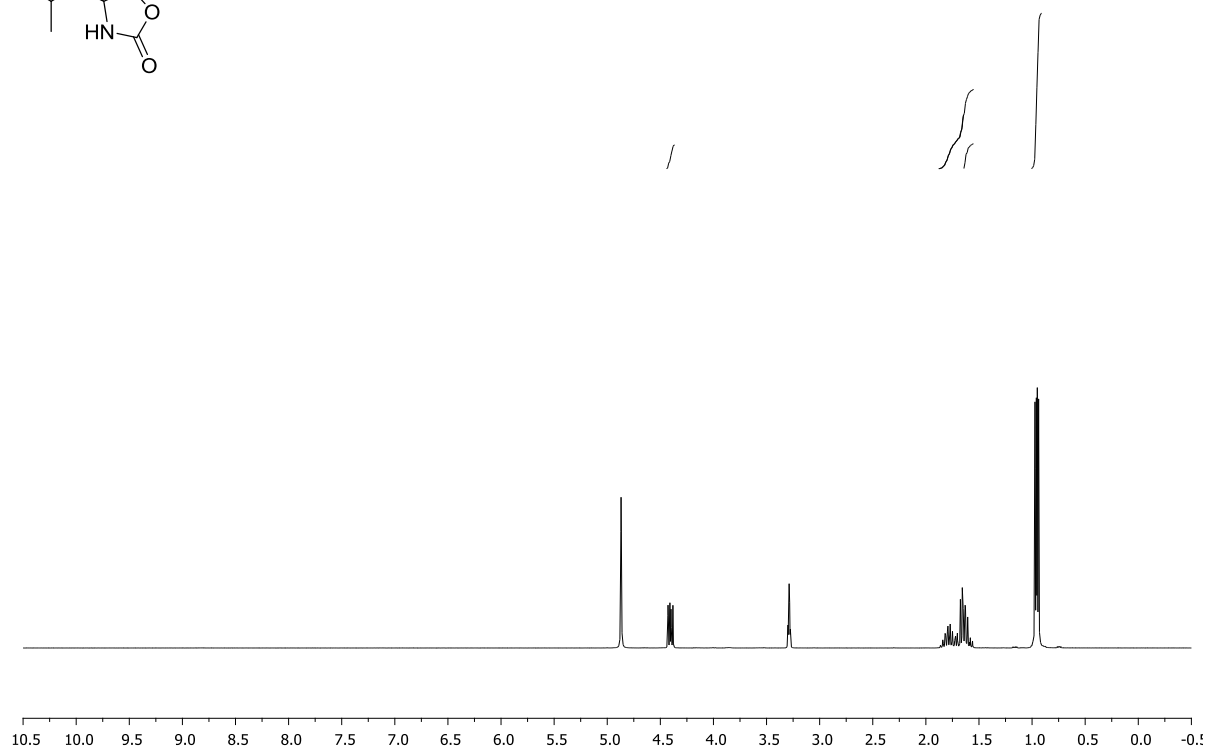
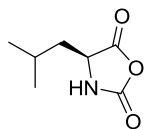
and the product purified by column chromatography (hexanes/EtOAc 30:1) yielding the product as white solid (21 mg, 0.12 mmol, 30%) with 92% *ee*.

**R<sub>f</sub>** = 0.48 (hexanes/EtOAc 5:1); **chiral HPLC analysis** (Phenomenex Lux Cellulose-2, *n*heptane/*i*PrOH 99:1, 1.0 mL/min, 254 nm): *t<sub>r</sub>* = 32.09 min, *t<sub>r</sub>* = 38.17 min; **<sup>1</sup>H NMR** (300 MHz, CDCl<sub>3</sub>): δ<sub>H</sub> = 8.01 (dd, *J* = 8.3, 1.2 Hz, 2H), 7.67 – 7.33 (m, 8H), 4.31 (d, *J* = 1.9 Hz, 1H), 4.08 (d, *J* = 1.8 Hz, 1H); **<sup>13</sup>C NMR** (101 MHz, CDCl<sub>3</sub>): δ<sub>C</sub> = 193.1, 135.5, 134.0 (2C), 129.1, 128.9, 128.8, 128.4, 125.8, 61.1, 59.4.

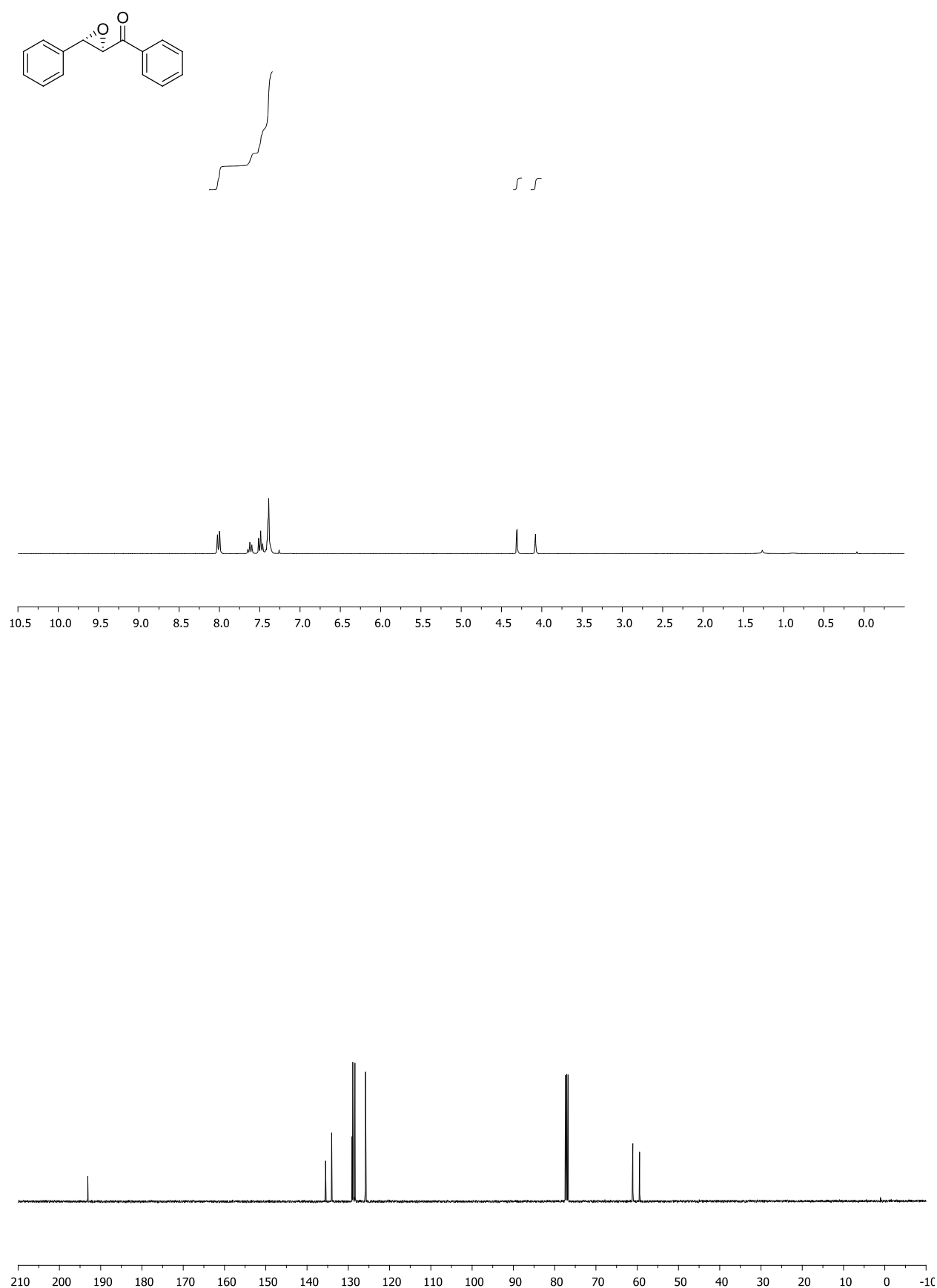
## NMR spectra

*(S)*-4-Isobutyloxazolidine-2,5-dione (**89**)

MeOD, 300 MHz





Phenyl((2*R*,3*S*)-3-phenyloxiran-2-yl)methanone **107**CDCl<sub>3</sub>, 300 MHz

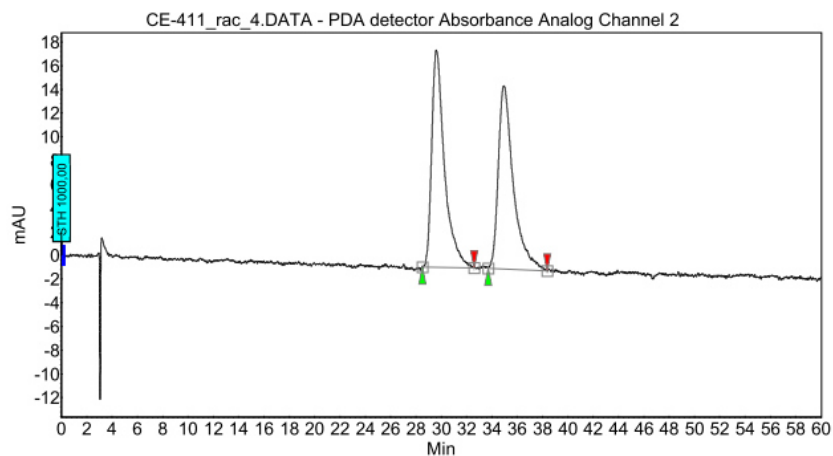
## Chiral HPLC spectra

Phenyl(3-phenyloxiran-2-yl)methanone ((*rac*)-**110**)

Vial : 4  
Method : Phex-Cel2\_99-1  
Run time : 60,00 min  
Inj. vol. : 10,000 µl

Column : Phenomenex Lux Cellulose-2,  
4.6 x 250 mm, 5 µm  
Eluents : A = n-Heptane  
B = i-Propanol  
Flow : 1.0 ml/min

λ : 254 nm



## Peak Results :

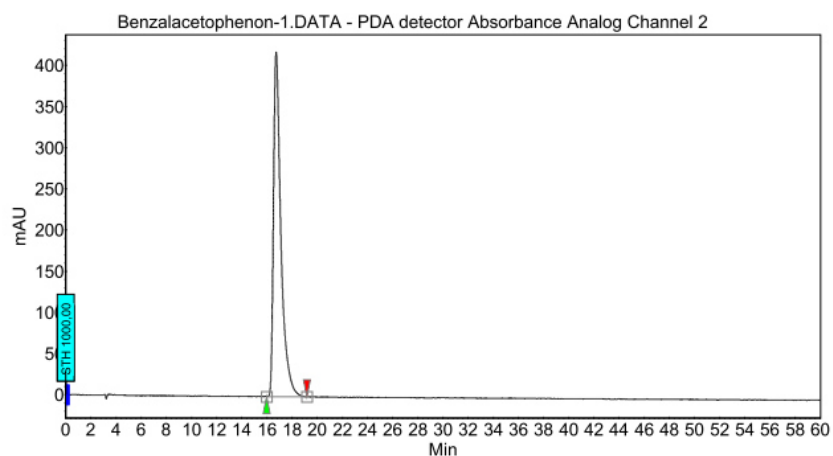
Index	Name	Time [Min]	Quantity [% Area]	Height [mAU]	Area [mAU.Min]	Area % [%]
1	UNKNOWN	29.59	50.11	18.3	21.4	50.112
2	UNKNOWN	34.93	49.89	15.5	21.3	49.888
Total			100.00	33.8	42.8	100.000

(*E*)-chalcone **106**

Vial : 151  
Method : Phex-Cel2\_99-1  
Run time : 60,00 min  
Inj. vol. : 10,000 µl

Column : Phenomenex Lux Cellulose-2,  
4.6 x 250 mm, 5 µm  
Eluents : A = n-Heptane  
B = i-Propanol  
Flow : 1.0 ml/min

λ : 254 nm



## Peak Results :

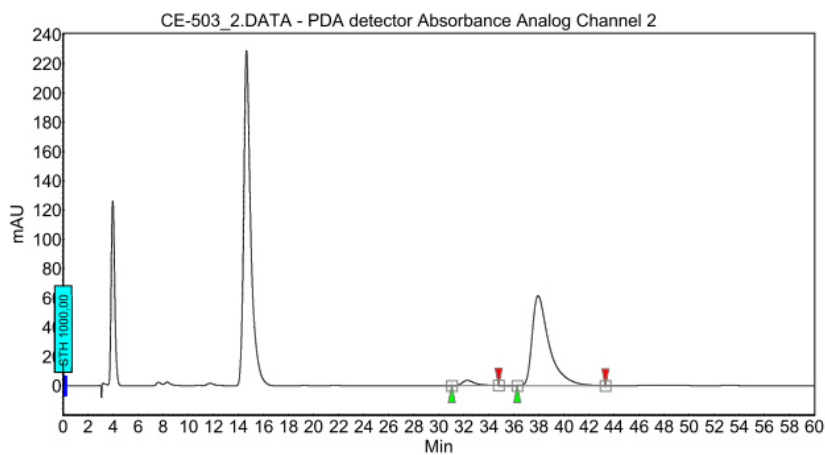
Index	Name	Time [Min]	Quantity [% Area]	Height [mAU]	Area [mAU.Min]	Area % [%]
1	UNKNOWN	16.73	100.00	418.4	287.1	100.000
Total			100.00	418.4	287.1	100.000

Phenyl((2*R*,3*S*)-3-phenyloxiran-2-yl)methanone **107** (91% *ee*)

Vial : 122  
 Method : Phex-Cel2\_99-1  
 Run time : 60,00 min  
 Inj. vol. : 10,000 µl

Column : Phenomenex Lux Cellulose-2,  
 4.6 x 250 mm, 5 µm  
 Eluents : A = n-Heptane  
 B = i-Propanol  
 Flow : 1.0 ml/min

λ : 254 nm



## Peak Results :

Index	Name	Time [Min]	Quantity [% Area]	Height [mAU]	Area [mAU.Min]	Area % [%]
1	UNKNOWN	32.27	4.35	3.6	4.4	4.355
2	UNKNOWN	37.94	95.65	61.4	96.1	95.645
Total			100.00	65.0	100.5	100.000

### 3.5 References

- [1] S. Juliá, J. Masana, J. C. Vega, *Angew. Chem. Int. Ed.* **1980**, *19*, 929–931.
- [2] D. R. Kelly, S. M. Roberts, *Chem. Commun.* **2004**, 2018–2020.
- [3] S. Baars, K.-H. Drauz, H.-P. Krimmer, S. M. Roberts, J. Sander, J. Skidmore, G. Zanardi, *Org. Process Res. Dev.* **2003**, *7*, 509–513.
- [4] A. Gerlach, T. Geller, *Adv. Synth. Catal.* **2004**, *346*, 1247–1249.
- [5] a) A. Berkessel, N. Gasch, K. Glaubitz, C. Koch, *Org. Lett.* **2001**, *3*, 3839–3842; b) T. Geller, A. Gerlach, C. M. Krüger, H.-C. Militzer, *J. Mol. Catal. A: Chem.* **2006**, *251*, 71–77; c) T. Geller, C. M. Krüger, H.-C. Militzer, *Tetrahedron Lett.* **2004**, *45*, 5069–5071; d) S. B. Tsogoeva, J. Wöltinger, C. Jost, D. Reichert, A. Kühnle, H.-P. Krimmer, K. Drauz, *Synlett* **2002**, 2002, 707–710; e) D. R. Kelly, A. Meek, S. M. Roberts, *Chem. Commun.* **2004**, 2021–2022; f) A. Berkessel, B. Koch, C. Toniolo, M. Rainaldi, Q. B. Broxterman, B. Kaptein, *Biopolymers* **2006**, *84*, 90–96; g) Bentley, P. A., W. Kroutil, Littlechild, J. A., S. M. Roberts, *Chirality* **1997**, *9*, 198–202; h) S. Banfi, S. Colonna, H. Molinari, S. Julia, J. Guixer, *Tetrahedron* **1984**, *40*, 5207–5211; i) B. M. Adger, J. V. Barkley, S. Bergeron, M. W. Cappi, B. E. Flowerdew, M. P. Jackson, R. McCague, T. C. Nugent, S. M. Roberts, *J. Chem. Soc., Perkin Trans. 1* **1997**, 3501–3508.
- [6] T. Geller, A. Gerlach, C. M. Krüger, H.-C. Militzer, *Tetrahedron Lett.* **2004**, *45*, 5065–5067.
- [7] A. Gerlach, T. Geller, *Adv. Synth. Catal.* **2004**, *346*, 1247–1249.
- [8] P. A. Bentley, S. Bergeron, M. W. Cappi, D. E. Hibbs, M. B. Hursthouse, T. C. Nugent, R. Pulido, S. M. Roberts, L. Eduardo Wu, *Chem. Commun.* **1997**, 739–740.
- [9] J. V. Allen, K.-H. Drauz, R. W. Flood, S. M. Roberts, J. Skidmore, *Tetrahedron Lett.* **1999**, *40*, 5417–5420.
- [10] a) S. Itsuno, M. Sakakura, K. Ito, *J. Org. Chem.* **1990**, *55*, 6047–6049; b) M. W. Cappi, R. W. Flood, S. M. Roberts, J. Skidmore, N. M. Williamson, W.-P. Chen, Y.-W. Liao, J. A. Smith, *Chem. Commun.* **1998**, 1159–1160.
- [11] a) L. Carde, H. Davies, T. P. Geller, S. M. Roberts, *Tetrahedron Lett.* **1999**, *40*, 5421–5424; b) T. Geller, S. M. Roberts, *J. Chem. Soc., Perkin Trans. 1* **1999**, 1397–1398; c) A. Dhanda, K.-H. Drauz, T. Geller, S. M. Roberts, *Chirality* **2000**, *12*, 313–317.
- [12] H. Yi, G. Zou, Q. Li, Q. Chen, J. Tang, M.-y. He, *Tetrahedron Lett.* **2005**, *46*, 5665–5668.
- [13] W. H. Daly, D. Poché, *Tetrahedron Lett.* **1988**, *29*, 5859–5862.
- [14] M. Oya, R. Katakai, H. Nakai, Y. Iwakura, *Chem. Lett.* **1973**, 1143–1144.
- [15] R. N. Grass, E. K. Athanassiou, W. J. Stark, *Angew. Chem. Int. Ed.* **2007**, *46*, 4909–4912.
- [16] S. Fernandes, C. M. Eichenseer, P. Kreitmeier, J. Rewitzer, V. Zlateski, R. N. Grass, W. J. Stark, O. Reiser, *RSC Adv.* **2015**, *5*, 46430–46436.
- [17] A. Giannis, K. Sandhoff, *Angew. Chem. Int. Ed.* **1989**, *28*, 218–220.
- [18] Q. M. Kainz, S. Fernandes, C. M. Eichenseer, F. Besostri, H. Körner, R. Müller, O. Reiser, *Faraday Discuss.* **2014**, *175*, 27–40.
- [19] Y. Liu, D.-C. Wu, W.-D. Zhang, X. Jiang, C.-B. He, T. S. Chung, S. H. Goh, K. W. Leong, *Angew. Chem. Int. Ed.* **2005**, *44*, 4782–4785.
- [20] H. R. Kricheldorf, D. Müller, *Int. J. Biol. Macromol.* **1983**, *5*, 171–178.
- [21] S. Juliá, J. Guixer, J. Masana, J. Rocas, S. Colonna, R. Annuziata, H. Molinari, *J. Chem. Soc., Perkin Trans. 1* **1982**, 1317–1324.
- [22] G. Carrea, S. Colonna, A. D. Meek, G. Ottolina, S. M. Roberts, *Chem. Commun.* **2004**, 1412–1413.
- [23] M. Rossier, F. M. Koehler, E. K. Athanassiou, R. N. Grass, B. Aeschlimann, D. Günther, W. J. Stark, *J. Mater. Chem.* **2009**, *19*, 8239–8243.

- [24] Smeets, N. M. B., van der Weide, P. L. J., J. Meuldijk, Vekemans, J. A. J. M., L. A. Hulshof, *Org. Process Res. Dev.* **2005**, *9*, 757–763.
- [25] Boal, A. K., Galow, T. H., F. Ilhan, V. M. Rotello, *Adv. Funct. Mater.* **2001**, *11*, 461–465.
- [26] X.-L. Geng, Z. Wang, X.-Q. Li, C. Zhang, *J. Org. Chem.* **2005**, *70*, 9610–9613.

## C Summary

The present dissertation deals with the immobilization of scavengers as well as transition metal and organocatalysts on highly magnetic carbon-coated iron (Fe/C) or cobalt (Co/C) nanoparticles. The graphene-like surface of the particles allows for an easy functionalization while the metal core ensures a facile and rapid separation by magnetic decantation. The attachment of polymeric structures onto the surface had various effects, for instance, it increased the achievable loading capacities. Additionally, it also altered the dispersibility of the particles in various solvents, rendering even the application of water as environmentally friendly solvent possible.

The first chapter of the main part describes the synthesis of a novel nanoparticle-poly(ethylenimine) hybride (Co/C-PEI, **40**) by direct cationic polymerization of aziridine with amino functionalized NPs **38** as initiator. The material was successfully applied in mercury extraction from aqueous samples at relevant concentrations (ppm/ppb), exhibiting an extraction capacity of 550 mg  $\text{Hg}^{2+}$  per gram nanomaterial. It could also be demonstrated that Co/C-PEI NPs **40** have a high preference for mercury, even in the presence of several competitive metals. A recycling protocol comprising an extraction step and a subsequent release in acidic medium has been established for at least six consecutive runs (Figure 24). The material's applicability in an industrial process close to reality was proven by decontaminating 20 L of water with an initial mercury concentration of 30 ppb. By using just 3 mg nanoparticles **40** per liter, the mercury content could be decreased to 2 ppb within one hour.

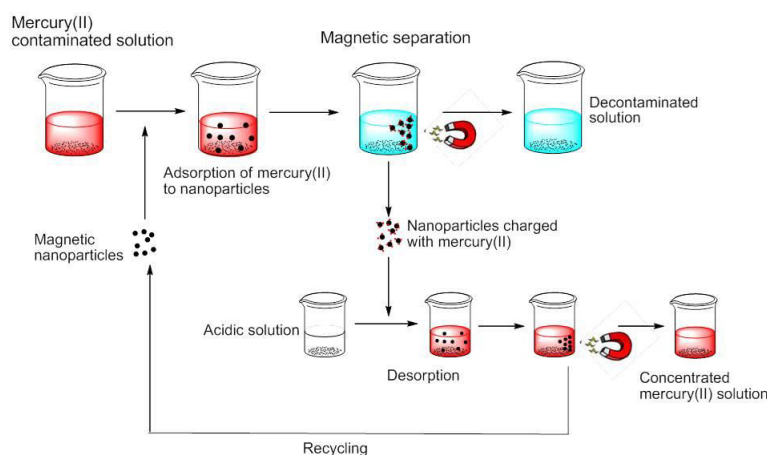
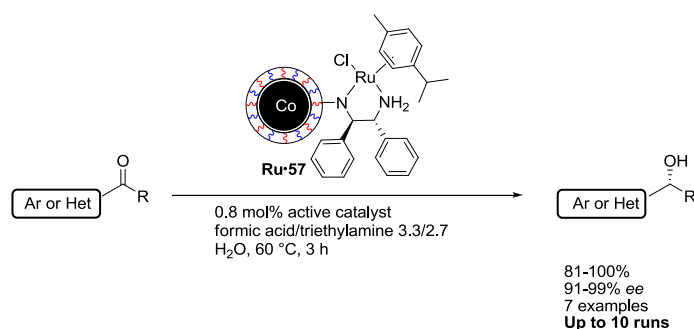


**Figure 24.** Recycling protocol for the extraction of mercury in tap water samples.

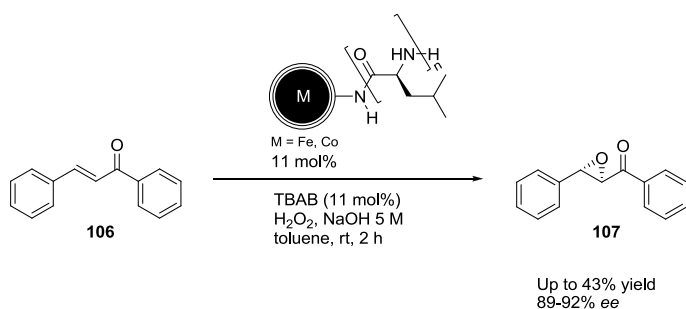
Chapter 2 is devoted to the synthesis and application of magnetic Noyori-type ruthenium catalysts for the asymmetric transfer hydrogenation. Carbon-coated cobalt nanoparticles in combination with different polymers served as magnetic platforms for the immobilization of the transition metal catalyst. The activity and enantioselectivity of these catalysts were benchmarked in the asymmetric transfer hydrogenation of acetophenone in an aqueous medium. The best results were obtained when the chiral 1,2-diamine ligand bearing a vinyl group in the organic framework was attached via co-polymerization with divinylbenzene to vinylbenzene functionalized Co/C nanoparticles followed by complexation with  $[\text{RuCl}_2(p\text{-cymene})]_2$ . This catalyst **Ru-57** was characterized by infrared spectroscopy, superconducting quantum interference device magnetometry analysis, transmission electron microscopy and energy-dispersive x-ray spectroscopy. The catalyst was applied in asymmetric hydrogen transfer reactions in water, reducing various aryl methyl ketones to their corresponding alcohols with good yields (81–100%) and enantioselectivities (91–99% *ee*) (Scheme 27). A non-hazardous mixture of formic acid and triethylamine could be employed as hydrogen source, which can be handled in a simple manner compared to gaseous hydrogen. Moreover, the catalyst could be recycled over ten runs with just minor ruthenium contaminations into the product (between 0.8 and 3.3 ppm per run).



**Scheme 27.** ATH with immobilized ruthenium catalyst **Ru-57**.

The immobilization of poly(*L*-leucine) on magnetic Co/C and Fe/C nanoparticles is presented in chapter 3 of the main part. Amino groups were covalently attached to the surface of the nanoparticles by different routes before they were used as initiators in the direct polymerization with *L*-leucine-NCA at room temperature and at 90 °C. Under both reaction conditions high leucine loadings could be obtained (1.5–6.6 mmol leucine per gram nanoparticles). The resulting magnetic poly(*L*-leucine) catalysts were subsequently studied in the asymmetric epoxidation of

(*E*)-chalcone (Scheme 28). The activity and selectivity of the high-temperature and low-temperature catalysts were compared using different reaction conditions. The triphasic system, consisting of an aqueous H<sub>2</sub>O<sub>2</sub> solution, toluene and the insoluble immobilized catalyst, with an additional phase transfer catalyst (TBAB), was identified as the best condition with regard to enantioselectivity (up to 43% yield, 89-92% *ee*). Despite different approaches, the reaction yield could not be increased. Finally, the recyclability of the catalyst was studied but already in the second run reduced activity has been observed.



**Scheme 28.** Asymmetric epoxidation of (*E*)-chalcone **106** with magnetic poly(*L*-leucine) catalyst.



## D Zusammenfassung

Die vorliegende Dissertation beschreibt die Immobilisierung von “Abfang-Gruppen” sowie Übergangsmetall- und Organokatalysatoren auf hoch magnetischen Kohlenstoff-beschichteten Eisen (Fe/C) oder Cobalt (Co/C) Nanopartikeln. Die graphen-artige Oberfläche der Partikel ermöglicht eine einfache Funktionalisierung während der metallische Kern eine mühelose und schnelle Abtrennung durch magnetisches Dekantieren gestattet. Das Anbringen von zusätzlichen Polymeren-Schichten auf der Oberfläche hatte verschiedene Effekte, beispielsweise erhöhte es die Beladungskapazität der Partikel. Ebenso konnte die Dispergierbarkeit der Nanopartikel in unterschiedlichen Lösungsmitteln verändert werden, so dass die Verwendung von Wasser als umweltschonendes Lösungsmittel ermöglicht wurde.

Das erste Kapitel des Hauptteils beschreibt die Synthese einer neuartigen Nanopartikel-Poly(ethylenamin) Hybrid Spezies (Co/C-PEI, **40**). Diese wurde ausgehend von Amino-funktionalisierten Nanopartikeln **38**, welche als Initiatoren fungieren, durch direkte kationische Polymerisierung mit Aziridin hergestellt. Die Nanopartikel wurden erfolgreich in der Extraktion von Quecksilber aus wässrigen Proben in relevanten Konzentrationsbereichen (ppm/ppb) eingesetzt, wobei eine Extraktionskapazität von 550 mg  $\text{Hg}^{2+}$  pro Gramm Nanomaterial bestimmt werden konnte. Weiterhin konnte gezeigt werden, dass Co/C-PEI Nanopartikel **40** sogar in Gegenwart mehrerer konkurrierender Metalle eine hohe Präferenz für Quecksilber aufwiesen. Zudem konnte ein Recycling Protokoll für mindestens sechs aufeinanderfolgende Läufe entwickelt werden, welches jeweils pro Lauf aus einem Extraktionsschritt gefolgt von einer Freisetzung im sauren pH Bereich bestand (Abbildung 1). Außerdem konnte die Anwendbarkeit der hergestellten Nanopartikel in einem realitätsnahen industriellen Prozess demonstriert werden. Hierfür wurden 20 L Wasser, welche mit einer anfänglichen Quecksilber-Konzentration von 30 ppb versetzt wurden, durch den Einsatz von nur 3 mg Nanopartikel **40** pro Liter dekontaminiert. Dadurch konnte der Quecksilber-Gehalt innerhalb einer Stunde auf 2 ppb herabgesenkt werden.

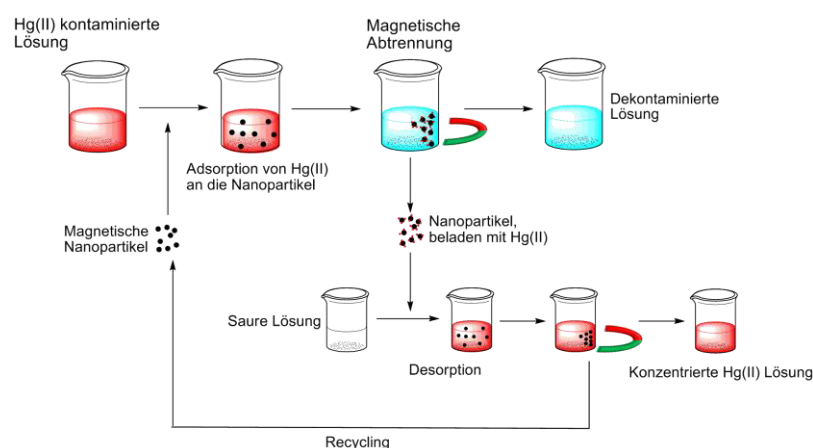
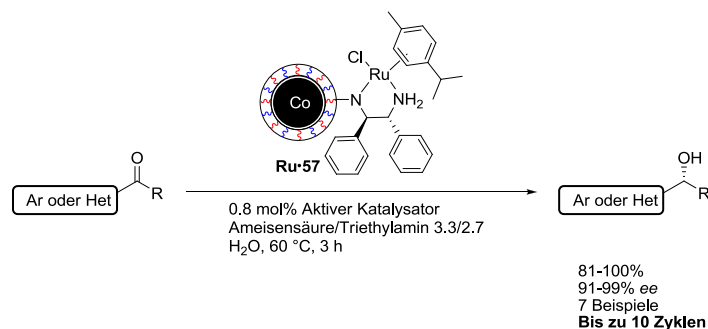


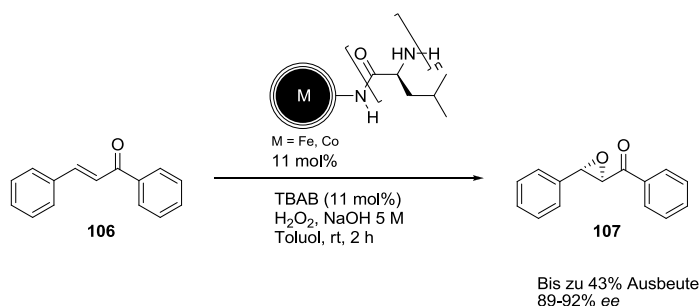
**Abbildung 1.** Recycling Protokoll für die Quecksilber-Extraktion aus Leitungswasser-Proben.

Kapitel 2 behandelt die Synthese von magnetischen Noyori-Typ Ruthenium Katalysatoren und deren Anwendung in der asymmetrischen Transferhydrierung. Hierbei wurden Übergangsmetall-Katalysatoren auf Kohlenstoff-beschichtete Cobalt Nanopartikel in Kombination mit unterschiedlichen Polymeren immobilisiert. Die Aktivität und Enantioselektivität dieser Katalysatoren wurde in der asymmetrischen Transferhydrierung von Acetophenon in wässrigem Medium bewertet. Die besten Ergebnisse konnten erzielt werden, indem der chirale 1,2-Diamin Ligand mit einer Vinyl Gruppe funktionalisiert wurde, bevor er durch Copolymerisation mit Divinylbenzol auf Vinylbenzol substituierten Co/C Nanopartikel immobilisiert und mit  $[\text{RuCl}_2(p\text{-cymene})]_2$  komplexiert wurde. Dieser Katalysator **Ru-57** wurde durch unterschiedliche Messmethoden, wie zum Beispiel Infrarotspektroskopie, Magnetometermessung mit einem supraleitenden Quantum Interferenz Gerät (SQUID), Transmissionselektronenmikroskopie und energiedispersive Röntgenspektroskopie (EDX) charakterisiert. Als Wasserstoff-Quelle wurde eine Mischung von Ameisensäure und Triethylamin verwendet, welche im Vergleich zu gasförmigem Wasserstoff einfacher zu handhaben ist. So konnten verschiedene Arylmethylketone in Wasser in guten Ausbeuten (81–100%) und Enantioselektivitäten (91–99% *ee*) zu den korrespondierenden Alkoholen reduziert werden (Schema 1). Die Wiederverwendung des Katalysators war über zehn Läufe möglich, wobei nur geringfügige Ruthenium Kontaminationen im Produkt detektiert werden konnten (zwischen 0.8 und 3.3 ppm pro Lauf).



**Schema 1.** ATH mit immobilisierten Ruthenium Katalysator **Ru-57**.

Die Immobilisierung von Poly(*L*-Leucin) auf magnetischen Co/C und Fe/C Nanopartikel wird in Kapitel 3 vorgestellt. Anfangs wurden durch verschiedene Synthesestrategien Amino-Gruppen kovalent auf der Oberfläche der Nanopartikel verankert, welche anschließend als Initiatoren für die direkte Polymerisation mit *L*-Leucin-NCA verwendet wurden. Diese wurde sowohl bei Raumtemperatur als auch bei 90 °C durchgeführt, wobei unter beiden Bedingungen gute Beladungen (1.5–6.6 mmol Leucin pro Gramm Nanopartikel) erzielt werden konnten. Die hergestellten magnetischen Poly(*L*-Leucin) Katalysatoren wurden in der asymmetrischen Epoxidierung von (*E*)-Chalkon getestet (Schema 2). Die Aktivität und Selektivität der unterschiedlich hergestellten Katalysatoren wurde unter verschiedensten Reaktionsbedingungen untersucht. Anschließend wurden die erhaltenen Ergebnisse verglichen. Hierbei lieferte ein dreiphasiges System aus wässriger H<sub>2</sub>O<sub>2</sub>, Toluol und dem unlöslichen immobilisierten Katalysator unter Zusatz eines Phasentransferkatalysators in Bezug auf die Enantioselektivität die besten Ergebnisse (bis zu 43% Ausbeute, 89-92% *ee*). Trotz unterschiedlichster Bemühungen konnten aber die Reaktionsausbeuten nicht verbessert werden. Ebenso misslang die Wiederverwendung des Katalysators, da bereits im zweiten Lauf eine verringerte Aktivität festgestellt werden musste.



**Schema 2.** Asymmetrische Epoxidierung von (*E*)-Chalkon **106** mit magnetischem Poly(*L*-Leucin) Katalysator.

## E List of abbreviations

AFS	atomic fluorescence spectroscopy	HPLC	high-performance liquid chromatography
AIBN	azobisisobutyronitrile		
ATR	attenuated total reflection	ht	high temperature
ATH	asymmetric transfer hydrogenation	<i>i</i>	iso
BINAP	(2,2'-bis(diphenylphosphino)-1,1'-binaphthyl)	ICP-OES	inductively coupled plasma optical emission spectrometry
CNT	carbon nano tube	IR	infrared spectroscopy
Co/C	carbon-coated cobalt nanoparticles	lt	low temperature
conc	concentrated	Me	methyl
CuAAC	copper(I)-catalyzed azide-alkyne cycloaddition	min	minute
d	day, diameter	MNP	magnetic nanoparticle
dba	dibenzylideneacetone	MS	Mass spectrometry
DCM	dichloromethane	MW	microwave
DEE	diethyl ether	n.d.	not determined
DIPEA	<i>N,N</i> -diisopropylethylamine	NMR	Nuclear magnetic resonance
DMAP	4-(dimethylamino)-pyridine	NPs	nanoparticles
DMF	dimethylformamide	PEI	poly(ethyleneimine)
DMSO	dimethylsulfoxide	Ph	phenyl
DPEN	1,2-Diphenyl-1,2-ethylenediamine	ppb	parts per billion
DVB	1,4-divinylbenzene	ppm	part per million
<i>ee</i>	enantiomeric excess	PrOH	propanol
emu	electromagnetic unit	PTC	phase transfer catalyst
equiv.	equivalent	quant.	quantitative
Et	ethyl	R	arbitrary rest
EtOAc	ethylacetate	ROMP	ring-opening metathesis polymerization
Fe/C	carbon-coated iron nanoparticles	rt	room temperature
FT	fourier transformation	s	second
GC	gas chromatography	SPION	superparamagnetic iron oxide nanoparticles
GP	general procedure		
h	hour		

SQUID	superconducting quantum interference device
<i>t</i>	tert
T	temperature
TEM	transmission electron microscopy
TGA	thermogravimetric analysis
THF	tetrahydrofuran
TLC	thin layer chromatography
TOF	turn over frequency
US	ultrasound
UV	ultra violet
vs.	versus
XPS	photoelectron spectroscopy
XRD	x-ray diffraction



# **Declaration**

Herewith I declare that this present thesis is a presentation of my original work prepared single-handed. Wherever contributions from others are involved, all of them are marked clearly, with reference to the literature, license, and acknowledgement of collaborative research.

Regensburg, April 11, 2016

Corina M. Eichenseer